Investigation of the reactive oxygen species metabolism during the life cycle of *Fusarium graminearum*

Dissertation

Submitted for the degree of Dr. rer. nat.
(*doctor rerum naturalium*) to the University of Hamburg,
Faculty of Mathematics, Informatics, and Natural Sciences, Department of Biology

by

Karl Lewin Günther

born 26.03.1990 in Kiel

Hamburg, August 2018

1. Reviewer: Prof. Dr. Wilhelm Schäfer

2. Reviewer: Prof. Dr. Jörg Bormann

Termin der Disputation: 09.10.2018

„Cells don’t make reactive oxygen species, they have happy accidents.”

Bob ROS

Table of contents

List of abbreviations

A. acetabulum	*Acetabularia acetabulum*
A. alternata	*Alternaria alternata*
A. brassicicola	*Alternaria brassicicola*
A. fumigatus	*Aspergillus fumigatus*
A. nidulans	*Aspergillus nidulans*
B. cinerea	*Botrytis cinerea*
BCS	Bathocuproinedisulfonic acid
bp	Base pairs
Br	Bromine
C	Carbon atom
Cd	Cadmium atom
cDNA	Complementary DNA
C. elegans	*Caenorhabditis elegans*
Cl	Chlorine
CLSM	Confocal laser scanning microscopy
cm	Centimetres
CM	Complete medium
C. neoformans	*Cryptococcus neoformans*
C. purpurea	*Claviceps purpurea*
cpYFP	Cyclic permutated yellow fluorescent protein
CSPD	[3-(1-chloro-3'-methoxyspiro[adamantane-4,4'-dioxetane]-3'-yl)phenyl] dihydrogen phosphate
CTAB	Cetyltrimethylammonium bromide
Cu	Copper atom
CWDE	Cell wall degrading enzyme
cytHyPer	Cytosolically expressed HyPer
DAB	Diaminobenzidine
DCF	Dichlorofluorescein
ddH_2O	Double-distilled water
df	Downstream flanking region
DHE	Dihydroethidium
dig-dUTP	Digoxygenin-labelled dUTP
DM	Deprivation medium
DMSO	Dimethyl sulfoxide
DNA	Deoxyribonucleic acid
DON	Deoxynivalenol
DOPA	Dihydroxyphenylalanine
dpi	Days post inoculation
dsDNA	Double-stranded DNA
dUTP	Deoxyuridine triphosphate
e^-	Electron
E. coli	*Escherichia coli*
E. festucae	*Epichloë festucae*
e.g.	For example (Latin: exempli gratia)
ER	Endoplasmic reticulum
FAD	Flavin adenine dinucleotide
Fe	Iron atom
F. graminearum	*Fusarium graminearum*
FHB	*Fusarium* Head Blight
FMN	Flavin mononucleotide

g	Grams
gDNA	Genomic DNA
GEN	Geneticin
GFP	Green fluorescent protein
GPI	Glycosylphosphatidylinositol
GPI-HyPer	HyPer attached to a GPI-anchor
GSH	Glutathione (reduced)
GSSG	Glutathione disulfide (oxidised glutathione)
GTP	Guanosine triphosphate
h	Hours
H^-	Hydrogen anion
H^+	Hydrogen cation/proton
HBSS	Hank's balanced salt solution
$HO^\bullet$	Hydroxyl radical
$HO_2^\bullet$	Perhydroxyl radical
H_2O_2	Hydrogen peroxide
HYG	Hygromycin
I	Iodine
IC	Infection cushion
i.e.	That is to say (Latin: id est)
l	Litres
LF	Left flanking region
M	Molar
MAM	Mitochondria-associated membrane
MAP	Mitogen-activated protein
MAPK	Mitogen-activated protein kinase
mg	Milligrams
min	Minutes
mJ	Millijoule
ml	Millilitres
mm	Millimetres
mM	Millimolar
Mn	Manganese atom
M. oryzae	*Magnaporthe oryzae*
mRFP	Monomeric red fluorescent protein
mRNA	Messenger RNA
N	Nitrogen atom
NAC	Nascent polypeptide-associated complex
NAD^+	Nicotinamide adenine dinucleotide (oxidised)
NADH	Nicotinamide adenine dinucleotide (reduced)
$NADP^+$	Nicotinamide adenine dinucleotide phosphate (oxidised)
NADPH	Nicotinamide adenine dinucleotide phosphate (reduced)
NAT	Nourseothricin
NBT	Nitroblue tetrazolium chloride
N. crassa	*Neurospora crassa*
Ni	Nickel atom
nm	Nanometre
NNT	Nicotinamide nucleotide transhydrogenase
Nox	NADPH oxidase
NPS	Non-ribosomal peptide synthase
p.a.	Analytically pure (Latin: pro analysi)
P450	Cytochrome P450 monooxygenase

PCR	Polymerase chain reaction
PDI	Protein disulfide isomerase
PKS	Polyketide synthase
O_2	Dioxygen
$O_2^{\bullet-}$	Superoxide radical
OH^-	Hydroxyl anion
ORF	Open reading frame
Pa	Pascal
PAMP	Pathogen-associated molecular pattern
P. anserina	*Podospora anserina*
PEG	Polyethylene glycol
PTI	PAMP-triggered immunity
qRT-PCR	Quantitative real-time PCR
RBOH	Respiratory burst oxidase homologue
RCI	Resistance cassette internal
RF	Right flanking region
RH	Runner hyphae
RNA	Ribonucleic acid
RNAseq	Ribonucleic acid sequencing
roGFP	Reduction-oxidation sensitive green fluorescent protein
ROI	Region of interest
ROS	Reactive oxygen species
rpm	Rounds per minute
S. cerevisiae	*Saccharomyces cerevisiae*
sec	Seconds
SM	Split marker
SOD	Superoxide dismutase
SRE	Secreted ROS-related enzyme
SRP	Signal recognition particle
SSC	Saline-sodium citrate
S. sclerotiorum	*Sclerotinia sclerotiorum*
S. tritici	*Septoria tritici*
TF	Transcription factor
uf	Upstream flanking region
U. maydis	*Ustilago maydis*
UPR	Unfolded protein response
USA	United States of America
UV	Ultraviolet
WT	Wildtype
YEPD	Yeast extract peptone dextrose medium
YFP	Yellow fluorescent protein
YPD	Yeast peptone dextrose medium
ZEA	Zearalenone
Zn	Zinc atom
µg	Micrograms
µl	Microlitres
µM	Micromolar
µm	Micrometres
°C	Degrees Celsius

Equations

Figures

Tables

1. Introduction

1.1 Fusarium graminearum and Fusarium Head Blight

Global food and feed production is constantly threatened by pathogenic microorganisms, animals, and weeds. It is estimated that all of these threats combined are lowering global agricultural productivity by 20-40% (Oerke, 2006). A major portion of this damage is dealt by phytopathogenic fungi. Calculations done by Fisher et al. (2012) estimate that fungal diseases of five important global crops (rice, wheat, maize, potatoes, and soybean) potentially lead to losses that would be able to feed 8.5% to up to 61% of the world's population. With regard to the global population growth, finding an answer to this problem has become one of the most prominent challenges of bio-science.

The necrotrophic, filamentous ascomycete *Fusarium graminearum* [teleomorph Gibberella zeae (Schwein.)] is a devastating pathogen of all major cereal crops and the main cause of *Fusarium* Head Blight (FHB) in wheat (*Triticum aestivum*) and barley (*Hordeum vulgare*) as well as ear rot in maize (*Zea mays*) (Figure 1). These diseases render the infected plants useless for food and feed purposes due to reduced test weight (Windels, 2000) and an accumulation of fungal mycotoxins in the grain, some of which are harmful to both animals and humans.

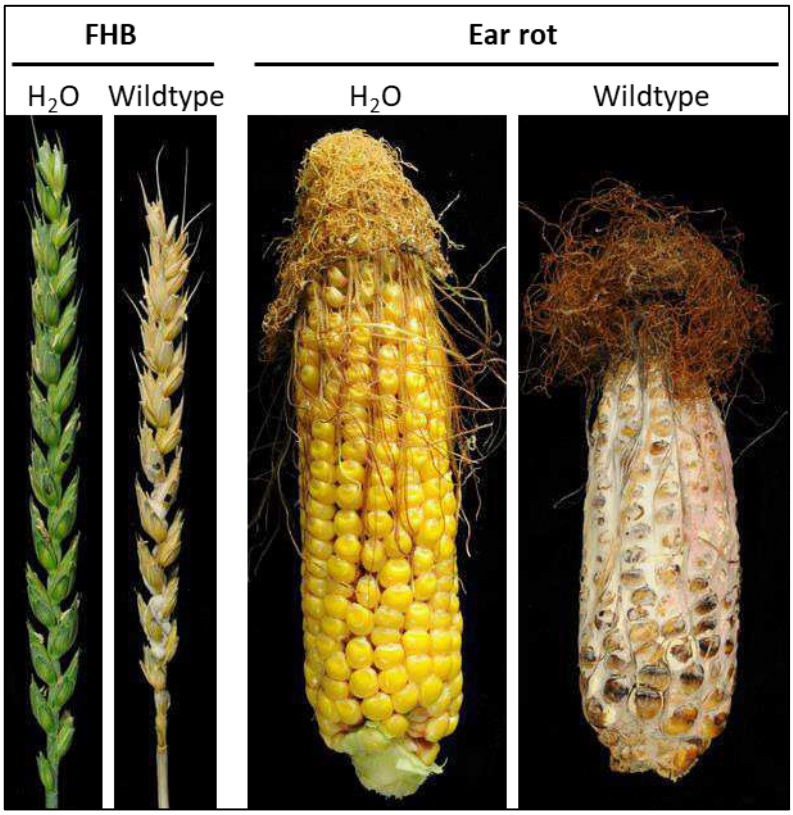

Figure 1: Symptoms of *Fusarium* Head Blight (FHB) on wheat (left) and ear rot on maize (right). Phenotypes of non-infected plants (H_2O) and infected plants (Wildtype) are shown. Infected wheat heads show premature bleaching in infected spikelets. Infected maize cobs are covered by white mycelia and show dark coloured kernels.

The mycotoxins deoxynivalenol (DON) and zearalenone (ZEA) are worth emphasizing as they are the main reasons for the fungus' toxicity. The trichothecenous toxin DON, also known as vomitoxin, inhibits protein biosynthesis at the ribosomes (Rocha et al., 2005) and causes nausea and vomiting when ingested (Pestka, 2010; Wu et al., 2014). Notably, DON constitutes an important virulence factor as it is involved in the effective spread of the fungus in plant tissue. The estrogenic polyketide ZEA has structural similarities with oestrogen and can bind to the respective receptors which may lead to hyperoestrogenism (Haschek & Voss, 2013). Both molecules are heat stable and remain active after sterilisation and processing of the contaminated grain, resulting in symptoms in humans and livestock (Desjardins & Proctor, 2001; Chen et al., 2017).

F. graminearum relies on a warm and humid climate during host anthesis for infection. Sexual ascospores or asexual conidiospores (conidia) are spread by wind, insects, rain, or irrigation, and land on flowering ears where they germinate. Growing hyphae penetrate the plant surface and proceed radially growing inside the host, causing necrosis of host cells and using the dead plant material as nutrition. Symptoms include water soaking followed by premature bleaching of wheat florets (Trail, 2009). In late infection stages, also after harvest, the fungus develops sexual reproductive organs (perithecia) in which ascospores are produced. It overwinters as mycelia or spores in crop residues, seeds, or in the soil. During springtime, ascospores are produced in newly formed perithecia on crop residues which constitute the major portion of the primary inoculum during the infection period (Wegulo, 2012). *F. graminearum* finds favourable conditions in southern Europe, China, South America, Australia, and the USA (McMullen et al., 2012) while colder regions such as central and northern Europe are dominated by the closely related species *Fusarium culmorum* (Kosiak et al., 2003; Wagacha & Muthomi, 2007). Besides climatic conditions, disease outbreaks are influenced by crop sequence, cultivar, and soil management (Evans et al., 2010; Scala et al., 2016).

The first FHB epidemic being officially published in 1890 in Indiana, USA (Arthur, 1891), reporting crop damage of up to 80%, further epidemics were reported throughout the 20th century with increasing severity and frequency especially in the USA and China (Atanasoff, 1920; Dickson, 1929 and 1942; Vestal et al., 1964; Moschini & Fortugno, 1996; Nganje et al., 2004; McMullen et al., 2012). During the last decade, in some areas in South America and China more than half of the local crop production has been destroyed by recurring Fusarium Head Blight epidemics (Yang et al., 2008; Pereyra & Lori, 2013). Protective measures against the disease are scarce. Highly resistant crop cultivars are not commercially available and the use of fungicides is cost intensive and problematic due to the narrow time window in which application is profitable (Gilbert & Haber, 2013; Cowger et al., 2016). These reports demonstrate that *F. graminearum* is still posing a global threat for agriculture and underline the need for further knowledge about the molecular basis of its infection process.

During infection *F. graminearum* forms different specialised epiphytical hyphal structures on the plant surface. Elongate non-invasive runner hyphae (RH) form an evenly distributed network covering the plant tissue. Invasive cells can be divided into three morphological classes (Boenisch & Schäfer, 2011): foot structures, lobate appressoria, and infection cushions (IC). Foot structures are formed when RH release short side branches which form small swellings directly on the plant surface and penetrate the cuticle. They are the first infection structures formed by *F. graminearum* and can be observed during the initial colonisation stage (infection stage I). Lobate appressoria are more complex multicellular infection structures formed by aggregation of hyphae. The most complex multicellular infectious organs are infection cushions (ICs) which are thought to be the fungus' most important tools for host invasion. They are formed by highly branched and agglomerated hyphae and cause multiple penetration events underneath them. Lobate appressoria and ICs belong to the class of compound appressoria and are formed during the main infection stage (infection stage II) (Boenisch & Schäfer, 2011; Bormann et al., 2014).

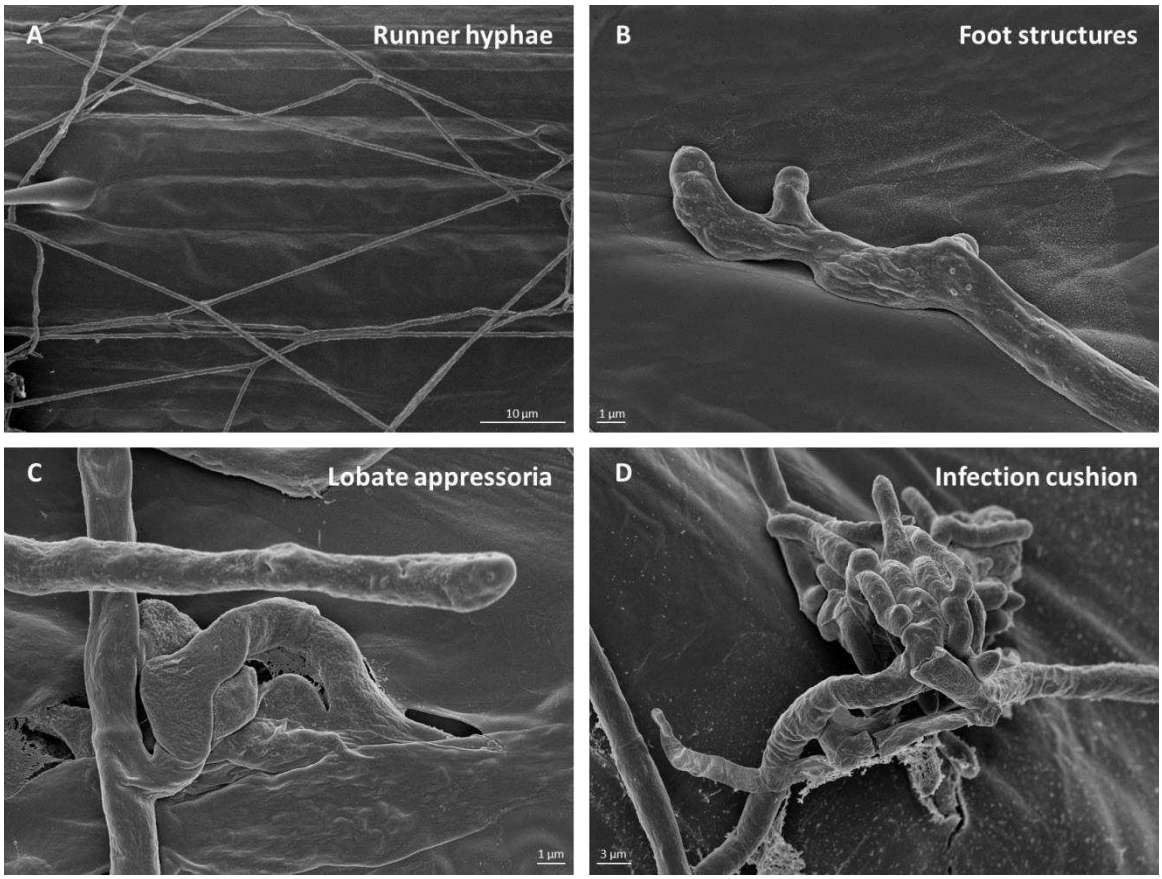

Figure 2: Scanning electron microscopy pictures of infection structures of *F. graminearum* on wheat palea. A: Mainly unbranched runner hyphae (RH) cover the plant surface. **B:** Small side branches form foot structures which are able to penetrate the plant cuticle. **C:** Lobate appressoria are further differentiated infection structures consisting of aggregated hyphae. **D:** Infection cushions (ICs) constitute the most complex infection structure of *F. graminearum*. They consist of multiple highly branched cells and penetrate the plant surface at multiple sites.

1.2 Transcriptomic data of the early infection stage

The exact molecular mechanisms leading to the initiation of infection structures still prove to be elusive. In previous work cDNA libraries of dissected RH, IC, and in-culture grown mycelia were established to gain further insight into gene regulatory processes (Mentges et al., unpublished data). RNAseq-based transcriptomic and functional analysis revealed major transcriptional rearrangements in the three types of hyphae (Mentges et al., unpublished data). Specific upregulation of putative virulence factors in ICs underlined their status as the major invasive structures of *F. graminearum*. Gene expression of DON, iron chelating siderophores, effector proteins, cell wall degrading enzymes, and enzymes involved in the metabolism of reactive oxygen species (ROS) is upregulated in ICs compared to RH and in-culture grown mycelia. The analysis of ROS-related enzymes was one of the core tasks of this thesis. An indication for the significance of ROS and ROS-related enzymes in the infection process of *F. graminearum* has been found previously by Mentges & Bormann (2015) who demonstrated an accumulation of the ROS H_2O_2 in ICs.

1.3 Oxygen and reactive oxygen species (ROS)

This thesis revolves entirely around the topic of ROS which are therefore introduced further in the following sections. Earth's atmosphere consists of 21% molecular oxygen, or dioxygen (O_2), which is used as an electron acceptor, and therefore as a reduction equivalent, by aerobic organisms. The energy potential of oxygen-dependent complete substrate oxidation is about 18 times higher compared to glycolysis (Cadet & Davies, 2017). While oxygen is commonly considered to be a highly reactive molecule it is abundant in the atmosphere without causing detrimental oxidative reactions with organic compounds in its vicinity. The reason for this lies in the special chemical properties of molecular oxygen. Its unique feature is that it exists in a triplet ground state ($^3O_2$) which distinguishes it from most other molecules that exist in the singlet state. Reactions between triplet and singlet molecules are energetically unfavourable (Hrycay & Bandiera, 2012). Large intrinsic resonance stabilisation energy protects dioxygen from polymerisation and from reaction with organic molecules (Borden et al., 2017). Therefore, molecular oxygen itself is comparably unreactive despite the fact that $^3O_2$ has two unpaired electrons making it a diradical. Through energy or electron transfer, however, it tends to form reactive oxygen species (ROS), e.g. during the reduction of O_2 to H_2O in the course of the mitochondrial electron transport chain (Equation 1).

$$O_2 \xrightarrow{e^-} O_2^{\bullet -} \xrightarrow{e^- + 2H^+} H_2O_2 \xrightarrow{e^- + H^+} OH\cdot \xrightarrow{e^- + H^+} H_2O$$

Equation 1: Sequential reduction of molecular oxygen to water. Transfer of one electron (e^-) to molecular oxygen (O_2) generates superoxide ($O_2^{\bullet -}$). This is further reduced to hydrogen peroxide (H_2O_2) by the transfer of another electron to superoxide. Two further electron transfer steps reduce hydrogen peroxide to hydroxyl radical (OH·) and hydroxyl radical to water (H_2O).

Four electrons are necessary for complex IV of the breathing chain to completely reduce molecular oxygen to water. The electron transport chain runs only at 97-99% efficiency which results in an electron leak at the FMN cofactor in complex I and the heme b_L cofactor in complex III (Liu et al., 2002; Kussmaul & Hirst, 2006; Jastroch et al., 2010). These electrons are capable of reducing dioxygen to the radical superoxide ($O_2^{\bullet-}$) which can spontaneously dismutate to hydrogen peroxide and oxygen (Equation 2).

$$O_2^{\cdot-} + H^+ \longrightarrow HO_2\cdot$$

$$2\ HO_2\cdot \longrightarrow H_2O_2 + O_2$$

Equation 2: Spontaneous dismutation of superoxide ($O_2^{\bullet-}$). Superoxide reacts with a proton (H^+) generating a perhydroxyl radical ($HO_2\cdot$). Two perhydroxyl radicals can react generating hydrogen peroxide (H_2O_2) and molecular oxygen (O_2).

H_2O_2 is more stable than superoxide and is generally considered membrane permeable. It is also the substrate for the Fenton-reaction during the course of which H_2O_2 reacts with a transition metal such as iron or copper forming the hydroxyl radical (OH·) (Equation 3). OH· is the most unstable and most reactive of all ROS. Within a radius of about 2 nm it can react with nucleic acids, proteins, carbohydrates, and lipids.

$$Fe^{2+} + H_2O_2 \longrightarrow Fe^{3+} + OH^- + OH\cdot$$

Equation 3: The Fenton-reaction. In presence of transition metal ions (Fe^{2+}) the relatively stable hydrogen peroxide molecule (H_2O_2) is converted to a hydroxyl ion (OH^-) and a highly reactive hydroxyl radical (OH·)

1.3.1 Benefits and dangers

The high reactivity of ROS, not only the hydroxyl radical, constitutes the danger these molecules can pose for all living organisms. ROS can react with DNA in multiple ways leading to more than 100 known modifications (Dizdaroglu, 1992). They can cause radical forming chain reactions when reacting with lipids and potentially inhibit or alter protein functions upon reactions with amino acids (Cooke et al., 2003; Møller et al., 2007). Together, the influence of ROS upon cellular components is potentially fatal leading to destructive chain reactions, consequential cell death, and aging of the organism. However, despite their toxicity ROS are of fundamental importance for the metabolism of every living organism. While toxic when accumulated, ROS in small amounts represent signalling molecules for cellular differentiation and development (Scott & Eaton, 2008). They are capable of oxidizing sulphur-containing groups such as cysteine residues in proteins, thereby potentially influencing the activity of phosphatases and transcription factors. Often, regulatory activity of ROS is indirect; e.g. instead of directly reacting with less reactive target molecules, H_2O_2 oxidizes highly reactive proteins such as peroxiredoxin which in turn oxidises the target molecule serving as an adapter protein (Winterbourn & Hampton, 2008).

The Janus-head character of ROS forced aerobic life forms to develop a sophisticated system of ROS-producing and –scavenging enzymes and transcriptional regulation in the course of evolution in order to avoid deleterious oxidation of cellular components. An arsenal of enzymatic and nonenzymatic defence systems protects cells from detrimental ROS-damages. Glutathione, phytochelatins, ascorbic acid, polyamines, flavonoids, alkaloids, or carotenoids all belong to the nonenzymatic defence systems (Jamieson, 1998). The enzymatic systems consist of two defence lines. Superoxide dismutase (SOD) catalyses the dismutation of superoxide to H_2O_2 which takes place 10,000 times faster than the spontaneous dismutation described above (Fridovich, 1983). Various peroxidases such as catalase, glutathione peroxidase, and peroxiredoxin convert H_2O_2 to H_2O. These proteins usually get recycled afterwards through reduction using an electron donor such as NADPH. Under physiological steady state conditions cells are therefore able to maintain a favourable ROS-equilibrium through tight balancing of ROS-production and ROS-scavenging. A disruption of this balance leads to oxidative stress.

1.3.2 ROS in plant-microbe interactions

ROS are of major importance for both sides of plant-pathogen interactions as a defence molecule and aggressive agent. Plant membrane-associated respiratory burst oxidase homologues (RBOHs) produce the majority of ROS necessary for the plant's first line of defence against aggressors, the oxidative burst (Torres et al., 1998). This rapid production of ROS is separated into two phases. The first one occurs within minutes after sensing a pathogen, is transient and low in amplitude. The second one can be observed hours after the contact and is sustained (Piedras et al., 1998; Grant & Loake, 2002; Able, 2003). In both pathogenic and mutualistic interactions between plants and other kingdoms the second phase of this defence mechanism is not observed and putatively suppressed as suggested by Shaw and Long (2003). The ROS-production itself is the earliest part of the pathogen-associated molecular pattern (PAMP)-triggered immunity (PTI). Apart from poisoning the aggressor, ROS additionally take part in cell wall strengthening and function as second messenger. The latter leads to induction of pathogenesis-related proteins and phytoalexins as well as apoptosis of neighbouring cells. Along with ROS, fungi are forced to deal with plant-produced antifungal xenobiotics such as benzoic acid and isoeugenol (Lah et al., 2011).

Different pathogenic fungal lifestyles brought forth different strategies of dealing with the PTI but all have in common that gaining control over the ROS-level in the area of contact between pathogen and host is pivotal for a successful invasion. Previous studies demonstrated the importance of ROS for phytopathogenic fungi: Mentges and Bormann (2015) used ratiometric imaging with *F. graminearum* ICs expressing the H_2O_2-sensitive reporter HyPer to demonstrate that ICs contain higher levels of H_2O_2 compared to RH. Nguyen et al. (2012) could show that the stress-activated MAP kinase (SAPK) FgOS-2 from *F. graminearum* orchestrates ROS generation and detoxification. Lack of FgOS-2 or of the FgOS-2 controlled transcription factor FgAtf1 which are involved in the regulation of catalases cause defects in pathogenic development and stress responses (Nguyen et al.,

2012; Nguyen et al., 2013; Mentges et al., unpublished results). Deletion of the superoxide-producing NADPH-oxidases NoxA and NoxB in *F. graminearum* leads to impaired pathogenicity (Wang et al., 2014). For other plant pathogenic fungi the literature shows a dependency on ROS as well. The biotroph *Ustilago maydis* is reliant on its ability to detoxify ROS in order to be fully virulent. Mutants of *U. maydis* unable to express the regulator Yap1p which mediates oxidative burst response (Toone & Jones, 1999) are impaired in virulence. This defect can be restored by inhibiting the ROS-producing NADPH-oxidase (Nox)-complex (Molina & Kahmann, 2007), showing the opposite effect as in *F. graminearum*. Similarly, deletion of the transcription factor Cptf1 of the biotroph *Claviceps purpurea* that controls the expression of multiple ROS-scavenging enzymes leads to an oxidative burst-like reaction which is usually not observed inside plant tissue during infection of the wildtype fungus (Nathues et al., 2004). Deletion of the histidine kinase CpHK2, a homologue of the oxidative stress sensor SpMAK2/3 of fission yeast, significantly lowers virulence of *C. purpurea* (Nathues et al., 2007). These examples demonstrate that biotrophic pathogens need to circumvent the plant defence response by ROS detoxification. The same is true for endophytes and other beneficial symbionts (Abbà et al., 2009; Kapoor & Singh, 2017). A different approach can be observed in necrotrophic pathogens. The necrotrophic grey mould fungus *Botrytis cinerea* causes a strong oxidative burst during all phases of infection (Schouten et al., 2002; Lyon et al., 2004). The dependency of this fungus on a beneficial ROS-equilibrium and at the same time the difference in ROS-dependency between biotrophic and necrotrophic fungi has been elegantly demonstrated by experiments with hypersensitive reaction-deficient *Arabidopsis* mutants (Tiedemann, 1997). The author observed that the virulence of *B. cinerea* correlates directly with the amount of ROS in the leaf tissue during infection. Indeed, almost no lesions were formed during infection of hypersensitive reaction-deficient plants. When co-infecting those plants with *B. cinerea* and the hypersensitive reaction-causing bacteria *Pseudomonas syringae* the fungus regains its virulence. This suggests that *B. cinerea* relies on a certain ROS concentration to be fully virulent which has been shown with other hosts as well (Asai and Yashioka, 2009). Similar results have been published for other necrotrophic fungi such as *Sclerotinia sclerotiorum* (Williams et al., 2011), *Alternaria solani* (Kobayashi et al., 2012), *Fusarium oxysporum* (Bai et al., 2013), *Colletotrichum coccodes* (Alkan et al., 2009), and *Aphanomyces euteiches* (Kiirika et al., 2012). While these findings seem to demonstrate a general rule regarding necrotrophic plant pathogen interactions, they do not apply for all examples of necrotrophic growth. The virulence of *S. tritici* for instance is enhanced by the addition of catalase during its necrotrophic infection phase (Shetty et al., 2007). Also, the character of the host-ROS-fungus relationship relies on timing. In initial stages of infection necrotrophic fungi are susceptible to ROS and can be inhibited in virulence by ROS production, contrary to their later dependency on high ROS-concentrations (Walz et al., 2008; L'Haridon et al., 2011; Williams et al., 2011) as suggested by the results of Zhang et al. (2012). This highlights the importance of differentiating between early and later colonisation phases of necrotrophic fungi.

1.4 ROS-related enzymes

The evident significance of ROS for *F. graminearum* pathogenicity led to the assumption that enzymes which are involved in the production or detoxification of ROS would consequentially be of similar importance for the fungus. Below, the enzyme classes that share this characteristic and were investigated in this study are described starting with the large enzyme family of oxidoreductases, which comprises the vast majority of studied enzymes, followed by cupredoxins and metallothioneins which exhibit a more indirect influence on cellular ROS.

1.4.1 Oxidoreductases

The term oxidoreductase comprises all enzymes catalysing the transfer of electrons from an electron donor molecule to an electron acceptor molecule, usually with the help of a cofactor such as heme, flavin and metal ions. In biochemistry oxidoreductases can be subdivided into oxidases, peroxidases, oxygenases/hydroxylases, and dehydrogenases/reductases (Xu, 2005). It has to be noted in this respect that redox reactions are usually reversible; for example an enzyme categorised as a reductase may function as an oxidase given suitable conditions. In fact, most of the enzyme classes described below exhibit multiple activities that would usually be described with the name of a different enzyme class. This functional redundancy and interchangeability between different classes of oxidoreductases makes the nomenclature in this regard somewhat imprecise. During all electron transfer reactions that are catalysed by these enzymes radical intermediates are generated which can - mostly unintentionally - get released. Therefore, all oxidoreductases are to some extent involved in the ROS metabolism of the cell. The following list starts with those oxidoreductases which have a direct impact on the cell's oxidation level with ROS being involved directly in the reactions they catalyse (superoxide dismutases, peroxidases, catalases, one-electron- and two-electron-transferring oxidases), followed by those oxidoreductases that have an indirect influence on the oxidation level, either by oxidation of the substrate using oxygen (four-electron-transferring oxidases) or dinucleotide cofactors (dehydrogenases) as the electron acceptor or by insertion of oxygen into the substrate (oxygenases/hydroxylases).

Superoxide dismutases (SOD)

The enzymatically catalysed dismutation of $O_2^{\bullet -}$ to H_2O_2 represents the first line of defence against oxidative stress. An alternative term for SOD is superoxide:superoxide oxidoreductase. The active centre carries a metal atom according to which these enzymes are classified. To date, manganese SODs (MnSOD), copper/zinc SODs (CuZnSOD), iron SODs (FeSOD), and nickel superoxide dismutases (NiSOD) are described. The dismutation

process is catalysed via sequential reduction and oxidation of the metal centre during the course of which $O_2^{\bullet -}$ is gradually reduced and oxidised (Abreu & Cabelli, 2010). In Eukaryotes the most abundant SOD is CuZnSOD which can be found in the cytosol, the chloroplast, and the extracellular space. MnSOD is usually found in mitochondria, FeSOD in chloroplasts, while NiSOD has not been found in Eukaryotes thus far. In prokaryotes all four types can be found (Abreu & Cabelli, 2010).

Peroxidases

The term peroxidase encompasses a large diversity of different enzymes all of which share the ability to catalyse the reduction of peroxides (Equation 4) in order to oxidise a wide array of inorganic or organic substrates.

$$ROOR' + 2e^- + 2H^+ \longrightarrow ROH + R'OH$$

Equation 4: Reduction of peroxides. The peroxide substrate (ROOR') is split at the O-O bond by reduction of both oxygen atoms. The donors of the reduction equivalents ($2e^-$ and $2H^+$) are oxidised in this process.

Many peroxidases use an oxygen-binding heme complex as a prosthetic group (e.g. horseradish peroxidase) but there are also cofactor-free variants using redox-active cysteine or selenocysteine residues (glutathione peroxidase, peroxiredoxin). In rare cases vanadate is used as a cofactor (Vilter, 1995).
Despite their common function of eliminating H_2O_2, peroxynitrite, and other peroxides, peroxidases are not to be regarded only as antioxidant enzymes. The reduction catalysed by heme-peroxidases is often achieved by one-electron transitions potentially turning the substrate into a radical. With the exception of catalases, heme-peroxidases are therefore generally prone to promote oxidative damage (Flohé & Ursini, 2008). On the other hand, peroxidases using selenium or sulphur as catalysing agents usually induce two-electron transitions which abolish the risk of producing free radical intermediates. With hydroperoxides as oxidizing agents these enzymes do lower oxidative stress; however this antioxidative function is often subordinate compared to the physiological role of substrate oxidation.

Lignin-peroxidases are secreted heme-containing peroxidases that catalyse the oxidative cleavage of ß-1 linkages in lignin while reducing H_2O_2 to H_2O. While these enzymes are of high interest for biotechnology due to their potential for the industrial biodegradation of wood (Kimura et al., 1990; Hammel & Cullen, 2008) it seems likely that they are involved in plant-invasion although sources regarding this matter are scarce.

Chloroperoxidases are heme-containing peroxidases that belong to the subgroup of haloperoxidases which catalyse the oxidation of halides by hydrogen peroxide. The oxidised halide can replace a hydrogen atom of the organic substrate compound, a process called halogenation (Equation 5). Haloperoxidases are divided into

iodoperoxidases which are able to oxidize I^-, bromoperoxidases which are able to oxidize I^- and Br^-, and chloroperoxidases which are able to oxidize I^-, Br^-, and Cl^-. Apart from halogenation chloroperoxidases catalyse a variety of reactions such as peroxidation or oxygenation, and have been shown to be involved in fungal delignification processes (Ortiz-Bermúdez et al., 2003). The highly electrophilic chlorine species generated via the oxidation of Cl^- by chloroperoxidases react with the electron-rich aromatic rings of lignin (Dence, 1971). Correspondingly, soil, litter, and decayed wood contain high-molecular-weight chloroaromatics (Flodin et al, 1997; Myneni, 2002).

$$R\text{-}H + Cl^- + H_2O_2 + H^+ \longrightarrow R\text{-}Cl + 2H_2O$$

Equation 5: Halogenation of an organic substrate (R) with concomitant reduction of H_2O_2. The negatively charged electrophilic halogen (in this case chlorine, Cl^-) replaces the hydrogen atom of the substrate molecule. Together with a free H^+ ion the hydrogen atom is used to reduce H_2O_2 to 2 water molecules ($2H_2O$).

Catalases

Catalases belong to the peroxidase enzyme group. The unique feature of these enzymes is the specificity to H_2O_2 as both electron donor and electron acceptor. Catalases catalyse the degradation of two H_2O_2 molecules to O_2 and H_2O (Equation 6). One of the H_2O_2 molecules is reduced to H_2O and one is oxidised to O_2. The enzyme's cofactor (usually heme) first provides an electron for the reduction process (Fe^{3+} to Fe^{4+} in case of heme) which it retrieves during the oxidation process (Fe^{4+} to Fe^{3+} in case of heme) returning to the initial state.

$$H_2O_2 + H_2O_2 \longrightarrow O_2 + 2H_2O$$

Equation 6: Reduction of hydrogen peroxide (H_2O_2) by catalase. Through the successive reaction of catalase two H_2O_2 molecules are reduced to molecular oxygen (O_2) and 2 water molecules ($2H_2O$).

The turnover frequency and catalytic efficiency of this group are among the highest of all enzymes in nature (Heck et al., 2010). Catalases can be divided into three classes: heme-containing monofunctional catalase or typical catalase, heme-containing bifunctional catalase-peroxidase, and pseudocatalase or Mn-catalase (Zhang et al., 2010). The pure antioxidative function and high turnover rate of monofunctional catalase make it a pivotal enzyme for oxidative stress resistance.

Oxidases

Oxidases catalyse the oxidation of their substrate using dioxygen as the electron acceptor. Depending on the number of electrons transferred to dioxygen the reaction product varies between different types of oxidases. Transfer of one electron to dioxygen leads to the production of superoxide (NADPH-oxidase, see below), transfer of two electrons leads

to hydrogen peroxide (e.g. xanthine oxidase), and transfer of four electrons leads to water (e.g. cytochrome c oxidase). While the transfer of one or two electrons always generates ROS, the production of ROS is possible by oxidases usually transferring four electrons as well when the reduction of oxygen gets attenuated and the radical intermediates are released. This potential for an unintended generation of ROS is in fact innate to all oxidoreductases since the sequential transfer of electrons is coupled to the production of unstable intermediates which usually get processed to stable products in a controlled manner by the enzymes.

The Nox-complex

A unique oxidase type that needs to be introduced specifically due to its important role in this study is the multicomponent NADPH oxidase enzyme complex (Nox) which plays a major role in the redox homeostasis of animals, plants and fungi. Nox couples one electron from NADPH to molecular oxygen, thereby producing superoxide. It is the only known cellular machinery whose sole purpose is the generation of ROS and the most important enzymatic ROS generating system (Bedard & Krause, 2007). In mammals the NADPH oxidase $gp91^{phox}$ is necessary for the oxidative burst defence response of neutrophils (Bedard & Krause, 2007). Several additional enzymatic components are necessary for its activity such as the regulatory subunit p67phox and the small GTPase Rac2 (Diebold & Bokoch, 2001; Bedard & Krause, 2007). The Nox machinery is also described in plants where it is required for defence against pathogens (Keller et al., 1998; Torres et al., 2002; Marino et al., 2012) and in fungi. While Nox is absent in some unicellular fungal species, filamentous fungi all contain one or multiple *nox* genes (Lara-Ortiz et al, 2003; Cano-Dominguez et al., 2008; Yang & Chung, 2012, 2013; Wang et al. 2014). To date, three Nox proteins FgNoxA, FgNoxB and the variant FgNoxC are identified in *F. graminearum* (Aguirre et al., 2005; Heller & Tudzynski, 2011; Ryder et al., 2013) of which FgNoxA and FgNoxB are well characterised in Wang et al., 2014. In contrast to NoxC which is regulated by its EF-hand motifs (Tudzynski et al., 2012) NoxA and NoxB are regulated by the regulatory subunit NoxR. Of special interest for this study is the localisation of the Nox complex. This matter has lately been subject of intense discussion due to the fact that the Nox isoforms are not restricted to a certain cellular locus. The dependency on different stimuli and post-translational processes leading to varying subcellular locations as well as the absence of a clear localisation signal within the Nox structure and a lack of reliable antibodies have made it difficult to assign mammalian Nox isoforms to a specific structure (Laurindo et al., 2014). For the plant pathogen *B. cinerea* it has been shown that NoxA and NoxB localise to the nuclear envelope and the ER (Siegmund et al. 2013, Marschall et al., 2016b). Marschall et al. also predict possible ROS production by NoxA inside of the ER.

Dehydrogenases/reductases

Dehydrogenases are oxidoreductase enzymes catalysing the reversible oxidation of their substrate via the transfer of a hydrogen anion (H^-) to an electron acceptor (NAD^+, $NADP^+$, or FAD). A cysteine residue in the active centre of the dehydrogenase covalently binds the substrate molecule and the cofactor (the electron acceptor) takes over the hydrogen anion ($2e^- + H^+ = H^-$), oxidising the substrate molecule. This electron transfer step is a potential source for ROS. The covalent bond with the enzyme is cleaved by hydrolysis and the reduced cofactor is exchanged for an oxidised one (Müller-Esterl et al., 2017). Dehydrogenases are classified according to their substrate, hence classes such as glucose dehydrogenases, ethanol dehydrogenases, or lipoamide dehydrogenases. Dehydrogenases are crucial for the energy metabolism of all organisms as the cleavage of hydrogen from organic substrates is one of the basic exothermal reactions of the cell.

Nicotinamide nucleotide transhydrogenase (NNT)

A special kind of hydrogen anion transferring enzyme is the nicotinamide nucleotide transhydrogenase (NNT). The NNT is a unique type of protein which is located in the inner mitochondrial membrane and catalyses the regeneration of NADPH by using energy from the mitochondrial proton gradient as the driving force (Nickel et al., 2015). $NADP^+$ is reduced by the translocation of a hydrogen anion from NADH (Equation 7). Under normal conditions the production of NADPH is highly favoured because the transhydrogenase reaction is coupled with the reflux of a proton from the intermembrane space to the matrix.

$$NADH + NADP^+ \rightleftharpoons NADPH + NAD^+$$

Equation 7: Regeneration of NADPH by the NNT. A hydrogen anion is transferred from NADH to $NADP^+$ generating NAD^+ and NADPH. This reaction is reversible but the equilibrium is strongly on the right side of the equation.

The coupling of NNT activity to the proton gradient ensures NADPH synthesis only during sufficient energy production by mitochondria. NADPH is needed for the upkeep of reduced glutathione/thioredoxin system making the NNT an important player in the avoidance of high ROS concentrations in mitochondria (Rydström, 2006).

Oxygenases/hydroxylases

Oxygenases and hydroxylases catalyse the oxygenation or hydroxylation of organic compounds by inserting one (monooxygenases/hydroxylases) or two (dioxygenases/hydroxylases) oxygen atoms into their substrate using molecular oxygen (O_2) as oxygen donor (Torres Pazmiño et al,. 2010).

Monooxygenases

To achieve the integration of an oxygen atom into the organic substrate molecule, molecular oxygen needs to be activated by the transfer of electrons. Hereby, ROS are formed. Monooxygenases are classified according to their cofactor (such as flavins, hemes, or NADH) which also determines the type of ROS produced (Torres Pazmiño et al., 2010). Their chemo-, regio-, and enantioselectivity make them highly attractive as industrial biocatalysts (Torres Pazmiño et al., 2010; Pigné et al., 2017). Below, different types of monooxygenases relevant for this study are described in further detail.

Cytochrome P450-monooxygenase

Cytochrome P450 enzymes (P450s) are heme-thiolate proteins found in all life forms (Nelson et al., 1996). Nearly all P450s function as monooxygenases (Shin et al., 2018) which means that they incorporate one oxygen atom into their substrate (Sono et al., 1996; Mansuy, 1998). This is achieved by the successive reduction of dioxygen (O_2). One oxygen atom is incorporated into the substrate while the other is reduced to H_2O. Most, but not all, P450s require an additional protein complex that transfers the two necessary electrons from NADH or NADPH to their catalytic centre for the reduction of oxygen (Črešnar & Petrič, 2011). The ability to hydroxylise an inoperable C-H bond into a C-OH bond accounts for the broad scope of different functions of P450s (Mansuy, 1998). Along with their most common role as monooxygenases in the metabolism of primary and secondary metabolites and degradation of xenobiotics (Črešnar & Petrič, 2011; Shin et al., 2018) P450s can function as peroxidases and peroxygenases and have a considerable impact on the redox status of cells. The monooxygenation cycle is a highly complex mechanism involving the constant oxidation and reduction of the enzyme's metal centre. During "unsuccessful" or uncoupled reactions, e.g. the transfer of electrons into unoccupied P450 molecules, $O_2^{\bullet-}$ and/or H_2O_2 are produced leading to oxidative stress (Hrycay & Bandiera, 2012; Feyereisen, 2012; Hrycay & Bandiera, 2015). Filamentous fungi depend on their large array of secreted proteins and secondary metabolites to be able to degrade their substrate, survive unfavourable conditions, or interact with their host. For this reason they contain a much larger diversity of P450s than animals which enables them to efficiently degrade environmental pollutants, plant-derived toxins, or fungicides (Sutherland, 1992; George et al., 1998), and, e.g. in case of *F. graminearum*, to produce mycotoxins. The majority of P450s are located in the smooth ER membrane facing the cytosol (Monier et al., 1988; Black, 1992). They carry an N-terminal signal peptide in their amino acid chain which directs them to the secretory pathway. However, instead of being secreted P450s are retained in the ER membrane due to retention signals which can function in two ways. Either the retention signal directly mediates exclusion of the polypeptide from transport vesicles or the polypeptide does get transported to the Golgi apparatus but is then sent back to the ER via the retrieval pathway (Andersson et al., 1999; Szczesna-Skorupa & Kemper, 2000).

Flavin-dependent monooxygenases

Rather than using transition metals like the heme in P450s, these enzymes rely on the organic cofactors FAD or FMN and usually catalyse aromatic ring oxygenations, epoxygenations, and halogenations (Torres Pazmiño et al., 2010). During oxygenation reaction NADPH reduces FAD to $FADH_2$ before O_2 binds to the FAD, thus generating the hydroperoxide intermediate FADH-4α-OOH that transfers one oxygen atom onto the substrate. Since the activated flavin cofactor is a weaker oxidant than the activated heme of P450s, flavin-dependent monooxygenases have a much narrower scope of functions (Totah & Rettie, 2007). They are common in microorganisms (Cochrane & Vederas, 2014; Huijbers et al., 2014) and, like P450s, are involved in xenobiotics degradation.

Tyrosinases

Tyrosinases are copper proteins that belong to the class of monophenol-monooxygenases. Catalysing the hydroxylation of phenolic compounds to quinones, the main biological task of fungal tyrosinases is the biosynthesis of melanin, a pigment involved in defence against different stresses such as free radicals, UV or gamma radiation or dehydration (Bell & Wheeler, 1986). During the tyrosinase-catalysed reaction the enzyme's copper centre binds molecular oxygen and first transfers one oxygen atom onto the monophenol substrate oxygenating it to a diphenol. In a second step the diphenol is oxidised to a quinone. The two hydrogen atoms and the remaining oxygen atom are released as water (Equation 8).

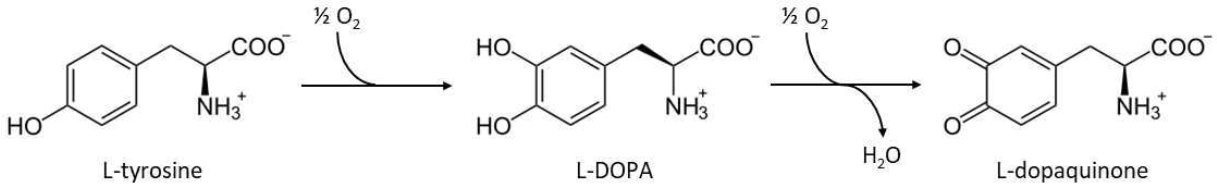

Equation 8: Oxidation of L-tyrosine to L-dopaquinone, a precursor of melanin, by tyrosinase with concomitant reduction of oxygen to water. First, one oxygen atom is introduced into the carbon ring of L-tyrosine generating a second hydroxyl group (L-DOPA). The hydrogen atoms of the hydroxyl groups are then transferred to the other oxygen atom reducing it to water (H_2O) and oxidising the hydroxyl groups to keto groups generating L-dopaquinone.

As with other oxidoreductases, the reduction of oxygen to water represents a potential source of ROS. Due to their broad substrate specificity, capability of cross-linking phenolic poylmers, and involvement in the synthesis of the pharmaceutically important compound L-DOPA, tyrosinases are of rising interest for industry and medicine (Chen et al., 2002; Sanz et al., 2005; Selinheimo et al., 2007a, 2007b; Zaidi et al., 2014)

1.4.2 Cupredoxins

There are many different types of proteins that contain one or more copper ions as prosthetic groups. These copper proteins are classified according to the spectroscopic properties of their copper centre (Choi & Davidson, 2011). Cupredoxins, also called blue copper proteins, carry a type I copper centre and function primarily as electron shuttles (Choi & Davidson, 2011). Along with mono-domain cupredoxins such as plastocyanin, amicyanin, and azurin there are multi-domain copper proteins such as laccase, ceruloplasmin, and nitrite reductase that contain multiple, but not exclusively, cupredoxin-type folds. However, when referring to the enzyme class the term cupredoxin describes only blue copper proteins. Cupredoxins bind toxic free copper ions and render them innocuous. One reason for the toxicity of free copper (Cu^{2+}) lies in its connection with ROS: cuprous ions can react with H_2O_2 forming hydroxyl radicals (Fenton-reaction) (Manzl et al., 2004).

1.4.3 Metallothioneins

Metallothioneins are low molecular weight, cysteine-rich, metal-binding proteins found in all eukaryotes and several prokaryotes (Coyle et al., 2002; Henkel & Krebs, 2004; Vasák, 2005). The high amount of cysteine residues (~30%) allows for binding of different heavy metal atoms, most notably copper and zinc, under physiological conditions. A variety of biological purposes are associated with metallothioneins such as cell growth and differentiation, maintenance of metal homeostasis, metal detoxification, and ROS-scavenging (Vasák & Hasler, 2000; Coyle et al., 2002; Ruttkay-Nedecky et al., 2013). The antioxidative function of metallothioneins is well researched in mammals (Ruttkay-Nedecky et al., 2013) where they bind mainly zinc but also copper or cadmium (Shaw et al., 1991). During oxidative stress in mammals metallothioneins release their zinc atom and reduce ROS-molecules forming metallothionein disulfides that are either degraded or regenerated to the thiol state if the environment is reducing, e.g. through an increase in the glutathione/glutathione disulfide ratio. This process increases the cellular concentration of free zinc. Zinc itself has no redox capacity but is still an important antioxidative agent (Oteiza, 2012) because it leads to a transcriptional up-regulation of metallothioneins and glutathione which constitutes the metallothionein redox cycle (Ruttkay-Nedecky et al. 2013). Adding to their antioxidative capabilities, metallothioneins are able to efficiently sequester copper which, when free, can potentially generate ROS by catalysing the Fenton reaction in the course of which hydroxyl radical is produced. While being well-investigated in mammals, fungal metallothioneins are still the subject of intensive research.

1.5 Endoplasmic reticulum and secretion

The enzyme families introduced above were the target of characterisation because they are involved in ROS-metabolism. A special focus of this study, however, lay on those ROS-related enzymes that were secreted by the fungus and might thereby potentially influence the ROS-equilibrium in the contact area between pathogen and host. Below, the general process of protein secretion is explained in further detail along with an explanation of the structure, function, and stress adaptation processes of the endoplasmic reticulum (ER) as this organelle plays an important role for experiments conducted in this study.

Filamentous fungi are life forms that produce and secrete large amounts of proteins such as secondary metabolites. 1665 of 13826 genes in *F. graminearum* (12%) are predicted for secretion. The endoplasmic reticulum (ER) is a type of organelle present in the vast majority of eukaryotic cells with few exceptions such as erythrocytes and spermatozoa. It is directly continuous with the outer nuclear membrane and spreads throughout the cell amounting to over half of the total cellular membrane mass (Campbell, 2000). The ER is differentiated into the rough ER and the smooth ER (Alberts et al., 2002). The term rough ER derives from ribosomes which are attached to the ER membrane giving it a rough appearance under the microscope and constitute the rough ER's role in protein synthesis. The smooth ER does not carry ribosomes. Depending on the cell type it can have different functions. It is usually associated with lipid and steroid synthesis and the degradation of harmful metabolites and xenobiotics by P450s bound to the smooth ER membrane. Most importantly, the ER represents the first station of the secretory pathway. Classically, the signal peptide of a nascent polypeptide synthesised by ribosomes binds to the signal recognition particle (SRP) which targets them to the ER's translocon where the polypeptide is further translated and fed into the ER lumen. There the polypeptide is processed, folded, modified, and eventually loaded in vesicles wherein it is sent to the Golgi apparatus for membrane insertion or secretion.
ROS constitute a major player for the function of the ER as for the correct folding of proteins the systematic formation of disulfide bonds is pivotal (Bardwell 2004; Santos et al., 2009; Laurindo et al., 2012). Protein folding is among the most vital functions of the ER and is largely dependent on the chaperone and dithiol-disulfide oxidoreductase protein disulfide isomerase (PDI) (Santos et al., 2009; Laurindo et al., 2012). Oxidised PDI oxidises cysteine residues in substrate proteins promoting formation of disulfide bonds. Regeneration of the oxidative state of PDI by the oxidase Ero1 is dependent on the reduction of oxygen to hydrogen peroxide, directly linking protein folding to oxidative stress (Santos et al., 2009; Laurindo et al., 2012; Zeeshan et al., 2016). Consequently, an increase of the protein cargo load or an impediment of the ER's processing efficiency can lead to an increase of cellular ROS generation. Un- or misfolded proteins are extremely harmful to cells due to loss of function or even potentially aberrated function and formation of aggregates (Santos et al., 2009). The collateral accumulation of unfolded proteins in the ER lumen triggers a cellular response mechanism termed the unfolded

protein response (UPR) (Marciniak & Ron, 2006) which includes attenuation of translation, degradation of mRNA for certain ER proteins active in the ER lumen, expression of UPR target genes such as chaperones and calreticulin, improvement of protein folding, and induction of misfolded protein degradation (Harding et al., 2003; Ron & Walter, 2007; Santos et al., 2009; Zeeshan et al., 2016). A sustained UPR triggers ER-specific caspases and thereby apoptosis (Marciniak et al., 2004; Tabas & Ron, 2011; Sano & Reed, 2013). Notably, ROS production is an integral part of the UPR as well, sustained not only by the PDI- and Ero1-induced protein folding but also by mitochondrial and Nox activity (Santos et al., 2009; Wu et al., 2010; Laurindo et al., 2012).

Not all extracellular proteins are secreted via the ER secretory pathway. In all eukaryotic cells there is a heterogeneous group of proteins that does not carry the N-terminal signal peptide but has been found active outside of the cell even after disruption of the ER secretory pathway (Nickel, 2005). This usually stress-induced phenomenon comprises three different pathways (Rabouille, 2017): Type I secretion involves the formation of plasma membrane pores that allow direct passage of specific folded cytoplasmic proteins, type II secretion is mediated by ABC transporters and specific to acylated peptides and yeast mating peptides, while type III secretion is based on autophagosomes or endosomes. Here, the proteins are postulated to be either released by late endosomes binding the plasma membrane or to translocate across the plasma membrane-bound organelle membrane in a similar fashion as type I secretion. Additionally, proteins that do carry an N-terminal signal peptide but bypass the Golgi apparatus during transport to the plasma membrane have been described (Grieve & Rabouille, 2011). This mechanism is termed type IV secretion. It is believed that these mechanisms, which are largely triggered by stress, have evolved to ensure secretion despite or in reaction towards ER stress, or that the respective proteins are to avoid ER-mediated modifications in order to maintain a specific function (Rabouille, 2017).

1.6 Measuring ROS: pros and cons of different techniques

Apart from the characterisation of ROS-related enzymes, this study aimed at gaining insight into the role of ROS in *F. graminearum* by the generation of a modified ratiometric H_2O_2 probe.

There is constant development regarding the means to visualize and quantify intracellular ROS in different phyla including colorimetric assays, immunoblotting, and immunofluorescence. A plethora of chemicals allow staining of specific ROS. Superoxide anion is usually detected with ferricytochrome C or nitroblue tetrazolium (NBT). When reacting with superoxide, these dyes are reduced to ferrocytochrome C and formazan, respectively, which have a different extinction coefficient than their precursors (Brandes & Janiszewski, 2005; Hare et al., 2008). Limitations of these methods include the relatively long incubation time (up to 1 h) and the small changes in optical density that are

frequently observed with the ferricytochrome C assay (Tarpey & Fridovich, 2001; Brandes & Janiszewski, 2005) and the potential of NBT to react with molecular oxygen and produce superoxide (Auclair et al., 1978). Lucigenin is a chemiluminescent detection molecule that emits light when reacting with superoxide (Brandes & Janiszewski, 2005). It is relatively specific for superoxide but is prone to generating superoxide through autooxidation (Janiszewski et al., 2002). The fluorescent dye dihydroethidium (DHE) forms 2-hydroxyethidium when reacting with superoxide, and ethidium when reacting with other ROS (Zhao et al., 2003, 2005). Hydrogen peroxide is most commonly detected using Amplex® Red (Zhou et al., 1997), homovanillic acid (Ruch et al., 1983), and diacetyldichlorofluorescein (Hinkle et al., 1967). In the presence of horseradish peroxidase Amplex® Red is oxidised to Resorufin which can be detected colorimetrically at 570 nm or by fluorescence using excitation of 570 nm and emission of 585 nm (Reszka et al., 2005). Homovanillic acid dimerizes when oxidised by hydrogen peroxide through horseradish peroxidase catalysis. As with Amplex red, homovanillic acid monomer is non-fluorescent, but as a dimer, it possesses a peak excitation wavelength of 315 nm, with an emission wavelength of 425 nm. Dichlorodihydrofluorescein gets oxidised by intracellular ROS to dichlorofluorescein which is highly fluorescent with 498 nm as excitation and 522 nm as emission wavelengths. While this list is far from complete, all of the described techniques share the disadvantages that they lack specificity for certain ROS, can be toxic to the stained cells, and are difficult to apply compartment-specifically (Lehmann et al., 2014). Furthermore, they can produce ROS upon light-exposure which results in artefactual ROS generation and signal amplification.

Sensitive but expensive detection of ROS can be achieved via magnetic resonance imaging (Thelwall et al., 2005), positron emission tomography (Ikawa et al., 2009), X-ray synchrotron (Debenham et al., 1996), or mass spectrometry (Fenaille et al., 2003; Weber et al., 2004; Greving et al., 2011). Similar to some staining procedures, the cell manipulations necessary for these techniques can potentially lead to ROS artefacts (Chiu et al., 2014).

1.6.1 HyPer: advantages of genetic encoding and ratiometry

A different way to approach the issue of visualising and quantifying ROS is the use of genetically encoded indicator proteins. Fluorescing proteins were first extracted by Shimomura et al. (1962) and are used in a variety of different applications today. In combination with redox sensory function they constitute ROS-probes with minimal invasiveness and high sensitivity. A typical example for such an engineered genetically encoded redox sensor is the reduction-oxidation-sensitive green fluorescent protein (roGFP) (Hanson et al., 2004; Dooley et al., 2004). Different variants with different properties have been developed but they all function in the same way. Through the addition of two cysteines in the beta barrel structure of GFP, the protein possesses a potential disulfide bonding site. Oxidation or reduction of the cysteines by oxidised (GSSG) or reduced glutathione (GSH) increases GFPs excitation peak at 400 nm or 480 nm,

respectively. Calculation of the ratio between the fluorescence intensities of both peaks offers redox-state-dependent units which are largely independent of cell quantity and growth speed. Sensors with this feature are called ratiometric sensors.
Belousov et al. (2006) combined the circularly permuted yellow fluorescent protein (cpYFP) with the regulatory domain of transcription factor OxyR from *Escherichia coli* creating a modified fluorescent protein named HyPer. OxyR serves as an intracellular H_2O_2-sensor. Two cysteine-residues in the regulatory domain form a disulfide bond after oxidation by H_2O_2, thereby altering its tertiary structure and that of the cpYFP that had been integrated in the regulatory domain. Just like roGFP, HyPer, therefore, has two states, oxidised and reduced, which differ in conformation and also in absorption maxima (Figure 3).

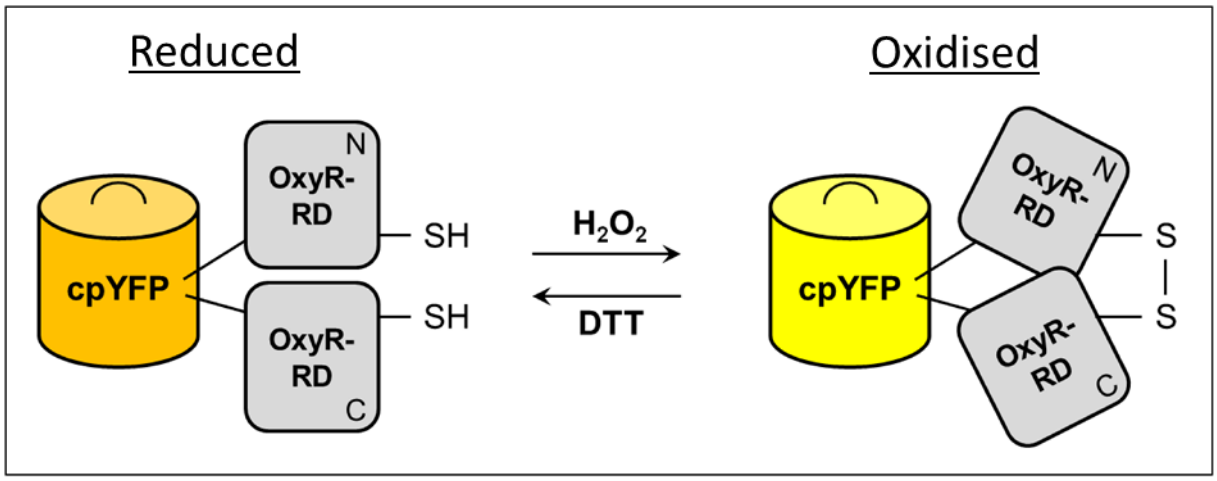

Figure 3: (According to Lukyanov & Belousov, 2014 and Mentges, 2014 (master thesis)) Structure and mechanism of HyPer. In the reduced state (left) the two cysteine residues in the regulatory domain of OxyR (OxyR-RD_N and OxyR-RD_C) are reduced and the attached circularly permutated yellow fluorescent protein (cpYFP) has two absorption peaks: one at 420 nm and one at 500 nm excitation wavelength. Upon oxidation by hydrogen peroxide (H_2O_2) the hydrogen atoms are removed from the cysteine residues and a disulfide bond is formed (right). This alters the conformation of HyPer raising the absorption maximum of cpYFP at 500 nm and lowering the maximum at 420 nm. The oxidation is reversible by addition of a reducing agent such as dithiothreitol (DTT).

The absorption peaks of the reduced and the oxidised state are 420 nm and 500 nm, respectively. The emission wavelength is at 516 nm for both (Belousov et al., 2006). After oxidation the absorption peak at 420 nm decreases and the one at 500 nm increases proportionally (Figure 4). This permits ratiometric detection of H_2O_2.

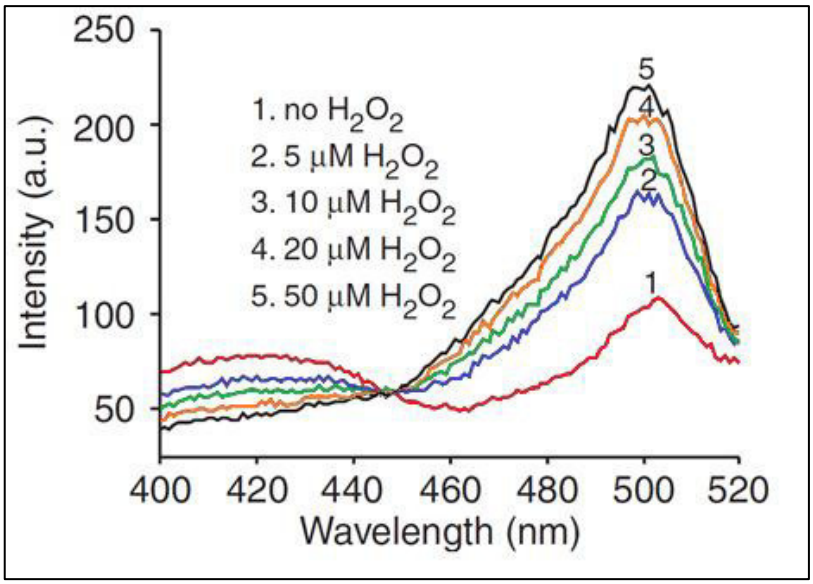

Figure 4: (According to Lukyanov & Belousov, 2014, courtesy of Michael Mentges) Concentration dependent ratiometric adaptation of HyPer's absorption maxima upon contact with hydrogen peroxide (H_2O_2). Without H_2O_2 HyPer exhibits two distinct absorption maxima at 420 nm and 500 nm excitation wavelength (red line). After addition of 5 µM H_2O_2 the fluorescence intensity peak at 420 nm decreases and the peak at 500 nm increases (blue line). The magnitude of both the decrease at 420 nm and the increase at 500 nm is proportional to the applied H_2O_2-concentration (green, orange, and black line). a.u.: arbitrary unit. nm: nanometres.

Through further modifications of the regulatory domain two new variants of HyPer have been established: HyPer-2 (Markvicheva et al., 2011) and HyPer-3 (Bilan et al., 2013). HyPer-2 shows stronger fluorescence intensity, a broader dynamic range, and a longer reaction time towards oxidation and reduction (Markvicheva et al., 2011). HyPer-3 has the same fluorescence qualities but does not show the reaction attenuation (Bilan et al., 2013). In this study HyPer-2 was used.

1.6.1.1 Targeted expression of HyPer in mammals

An important advantage of genetically encoded markers is the possibility to express them targeted to a specific cellular structure or organelle. In mammalian cells HyPer has been targeted to the nucleus, the cytosol, peroxisomes, mitochondria, and endoplasmic reticulum (ER) (Malinouski et al., 2011; Gehrmann and Elsner, 2011; Mehmeti et al., 2012). Localised expression of a ROS-sensor allows specific real-time monitoring of the redox status in the respective tissue under physiological and pathological conditions, thereby representing a powerful tool in understanding the role of localised redox processes which determine many if not all major cellular functions. Specific targeting of proteins can be achieved by taking advantage of the natural cellular protein targeting mechanisms that specify the destination of each synthesised polypeptide. Cells sort proteins for transportation to certain compartments through the recognition of targeting sequences, usually located at the N-terminus or the C-terminus of the polypeptide chain. These sequences are bound by carrier proteins which guide the polypeptide to the target organelle. Proteins that are to be secreted or are destined for the plasma membrane, ER,

Golgi apparatus or endosomes are usually translocated co-translationally. In this mechanism recognition of the N-terminal signal peptide of the nascent polypeptide and translocation take place before the translation is complete. Transportation to mitochondria, peroxisomes, or chloroplasts is usually mediated by post-translational recognition by a specific chaperone. By adding the respective specific signal elements to the protein sequence, such as an N-terminal signal peptide for secreted proteins, one can localise artificial proteins to the desired cellular structure or space.

Glycosylphosphatidylinositol (GPI) anchors

Another natural way for cells to control the localisation of their proteins is the attachment of glycosylphosphatidylinositol (GPI) anchors. GPI anchors are glycolipid structures post-translationally attached to the C-terminus of many eukaryotic proteins. Structurally they consist of an ethanolamine phosphate bridge that links the GPI to the C-terminus of a respective protein, a conserved carbohydrate linker, and a phospholipid tail that attaches the GPI anchor to the cell membrane. Proteins designated for cell surface attachment carry an N-terminal signal peptide which destines them for secretion and a C-terminal signal peptide containing a hydrophobic segment followed N-terminally by characteristic features (Ferguson & Williams, 1988; Takeda & Kinoshita 1995). Within the lumen of the rough ER the GPI-transamidase complex recognises and processes this C-terminal anchor addition sequence (Rittenour & Harris, 2013). At the residue to which the GPI anchor is to be linked (termed the ω site) the C-terminal signal peptide is cleaved off and the ethanolamine phosphate residue of the GPI attaches to the carboxyl residue of the protein by formation of a peptide bond. The protein-GPI complex continues the secretion pathway normally by delivery from the ER to the plasma membrane via the Golgi apparatus where it is retained in the outer leaflet of the membrane due to the GPI's lipophilic phospholipid residues. In fungi, many GPI-anchored proteins are released and covalently attached to the cell wall instead of being localised in the plasma membrane (Kapteyn et al., 1996).

1.7 Aim

Previous research has raised the assumption that precise regulation of a beneficial ROS equilibrium is essential for successful host colonisation by phytopathogenic fungi (Tanaka et al., 2006; Nguyen et al., 2012; Nguyen et al., 2013). MAPKs and TFs that control ROS and lead to reduced virulence are described, however so far only few ROS-related enzymes are known to be responsible for virulence. Transcriptomic analysis of the early infection stage of *F. graminearum* on wheat revealed an upregulation of ROS-related genes in ICs providing a clear indication of a pivotal role of ROS for virulence. This was affirmed by experiments with a *F. graminearum* strain expressing the H_2O_2 sensor HyPer showed that ICs contain much higher levels of H_2O_2 than RH (Mentges & Bormann, 2015). Furthermore, ROS are known to be essential players during fungal cellular differentiation

(Scott & Eaton, 2008). The specific enzymes taking part in these developmental ROS-fluctuations are as yet unknown. Based on this background, this study aimed at gaining a better understanding of ROS-based processes during different aspects of the life cycle of *F. graminearum*, specifically virulence, growth, ROS-resistance and -accumulation, and sexual reproduction through the generation of gene deletion mutants and the establishment of a novel modified H_2O_2 sensor (GPI-HyPer). Only few secreted virulence factors of *F. graminearum* are known to this day, such as DON and secreted lipases (Voigt et al., 2005; Maier et al., 2006; Blümke et al., 2014). Special attention was therefore paid to secreted ROS-related enzymes (ROS) which were assumed to constitute a part of ICs' mobile weaponry during plant infection.

2. Materials and methods

2.1 Materials

The twice deionised water which was used for all solutions, suspensions, and reactions was obtained from a Millipore Purification System (Milli-Q Water Systems, Millipore, Eschborn, Germany) and is referred to as H_2O in the following.

Media, solutions, buffers, bottles, containers, and pipette tips were sterilised by autoclaving for 20 min at 121 °C and 2×10^5 Pa. Heat-sensitive solutions and buffers were sterilised by filtration (pore diameter 0.2 µm).

***Fusarium graminearum* genome database**

DNA-sequences of *F. graminearum* genes were taken from "MIPS-*Fusarium graminearum* Database Pedant" established by Helmholtz Centre Munich (http://pedant.helmholtz-muenchen.de).

Sequence editing and primer design

As a tool for sequence editing and annotating as well as primer design the program SeqBuilder from DNASTAR was used.

Enzymes

The restriction enzymes used in this study were purchased from New England Biolabs (Ipswich, MA, USA). For amplification of DNA fragments OneTaq-MasterMix or Q5-polymerase (New England Biolabs) were used. Diagnostic PCRs were performed with Phire Hot Start II DNA polymerase (ThermoFisher). For ligation T4-DNA-ligase (New England Biolabs) was used.

Molecular-weight size marker

GeneRuler™ DNA Ladder Mix (abbreviated M1), GeneRuler™ 1 kb DNA Ladder (abbreviated M2), and GeneRuler™ 1 kb Plus DNA Ladder (abbreviated M3) (ThermoFisher) were used as size indicators in all PCR experiments. One exception is the Southern Blot analysis where DNA Molecular Weight Marker VII, DIG labeled (Roche) was used.

2.1.1 Organisms

Fungal strains:

F. graminearum wild-type strain 8/1 was used for this study (Courtesy of T. Miedaner, Landessaatzuchtanstalt Hohenheim). Gene deletions were carried out in strain 8/1. As a positive control for perithecia formation experiments *F. graminearum* wild-type strain PH1 was used (Strain Passport: NRRL 31084).
For yeast recombinational cloning the uracil-auxotrophic *Saccharomyces cerevisiae* strain FGSC 9721 (FY 834) was used.

Plants:

For pathogenicity experiments the susceptible wheat cultivar Nandu (*Tricium aestivum* L, European Wheat Database[5] [EWDB] 58436, accession number RICP 01C0203421) and the maize cultivar W64 were used.

Bacteria:

For vector amplification via *Escherichia coli* transformation the strain DH5α (Gibco BRL) was used.

2.1.2 Primers

The primers used in this study were synthesised by Eurofins Genomics GmbH (Ebersberg, Germany). The following tables show the oligonucleotides used for amplification of resistance cassettes, amplification of gene deletion constructs, verification of gene deletions, and quantitative real-time PCR. The left column shows the purpose of the respective set of primers with the shown FGSG-number indicating the gene-ID of the target genes. The second column from the left shows the primer abbreviations. HYG, NAT, and GEN stand for resistance cassettes for hygromycin, nourseothricin, and geneticin, respectively. The endings “f” and “r” indicate forward and reverse primers, respectively. Abbreviations “uf” and “df” indicate the upstream and downstream flanking region, respectively. Diagnose primers bind with the open reading frame (ORF) of the target gene to verify the deletion. Locus-check primers are two primer pairs of which one primer binds inside the resistance cassette and one in the non-transgenic genomic region – thereby spanning over the flanking region - at both the 3’ and the 5’ end of the deletion construct to verify the localisation of the deletion construct. The split marker nested primers are used for all split marker deletion constructs. The long primers for split marker flanking region amplification produce the same overhang independent of the target gene which constitutes the binding site for the overhang nested primers. This circumvents the necessity of designing exterior 3’ and 5’ primers for every target gene. The resistance cassette nested primers form a pair with the respective overhang nested primer to amplify the split markers.

Table 1: Primers used for the amplification of resistance cassettes and their validation in deletion mutants

Purpose	Primer type	Sequence	Product length (bp)
Hygromycin resistance cassette amplification	1F-Hyg	GAGCGAGGTGGGTGATGTAG	1740
	2R-Hyg	CGGTCGGCATCTACTCTATTC	
Geneticin resistance cassette amplification	1F-NptII	GCCAGTTGTTCCCAGTGATCT	2323
	2R-NptII-vect	GCTCTAGAACTAGTGGATCCCCCGGGCTGGCGAGGTCCAATGCATTAATG	
Resistance cassette internal primers (RCI primers) for validation	HYG_f	GCCGTATCTGACAATGATCC	1540
	HYG_r	GTACTTCTACACAGCCATCG	
	NAT_f	CGTCAAGAGTGGTCATATGG	794
	NAT_r	ATCATTCTAGCTTGCGGTCC	
	GEN_f	AATATCACGGGTAGCCAACG	422
	GEN_r	GAAGGGACTGGCTGCTATTG	

Table 2: Primers used for the generation of deletion plasmids and for the validation of the respective deletion mutants

Genes deleted by knock-out-plasmids			
Purpose	**Primer type**	**Sequence**	**Product length (bp)**
FGSG_00576	LF_f (df)	GGCCCCCCCTCGAGGTCGACGGTATCGATTAATCCCTTGACTGTCAGCC	1035
	LF_r (df)	ACATGAGCATGCCCTGCCCCTGAGCGGCCGAAGCCAGTGATGGAAATGG	
	RF_f (uf)	CCCGAATCGGGAATGCGGCTCTAGAGTAGGCAGATGGTGCAACTAAAGG	1061
	RF_r (uf)	GCTCTAGAACTAGTGGATCCCCCGGGCTGTCAACGAGGGTCATGTATCG	
	Diagnose_f	TACTTTAGAGCTGGGAGTGG	582
	Diagnose_r	TCCTTCTTCAAGGATGCTGC	
	Left Locus-check_f	AGATACAAACGATCCACGGG	2007
	Left Locus-check_r	CCATATGACCACTCTTGACG	
	Right Locus-check_f	AACTTGGGAACAACCCTACG	1927
	Right Locus-check_r	AACAGGTTAGTCCTGTCTCC	
FGSG_06023	LF_f (uf)	GGCCCCCCCTCGAGGTCGACGGTATCGATAGGGATCAGGTATAGGGA	976
	LF_r (uf)	ACATGAGCATGCCCTGCCCCTGAGCGGCCGTCTGGGGATGTGGATAT	
	RF_f (df)	CCCGAATCGGGAATGCGGCTCTAGAGTAGCTCCGATGATGACTCTTC	646
	RF_r (df)	GCTCTAGAACTAGTGGATCCCCCGGGCTGCCTTCGCACGTATGTACT	
	Diagnose_f	ACAGGTCTCAGATTCTGG	600
	Diagnose_r	ATCGGAAGAAGAGTCACC	
	Left Locus-check_f	CCCACAGTAAACTTGCAACC	1669
	Left Locus-check_r	CCATATGACCACTCTTGACG	
	Right Locus-check_f	GAAAGGAAGATGGACTGAGG	1597
	Right Locus-check_r	TGAGCTCAAGGTTAAGGAGC	

FGSG_09742	LF_f (df)	GGCCCCCCCTCGAGGTCGACGGTATCGATGTCGGGTACAGATAGAAACG	823
	LF_r (df)	GAGGGCAAAGGAATAGAGTAGATGCCGGTTTGTGGTAAGGATGGTGG	
	RF_f (uf)	GCTTCCAAGCGGAGCAGGCTCGACGTATTAATAGTACTAGCGGACAGCG	533
	RF_r (uf)	GCTCTAGAACTAGTGGATCCCCCGGGCTGTCACTAGTCATCGGTTCTCG	
	Diagnose_f	CTCTCCCATTACTCTTCTCG	366
	Diagnose_r	GAAGCTTGAACTTACGGAGC	
	Left Locus-check_f	CAGTATACAAGTGGCTTGCC	1800
	Left Locus-check_r	ATCTCGTGCTTTCAGCTTCG	
	Right Locus-check_f	TGGCTTCACATTCTCCTTCG	2083
	Right Locus-check_r	TAGCCAATACCATGTCAGGC	
FGSG_11399	LF_f (uf)	GGCCCCCCCTCGAGGTCGACGGTATCGATGTCTCATCATATTTCTCATAT	1157
	LF_r (uf)	ACATGAGCATGCCCTGCCCCTGAGCGGCCGTCTTGGCGAAAGAGGGTTGG	
	RF_f (df)	CCCGAATCGGGAATGCGGCTCTAGAGTAGGTCCGAGACATTCTGCACGAG	775
	RF_r (df)	GCTCTAGAACTAGTGGATCCCCCGGGCTGGCTTTGAGCGATTTGCTGACC	
	Diagnose_f	TCTGCAAAGGTCTACTTCCCTG	1214
	Diagnose_r	CGTTGAAGATGGAGTCGCCT	
	Left Locus-check_f	AGGAGTGACACAAGAAGTGG	1754
	Left Locus-check_r	CCATATGACCACTCTTGACG	
	Right Locus-check_f	TCTATCGTGAATCCGTGACG	1428
	Right Locus-check_r	TATGTCATGTTGGCTGAGGG	
FGSG_16013	LF_f (df)	GGCCCCCCCTCGAGGTCGACGGTATCGATCGACCCCCTGAGAGACTGATA	986
	LF_r (df)	CTATCGCCTTCTTGACGAGTTCTTCTGAGACTGTAATGCCTGCTGGCTTG	
	RF_f (uf)	CCACAGCCAGGTAGGCCGAATAACTTGCACAAATTGGTGTCTACAAGTTCCCTAGTGAC	653
	RF_r (uf)	GCTCTAGAACTAGTGGATCCCCCGGGCTGCATGCCAAGTGGCATGCTCT	
	Diagnose_f	GAACAGAATATCCCAGACACCC	675
	Diagnose_r	ATATCAAGAAGATCCTCCAAGGCA	
	Left Locus-check_f	GCTACGAAATTTGGAGGTGG	1216
	Left Locus-check_r	ATCATGGCTGATGCAATGCG	
	Right Locus-check_f	GATGAAATCAACGCGCTTCG	1342
	Right Locus-check_r	TCATCAAGTGGATACTCGCG	

Table 3: Primers used for the generation of split markers and the validation of the respective deletion mutants

Genes deleted by split-markers			
Gene ID	**Primer type**	**Sequence**	**Product length (bp)**
Overhang nested primers	AL-1F-Split	TAGTGGATCCCCCGGGCTG	
	AL-2F-Split	CGGCCAGTGAGCGCGCGT	
Resistance cassette nested primers	Hygromycin Split f (9F-HY)	GCCATGAGCGCCCCTACAG	
	Hygromycin Split r (10R-YG)	GCAGTCCTCGGCCCAAAGC	
	Nourseothricin Split f (LG_NAT_overlap_f)	AGCTCAGACCGCTCCACGG	
	Nourseothricin Split r (LG_NAT_overlap_r)	CGTCCGATTCGTCGTCGGG	
	Geniticin Split f (LG_GEN_overlap_SM_f)	TTCATCGGTGATGCTTTCGG	
	Geniticin Split r (LG_GEN_overlap_SM_r)	CGATGCTTGGGTAGAATAGG	
FGSG_11215	LF_f_SM	GTTGTAAAACGACGGCCAGTGAGCGCGCGTCCAGGTATGCAATGCAATGC	558
	LF_r_SM	AAAGGAATAGAGTAGATGCCGACCGAACCCCATAGTTCCTGTTGATCG	
	RF_f_SM	AGTCAATGCTACATCACCCACCTCGCTCAATCTTCACTGACGTCCAGG	566
	RF_r_SM	CTCTAGAACTAGTGGATCCCCCGGGCTGATTGATGACTGTATGCCGGG	
	Diagnose_f	ACTGGTTGGTTAGTACTCCC	403
	Diagnose_r	ATCCTTCGATAATGCCACCG	
	Left Locus-check_f	CAGCTCGTCGATTTGATTCG	1449
	Left Locus-check_r	TTATCGGCACTTTGCATCGG	
	Right Locus-check_f	AAAGCACGAGATTCTTCGCC	1516
	Right Locus-check_r	AGCCGAGAAGTTGGTTGATC	
FGSG_09006	LF_f_SM	CTCTAGAACTAGTGGATCCCCCGGGCTGGGATGAGATGCGGTTAAGTG	485
	LF_r_SM	CCCGAATCGGGAATGCGGCTCTAGAGTAGCCAAGCAGGTTGTGGTTATG	
	RF_f_SM	ACATGAGCATGCCCTGCCCCTGAGCGGCCAAGAGTCATGAGCGCGATAG	483
	RF_r_SM	GTTGTAAAACGACGGCCAGTGAGCGCGCGTAAGGAAGAAGTTCTGGGTGG	
	Diagnose_f	GGAAGCAAGACTAGAGATGG	689
	Diagnose_r	AGTTGTAAGAGGTGCCATCG	
FGSG_01988	LF_f_SM	CTCTAGAACTAGTGGATCCCCCGGGCTGACTTGGCGGATGGTTCATTG	714
	LF_r_SM	CCCGAATCGGGAATGCGGCTCTAGAGTAGGATCAACTGTCGTTGCCAAC	
	RF_f_SM	ACATGAGCATGCCCTGCCCCTGAGCGGCCGATTGTGACTTGAGTGACCG	771
	RF_r_SM	GTTGTAAAACGACGGCCAGTGAGCGCGCGTATACCTTTCTCCACCTGACG	
	Diagnose_f	ACGCTCATATCCTTGAAGGG	466
	Diagnose_r	TGTCTTCAGTCTAAGCCTGC	
FGSG_16458	LF_f_SM	CTCTAGAACTAGTGGATCCCCCGGGCTGTATGATGGCACAGACAAGCC	1083
	LF_r_SM	AGTCAATGCTACATCACCCACCTCGCTCATACACTAGTCACCCAGAGC	
	RF_f_SM	AAAGGAATAGAGTAGATGCCGACCGAACTAGTTAGGCAAAGAGGCAGG	883
	RF_r_SM	GTTGTAAAACGACGGCCAGTGAGCGCGCGTATACAGCCTCTTAGTCTCGG	

	Diagnose_f	TCATGCCAATGCTAGGTAGG	401
	Diagnose_r	CTCTGGATGACATCAAAGGG	
FGSG_07765	LF_f_SM	CTCTAGAACTAGTGGATCCCCCGGGCTGCAAGCTTCATCCAAGTCTGC	681
	LF_r_SM	CCCGAATCGGGAATGCGGCTCTAGAGTAGTTTGAAGCAGGGACAGAAGG	
	RF_f_SM	ACATGAGCATGCCCTGCCCCTGAGCGGCCACCACAACTTTCTGATCCGG	719
	RF_r_SM	GTTGTAAAACGACGGCCAGTGAGCGCGCGTATAGAGAGAGGTCCACATGC	
	Diagnose_f	CTGATCTCACTTCGTTGACG	398
	Diagnose_r	TTCATCACCACTATGGCTCG	
FGSG_17478	LF_f_SM	CTCTAGAACTAGTGGATCCCCCGGGCTGTAGAGATCGATGGGTTGTGG	894
	LF_r_SM	GGTAGGCCGAATAACTTGCACAAATTGGATGGTCTGGGATGAGTTTGG	
	RF_f_SM	CTATCGCCTTCTTGACGAGTTCTTCTGATAACTGAATTACCCGACGGG	857
	RF_r_SM	GTTGTAAAACGACGGCCAGTGAGCGCGCGTATGATGGTGTGCTATCGAGG	
	Diagnose_f	ATATCAGTCTCAGCCTCTGG	456
	Diagnose_r	TGAGAGATCAGATGGTAGCC	
FGSG_03436	LF_f_SM	CTCTAGAACTAGTGGATCCCCCGGGCTGTCTCGTCACCCATATCAAGG	831
	LF_r_SM	CCCGAATCGGGAATGCGGCTCTAGAGTAGTCTTGCTGAAGCTCTAGTGC	
	RF_f_SM	ACATGAGCATGCCCTGCCCCTGAGCGGCCATCAGCAAACGAGCCAATGG	762
	RF_r_SM	GTTGTAAAACGACGGCCAGTGAGCGCGCGTCCCTCGTGTTACTCAATTGC	
	Diagnose_f	CATCTGCACATCCGTAAAGC	512
	Diagnose_r	TTGATGACTTGATCGAGGGC	
	Left Locus-check_f	GAGGTGCCATGGTAAATTCG	1737
	Left Locus-check_r	CGTCAAGAGTGGTCATATGG	
	Right Locus-check_f	TTCGTGGTCATCTCGTACTC	1198
	Right Locus-check_r	CTGGAGATGCCATAGTGTTG	
FGSG_03498	LF_f_SM	CTCTAGAACTAGTGGATCCCCCGGGCTGTGAAACCAGGATGGTTGAGC	765
	LF_r_SM	AGTCAATGCTACATCACCCACCTCGCTCGTTATTCTGAGATGACCGCC	
	RF_f_SM	AAAGGAATAGAGTAGATGCCGACCGAACGACAACAGTATCACGGTTCC	787
	RF_r_SM	GTTGTAAAACGACGGCCAGTGAGCGCGCGTTCTAACAGAACAAGGAGGGC	
	Diagnose_f	ATCCTAAGATCGATGCAGCG	400
	Diagnose_r	AGCATGTTCGATCACTTCCC	
FGSG_03700	LF_f_SM	CTCTAGAACTAGTGGATCCCCCGGGCTGCGAGTTGGTGATGATGAAGG	581
	LF_r_SM	CCCGAATCGGGAATGCGGCTCTAGAGTAGCTGTCGATTACGCTTACAGC	
	RF_f_SM	ACATGAGCATGCCCTGCCCCTGAGCGGCCGACAAGAAGAGTTATGCGGG	606
	RF_r_SM	GTTGTAAAACGACGGCCAGTGAGCGCGCGTATGCATTCTGTCCACTGTCG	
	Diagnose_f	CTAGCTTCAAGAAGACTGCC	399
	Diagnose_r	GAAGAGCTTCCTTGCATAGG	
FGSG_03708	LF_f_SM	CTCTAGAACTAGTGGATCCCCCGGGCTGCGCATAGAGATGGGTTTTAATG	618
	LF_r_SM	AGTCAATGCTACATCACCCACCTCGCTCATTGTCACCCACAGCCACCC	

	RF_f_SM	AAAGGAATAGAGTAGATGCCGACCGAACGAATGCGAATGAGAGGCTGC	941
	RF_r_SM	GTTGTAAAACGACGGCCAGTGAGCGCGCGTGGATGCAACGTTCGAGCCAA	
	Diagnose_f	ACACCGAAGTCAGTGTAACG	492
	Diagnose_r	CAAGCACATGAGCAACAACC	
	Left Locus-check_f	TCCTTTCCTCTACGCTATGG	956
	Left Locus-check_r	GACCCAATTACACCCTTTGC	
	Right Locus-check_f	CCAACTCTATCAGAGCTTGG	1330
	Right Locus-check_r	ACTAGTGTTCGAAACGACGG	
FGSG_04434	LF_f_SM	CTCTAGAACTAGTGGATCCCCCGGGCTGAAAGGATTTGACCCTGCTCG	858
	LF_r_SM	AGTCAATGCTACATCACCCACCTCGCTCTTCATCCCTCACTCTGTAGC	
	RF_f_SM	AAAGGAATAGAGTAGATGCCGACCGAACCCCACTCTGTAGTCTAAAGG	883
	RF_r_SM	GTTGTAAAACGACGGCCAGTGAGCGCGCGTATGATTTGCTCTGTACCGGG	
	Diagnose_f	TTATTGGTGGTCATGAGGCG	390
	Diagnose_r	TGATGTCACTGGCATCAAGG	
FGSG_09124	LF_f_SM	CTCTAGAACTAGTGGATCCCCCGGGCTGGATCAAATTGGATGCCACGC	637
	LF_r_SM	AGTCAATGCTACATCACCCACCTCGCTCATGAGCGCTGATAGAAGTCC	
	RF_f_SM	AAAGGAATAGAGTAGATGCCGACCGAACGCCTCTCTCGTATAAGATGG	576
	RF_r_SM	GTTGTAAAACGACGGCCAGTGAGCGCGCGTTGACTGAGGACAAGTGATGG	
	Diagnose_f	TCTGGTGCAAACCAATCTCC	213
	Diagnose_r	GGACGATGTGAAAGGAAACC	
FGSG_11528	LF_f_SM	CTCTAGAACTAGTGGATCCCCCGGGCTGGGCAGAAAGATCAGACAAGG	600
	LF_r_SM	CCCGAATCGGGAATGCGGCTCTAGAGTAGAATATCACCCTCGGCAAAGC	
	RF_f_SM	ACATGAGCATGCCCTGCCCCTGAGCGGCCTTGCAGTTCTCTTACGCACC	616
	RF_r_SM	GTTGTAAAACGACGGCCAGTGAGCGCGCGTGCCTGTATGCATTGAGATCC	
	Diagnose_f	GTTAGTAGCAAAGTCACCGG	402
	Diagnose_r	TTTGCAGGAAGACACTCTCC	
FGSG_12456	LF_f_SM	CTCTAGAACTAGTGGATCCCCCGGGCTGCCAGAGAGGCAAGTCTAAAG	550
	LF_r_SM	CCCGAATCGGGAATGCGGCTCTAGAGTAGACGTACAGCATCCAGCAAAG	
	RF_f_SM	ACATGAGCATGCCCTGCCCCTGAGCGGCCAAGAGGAAGCTTGGAGGTTC	472
	RF_r_SM	GTTGTAAAACGACGGCCAGTGAGCGCGCGTTTCAATCTGGATAGCCTGGG	
	Diagnose_f	TCAACATGGCTTGCGATTGC	109
	Diagnose_r	GACCAGTCAGTACTAACACC	
	Left Locus-check_f	CATAATCTGCGAGAACGACC	1275
	Left Locus-check_r	TCAGTCCATCTTCCTTTCCC	
	Right Locus-check_f	AGGCTGATATAGCCTTCTCC	1201
	Right Locus-check_r	ACAGTGAAGTCTGGTAGACG	
FGSG_17054	LF_f_SM	CTCTAGAACTAGTGGATCCCCCGGGCTGGATGATGTTGGTGGAGTGAG	444
	LF_r_SM	AGTCAATGCTACATCACCCACCTCGCTCCGGATACCACTTGTTCTAGG	
	RF_f_SM	AAAGGAATAGAGTAGATGCCGACCGAACTGGTGGTTGGAAGGAAGTTG	564

	RF_r_SM	GTTGTAAAACGACGGCCAGTGAGCGCGCGTAGTGGCAATCAGCCTTGAAG	
	Diagnose_f	GTTGTTTATTTGCCGCAGCC	148
	Diagnose_r	CAATCTTCACAATGGCTGGC	
	Left Locus-check_f	CGAAAGGTTTCGTGGTTTGC	1087
	Left Locus-check_r	GGGTTAGATATCGAGCTTGG	
	Right Locus-check_f	TTTCGATGATGCAGCTTGGG	1293
	Right Locus-check_r	CAGAACTTCCACTCAGATGC	
FGSG_02341	LF_f_SM	CTCTAGAACTAGTGGATCCCCCGGGCTGAATGGCCTTCCATCAGTACG	558
	LF_r_SM	GGTAGGCCGAATAACTTGCACAAATTGGGTCTGCCTACAGAAATTGG	
	RF_f_SM	CTATCGCCTTCTTGACGAGTTCTTCTGAGACTGTTATCGAACCTGTCG	753
	RF_r_SM	GTTGTAAAACGACGGCCAGTGAGCGCGCGTCACGTTAGCTTTCTACTGC	
	Diagnose_f	AAGAAAGAAGCCATCTCGCC	489
	Diagnose_r	AACACATTGGCCAACCATGG	
	Left Locus-check_f	TAGGACGAAGTATCGAAGCC	1021
	Left Locus-check_r	GATGAAATCAACGCGCTTCG	
	Right Locus-check_f	TCTGGATTCATCGACTGTGG	1090
	Right Locus-check_r	TTGTGGTTGTAAGCGAGTCG	

Table 4: Primers used for quantitative real-time PCR of FGSG_03708.

qRT-PCT FGSG_03708	LG_qRT_03708_f4	GGAATAGTTGGCAGCAAGAC	133
	LG_qRT_03708_r4	GTACGAGCACAACAAGAACC	
qRT-PCR Tubulin	AL-qF-Tub	TGTCGACGACCAGTTCTCAGC	152
	AL-qR-Tub	CGATGTCGGCGTCTTGGTAT	

Table 5: Primers used for the cloning of pII99_GPI-HyPer. The primers for amplification of GPI-HyPer contain binding sequences for restriction enzymes *Sac*I (_fw) and *Xba*I (_rv) (*italic* bases), the sequences of the N-terminal (_fw) and the C-terminal (_rv) signal peptide, a sequence complementary to the 5' (_fw) and the 3' (_rv) end of HyPer-2 (underlined bases), as well as the sequence of the GAGAGA spacer (_rv) (dotted bases). The primers for amplification of the promotor region of FGSG_04399 contain binding sequences for restriction enzymes *Sac*I (_fw) and *Nde*I (_rv) (*italic* bases).

Amplification of GPI-HyPer	LG_GPI_HyPer_fw	*GAGCTC*ATGCGCGCCCAGGCTCTTGCTGCTGTTCTTCTCTCTGCATGCGCTGGTCAAGCTATCGCTGAGATGGCAAGCCAG	1593
	LG_GPI_HyPer_rv	*TCTAGA*CAGAGCGAAAGCGAGAGCAAAGACACCAGCAAGAACCAGGTTGACCGGAACAGCCATAGAAGAGCCAGCGTTTGCACCTGCTCCAGCTCCAACCGCCTGTTTTAAAACTTTATC	
Promotor region of FGSG_04399	LG_Pro04399_*Sac*I	CTTGAAAGTT*GAGCTC*GAGAGATGTATGTG	879
	LG_Pro04399_*Nde*I	CGCCACCCTTTTTTACTTTTATT*CATATG*GC	

2.1.3 Plasmids

Table 6: Plasmids used in this study

Name	Use	Restriction enzymes	References
pRS426	Yeast cloning method		Christianson, T. W. et al., 1992
pGEM-Hyg	Hygromycin (Hyg) selectable marker		Maier, F. et al., 2005
pII99	Geneticin (NptII) selectable marker		Beck, E. et al., 1982
pNR1	Nourseothricin (NatI) selectable marker	*Eco*RI and *Xba*I	Malonek, S. et al., 2004
pRS426_Δ00576	FGSG_00576 deletion construct	*Sac*I and *Sal*I	This study
pRS426_Δ06023	FGSG_06023 deletion construct	*Sac*I and *Sal*I	This study
pRS426_Δ09742	FGSG_09742 deletion construct	*Bam*HI and *Cla*I	This study
pRS426_Δ11399	FGSG_11399 deletion construct	*Sal*I and *Spe*I	This study
pRS426_Δ16013	FGSG_16013 deletion construct	*Spe*I and *Xho*I	This study
pRS426_Δ04123	FGSG_04123 deletion construct	*Not*I and *Xho*I	Master thesis Michael Mentges
pAN71GluA_HyPer-2	HyPer-2 template		Master thesis Michael Mentges
pII99_GPI-HyPer	GPI-HyPer expression	*Pvu* I	This study

2.2 Methods

Solid media

For making solid medium of the media specified below 1.6% granulated Agar were added to these media before autoclaving.

***F. graminearum* mycelia cultivation**

Mycelium was generated by incubating conidiospores or mycelial plugs in liquid or solid CM at 28 °C. Liquid media was shaken at 145 rpm.

Complete medium (CM):

Solution A (100 g/l $Ca(NO_3)_2 \times 4\ H_2O$)	1%
Solution B (20 g/l KH_2PO_4, 25 g/l $MgSO_4 \times 7\ H_2O$, 15 g/l NaCl)	1%
D-glucose	1%
Yeast-Casein-Extract	0.2%
Trace-elements-solution (60 mg/l H_3BO_3, 390 mg/l $CuSO_4 \times 5\ H_2O$, 13 mg/l KI, 60 mg/l $MnSO_4 \times H_2O$, 51 mg/l $(NH_4)_6Mo_7O_{24} \times 4H_2O$, 5.48 g/l $ZnSO_4 \times 7\ H_2O$, 932 mg/l $FeCl_3 \times 6\ H_2O$)	0.1%
Dilute in H_2O	

Minimal medium (MM):

Solution A (100 g/l $Ca(NO_3)_2 \times 4\ H_2O$)	1%
Solution B (20 g/l KH_2PO_4, 25 g/l $MgSO_4 \times 7\ H_2O$, 15 g/l NaCl)	1%
D-glucose	1%
Trace-elements-solution (60 g/l H_3BO_3, 390 mg/l $CuSO_4 \times 5\ H_2O$, 13 mg/l KI, 60 mg/l $MnSO_4 \times H_2O$, 51 mg/l $(NH_4)_6Mo_7O_{24} \times 4H_2O$, 5.48 g/l $ZnSO_4 \times 7\ H_2O$, 932 mg/l $FeCl_3 \times 6\ H_2O$)	0.1%
Dilute in H_2O	

Solution A and B were sterilised by sterile filtration. Trace-elements-solution was sterilised by adding chloroform in the ration 1:1000 (v/v).

For the production of selection media for transformed strains the following antibiotics were added to the media after autoclaving:

Hygromycin	100 µg/ml
Nourseothricin	100 µg/ml
Geneticin	100 µg/ml

Conidiogenesis

Formation of conidiospores was induced by incubation of mycelial plugs in wheat-medium for 3-7 days at 28 °C in darkness.

Wheat medium:
For 1 l of wheat medium 15 g of sliced wheat leaves were autoclaved in 1 l H_2O. After 12h the liquid was filtered through a folded filter (grade 3 hw) and autoclaved again.

Storage

For long-term storage conidiospores of *F. graminearum* suspended in H_2O were frozen at -70 °C.

2.2.1 Generation of deletion plasmids

For construction of deletion plasmids flanking regions (300 – 1500 bp upstream and downstream) of the genes of interest were cloned by PCR from gDNA of the wild type strain using appropriate primers (Table 2) carrying overhangs complementary to the resistance cassette and the linearised vector backbone. The resistance cassettes nourseothricin, hygromycin, and geneticin were obtained from the plasmids pNR1 (Malonek et al., 2004), pGEMT-Hyg (Maier et al., 2005), and pII99 (Beck et al., 1982), respectively. The nourseothricin resistance cassette was cut out from pNR1 with *Eco*RI and *Xba*I (37 °C, 2 h). The cassette was separated from the plasmid backbone via gel electrophoresis, cut out of the gel and purified using the NucleoSpin® Gel and PCR Clean-up Kit (Macherey-Nagel, Düren, Germany). Hygromycin and geneticin resistance cassettes were amplified from pGEMT-Hyg and pII99 via PCR using the appropriate primers (Table 1), respectively. The PCR products were also gel-purified. Flanking regions and desired resistance cassette were cloned into the plasmid pRS426 by transforming all fragments (3'-flanking region, 5'-flanking region, resistance cassette, linearised pRS426) into the uracil-auxotrophic *Saccharomyces cerevisiae* strain FGSC 9721 (FY 834).

Yeast-transformation

Deletion plasmids were assembled via yeast-recombination based on Colot et al. (2006). A 5 ml starter culture of the uracil-auxotrophic *Saccharomyces cerevisiae* strain FGSC 9721 (FY 834) in YPD medium was incubated at 200 rpm and 30 °C for 12 h. 50 ml YPD medium were inoculated with 3 ml of this culture and incubated for 4 h under the same conditions. The culture was centrifuged for 5 minutes at 2000 rpm and the supernatant

was discarded. The pellet was washed in 10 ml H_2O. The solution was centrifuged again and washed with 1 ml 100 mM lithium acetate. After another centrifugation the pellet was resuspended in a high enough volume of 100 mM lithium acetate for all desired transformation reactions. 50 µl of this cell suspension as well as 50 µl of freshly denatured salmon sperm DNA (2 µg/ml) were added to a solution containing

50 % PEG 3350	240 µl
1 M lithium acetate	36 µl
Yeast shuttle plasmid pRS426	100 ng
Flanking regions and resistance cassette	500 ng each
H_2O	ad 360 µl

and incubated at 30 °C for 30 min. Heat shock was induced by incubating the solution 45 °C for 15 min. Cells were plated on uracil-free SD agar (SD –uracil agar) and incubated at 30 °C in the dark until colonies are visible. Colonies were used for plasmid isolation.

YPD-medium:

Yeast extract	10 g/l
Difco-Bacto-Trypton	20 g/l
D-glucose	20 g/l
Dilute in H_2O	

SD –uracil-medium:

D-glucose	20 g/l
Difco© yeast nitrogen base without amino acids	6.7 g/l
CLontech –Ura DO supplement	0.77 g/l
Dilute in H_2O	

Plasmid DNA isolation from yeast

Transgenic yeast colonies were each cultivated in 15 ml uracil-free SD medium at 30 °C and 120 rpm overnight. Cells were harvested by centrifugation at 1500 rpm for 5 min washed with 500 µl H_2O. After discarding the H_2O, 200 µl yeast lysis buffer, 200 µl phenol:chloroform:isoamylalcohol (25:24:1 v/v), and 0.3 g of acid washed glass beads (diameter 425-600 µm, Sigma-Aldrich, USA) were added in this order. The solution was homogenised in a vibration mill (MM 200, Retsch, Haan, Germany) for 5 min at maximum speed. The homogenised solution was then centrifuged at 14000 rpm for 5 min. The aqueous phase was transferred to a fresh tube and separated by adding 200 µl chloroform and centrifuging at 14000 rpm for 5 min. After transferring the aqueous phase to a new tube $1/10^{th}$ volume 3 M sodium acetate (pH 5.5) and 1 ml ethanol were added before incubating the solution at -20 °C for 15 min. The solution was centrifuged at 14000 rpm for 20 min. The pellet was resuspended in 400 µl TE-buffer, and 4 µl RNase A (10

mg/ml) were added. Resuspension of the pellet was accelerated by incubation at 37 °C. 50 µl 4 M ammonium acetate and 1 ml ethanol were added before centrifugation at 14000 rpm for 20 min. The pellet was washed with 70% ethanol, air dried, and resuspended in 20 µl H_2O. For plasmid amplification up to 10 µl of the solution were transformed in *E. coli*.

Yeast lysis buffer:

Triton X-100	2%
SDS 10%	10%
NaCl 5 M	2%
EDTA 0.5 M	0.2%
Tris 1 M	1%
Dilute in H_2O	

E. coli-transformation

For amplification the plasmids were transformed into *Escherichia coli* strain DH5α (Green, M. R. & Sambrook, J. (eds) Molecular cloning: a laboratory manual 4th edn (Cold Spring Harbor Laboratory, 2012)). 1-10 µl of plasmid solution were carefully added to 1 ml competent *E. coli* DH5α suspension. The cells were incubated on ice for 20 min before applying a heat shock (42 °C) for 90 sec. After another incubation on ice for 5 min the cells were incubated for 1 h at 37 °C shaking lightly. The cells were then centrifuged for 1 min at 2000 rpm and 900 µl of the supernatant were discarded. After resuspension of the pellet in the remaining supernatant the cells were spread on LB-agar plates with suitable antibiotics.

LB-medium:

Tryptone	10 g/l
Yeast-Extract	5 g/l
NaCl	10 g/l
Dilute in H_2O	

For selection medium 100 µg/ml ampicillin were added to the medium after autoclaving.

Plasmid DNA isolation from _E. coli_

For a first screening of transgenic *E. coli* cells, the respective colonies were each cultivated in 1 ml LB-medium with 200 µg/ml ampicillin at 37 °C and light shaking overnight. The cells were centrifuged at 14000 rpm for 10 min before resuspending the pellet in 100 µl resuspension buffer P1. 100 µl denaturation buffer P2 were added and the solution inverted until becoming transparent. 100 µl neutralisation buffer P3 were added and the tube inverted ten times. The solution was incubated on ice for 5 minutes before centrifugation at 14000 rpm for 10 min. The supernatant was transferred to a fresh tube and 1/10th volume of sodium acetate (pH 5.5) as well as 700 µl isopropanol were added.

The solution was centrifuged at 14000 rpm and 4 °C for 30 min. The supernatant was discarded and the pellet washed with 70% ethanol before resuspension in 30 µl H_2O.

For isolation of high concentrations of pure plasmid DNA, cells from colonies carrying the desired plasmid were incubated in 100 ml LB-medium with 200 µg/ml ampicillin at 37 °C shaking overnight. The cells were harvested in 50 ml centrifuge tubes by centrifugation at 4000 rpm for 5 min. The plasmid isolation was performed using the Quiagen Plasmid Midiprep Kit. The manufacturer's instructions were followed until the precipitation step. The 5 ml plasmid DNA suspension in elution buffer (Buffer ELU) were distributed over 5 2 ml centrifugation tubes to facilitate high rpm centrifugation. The suspension was substituted with 700 µl isopropanol before centrifugation at 14000 rpm and 4 °C for 30 min. The supernatant was discarded and the pellet washed with 70% ethanol before resuspension in 500 µl H_2O.
After plasmid isolation the deletion constructs (resistance cassette framed by the two flanking regions) were cut out from the plasmid using suitable restriction enzymes (indicated in Supplementary figures 1-5). The deletion constructs were separated from the plasmid backbone via gel electrophoresis, cut out of the gel and purified using the NucleoSpin® Gel and PCR Clean-up Kit (Macherey-Nagel, Düren, Germany). The isolated and purified deletion constructs were transformed in *F. graminearum* strain 8/1.

P1 buffer:

Tris-HCl (pH 8.0)	50 mM
EDTA 0.5 M	10 mM
RNase A	10 µg/ml
Dilute in H_2O	

P2 buffer:

NaOH 5 M	20%
SDS 10%	10 mM
Dilute in H_2O	

P3 buffer:

Sodium acetate	3 M
Dilute in H_2O, adjust pH to 4.8	

2.2.2 Generation of split markers

Split marker construction was carried out as described by Harrison et al. (2013) with the following addition: Primers annotated F1 and F4 in Harrison et al. (2013) were augmented by an overhang which serves as a binding site for embedded primers in this study. This allowed using the same primers for the fusion PCRs of all split-markers.

A schematic view of split marker generation is shown in Figure 5.

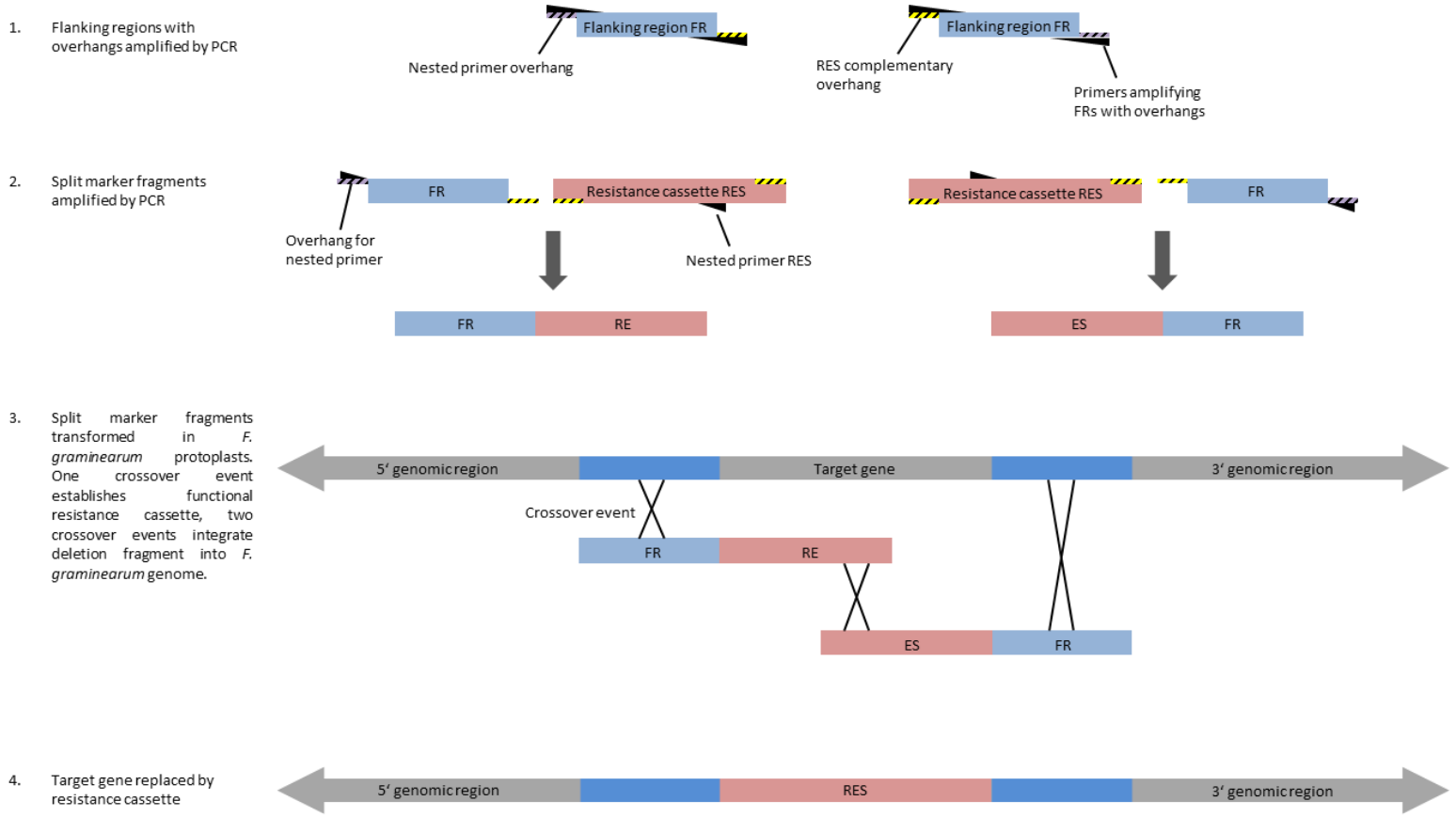

Figure 5: Split marker amplification and gene deletion. **1.:** Flanking regions of target genes were amplified with primers carrying specific overhangs; one overhang was complementary to the first 28-30 bp of the respective resistance cassette, one served as a binding site for nested primers. The respective resistance cassette was amplified by PCR as in case of HYG and GEN, or cut out of the vector pNR1 as in case of NAT. **2.:** In a PCR using the upstream or downstream flanking region (FR) and the resistance cassette (RES) as templates a split marker was amplified with primers binding the respective overhang of the flanking region and in the resistance cassette sequence amplifying a DNA fragment consisting of the flanking region and approximately two thirds of the resistance cassette. The second split marker was amplified using the respective other flanking region and the resistance cassette as template and consisted of the flanking region and the other two thirds of the resistance cassette. Hence, the sequences of the two split markers were identical in the centre region of the resistance cassette. **3.:** After transformation of *F. graminearum* protoplasts with the split markers, three cross over events take place. The flanking regions recombine with the respective identical regions in the genome and the centre regions of the truncated resistance cassettes of the split markers recombine forming the complete functional resistance cassette. **4.:** After three successful cross over events the target gene is replaced by the resistance cassette.

2.2.3 Protoplast-transformation of *F. graminearum*

For the generation of *F. graminearum* protoplasts, 50 ml YEPD-medium were inoculated with 1×10^6 of the respective *F. graminearum* strain and incubated overnight shaking at 150 rpm and 28 °C. Grown mycelia was separated from the media using a sieve with a mesh diameter of 40 µm and washed with at least 200 ml sterile ddH_2O. While drying the mycelia on sterile Whatman paper, the cell wall degrading enzyme mix was prepared and stirred for 30 minutes before being centrifuged at 4100 rpm (room temperature) and sterilised via filtering. The enzyme mix was transferred to a 100 ml Erlenmeyer flask, inoculated with 0.5 g mycelia, and incubated at 30 °C shaken at 80 rpm for 2.5 h. The resulting protoplasts were successively filtered through sieves with 100 µm and 40 µm mesh diameter in order to rid the protoplasts of any remaining mycelia. The protoplasts were washed with 10 ml 1.2 M potassium chloride and centrifuged at 2000 rpm for 10 min. The supernatant was discarded and the pellet washed with 10 ml STC-CO buffer. The centrifugation was repeated and the protoplast pellet resuspended in an appropriate amount of STC-CO buffer to reach a protoplast concentration of 1×10^8/ml. For one transformation 3-10 µg of DNA (linearised plasmid, deletion construct, or split marker) were added to 200 µl (2×10^7 protoplasts) of the protoplast suspension, which was then carefully mixed and incubated at room temperature for 20 min. 1 ml PEG-CO buffer was added, the suspension carefully mixed and centrifuged and incubated at room temperature for another 20 min. For regeneration of the protoplasts, 5 ml TB3-buffer were added and the suspension was incubated for 30 min. Then, 50 ml of TB3-agar (~50 °C) were added to the suspension which was distributed to five petri dishes (Ø 96 mm). To allow sufficient regeneration of the transformed protoplasts the plates were incubated at 28 °C overnight. The following day 10 ml of a 1.5% water agar solution containing the desired antibiotic (in case of transformed *F. graminearum* strain 8/1: 100 µg/ml for hygromycin, nourseothricin, and geneticin) were added to each plate forming an even layer. The plates were incubated for another 3-4 days at 28 °C until mycelia originating from transgenic protoplasts was visible on top of the selection agar layer. Small mycelia blocks (~1 mm²) were cut out from the centre of these primary transformants and transferred to small plates with selection agar.

YEPD-medium:

Yeast extract	0,3%
Bacto-Pepton	1%
D-glucose	2%
Dilute in H_2O	

Enzyme mix for protoplast transformation (10 ml / transformation):

Driselase™	
Basidiomycetes sp.	2.5%
Lysing enzymes from	
Trichoderma harzianum	0.5%

Dilute in 1,2 M potassium chloride, sterilize by filtration

STC-CO-buffer:

Saccharose	20%
Tris-HCl (pH 8,0)	10 mM
$CaCl_2$	50 mM

Dilute in H_2O

PEG-CO-buffer:

PEG 4000 (sterile)	40%
STC-CO-buffer	60%

Dilute in H_2O

TB3-medium:

Saccharose	20%
Yeast extract	0.3%
Acid hydrolysed casein	0.3%

Dilute in H_2O

Methods for diagnosis of deletion mutant candidates

2.2.4 Polymerase chain reaction (PCR) and gel electrophoresis

Amplification of DNA fragments was achieved by PCR. This included amplification of DNA fragments used for cloning, screening of deletion mutant candidates, and amplification of DNA probes for Southern Blotting. Composition of PCR reaction mixes as well as denaturation and elongation temperatures were applied following the manufacturers' instructions. Verification of PCR results was performed via gel electrophoresis using 0.8% agarose gels and 1× TAE buffer. Depending on the expected concentration of the DNA product, 1-10 µl were diluted in 6× loading dye and pipetted into the agarose gel chambers. Electrophoresis took place at 100-150 volts. Gels were stained in an ethidium bromide bath for 20 min before documentation in a UV transilluminator (SynGene Genius, Bio Imaging System, United Kingdom).

50× TAE buffer:

Tris	2 M
Na_2EDTA (pH 8)	50 mM
Glacial acetic acid	5.41%
Dilute in H_2O	

6× loading dye:

Bromophenol blue	250 mg
Xylene cyanol FF	250 mg
Tris 150 mM (pH 7.6)	33 ml
Glycerol	60 ml
Dilute in 7 ml H_2O	

2.2.5 Digestion of *F. graminearum* cells to obtain gDNA for PCR

To obtain genomic DNA (gDNA) of transgenic *F. graminearum* strains for target gene deletion verification, the Phire Plant Direct PCR Master Mix (ThermoFisher) was used. gDNA from the cells was released by grinding a small amount of mycelia (a few hyphae are sufficient) shortly in a 1.5 ml centrifugation tube containing 20 µl Dilution Buffer with a pipette tip. This way, intracellular cell components are released and the gDNA diffuses into the supernatant. 0.5 µl of the supernatant were used as a template for test PCRs using 2 × Phire Plant PCR Master Mix in a 10 µl PCR setup.

2.2.6 Verification of successful transformation

gDNA of transformed strains was used as template for PCR aimed at verifying the deletion of the target gene. First, a PCR was conducted with primers that bind inside of the target gene ("Diagnose"-primers. Abbreviation: diag_) (Figure 6). With WT gDNA as template this PCR would generate a fragment of known length which would be visible after gel electrophoresis. With deletion mutant gDNA as template no band would be visible in the gel; the diag-primers have no complementary binding site in the mutant's genome as the target gene had been replaced with the respective resistance cassette. gDNA of transformants that showed no band after the diagnose PCR was analysed in a second PCR which aimed at verifying the correct integration of the resistance cassette into the genome and proving that the lack of a band in the first PCR did not derive from damaged gDNA. Two different techniques were applied in this second PCR.

1. Resistance-cassette-internal (RCI)-primers (Figure 6): The primers in this PCR bind inside the resistance cassette. Therefore, WT gDNA as template would not generate any fragment due to a lack of binding sites. With deletion mutant gDNA as template a fragment of known size is generated.

2. Locus-primers (Figure 6): Two primer pairs are used in this PCR. Of each pair only one primer would bind in the resistance cassette, directed in upstream or downstream direction, respectively. The other primer of each pair would bind outside of the respective upstream or downstream flanking region in the genome. With WT gDNA as template no fragments would be generated because only one primer of each pair would be able to bind. gDNA of a deletion mutant with the resistance cassette being correctly integrated in the desired location would generate two fragments of known size.

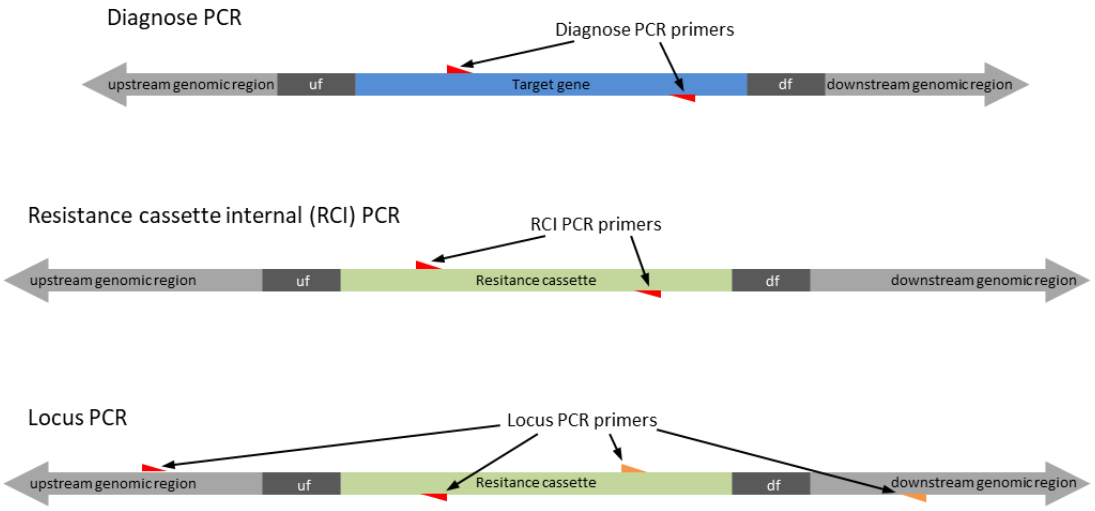

Figure 6: Primer setups for gene deletion verification PCRs. Primers are depicted as red or orange triangles. Diagnose PCR primers bind inside the target gene sequence generating a DNA fragment with WT gDNA but not with deletion mutant gDNA. Resistance cassette internal (RCI) PCR primers bind inside the resistance cassette sequence generating a DNA fragment with deletion mutant gDNA but not with WT gDNA. Locus PCR primers are made up of two primer pairs. Of each pair one primer binds inside the resistance cassette and outside of the respective flanking region, generating DNA fragments with deletion mutant gDNA but not with WT gDNA. uf: upstream flanking region; df: downstream flanking region.

2.2.7 Conidia isolation

In some cases the diagnose PCR of transgenic strains revealed faint bands of the target gene, raising doubt concerning the homokaryocity of the transformant. In these cases, conidia of the strain were isolated. Each conidiospore contains only nuclei that have formed through mitotic division making it homokaryotic. Nuclei of mycelium that originates from one conidiospore therefore derive from one single nucleus. For this purpose, conidia were isolated with the following procedure. After successful transformation, primary transformants were transferred to small plates with selection agar. From these plates conidia were washed off with sterile ddH_2O and distributed on a water agar plate (Ø 96 mm) with a spatula. After an incubation period of 5-6 h at 28 °C (or overnight at room temperature), germinated conidia were magnified under a binocular loupe, cut out with a scalpel, and transferred to a fresh selection agar plate. DNA of grown mycelia from these secondary transformants was again diagnosed via PCR.

2.2.8 gDNA-isolation

For obtaining large amounts of genomic DNA (gDNA) from *F. graminearum*, aerial mycelium from the respective strains was lyophilised overnight in centrifugation tubes with punctured lids. The lyophilised mycelia was ground with a pestle and further lysed by addition of 1 ml CTAB buffer and incubation at 65 °C for 1 h. After centrifugation at 13000 rpm for 10 min, the supernatant was transferred to a fresh 2 ml tube and 1 ml chloroform was added. The centrifugation step was repeated after inverting the solution ten times. The aqueous phase was transferred to a new tube and 750 µl isopropanol were added. The solution was inverted ten times and incubated at -20 °C for 30 min. After centrifugation at 4 °C and 13000 rpm for 30 min, the supernatant was discarded and the pellet washed by addition of 500 µl 70% ethanol and centrifugation at room temperature for 10 min. The washing step was performed twice. After discarding the supernatant and air drying the pellet, the DNA was resuspended in the desired amount of ddH_2O.

CTAB lysis buffer:

CTAB	2%
Tris-HCl (pH 8)	0.1 M
NaCl	1.4 M
EDTA (pH 8)	20 mM
Dilute in H_2O	

2.2.9 Southern-blotting

Southern blotting is a diagnosis method able to detect specific DNA sequences, gene deletions, or multiple integrations of DNA after a transformation. In this study southern blotting was used to investigate the presence of a second integration of the KO-construct in the metallothionein deletion mutant Δ*FGSG_17054*.

Buffers:

Depurination buffer:

HCl	0.25 M
Dilute in H_2O	

Denaturation buffer:

NaOH	0.5 M
NaCl	1.5 M
Dilute in H_2O	

Neutralisation buffer:

Tris-HCl (pH7.5)	0.5 M
NaCl	1.5 M

Dilute in H_2O

20 × SSC buffer:

NaCl	3 M
Sodium citrate	0.33 M

Dilute in H_2O

5 × B1 buffer:

Maleic acid	0.5 M
NaCl	0.75 M

Dilute in H_2O, adjust pH to 7.5

10% blocking solution:

Dilute 10% blocking reagent (Roche) in 1 × B1 buffer

B2 buffer:

Blocking solution	1%

Dilute in 1 × B1 buffer

B3 buffer:

Tris-HCl	0.1 M
NaCl	0.1 M

Dilute in H_2O

Prehybridisation buffer:

N-lauryl sarcosine	0.1%
SDS	0.2%
Blocking solution	2%

Dilute in 5 × SSC buffer

Hybridisation buffer:

Prehybridisation buffer + digoxigenin-labelled probe

Purified HYG was used as a probe. For the amplification of HYG via PCR, digoxigenin-labelled dUTPs (deoxyuridine triphosphate) were added to the reaction mix leading to intermittent integration of dig-dUTP instead of dTTP (deoxythymidine triphosphate).

W1 buffer:

SDS	0.1%

Dilute in 2 × SSC buffer

W2 buffer:

SDS 0.1%

Dilute in 0.2 × SSC buffer

WP buffer:

Tween 20 0.3%

Dilute in 1 × B1 buffer

Antibody solution:

Anti-digoxigenin-AP Fab fragments diluted 1:10,000 in B2 buffer

CSPD solution:

Dilute chemoluminscense reagent CSPD (Roche) 1:100 in B3 buffer

At least 2 µg of gDNA of ΔFGSG_17054 were digested in reaction mixture volume of 500 µl with 20 U *Hin*dIII overnight. After digestion, 20 µl of the restriction mixture were gel electrophorised in order to verify a complete digestion of the DNA. A continuous smear containing no bands should be visible on the respective UV picture if the digestion was successful. The rest of the restriction mixture was treated with 1/10 volumes 3 M sodium acetate and 1 volume isopropanol at -20 °C for 30 min to precipitate the DNA. After centrifugation at 4 °C for 30 min, the pellet was washed with 500 µl 70% ethanol and centrifuged at room temperature for 10 min. The pellet was resuspended in 30 µl ddH_2O and the whole volume separated by gel electrophoresis using 15 µl of dig-labeled DNA Molecular Weight Marker VII (Sigma-Aldrich, St. Louis, Missouri, USA). After electrophoresis, the gel was treated with depurination buffer, denaturation buffer, and neutralisation buffer for 10 min each. For the blotting process a basin was filled with 500 ml 20 × SSC and the blotting tower set up as indicated in Figure 7.

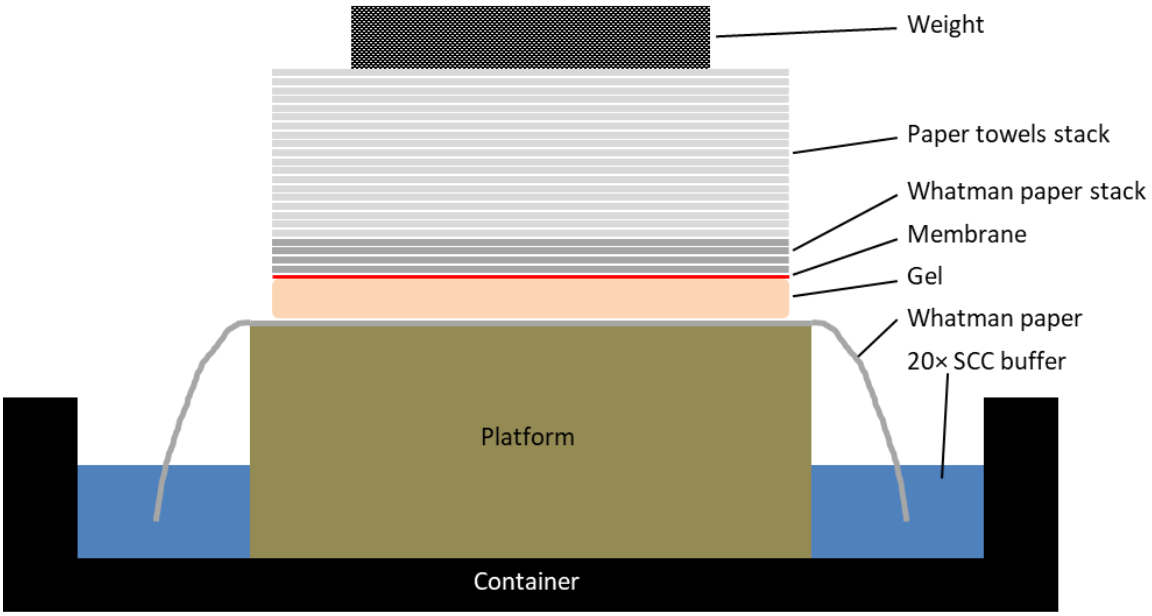

Figure 7: Southern blot setup. A container was filled with 500 ml 20× SSC buffer. A platform was put into the buffer with a sheet of Whatman paper on top whose ends were submerged in the buffer. The electrophorised gel was laid on top of the sheet of Whatman paper and any air bubbles were removed. A nylon membrane and 4 layers of Whatman paper of the size of the gel were added on top followed by a 10 cm thick stack of paper towels. A weight of approximately 500 g was put on top to apply pressure and facilitate capillary flow of the buffer.

The blotting process took place overnight. The next day the membrane was rinsed in 2 × SSC before fixing the DNA to the membrane via UV exposure with a Stratalinker UV Crosslinker (120 mJ) (Stratagene California, La Jolla, California, USA). The following incubation steps were performed in a hybridisation tube with the DNA side of the membrane facing inwards. The membrane was washed with 2 × SSC for 2 min. The SSC was removed and 20 ml prehybridisation buffer were added for incubation at 68 °C for 5 h. The prehybridisation solution was replaced with 10 ml of hybridisation solution. Hybridisation was carried out overnight at 68°C. The hybridisation solution was discarded and the membrane washed twice with 50 ml W1 buffer for 5 min at room temperature before washing twice with W2 buffer for 15 min at room temperature. The membrane was rinsed with WP buffer and incubated in 10 ml B2 blocking buffer for 60 min. The B2 blocking buffer was discarded and 10 ml antibody solution was added for incubation at room temperature for 30 min in the course of which the antibody would bind the digoxigenin residues of the labelled probe. The antibody solution was discarded and the membrane was washed thrice with 50 ml WP buffer for 20 min at room temperature. The WP buffer was replace with 10 ml B3 buffer for an incubation at room temperature for 5 min. 500 µl CSPD-solution were distributed over a plastic film (large enough for the dimensions of the membrane). The membrane was place on the CSPD drops with the DNA side facing downwards and covered with a second plastic film. Air bubbles were carefully removed before incubating at room temperature for 5 min in the course of which the luminescence reaction of the antibody-bound enzyme is triggered. The membrane was removed and sealed in a fresh plastic bag. Luminescence detection was performed with a LAS 3000 Image Analyser (Fujifilm-Europe, Düsseldrof, Germany).

2.2.10 RNA-isolation

The determination of the expression of the *F. graminearum* chloroperoxidase gene FGSG_03708 with and without oxidative stress via quantitative real time PCR required the extraction of RNA from the respective strain. To obtain the necessary mycelia, *F. graminearum* 8/1 was cultivated on a layer of cellophane spread on CM-agar without admixture and CM-agar containing 20 mM H_2O_2 or 50 µM menadione, respectively, at 28 °C. After three days the cellophane was detached from the agar and lyophilised together with the attached mycelia. After lyophilisation the cellophane and mycelia were frozen in liquid nitrogen and ground with a mortar. To extract total RNA from the powder, pegGOLD TriFast reagent (peqlab, VWR Life Science, Erlangen, Germany) was used following the manufacturer's guidelines.

2.2.11 cDNA-synthesis and purity verification

To rid the isolated RNA from any gDNA residues, it was treated with DNase from the First Strand cDNA Synthesis Kit (Fermentas, Thermo Fisher Scientific, Waltham, Massachusetts, USA) which was also used for cDNA synthesis using the producer's guidelines. 1 µg RNA was used as template. To assess the purity of the gained cDNA, i.e. the absence of gDNA residues, control PCRs were performed using primers that amplify a gene section containing a large intron. As cDNA contains no introns, the resulting band of the PCR with cDNA as template differs in length to the resulting band with gDNA as template. gDNA impurities in the cDNA sample would result in a double band. The gained cDNA was diluted 1:20 to be used as template for qRT-PCR.

2.2.12 Quantitative real time PCR (qRT-PCR)

For the determination of the expression of the *F. graminearum* chloroperoxidase gene FGSG_03708 with and without oxidative stress, a quantitative real time PCR with LightCycler® 480 SYBR Green I Master (Roche, Basel, Switzerland) was performed. SYBR Green is a cyanine fluorescent dye that absorbs light with 494 nm wavelength and emits light with 522 nm wavelength. It preferentially binds to double stranded DNA (dsDNA) but has some performance with single stranded DNA and RNA as well. During a qRT-PCR the increase of fluorescence is proportional to the amount of PCR-product. This allows for a relative quantification of the mRNA of interest when compared to a known housekeeper gene. Because SYBR Green unspecifically binds all types of dsDNA, i.e. also primer dimers, contaminating DNA, or PCR products due to mis-annealed primers, a melting curve is necessary to test whether the PCR has produces a single specific product. For this purpose the temperature is continually raised from 50 °C to 95 °C denaturing all amplificates at a certain temperature. Upon denaturing of the amplificate SYBR Green detaches leading to

a measurable decrease of fluorescence intensity. In case of one specific product a single sudden drop of fluorescence should be detectable preceded by a less intense persistent drop of fluorescence. For the relative quantification of FGSG_03708 mRNA the housekeeper gene ß-tubulin was used as a reference gene since it is constitutively expressed in all cells. One assay consisted of samples from *F. graminearum* 8/1 grown on CM-agar, on CM-agar + 20 mM H_2O_2, and on CM-agar + 50 µM menadione. ddH_2O was used as contamination control. Each sample was probed with FGSG_03708-specific and ß-tubulin-specific primers with three technical replicates each. The primer sequences are shown in Table 4.

In the following, the composition of the reaction mixture for one technical replicate is shown:

SYBR Green 2× Master-Mix	5 µl
Primer forward (10 µM)	0.2 µl
Primer reverse (10 µM)	0.2 µl
ddH_2O	3.6 µl
Template (cDNA or ddH_2O)	1 µl

The qRT-PCR reaction took place in the real-time PCR cycler Rotor Gene Q (Quiagen, Hilden, Germany) with the following temperature settings:

Initial denaturation	95 °C	10 min	
Denaturation	95 °C	15 sec	45 ×
Annealing	58 °C	30 sec	
Polymerisation	72 °C	30 sec	
Pause	4 °C	∞	

For evaluation of the acquired ct (cycle threshold)-values, the program REST-348 (Relative Expression Software Tool, Pfaffl et al., 2002) was used. The ct value describes the part of a fluorescence curve that exponentially excels the background value and marks the time point in which all reaction tubes contain the same amount of newly synthesised DNA. Significant deviations between curves of different samples were calculated using the Pair Wise Fixed Reallocation Randomisation Test (Pfaffl et al., 2002).

2.2.13 Pathogenicity assays on wheat

To determine the ability of the tested strains to infect wheat heads, the space between the palea and the lemma of the two centre spikelets of wheat heads in early anthesis was inoculated with 10 µl of a conidia suspension (20 conidia/µl H_2O). The plants were incubated in artificial day-night-cycle conditions with 16 h illumination at 21 °C and 8 h

darkness at 16 °C for 21 days. To avoid cross-contaminations and to ensure sufficient ambient humidity, the inoculated wheat heads were covered with moisturised plastic bags during the first 72 h of incubation. After 21 days, the inoculated wheat heads were removed and photographed. The spreading of the prematurely bleached plant tissue indicated the virulence of the tested strains.

2.2.14 Pathogenicity assays on maize

Fungal virulence on maize was achieved by injecting 1 ml of a conidia suspension (200 conidia/µl H_2O) into the silk channel of young maize cobs using a 2 ml syringe. The plants were incubated in a greenhouse with a 16 h photoperiod at 21 °C. To avoid cross-contaminations and to ensure sufficient ambient humidity, the inoculated maize cobs were covered with moisturised plastic bags during the first 72 h of incubation. After 5 weeks the inoculated maize cobs were harvested and photographed. The spreading of mycelia and necrotic plant tissue indicated the virulence of the tested strains.

2.2.15 ROS-sensitivity-assays

To determine the sensitivity of the mutants towards ROS-stress, mycelia plugs were cut out from the rims of 3-day-old colonies grown on CM agar and placed on plates with CM agar containing increasing concentrations of H_2O_2 or menadione (10 mM, 15 mM, 20 mM, and 10 µM, 50 µM, 100 µM respectively). Plates were incubated at 28 °C in the dark for 3 days before being documented. The colony area was determined with ImageJ. Differences in colony areas between mutants and WT 8/1 were considered significant at $p \leq 10^{-3}$, very significant at $p \leq 10^{-4}$, and highly significant at $p \leq 10^{-5}$, calculated with a two-tailed homoscedastic t-test.

2.2.16 4-nitro blue tetrazolium chloride (NBT) staining

To quantify the production of superoxide by the mutants, fresh mycelia was placed on CM-agar plates and incubated at 28 °C for 3 days. The plates were flooded with 5 ml 0.2% 4-nitro blue tetrazolium chloride (NBT) and incubated in the dark at room temperature for 30 minutes. NBT reacts with superoxide forming a blue precipitate which stains the mycelia. The resulting colour intensity is superoxide concentration dependent until reaching saturation. After the incubation, the NBT solution was discarded, 3 ml ethanol p.a. were added to stop the reaction, and plates were incubated in the dark at room temperature for another 20 minutes. The ethanol was then discarded and plates were allowed to dry. Blue precipitates in the mycelia were photographed.

2.2.17 Fertility assay

To determine the capability of strains for sexual reproduction, perithecia formation was induced on detached wheat nodes on water agar plates. Wheat nodes were collected from dried wheat straw. They were inoculated by dropping 10 µl of a conidia suspension (100 conidia/µl H_2O) of the respective strain on the node. 7 wheat nodes were inoculated per plate. WT PH1 was used as a positive control in this experiment as this strain is known to be hyperfertile (Trail & Common, 2000). The plates were sealed with Parafilm and incubated at 25 °C with a 16-hour photoperiod for 12 weeks. The time point of perithecia formation and amount of produced perithecia were documented. Evaluation of perithecia assays revealed extreme fluctuations in the fertility of the tested strains. Perithecia may grow separately or in large clusters, making them difficult to quantify. Also, strains tended to span from not producing any perithecia to producing large amounts within technical replicates of the same experiment. To avoid immense standard deviations or false positive results during statistical evaluation of this assay, each photographed wheat node was divided in three sections: left edge, centre, and right edge (Figure 8). Any amount of perithecia visible in one of these sections was counted as 1 "perithecia nest". Therefore, the maximum amount of perithecia nests on a plate with 7 inoculated wheat nodes was 21. The parameter for fertility of the tested strains was the ratio perithecia nests/wheat nodes which had a maximal possible value of 3. Differences in this ratio between mutants and WT 8/1 were considered significant at $p \leq 0.05$, very significant at $p \leq 0.005$, and highly significant at $p \leq 0.0005$ calculated with a two-tailed homoscedastic t-test.

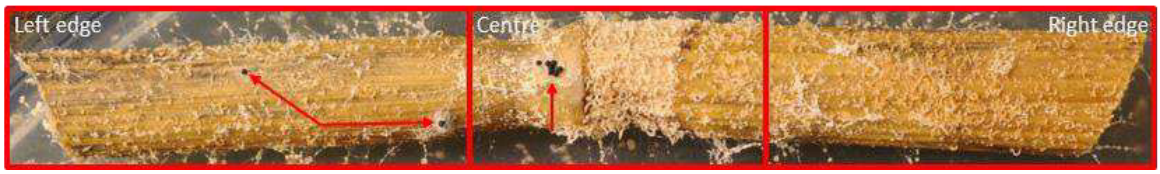

Figure 8: Subdivision of a detached wheat node in left edge, centre, and right edge. On the left edge the red arrows indicate two single perithecia which were together counted as 1 perithecia nest. The centre contains a perithecia aggregate (red arrow) which also counted as 1 perithecia nest. No perithecia have grown on the right edge.

2.2.18 Metal-sensitivity assays

Sensitivity of metallothionein deletion mutants towards high concentrations of metal ions was assessed by cutting mycelia plugs out of the rims of 3-day-old colonies grown on CM and placing them on plates with CM containing increasing concentrations of $CuCl_2$, $ZnCl_2$, $CdCl_2$, and NaCl ($CuCl_2$: 0.1 mM, 0.5 mM, 1.0 mM; $ZnCl_2$: 5 mM, 10 mM; $CdCl_2$: 50 µM, 100 µM, 200 µM). Plates were incubated at 28 °C in the dark for 3 days before being documented. The colony area was determined with ImageJ. Differences in colony areas between mutants and WT 8/1 were considered significant at $p \leq 10^{-3}$, very significant at $p \leq 10^{-4}$, and highly significant at $p \leq 10^{-5}$ calculated with a two-tailed homoscedastic t-test.

2.2.19 Metal-starvation assays

Susceptibility of metallothionein deletion mutants towards metal starvation was assessed by cutting mycelia plugs out of the rims of 3-day-old colonies grown on deprivation media (DM)-agar and placing them on DM-agar plates containing increasing concentrations of bathocuproinedisulfonic acid (BCS) (30 µM, 60 µM, 100 µM) which functions as a potent metal chelator. Plates were incubated at 28 °C in the dark for 3 days before being documented. The colony area was determined with ImageJ. Differences in colony areas between mutants and WT 8/1 were considered significant at $p \leq 10^{-3}$, very significant at $p \leq 10^{-4}$, and highly significant at $p \leq 10^{-5}$ calculated with a two-tailed homoscedastic t-test.

Metal deprivation medium (DM) agar:

Noble agar	1.6%
Solution A (100 g/l $Ca(NO_3)_2 \times 4\ H_2O$)	1%
Solution B (20 g/l KH_2PO_4, 25 g/l $MgSO_4 \times 7\ H_2O$, 15 g/l NaCl)	1%
D-glucose	1%
Reduced trace-elements-solution (60 g/l H_3BO_3, 13 mg/l KI, 60 mg/l $MnSO_4 \times H_2O$, 51 mg/l $(NH_4)_6Mo_7O_{24} \times 4H_2O$	0.1%
Dilute in H_2O	

After autoclaving, sterile bathocuproinedisulfonic acid solution was added (final concentrations: 30 µM, 60 µM, 100 µM).

2.2.20 Modification of the H_2O_2-sensor HyPer

GPI-HyPer-Vector construction

In this study a glycosylphosphatidylinositol anchor (GPI anchor) was attached to the H_2O_2-sensor HyPer. The putatively cell surface attached superoxide dismutase FGSG_00576 is predicted to be bound to a GPI-anchor. The online tools SignalP (http://www.cbs.dtu.dk/services/SignalP/) and big-PI Predictor (http://mendel.imp.ac.at/sat/gpi/gpi_server.html; Eisenhaber et al., 2004) were used to determine the sequence of the N-terminal signal peptide and the GPI modification site (C-terminal signal peptide) of FGSG_00576, respectively. With the primers LG_GPI-HyPer_fw and LG_GPI-HyPer_rv (Table 5) a DNA fragment consisting of the complete ORF of HyPer-2, the binding sequences of the restriction enzymes *Sac*I (5' end) and *Xba*I (3' end) (cloning sites of the vector pII99), the N-terminal and C-terminal signal peptide, as well as a spacer consisting of three glycine and three adenine molecules (GAGAGA), was amplified in one PCR using the HyPer-2-containing vector pAN71GluA_HyPer-2 (Michael Mentges, Master thesis) as template. This DNA fragment and the vector pII99 (Beck et al., 1982) were digested with *Sac*I and

*Xba*I and the fragment was ligated into the vector. Ligation was performed following NEBs Ligation Protocol with T4 Ligase (M0202). Optimal molar ratios were calculated using NEBs online tool NEBioCalculator. As promoter 843 bp upstream of the uncharacterised gene FGSG_04399 were used which was determined as one of the highest constitutively expressed genes in the genome of *F. graminearum* using transcriptomic data established previously (Mentges et al., unpublished data). With the primers LG_Pro04399_*Nde*I and LG_Pro04399_*Sac*I the region was amplified from *F. graminearum* 8/1 gDNA and binding sites for the restriction enzymes *Nde*I and *Sac*I (cloning sites of the promotor in pII99) were added. The amplified DNA fragment and the vector pII99 were cut with *Nde*I and *Sac*I and the promotor region was ligated into the plasmid. After cloning was finished, the vector was linearised via digestion with *Pvu*I and transformed into *F. graminearum* 8/1.

Application of fluorescent dyes

Staining of specific organelles was achieved by incubation of conidia of the tested strains in minimal media (MM) for 12 h. Grown mycelium was twice washed in Hank's balanced salt solution (HBSS) before staining. For staining of mitochondria, ER, and endomembranes MitoTracker™ Red FM, ER-Tracker™ Blue-White DPX, and FM™ 4-64 (Thermo Scientific, Schwerte, Germany) were used, respectively. Staining was performed following the producer's guidelines. Chosen concentrations were 50 nM of MitoTracker™ Red FM, 1 µM of ER-Tracker™ Blue-White DPX, and 5 µg/ml of FM™ 4-64.

Hank's Balanced Salt Solution:

NaCl	140 mM
KCl	5 mM
$CaCl_2$	1 mM
$MgSO_4 \times 7H_2O$	0.4 mM
$MgCl_2 \times 6H_2O$	0.5 mM
Na_2HPO_4	0.3 mM
KH_2PO_4	0.4 mM
$NaHCO_3$	4 mM
Glucose	6 mM
Dilute in H_2O	

Application of ER-stress

The reaction of GPI-HyPer towards ER-stress-inducing agents was observed as follows. Each well of a black 96-well plate (Greiner Bio-One, Kremsmünster, Austria) was filled with 100 µl of MM agar. After hardening, the wells were inoculated with 200 conidia of the WT strain and the GPI-HyPer mutant, respectively. The plate was incubated at 28 °C for 3 days. Brefeldin A and tunicamycin were used as ER-stress-inducing agents. Chosen concentrations were 50 µg/ml and 20 µg/ml, respectively. DMSO was used as solvent. Immediately before measurement 200 µl of ER-stress-inducing agent solution was added to each well. Fluorescence was excited at 380/10 nm and 485/14 nm and fluorescence emission monitored at 520/10 nm continuously for 12 h. To increase fungal cell permeability in this assay, 0.2% Triton X-100 or 0.02% Tween 20 were added to the solvent.

Oxidation and reduction of GPI-HyPer by H_2O_2- and DTT-injection

Ratiometric analysis of the HyPer signal for graphical visualisation was performed using a microtiter plate reader equipped with multiple injectors (Mithras² LB 943, Berthold Technologies, Bad Wildbad, Germany) as described by Mentges and Bormann, 2015. Each well of a black 96-well plate (Greiner Bio-One, Kremsmünster, Austria) was filled with 100 µl of MM agar. After hardening, each well was inoculated with 200 conidia of the WT strain and the GPI-HyPer mutant, respectively. The plate was incubated at 28 °C for 3 days. Directly before measurement, 50 µl H_2O were distributed in each well. The injectors were programmed to inject 50 µl 100 mM H_2O_2 or 100 mM DTT at specific time points, respectively, to reach a final concentration in the wells of 50 mM. Fluorescence was excited at 380/10 nm and 485/14 nm and fluorescence emission was monitored at 520/10 nm.

Preparation of slides for CLSM live imaging

Slides for real-time imaging of cells during injection of H_2O_2 were prepared as described by Mentges & Bormann, 2015. A double-sided adhesive frame (Gene Frame, 25 µl [1 cm²], Thermo Scientific, Schwerte, Germany) was attached to a microscopy slide. 30 µl of MM agar were filled in the centre of the frame. A second slide was pressed on top of the frame to create a plane agar surface. After drying of the agar, the second slide was removed with a lateral movement and the agar inoculated with 15 µl containing 300 conidia. Slides were incubated for 12 h in a humid surrounding. After 12 h, a second frame was installed on top of the first one. Two openings were cut into the double frame, one serves as injection port (width: 1 mm), one as efflux opening.

Real-time CLSM imaging during H_2O_2-injection

Cells cultivated on MM in Gene Frames (described above) were to be supplemented with H_2O_2 during live imaging. Suspensions were injected using a syringe attached to a Heidelberger extension (Fresenius Kabi AG, Bad Homburg, Germany) and an endoneedle for root canal rinsing (Vedefar N.V., Dilbeek, Belgium). A syringe pump (Precidor, Infors AG, Basel, Switzerland) was used to apply minimal pressure to the syringe (thrust: 0.01 mm/min). Imaging was performed using confocal laser scanning microscopy (Zeiss Axio Imager Z2 with LSM 780 module, Zeiss, Oberkochen, Germany). HyPer was excited at 405 nm using a solid-state laser and at 488 nm using an argon ion laser. Fluorescence was recorded at a range from 508 nm to 548 nm. For calculation of ratios, regions of interest (ROIs) were defined in which pixels were counted. Photo-multiplier sensitivity was adjusted in a way that excitation at 405 nm and 488 nm led to similar fluorescence intensities in the non-stressed situation, leading to a ratio of approximately 1.

Deletion of *noxR*

Deletion of *noxR* was achieved via homologous recombination. Previously, a nourseothricin-resistance cassette flanked by upstream and downstream regions of *noxR* was cloned into the vector pRS426 by transforming all fragments (3'-flanking region, 5'-flanking region, resistance cassette, linearised pRS426) into the uracil-auxotrophic *S. cerevisiae* strain FGSC 9721 (FY 834) (Michael Mentges, Master thesis). The isolated vector was amplified in *E. coli* and re-isolated. The deletion construct (nourseothricin-resistance cassette with flanking regions) was cut out with *Xho*I and *Not*I and separated from the pRS426-backbone via gel electrophoresis. The isolated and purified deletion constructs were used to transform the desired *F. graminearum* strains.

3. Results

This study aims to clarify the role of reactive oxygen species (ROS) in the life cycle of *Fusarium graminearum*. Previous work by Nguyen et al. (2012 and 2013) showed that loss of the stress-activated MAP kinase FgOS-2, which orchestrates ROS generation and detoxification, leads to defects in infection structure development, stress responses, and virulence. This suggests importance of ROS in pathogenicity and defence reactions. While it is evident that ROS are pivotal for the penetration and dispersion of phytopathogenic and endophytic fungi, the ROS-fluctuations between pathogen and host and the involved enzymes are still not known in detail. Further research of this topic is required as understanding the exact ROS-fluctuations necessary for a successful infection of a pathogen might yield potential new drug targets or prevention methods against *Fusarium* related crop diseases. The characterisation of ROS-related enzymes which partake in the infection process of *F. graminearum* was therefore among the main amibitions of this work.

3.1 Characterisation of ROS-related enzymes

3.1.1 Transcriptomic profiling reveals potential ROS-related virulence factors in *F. graminearum*

The selection process of target genes for characterisation was based to a large extent on a differential transcriptomic analysis of ICs, RH, and axenic *in vitro* mycelia. For the establishment of this transcriptomic data, *F. graminearum* conidiospores were cultivated on detached wheat palea until ICs were formed. ICs and RH were isolated separately by laser capture microdissection to be able to generate cDNA libraries specific for ICs and RH (Mentges et al, unpublished data). These libraries allowed comparative analyses of gene regulation in invasive (ICs) and non-invasive (RH) *in planta* tissue and *in vitro* mycelia in order to identify genes which are differentially expressed during the infection process. The transcriptomic data set included a value of up- or downregulation of each gene in each analysed tissue in comparison with its expression in the respective other tissues. Genes were considered plant-regulated when their expression value exhibited a $\log_2$-fold change above the threshold of +2 (plant-induced) or below the threshold of -2 (plant-repressed) compared to expression in *in vitro* mycelia. The base 2 logarithm was used to facilitate comparisons between the regulations of different genes by scaling down the very high margins between the expression values of different genes and different tissues. The $\log_2$-threshold of 2 was chosen so that only highly regulated genes are taken into account. Analysis of the transcriptomic data revealed that of the 13826 predicted genes in *F. graminearum* 1073 encode proteins involved in ROS metabolism (ROS-related proteins). *In planta*, 173 of these genes are repressed, whereas 149 are induced with 10 genes being specifically up-regulated in RH and 34 in IC. Among the plant-regulated genes

45 code for secreted enzymes (secreted ROS-related enzymes, henceforth termed SREs). This study's classification of ROS-related proteins included components of the NADPH oxidase (Nox) complex, cupredoxins, metallothioneins, dehydrogenases, superoxide dismutases, catalases, reductases, peroxidases, oxidases, oxygenases, hydrolases, glutaredoxins, thioredoxins, peroxisomal proteins, as well as ROS-related transcriptional regulators (e.g. Fgap1, Fgskn7, FgOS-2, Fgatf1). Figure 9 shows the regulation of SREs and non-secreted genes relevant for this study. For a better visual representation the regulation of selected genes is presented in Figure 10 as a bar diagram. 29 SREs are plant-induced, 16 plant-repressed. The data show that high upregulation or downregulation in ICs compared to *in vitro* mycelia often correlates with upregulation or downregulation in RH compared to *in vitro* mycelia. 11 SREs (FGSG_02341, FGSG_11399, FGSG_03531, FGSG_11528, FGSG_07761, FGSG_03436, FGSG_07829, FGSG_09742, FGSG_09124, FGSG_06023, FGSG_11215) are upregulated in ICs compared to *in vitro* mycelia. 5 SREs (FGSG_09093, FGSG_17478, FGSG_02328, FGSG_FGSG_17417, FGSG_02327) are upregulated in RH compared to *in vitro* mycelia. 7 SREs (FGSG_08037, FGSG_02341, FGSG_11399, FGSG_03531, FGSG_07661, FGSG_03436, FGSG_09742) are upregulated in ICs compared to the expression in RH. 5 SREs (FGSG_17459, FGSG_02328, FGSG_02327, FGSG_11032, FGSG_16013) are upregulated in RH compared to the expression in ICs. It is striking that two neighbouring genes, FGSG_02327 and FGSG_02328 are in this list. Indeed, these genes belong to a polyketide synthase gene cluster that fulfils the biosynthesis of the pigment aurofusarin.

In addition to SREs 9 non-secreted ROS-related enzymes were studied for this thesis: 5 cytochrome P450 monooxygenases (P450s) (FGSG_03700, FGSG_07765, FGSG_01745, FGSG_16458, FGSG_03498), 3 metallothioneins (FGSG_17054, FGSG_12456, FGSG_16151), and 1 NAD(P) transhydrogenase (FGSG_09006). 3 of the studied P450s are plant-induced (FGSG_03700, FGSG_07765, FGSG_16458). FGSG_01745 shows a $\log_2$-fold difference towards *in vitro* mycelia of 1.8, not quite reaching the $\log_2$ threshold of 2. FGSG_03498 shows no differential expression *in planta* but gets upregulated after tebuconazole treatment according to Liu et al. (2009). Most noticeable is the regulation of the metallothioneins FGSG_17054 and FGSG_12456. FGSG_17054 shows the highest, FGSG_12456 the fifth highest *in planta* upregulation of all genes in *F. graminearum*. Both proteins contain a characteristic motif regarding the arrangement of their cysteines ([CXC]-X_5-[CXC]-X_3-[CXC]-X_2-C; C = cysteine, X = other amino acid) which represent up to a third of the polypeptide. While this motif is not present in the third annotated metallothionein in the *F. graminearum* genome, FGSG_08172, it was found via a BLAST analysis in gene FGSG_16151, former FGSG_04088, encoding an unknown protein. Contrary to NCBI database that describes FGSG_16151 as a gene of 95 amino acids length, RNA sequencing showed FGSG_16151 to be only 26 amino acids long and contain the metallothionein motif. Therefore, FGSG_16151 was considered a metallothionein. In opposite to FGSG_17054 and FGSG_12456 however, FGSG_16151 is not plant-regulated. The sole NAD(P) transhydrogenase (NNT) is downregulated in ICs and RH.

			IC vs. *in vitro*		RH vs. *in vitro*		IC vs. RH	
	Locus	Description	Log_2 difference	regulation	Log_2 difference	regulation	Log_2 difference	regulation
SREs	FGSG_08037	Intradiol ring-cleavage dioxygenase	6,718	up	4,316	up	2,401	up
	FGSG_02341	Chloroperoxidase	5,852	up	0,946	non	4,906	up
	FGSG_11399	FAD-linked oxidase	5,445	up	1,476	non	3,969	up
	FGSG_03708	Chloroperoxidase	5,253	up	4,638	up	0,615	non
	FGSG_10631	FAD-linked oxidase	4,871	up	4,327	up	0,544	non
	FGSG_03531	Tyrosinase	4,869	up	1,639	non	3,231	up
	FGSG_10587	Copper amine oxidase	4,414	up	2,694	up	1,720	non
	FGSG_09085	Cellobiose dehydrogenase	4,327	up	3,517	up	0,809	non
	FGSG_03416	FAD-dependent oxidoreductase	4,142	up	4,374	up	-0,231	non
	FGSG_04736	Choline monooxygenase	4,003	up	4,546	up	-0,543	non
	FGSG_04510	Tyrosinase	3,402	up	4,101	up	-0,699	non
	FGSG_11528	Tyrosinase	3,155	up	1,950	non	1,205	non
	FGSG_05983	Cellobiose dehydrogenase	3,002	up	3,189	up	-0,187	non
	FGSG_11228	Choline dehydrogenase	2,979	up	2,566	up	0,413	non
	FGSG_17459	FAD-linked oxidase	2,861	up	5,203	up	-2,342	down
	FGSG_10986	Alcohol oxidase	2,815	up	2,457	up	0,358	non
	FGSG_07661	FAD-linked oxidase	2,784	up	0,715	non	2,069	up
	FGSG_03436	Chloroperoxidase	2,583	up	0,399	non	2,185	up
	FGSG_07829	Cupredoxin	2,573	up	0,978	non	1,595	non
	FGSG_09742	Cupredoxin	2,567	up	-0,306	non	2,873	up
	FGSG_01988	Tyrosinase	2,481	up	2,004	up	0,477	non
	FGSG_09124	related to NADPH-dependent beta-ketoacyl reductase (rhlG)	2,327	up	0,385	non	1,942	non
	FGSG_06023	Cupredoxin	2,284	up	0,571	non	1,713	non
	FGSG_11215	FAD-binding monooxygenase	2,033	up	0,296	non	1,737	non
	FGSG_09093	Galactose oxidase	1,917	non	2,585	up	-0,667	non
	FGSG_17478	FAD-binding monooxygenase	1,832	non	2,292	up	-0,460	non
	FGSG_02328	Laccase	1,632	non	5,947	up	-4,315	down
	FGSG_17417	Amine oxidase	1,138	non	2,189	up	-1,051	non
	FGSG_02327	FAD-binding monooxygenase	-0,991	non	4,467	up	-5,458	down
	FGSG_04793	Amine oxidase	-2,019	down	-0,753	non	-1,266	non
	FGSG_07539	related to FAT1 - very long-chain fatty acyl-CoA synthetase	-2,137	down	-1,965	non	-0,172	non
	FGSG_00576	Superoxide dismutase	-2,156	down	-1,209	non	-0,947	non
	FGSG_11081	FAD-binding monooxygenase	-2,249	down	-3,202	down	0,952	non
	FGSG_12369	Catalase-peroxidase	-2,461	down	-0,898	non	-1,563	non
	FGSG_06053	Amine oxidase	-2,687	down	-1,920	non	-0,767	non
	FGSG_09646	Laccase	-2,967	down	-1,197	non	-1,770	non
	FGSG_11032	Galactose oxidase	-3,088	down	-0,686	non	-2,402	down
	FGSG_16013	Lignin peroxidase	-3,237	down	0,373	non	-3,610	down
	FGSG_05763	Glyoxal oxidase	-3,241	down	-3,085	down	-0,156	non
	FGSG_04368	FAD-binding monooxygenase	-3,339	down	-2,971	down	-0,368	non
	FGSG_16111	FAD-linked oxidase	-3,571	down	-1,792	non	-1,778	non
	FGSG_02477	NADH dehydrogenase	-3,597	down	-2,656	down	-0,941	non
	FGSG_05606	Cupredoxin	-4,211	down	-2,213	down	-1,998	non
	FGSG_17550	Laccase	-4,892	down	-3,177	down	-1,715	non
	FGSG_03616	isoamyl alcohol oxidase	-5,433	down	-5,456	down	0,023	non
non-secreted		**P450s**						
	FGSG_03700	Cytochrome P450 monooxygenase	6,044	up	4,270	up	1,774	non
	FGSG_07765	Cytochrome P450 monooxygenase	5,472	up	2,267	up	3,205	up
	FGSG_01745	Cytochrome P450 monooxygenase	1,801	non	0,471	non	1,330	non
	FGSG_16458	Cytochrome P450 monooxygenase	1,401	non	3,498	up	-2,098	down
	FGSG_03498	Cytochrome P450 monooxygenase	1,242	non	-0,331	non	1,573	non
		Metallothioneins						
	FGSG_17054	Metallothionein	19,116	up	18,219	up	0,897	non
	FGSG_12456	Metallothionein	11,804	up	10,314	up	1,490	non
	FGSG_16151	hypothetical protein	-0,404	non	0,256	non	0,660	non
	FGSG_08172	Metallothionein	-1,731	non	-2,834	down	1,103	non
		NNT						
	FGSG_09006	NAD(P) transhydrogenase	-2,236	down	-2,007	down	-0,229	non

Figure 9: Transcriptomic data analysis. This figure represents a list of *F. graminearum* genes (column 'locus'), each with its putative function (column 'description'), its regulation in ICs compared to expression in *in vitro* mycelia (column 'IC vs. *in vitro*'), its regulation in RH compared to expression in *in vitro* mycelia (column 'RH vs. *in vitro*'), and its expression in ICs compared to RH (column 'IC vs RH'). Genes were considered up- or downregulated if their log_2-fold change was ≥2 or ≤2, respectively. Those genes received the annotation 'up' (upregulated) or 'down' (downregulated). Genes with a log_2-fold change that did not surpass these thresholds were considered non-regulated and received the annotation 'non'. The genes are sorted in order of their upregulation in IC vs. *in vitro* mycelia from highest to lowest with a colour code ranging from green (strong upregulation) to red (strong downregulation). Genes FGSG_17054 and FGSG_12456 are excluded from this code as their upregulation is exceptionally high. Their regulation is highlighted yellow. Genes deleted in this study are highlighted blue. The 'SREs' bracket shows all plant-regulated secreted ROS-related enzymes (SREs) of *F. graminearum* with 29 SREs being upregulated and 16 downregulated *in planta*. The 'non-secreted' bracket shows intracellular ROS-related genes relevant for this study. These are further divided into their functional categories cytochrome P450 monooxygenases (P450s), metallothioneins, and NNT.

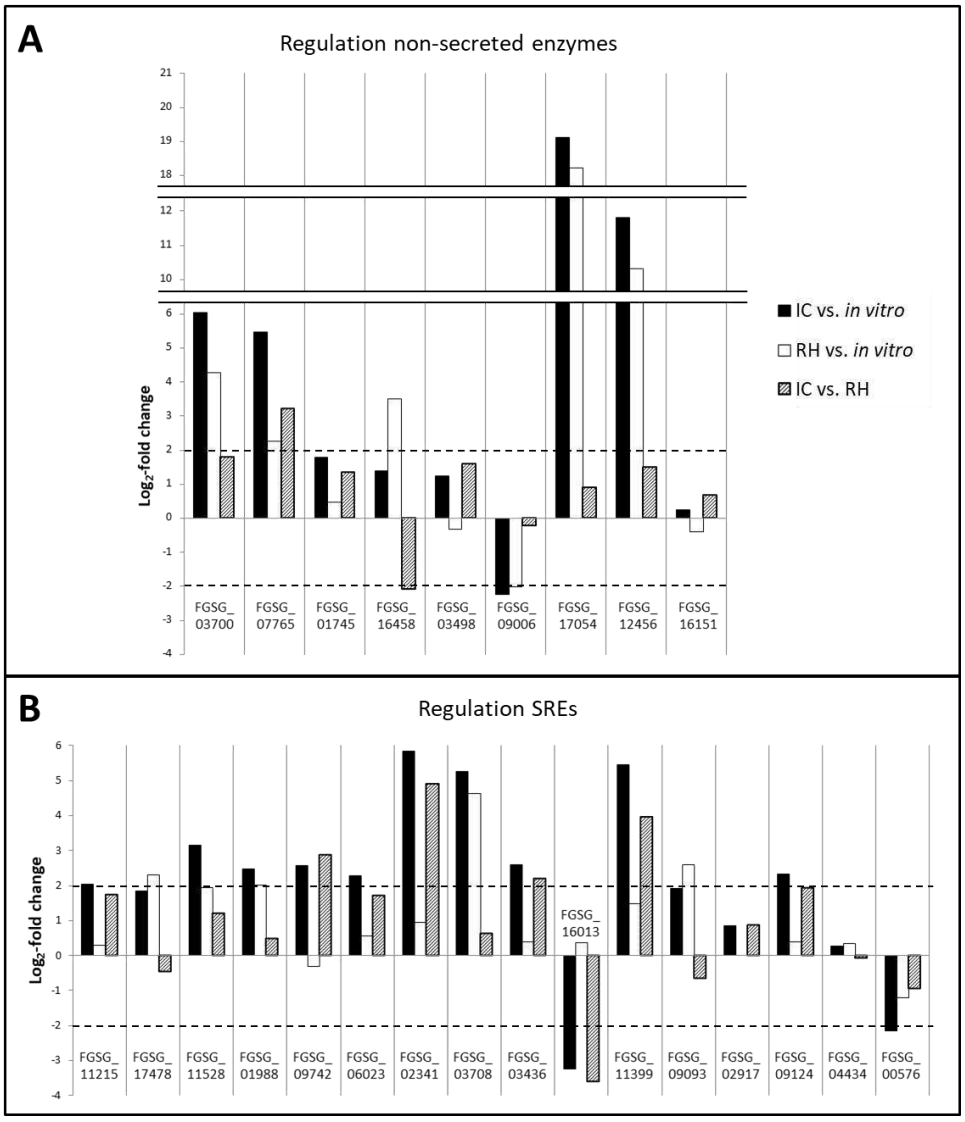

Figure 10: Bar diagram representing the expression of all genes studied in this thesis as the log_2-fold difference towards the expression in *in vitro* mycelia. Black bars represent the log_2-fold change in ICs compared to expression in *in vitro* mycelia, white bars the log_2-fold change in RH compared to expression in *in vitro* mycelia, and dashed bars the log_2-fold difference between expression in ICs compared to RH. Dashed lines show the log_2-values of 2 and -2 which mark the chosen threshold for up- or downregulation, respectively. **A:** Regulation of non-secreted enzymes. Except for the P450s FGSG_01745 and FGSG_03498, and the metallothionein FGSG_16151 all surpass the log_2-threshold in either ICs or RH (compared to *in vitro* mycelia). Notably, metallothioneins FGSG_17054 and FGSG_12456 show exceptionally high log_2-fold changes in ICs (19.1 for FGSG_17054 and 11.8 for FGSG_12456) and RH (18.2 for FGSG_17054 and 10.3 for FGSG_12456) compared to expression in *in vitro* mycelia. **B:** Regulation of SREs. Except for FGSG_02917 and FGSG_04434 all surpass the log_2-threshold in either ICs or RH.

3.1.2 Deletion of 25 ROS-related genes

An array of deletion mutants of *F. graminearum* was established through gene knock-outs via protoplast transformation with deletion plasmids and split markers in order to gain insight into the enzymes involved in the ROS-based interactions between *F. graminearum* and its host. Target genes were selected with regard to their connection to ROS-

metabolism (ROS being part of the enzyme's reaction process), expression profile (plant induced or plant repressed, see figures 9 and 10), functional redundancy (few other genes with similar function), and secretion. Figure 11 gives an overview of the deleted genes with regard to these parameters ordered by enzyme classes. The genes FGSG_11399, FGSG_06023, FGSG_00576, FGSG_16013, and FGSG_09742 where deleted by using deletion plasmids established via yeast recombinational cloning (see 'methods' section). For plasmid generation, flanking regions upstream and downstream of the respective gene locus as well as the respective resistance cassette were amplified by PCR using the appropriate primer pairs (Figure 12 A and C). The deletion vector pRS426 was linearised by three consecutive digestions with *Hin*dIII, *Eco*RI, and *Hin*dIII, respectively (Figure 12 C). Together with the linearised vector pRS426 the flanking regions and the resistance cassette were transformed into the uracil-auxotrophic yeast strain FY834 where the assembly of the fragments to the complete deletion vector took place. Isolated deletion plasmids were examined for correct assembly via specific digestion using the restriction enzymes indicated in Supplementary figures 1-5. The deletion construct consisting of flanking regions and resistance cassette was cut out of the deletion vector using appropriate restriction enzymes, isolated, and transformed into *F. graminearum* 8/1 protoplasts. Maps of the deletion plasmids with the restriction sites of the applied restriction enzymes are shown in Supplementary figures 1-5. Homologous recombination into the *F. graminearum* genome took place through double cross over.

Enzyme class			FGSG_number	Secreted	Regulation in infection structures	Proportion of the exome / Functional redundancy
Oxidoreductases	Monooxygenases	P450s	**FGSG_03700**	✗	Plant induced	9.55 ‰ / High
			FGSG_07765	✗	IC up	
			FGSG_01745	✗	Not differentially regulated	
			FGSG_16458	✗	RH up	
			FGSG_03498	✗	Not differentially regulated	
		FAD-dependent	**FGSG_11215**	✓	Plant induced	
			FGSG_17478	✓	Plant induced	
		Tyrosinases	**FGSG_11528**	✓	Plant induced	
			FGSG_01988	✓	Plant induced	
	Peroxidases	Ascorbate/Cytochrome c peroxidases	**FGSG_04434**	✓	Not differentially regulated	2.09 ‰ / Medium
		Chloroperoxidases	**FGSG_03708**	✓	Plant induced	
			FGSG_03436	✓	IC up	
			FGSG_02341	✓	IC up	
		Lignin peroxidases	**FGSG_16013**	✓	Plant repressed	
	Oxidases	Oxidases	**FGSG_11399**	✓	IC up	18.15 ‰ / High
		Galactose oxidases	**FGSG_09093**	✓	Plant induced	
	Dehydrogenases	Cellobiose dehydrogenases	**FGSG_02917**	✓	Not differentially regulated	37.38 ‰ / High
	Reductases		**FGSG_09124**	✓	Plant induced	44.25 ‰ / High
Cupredoxins			**FGSG_06023**	✓	Plant induced	0.43 ‰ / Low
			FGSG_09742	✓	IC up	
Metallothioneins			**FGSG_17054**	✗	Plant induced	0.21 ‰ / Low
			FGSG_12456	✗	Plant induced	
			FGSG_16151	✗	Not differentially regulated	
NNT			**FGSG_09006**	✗	Plant repressed	0.07 ‰ / Low
SOD			**FGSG_00576**	✓	Plant repressed	0.43 ‰ / Low

Figure 11: Deleted genes ordered by their enzyme class with information regarding secretion, regulation, and functional redundancy. Enzymes with a $\log_2$-fold change ≥ 2 *in planta* compared to *in vitro* mycelia are labeled as 'plant induced', with a $\log_2$-fold change ≤ 2 as 'plant repressed', others as 'not differentially regulated'. Enzymes with a $\log_2$-fold change ≥ 2 in ICs compared to RH are labeled as specifically upregulated in IC ('IC up'), vice versa as specifically upregulated in RH ('RH up'). Functional redundancy of the individual enzyme classes is based on the abundance of the enzyme class in the exome of *F. graminearum*. Enzyme classes with a genome proportion < 0.5‰ are attributed low functional redundancy, with a proportion < 5‰ medium functional redundancy, and with a proportion > 5‰ high functional redundancy.

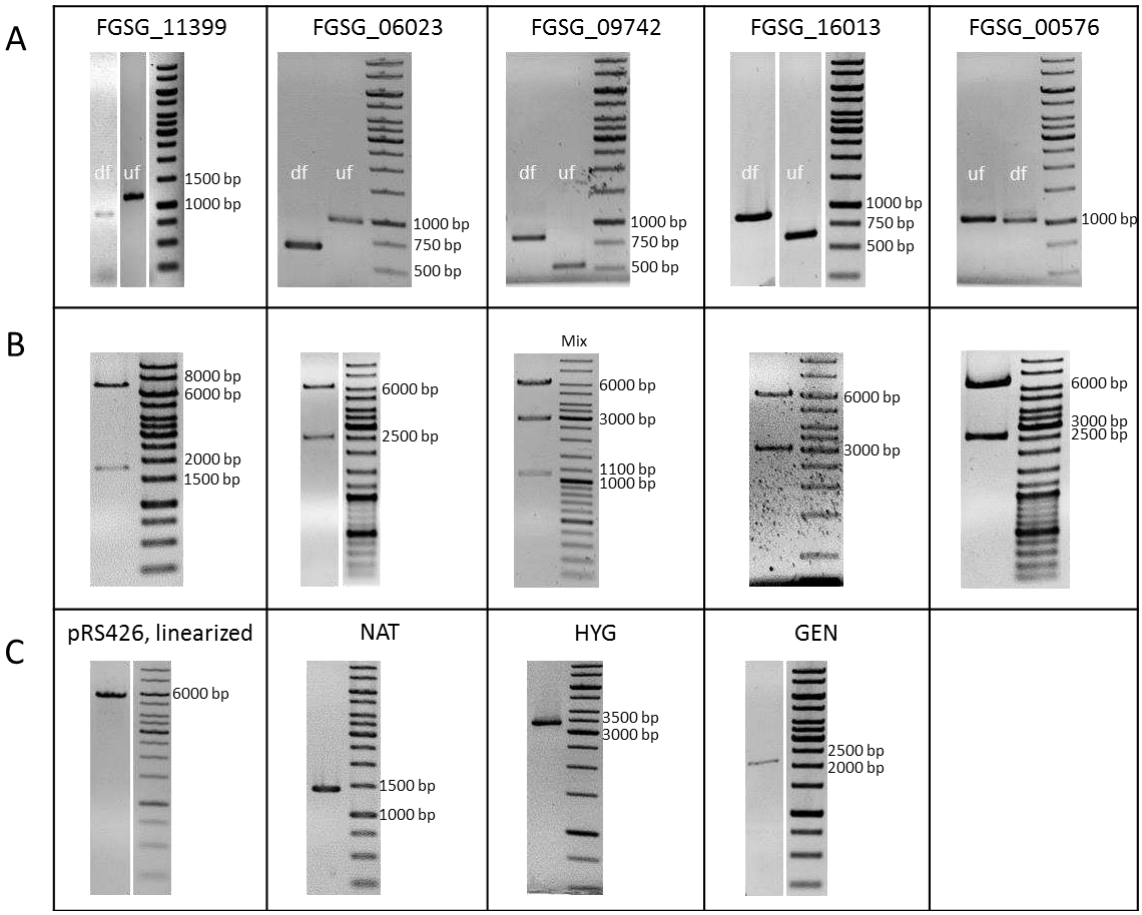

Figure 12: Agarose gel scans of the generation of deletion plasmids. A: Upstream flanking regions (uf) and downstream flanking regions (df) of target genes were amplified via PCR. Primers 11399_RF_f and 11399_RF_r produce a fragment size of 775 bp (FGSG_11399 df), primers 11399_LF_f and 11399_LF_r a fragment size of 1157 bp (FGSG_11399 uf). Primers 06023_RF_f and 06023_RF_r produce a fragment size of 646 bp (FGSG_06023 df), primers 06023_LF_f and 06023_LF_r a fragment size of 976 bp (FGSG_06023 uf). Primers 09742_LF_f and 09742_LF_r produce a fragment size of 823 bp (FGSG_09742 df), primers 09742_RF_f and 09742_RF_r a fragment size of 533 bp (FGSG_09742 uf). Primers 16013_LF_f and 16013_LF_r produce a fragment size of 986 bp (FGSG_16013 df), primers 16013_RF_f and 16013_RF_r a fragment size of 644 bp (FGSG_16013 uf). Primers 00576_LF_f and 00576_LF_r produce a fragment size of 1035 bp (FGSG_00576 df), primers 00576_RF_f and 00576_RF_r a fragment size of 1061 bp (FGSG_00576 uf). **B:** Deletion vectors were screened for correct assembly by digestion with specific restriction enzymes. Deletion vector pRS426_Δ11399 was digested with *Msc*I and *Bgl*II producing two fragments with 1840 bp and 7218 bp length. Deletion vector pRS426_Δ06023 was digested with *Bsr*GI producing two fragments with 2491 bp and 6142 bp length. Deletion vector pRS426_Δ09742 was digested with *Nhe*I and *Asc*I producing three fragments with 1109 bp, 2928 bp, and 6088 bp length. Deletion vector pRS426_Δ16013 was digested with *Bgl*II producing two fragments with 3076 bp and 6120 bp length. Deletion vector pRS426_Δ00576 was digested with *Spe*I producing two fragments with 2571 bp and 6536 bp length. **C:** The deletion vector backbone pRS426 was linearised with three consecutive restrictions with *Eco*RI, *Hin*dIII, and *Eco*RI producing a fragment with 5726bp length. The nourseothricin resistance cassette (NAT, 1416) was cut out of the vector pNR1 using *Eco*RI and *Xba*I. The hygromycin resistance cassette (HYG, 1743) was amplified from the vector pGEM-Hyg using primers 1F-Hyg and 2R-Hyg. The geneticin resistance cassette (GEN, 2029 bp) was amplified from the vector pII99 using primers 1F-NptII and 2R-NptII-vect.

All other characterised genes were deleted by applying the split marker method (see 'methods' section). In this variant no vector and no assembly of the fragments in yeast is necessary. In two PCRs the resistance cassette and one of the flanking regions serve as

templates and get amplified and fused to one continuous stretch of DNA using primers that bind at the end of the flanking region and two thirds down the length of the resistance cassette. Upon transformation of the two split markers in *F. graminearum* protoplasts the two resistance cassette fragments are assembled within the fungus and the deletion construct is integrated into the genome which requires three cross-over events.

Transformed protoplasts were regenerated on TB3-agar for 1 day before the TB3-agar was covered with antibiotic-containing water-agar. Antibiotic-resistant primary transformants were visible as colonies on top of the water agar after 2-3 days. These colonies were isolated and cultivated on antibiotic containing agar. Grown mycelium was harvested and genomic DNA (gDNA) isolated. To verify if transformed strains contain the desired deletions, the gDNA was screened by two PCRs. The primers of the first PCR bind inside the target gene. While they bind and allow amplification with WT gDNA as template, the deletion mutants' gDNAs do not generate a band because the target gene has been replaced by the resistance cassette. The second PCR served as a positive control for identifying deletion mutants. For this second PCR two different techniques were applied. 1.: The primers target the resistance cassette. Therefore, with deletion mutant gDNA serving as template a DNA product with specific length is amplified. With WT gDNA serving as template no product is amplified. This variant is termed 'resistance cassette-internal' (RCI). 2.: One primer binds inside the resistance cassette, the other one in the gDNA outside of the chosen flanking region. This was performed for both ends of the resistance cassette; upstream and downstream. This variant is termed 'locus'. The results of these PCRs are summarised in Figure 13.

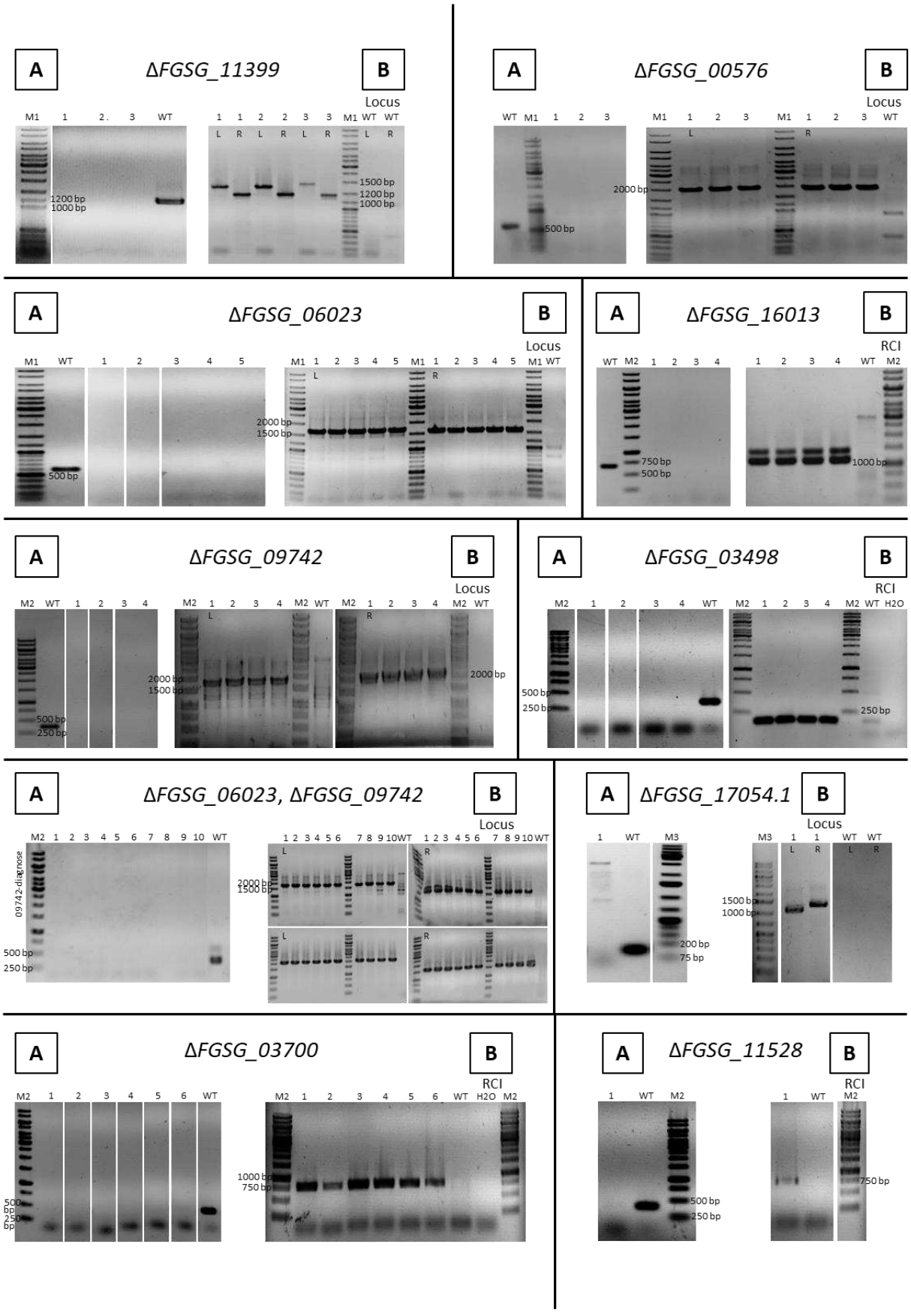
A
ΔFGSG_11399
B
Locus
M1 1 2. 3 WT
1200 bp
1000 bp
1 1 2 2 3 3 M1 WT WT
L R L R L R L R
1500 bp
1200 bp
1000 bp
A
ΔFGSG_00576
B
Locus
WT M1 1 2 3
500 bp
M1 1 2 3 M1 1 2 3 WT
L
R
2000 bp
A
ΔFGSG_06023
B
Locus
M1 WT 1 2 3 4 5
500 bp
M1 1 2 3 4 5 M1 1 2 3 4 5 M1 WT
L
R
2000 bp
1500 bp
A
ΔFGSG_16013
B
RCI
WT M2 1 2 3 4
750 bp
500 bp
1 2 3 4 WT M2
1000 bp
A
ΔFGSG_09742
B
Locus
M2 WT 1 2 3 4
500 bp
250 bp
M2 1 2 3 4 M2 WT
L
2000 bp
1500 bp
M2 1 2 3 4 M2 WT
R
2000 bp
A
ΔFGSG_03498
B
RCI
M2 1 2 3 4 WT
500 bp
250 bp
M2 1 2 3 4 M2 WT H2O
250 bp
A
ΔFGSG_06023, ΔFGSG_09742
B
Locus
M2 1 2 3 4 5 6 7 8 9 10 WT
09742-diagnose
500 bp
250 bp
1 2 3 4 5 6 7 8 9 10 WT 1 2 3 4 5 6 7 8 9 10 WT
L
R
2000 bp
1500 bp
A
ΔFGSG_17054.1
B
Locus
1 WT M3
200 bp
75 bp
M3 1 1 WT WT
L R L R
1500 bp
1000 bp
A
ΔFGSG_03700
B
RCI
M2 1 2 3 4 5 6 WT
500 bp
250 bp
M2 1 2 3 4 5 6 WT H2O M2
1000 bp
750 bp
A
ΔFGSG_11528
B
RCI
1 WT M2
500 bp
250 bp
1 WT M2
750 bp

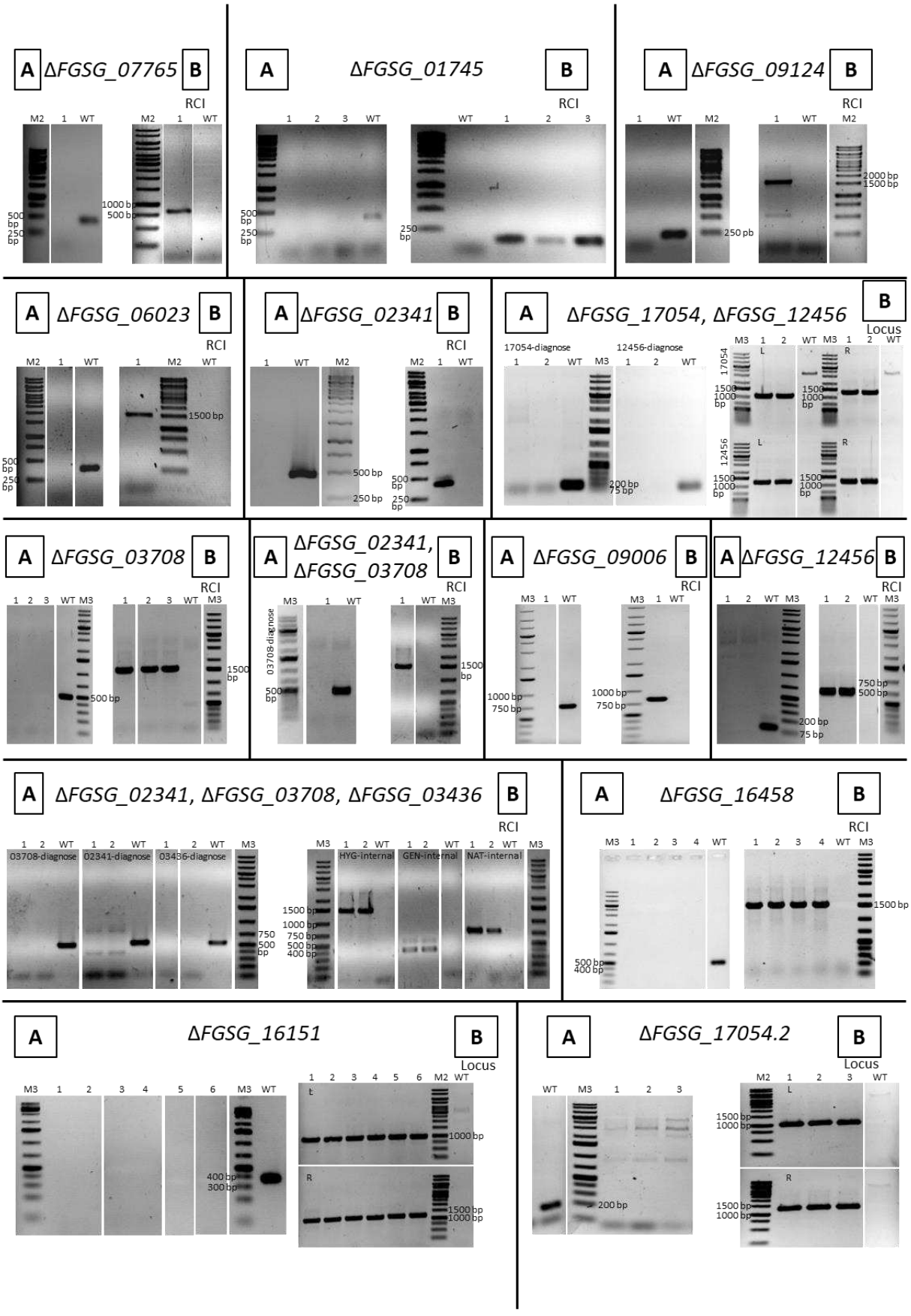
A
ΔFGSG_07765
B
RCI
M2 1 WT
500 bp
250 bp
1000 bp
500 bp
A
ΔFGSG_01745
B
RCI
1 2 3 WT
WT 1 2 3
500 bp
250 bp
250 bp
A
ΔFGSG_09124
B
RCI
1 WT M2
250 pb
1 WT M2
2000 bp
1500 bp
A
ΔFGSG_06023
B
RCI
M2 1 WT
1 M2 WT
500 bp
250 bp
1500 bp
A
ΔFGSG_02341
B
RCI
1 WT M2
500 bp
250 bp
M2 1 WT
500 bp
250 bp
A
ΔFGSG_17054, ΔFGSG_12456
B
Locus
17054-diagnose
12456-diagnose
1 2 WT M3 1 2 WT
200 bp
75 bp
M3 1 2 WT M3 1 2 WT
17054
L
R
1500
1000
bp
12456
L
R
1500
1000
bp
A
ΔFGSG_03708
B
RCI
1 2 3 WT M3
500 bp
1 2 3 WT M3
1500 bp
A
ΔFGSG_02341,
ΔFGSG_03708
B
RCI
M3 1 WT
03708-diagnose
500 bp
1 WT M3
1500 bp
A
ΔFGSG_09006
B
RCI
M3 1 WT
1000 bp
750 bp
M3 1 WT
1000 bp
750 bp
A
ΔFGSG_12456
B
RCI
1 2 WT M3
200 bp
75 bp
1 2 WT M3
750 bp
500 bp
A
ΔFGSG_02341, ΔFGSG_03708, ΔFGSG_03436
B
RCI
1 2 WT 1 2 WT 1 2 WT M3
03708-diagnose
02341-diagnose
03436-diagnose
750
500
bp
M3 1 2 WT 1 2 WT 1 2 WT M3
HYG-internal
GEN-internal
NAT-internal
1500 bp
1000 bp
750 bp
500 bp
400 bp
A
ΔFGSG_16458
B
RCI
M3 1 2 3 4 WT
500 bp
400 bp
1 2 3 4 WT M3
1500 bp
A
ΔFGSG_16151
B
Locus
M3 1 2 3 4 5 6 M3 WT
400 bp
300 bp
1 2 3 4 5 6 M2 WT
L
1000 bp
R
1500 bp
1000 bp
A
ΔFGSG_17054.2
B
Locus
WT M3 1 2 3
200 bp
M2 1 2 3 WT
L
1500 bp
1000 bp
R
1500 bp
1000 bp

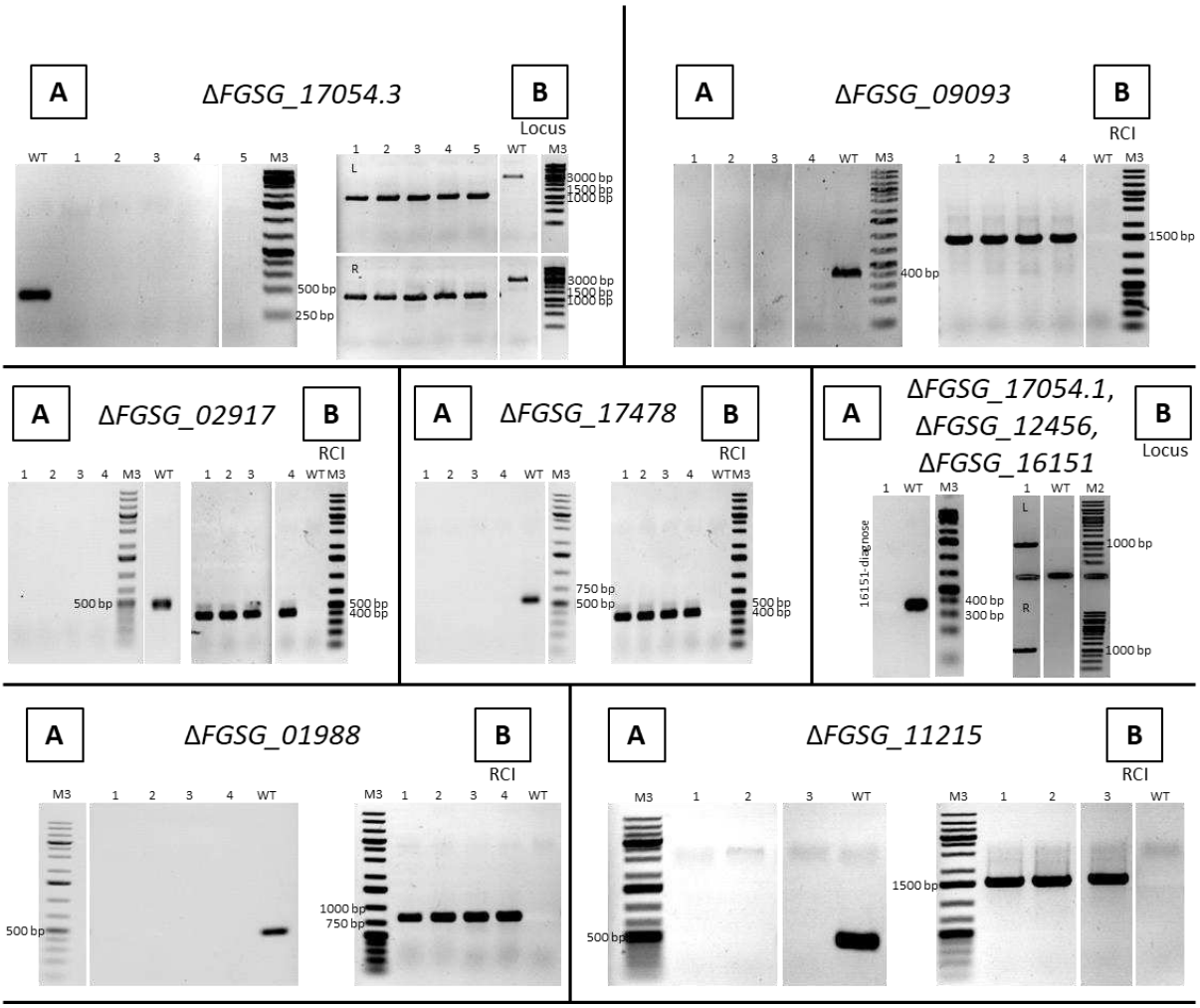

Figure 13: PCRs for deletion mutant verification. gDNA of antibiotics-resistant transformants was screened for the target gene (A) and the resistance cassette (B) by PCR. **A:** Internal PCRs of all genes deleted in this study. Primers bind within the DNA sequence of the target gene, thereby producing a band with a specific length with WT gDNA as template. With gDNA from deletion mutants as template the primers have no complementary binding site and no band is visible. **B:** Control PCRs of all genes deleted in this study. Two different techniques were used termed 'resistance cassette internal' ('RCI') and 'locus' PCR. RCI primers bind within the DNA sequence of the resistance cassette which is only present in deletion mutants. WT gDNA does not contain the respective sequence and no band is produced. Locus primers are two primer pairs of which one primer binds within the resistance cassette and the other primer outside of the upstream flanking region or the downstream flanking region, respectively. Here, both primer pairs generate a band with a specific length with deletion mutant gDNA as template. Corresponding to the respective flanking region the bands are marked L (left flanking region) or R (right flanking region). Since WT gDNA does not contain the resistance cassette, only the primer that binds outside of the flanking region can bind and no band is visible. Expected band lengths are listed in tables 2 and 3 in the materials and methods section.

25 single gene deletion mutants, 3 double deletion mutants, and 2 triple deletion mutants were established. Of the 25 single deletions, 16 targeted SREs. Specifically, 3 metallothioneins, 5 P450 monooxygenases, 2 FAD-binding monooxygenases, 2 tyrosinases, 2 cupredoxins, 3 chloroperoxidases, 1 lignin peroxidase, 1 galactose oxidase, 1 oxidase, 1 cellobiose dehydrogenase, 1 reductase, 1 ascorbate peroxidase, 1 nicotinamide nucleotide transhydrogenase (NNT), and 1 superoxide dismutase (SOD)

were deleted. An overview of all strains with storage code and number of individual mutants is provided in Supplementary table 1. In the following, the characterisation of all mutants ordered by their enzyme class is presented.

3.1.3 Characterisation of deletion mutants

The mutants were phenotypically characterised regarding virulence, vegetative growth, resistance towards oxidative stress, ROS-accumulation, and sexual reproduction. Virulence on wheat was assessed by inoculating flowering wheat spikelets with conidiospores of the tested strains. At 21 dpi the spreading of FHB-symptoms was documented. To test the mutants for radial growth and resistance against oxidative stress, CM agar plates containing H_2O_2, menadione, or no additive were inoculated with mycelia plugs of the tested strains and incubated at 28 °C for three days (3 dpi) before the colony areas were measured. Differences in colony areas were considered significant at $p \leq 10^{-3}$, very significant at $p \leq 10^{-4}$, and highly significant at $p \leq 10^{-5}$ calculated with a two-tailed homoscedastic t-test. ROS-accumulation was tested by soaking 3 days old mycelia grown on CM agar with 0.2% nitro blue tetrazolium chloride (NBT). Upon reaction with superoxide NBT forms a dark blue precipitate. Colour intensity of mutant mycelia was compared with WT mycelia. Fertility was assessed by cultivating the strains on wheat nodes and the ratio of generated “perithecia nests” (1 perithecia nest = occurrence of any amount of perithecia on a wheat node section) per wheat node was calculated and compared to the WT. Differences in this ratio between mutants and WT were considered significant at $p \leq 0.05$, very significant at $p \leq 0.005$, and highly significant at $p \leq 0.0005$ calculated with a two-tailed homoscedastic t-test. WT strain 8/1 was used as reference in all experiments and is referred to as WT. In fertility assays the hyperfertile WT strain PH1 was used as a positive control and is referred to as PH1.

3.1.3.1 Characterisation of monooxygenases

9 monooxygenases were deleted in this study, specifically 5 P450s (FGSG_03700, FGSG_07765, FGSG_01745, FGSG_16458, FGSG_03498), 2 secreted FAD-dependent monooxygenases (FGSG_11215, FGSG_17478), and 2 secreted tyrosinases (FGSG_11528, FGSG_01988). The deletion mutants showed the same colony diameter as the WT on CM agar (Figure 14). When growing on CM-agar containing H_2O_2 (10 mM, 15 mM, and 20 mM) or menadione (10 µM, 50 µM, and 100 µM), no significant differences to the WT colony area were observed (Figure 14).

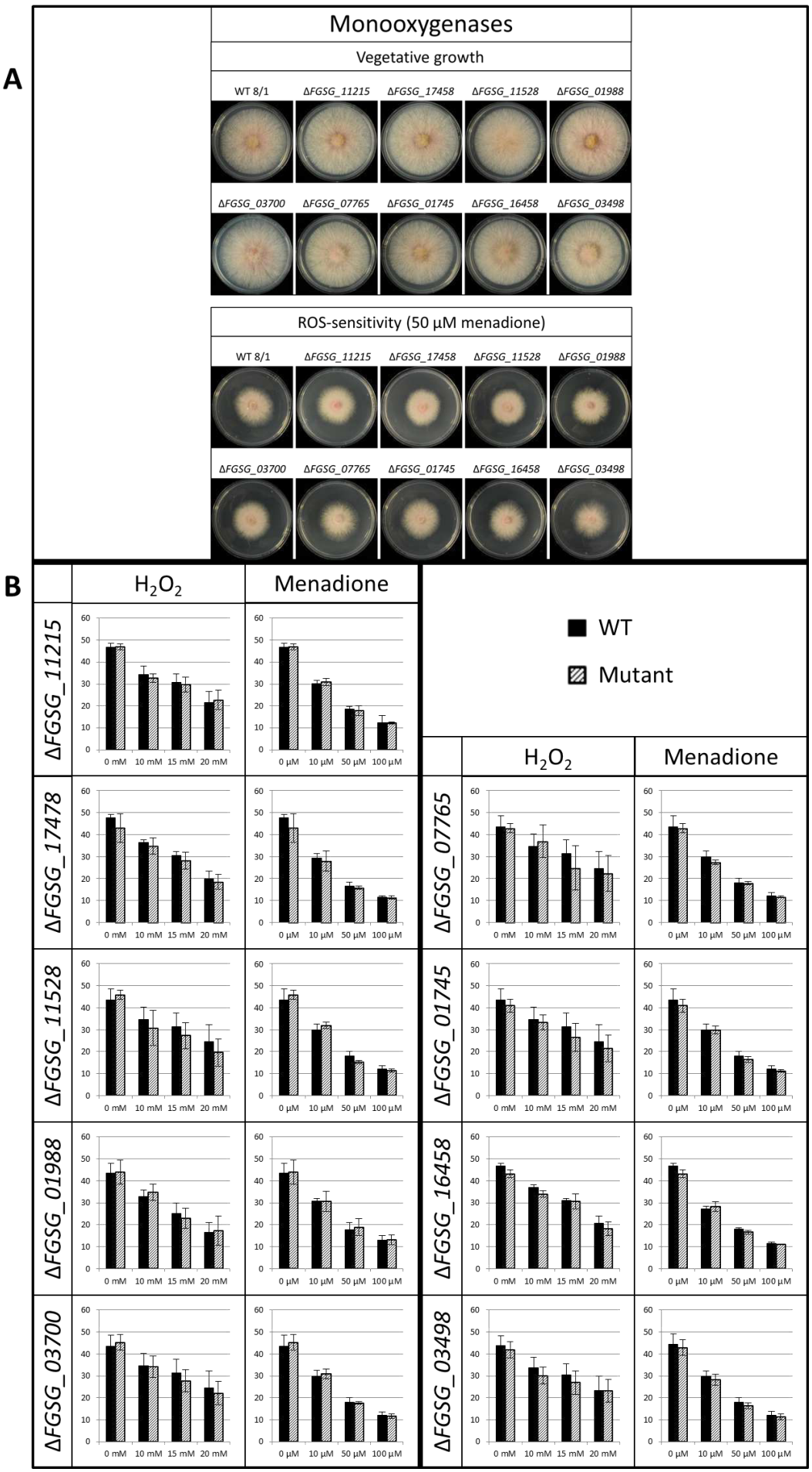
A
Monooxygenases
Vegetative growth
WT 8/1
ΔFGSG_11215
ΔFGSG_17458
ΔFGSG_11528
ΔFGSG_01988
ΔFGSG_03700
ΔFGSG_07765
ΔFGSG_01745
ΔFGSG_16458
ΔFGSG_03498
ROS-sensitivity (50 µM menadione)
B
H2O2
Menadione
WT
Mutant
0 mM 10 mM 15 mM 20 mM
0 µM 10 µM 50 µM 100 µM

Figure 14: Vegetative growth of monooxygenase deletion mutants with and without oxidative stress. Strains were cultivated on CM-agar without additives and CM-agar containing H_2O_2 (10 mM, 15 mM, 20 mM) or menadione (10 µM, 50 µM, 100 µM) for three days before the colony area was measured. **A:** Exemplary photographs showing colony morphology on CM-agar (vegetative growth) and on CM-agar containing 50 µM menadione (ROS-sensitivity). Colony morphology of monooxygenase deletion mutants did not differ from the WT. **B:** Colony area of all mutants compared to the WT represented as a bar diagram. Each mutant is presented individually because growth rate of WT (black bars) and mutants (striated bars) differed between individual experiments. Y-axis represents the colony area, X-axis the applied concentrations of H_2O_2 and menadione. Deviations from the WT were tested for significance using a two-tailed homoscedastic t-test (significant: $p < 10^{-3}$). None of the mutations led to significant colony area deviations on any of the applied additive concentrations. Error bars indicate the standard deviation (n = 6)

ROS-accumulation of monooxygenase deletion mutants was tested by staining 3 days old mycelia on CM agar with 0.2% NBT. After an incubation of 40 min the colouration of all mutants was WT-like (Figure 15).

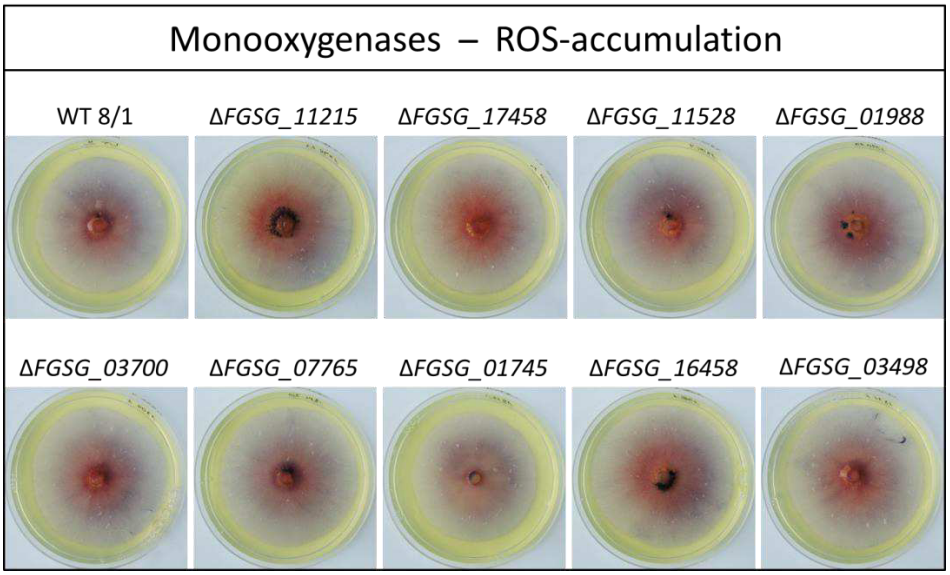

Figure 15: ROS-accumulation of monooxygenase deletion mutants. Strains were cultivated on CM-agar for 3 days before flooding the plates with 0.2% NBT. Upon reaction with superoxide NBT forms a blue precipitate. The intensity of blue colouration serves as an indicator for ROS-accumulation. None of the mutants show a deviation from the WT phenotype. (n = 2)

Pathogenicity of monooxygenase deletion mutants was assessed on wheat heads. At 21 dpi, all spikelets of wheat heads inoculated with WT and monooxygenase deletion mutant conidiospores showed premature bleaching, demonstrating that all mutants were able to fully infect wheat heads at 21 dpi (Figure 16).

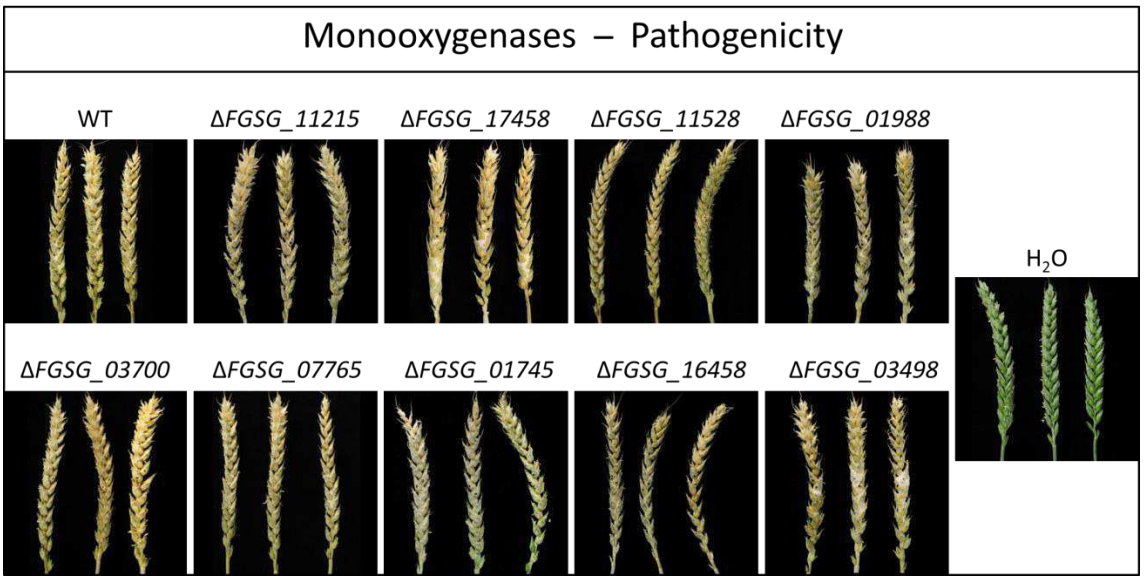

Figure 16: Pathogenicity of monooxygenase deletion mutants on wheat heads. 200 conidiospores of the tested strains were inoculated in 2 wheat spikelets in the centre of wheat heads in early anthesis. After an incubation period of 21 days in controlled conditions the disease pattern was assessed. The pictures show infected wheat heads at 21 dpi. Yellow spikelets indicate premature bleaching, a typical sign for infected plant tissue. Non-infected plant tissue is green, as shown in the water control (H_2O). All mutants and the WT were able to fully infect wheat heads. n = 5

Fertility of monooxygenase deletion mutants was tested by inoculating detached wheat nodes with conidiospores of the respective strains. The amount of produced perithecia on detached wheat nodes did not differ significantly from the WT (Figure 17).

Together, the results demonstrate that this subset of monooxygenases has no significant impact on vegetative growth, ROS-sensitivity, ROS-accumulation, virulence, and sexual reproduction.

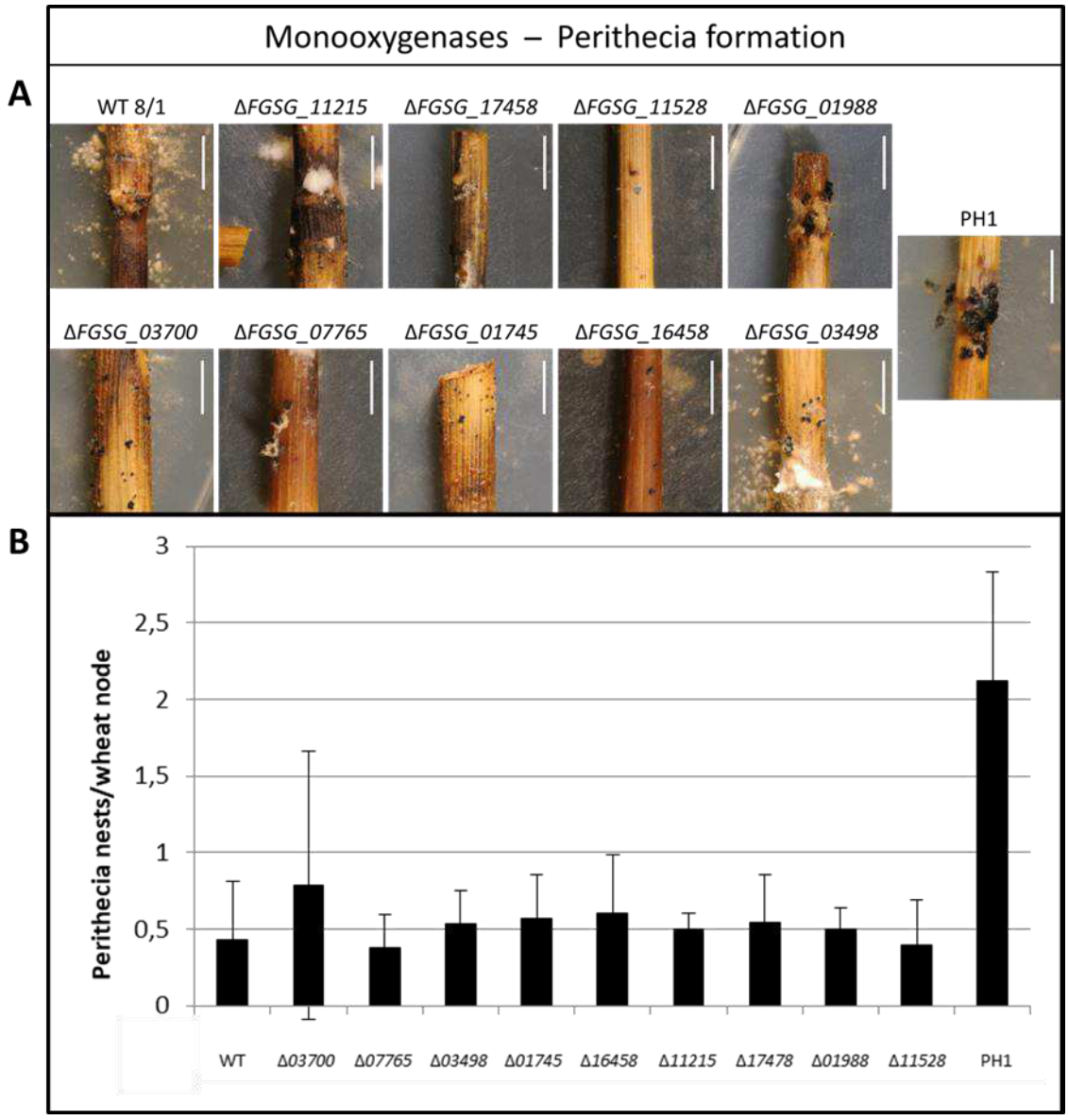

Figure 17: Fertility of monooxygenase deletion mutants. Detached wheat nodes from straw were inoculated with 1000 conidiospores of tested strains and incubated for 2 months with artificial night-daylight-cycle to induce perithecia formation. **A:** Close-up photographs of grown perithecia to demonstrate fertility. Clusters of perithecia are visible as little black dots on the wheat nodes. All monooxygenase deletion mutants were able to produce perithecia. Scale bars = 5 mm. **B:** Statistical evaluation of perithecia assays. Wheat nodes were subdivided in three sections (left edge, centre, right edge). If any amount of perithecia was present on one section this was counted as 1 perithecia nest. The sum of perithecia nests was divided by the number of assessed wheat node sections constituting the perithecia nests/wheat node ratio. Deviations from the WT were tested for significance using a two-tailed homoscedastic t-test (significant: $p < 0.05$). None of the mutants showed a statistically significant deviation from the WT ratio. Error bars indicate the standard deviation (n = 28).

3.1.3.2 Characterisation of peroxidases

Deletion mutants of 5 secreted peroxidases were established in this study. In detail, 3 chloroperoxidases (FGSG_03708, FGSG_03436, FGSG_02341), 1 ascorbate/cytochrome c peroxidase (FGSG_04434), and 1 lignin peroxidase (FGSG_16013) were disrupted. The

chloroperoxidase FGSG_03708 single deletion mutant (Δ*FGSG_03708*) was the only one that showed reduced vegetative growth on CM-agar (Figure 18). Simultaneous deletion mutants of FGSG_03708 with the other 2 secreted chloroperoxidases FGSG_02341 and FGSG_03436 were generated to see if this phenotype would intensify. However, the double deletion mutant ΔΔ*FGSG_02341;03708* and the triple deletion mutant ΔΔΔ*FGSG_02341;03708;03436* showed the same growth rate as Δ*FGSG_03708* (Figure 18).

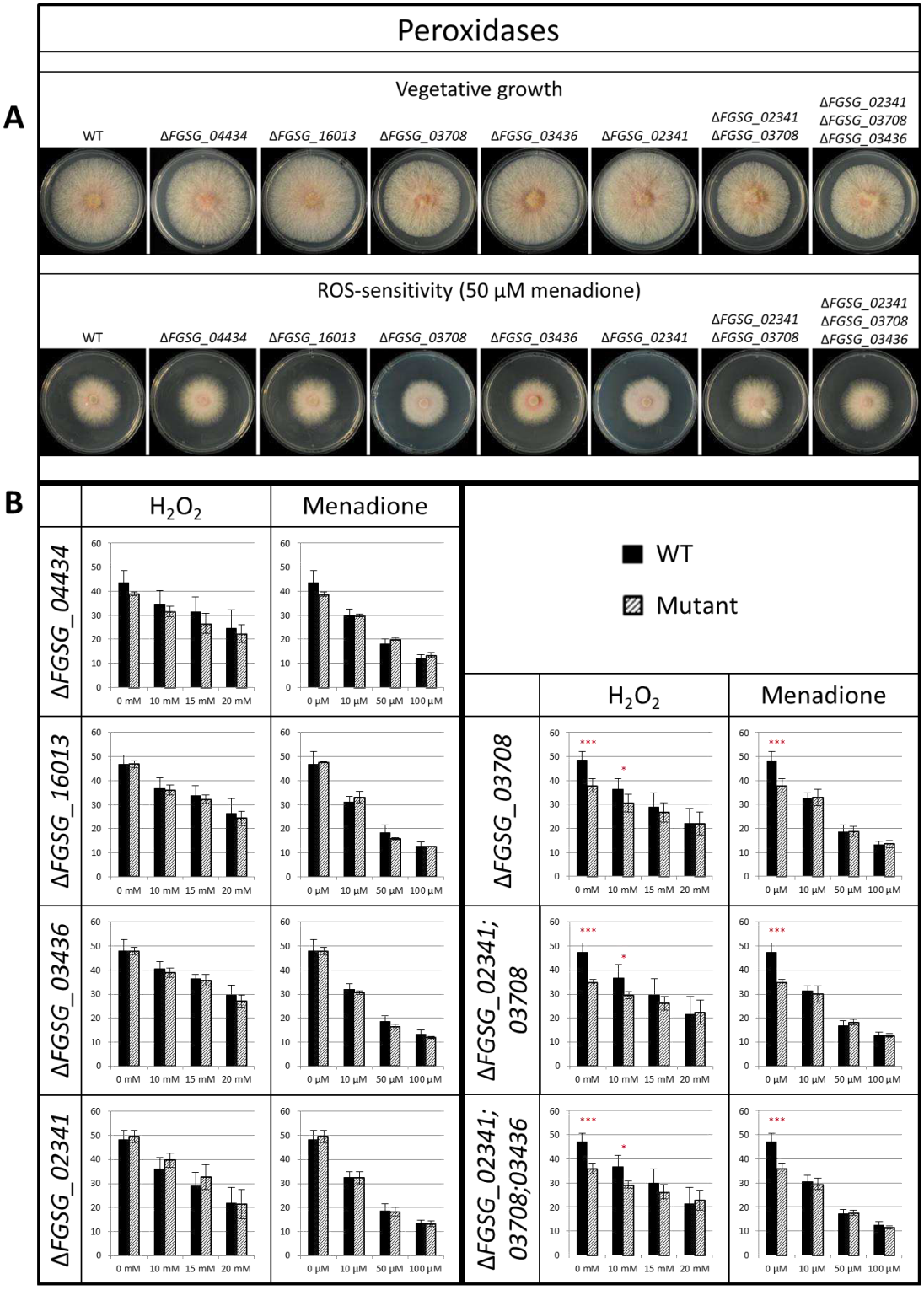

Figure 18: Vegetative growth of peroxidase deletion mutants with and without oxidative stress. Strains were cultivated on CM-agar without additives and CM-agar containing H_2O_2 (10 mM, 15 mM, 20 mM) or menadione (10 µM, 50 µM, 100 µM) for three days before the colony area was measured. **A:** Exemplary photographs showing colony morphology on CM-agar (vegetative growth) and on CM-agar containing 50 µM menadione (ROS-sensitivity). Vegetative growth of mutants lacking the chloroperoxidase FGSG_03708 (Δ*FGSG_03708*, ΔΔ*FGSG_02341;03708*, ΔΔΔ*FGSG_02341;03708;03436*) show a smaller colony area than the WT. **B:** Colony area of all mutants compared to the WT represented as a bar diagram. Each mutant is presented individually because growth rate of WT (black bars) and mutants (striated bars) differed between individual experiments. Y-axis represents the colony area, X-axis the applied concentrations of H_2O_2 and menadione. Deviations from the WT were tested for significance using a two-tailed homoscedastic t-test (1 asterisk: significant, $p < 10^{-3}$; 2 asterisks: very significant, $p < 10^{-4}$; 3 asterisks: highly significant, $p < 10^{-5}$). Mutants lacking the chloroperoxidase FGSG_03708 (Δ*FGSG_03708*, ΔΔ*FGSG_02341;03708*, ΔΔΔ*FGSG_02341;03708;03436*) are impaired in vegetative growth. Their colony area is approximately 10 cm² smaller than WT colonies (highly significant, $p < 10^{-5}$, three asterisks). In presence of 10 mM H_2O_2 the average colony area of those mutants is approximately 6 cm² smaller than WT colonies (significant, $p < 10^{-3}$, one asterisk). In presence of 15 mM H_2O_2 the difference is not statistically significant anymore. At 20 mM H_2O_2 colony areas of Δ*FGSG_03708* mutants and the WT are equal. Menadione stress does not show such concentration dependency. At all applied concentrations the colony areas of Δ*FGSG_03708* mutants and the WT are equal. The other peroxidase deletion mutants show no significant differences to the WT colony area. Error bars indicate the standard deviation (n = 6).

Interestingly, the vegetative growth-phenotype of Δ*FGSG_03708* can be linked to oxidative stress. Cultivating the mutant on CM-agar containing 10, 50, and 100 µM of the superoxide-stress inducing agent menadione restored WT-like growth (Figure 19). Cultivation on CM-agar containing 10, 15, and 20 mM H_2O_2 revealed a concentration dependency of the Δ*FGSG_03708* growth-phenotype. With increasing H_2O_2-concentration the growth of Δ*FGSG_03708* approached more and more WT-like behaviour (Figure 19).

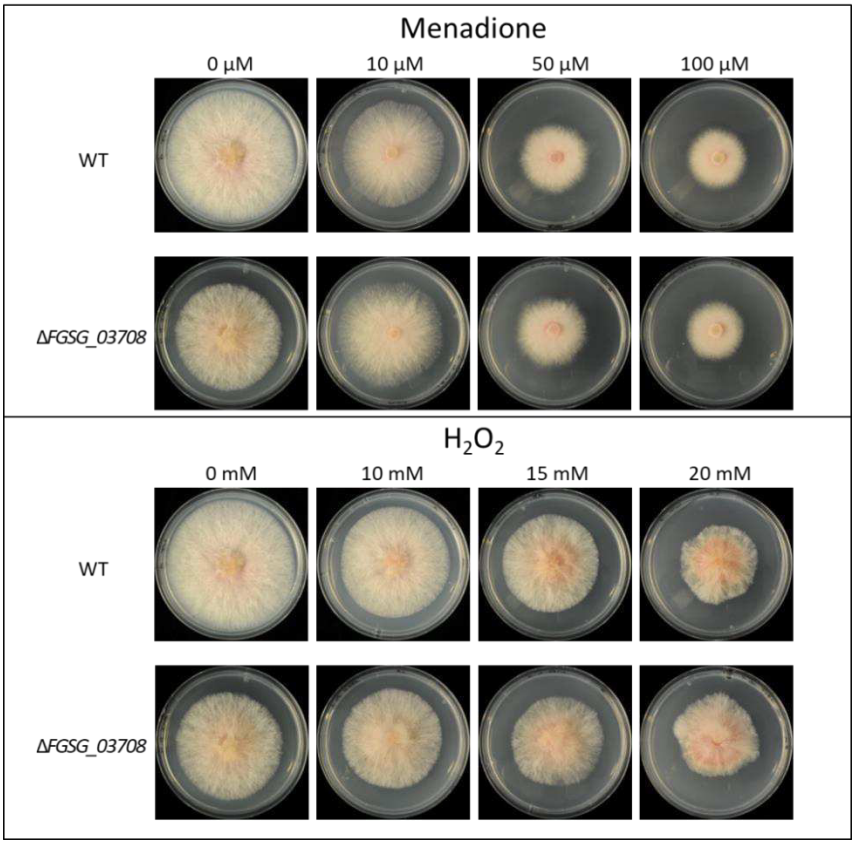

Figure 19: Vegetative growth reduction of Δ*FGSG_03708* is connected to oxidative stress. The photographs show the radial growth of *F. graminearum* WT and Δ*FGSG_03708* on CM-agar containing increasing concentrations of menadione or H_2O_2. At 10 µM, 50 µM and 100 µM the colony area of Δ*FGSG_03708* is WT-like. At 10 mM, 15 mM, and 20 mM H_2O_2 the colony area of Δ*FGSG_03708* gradually approaches the colony area of the WT.

Deducing from these observations that the role of FGSG_03708 is ROS-dependent, a quantitative real time PCR was performed comparing FGSG_03708-expression in the absence and the presence of oxidative stress inducing agents. The experiment revealed that FGSG_03708 is downregulated by the factor 5.4 (± 0.02) in the presence of 50 µM menadione and by the factor 1.4 (± 0.02) in the presence of 20 mM H_2O_2 (Figure 20).

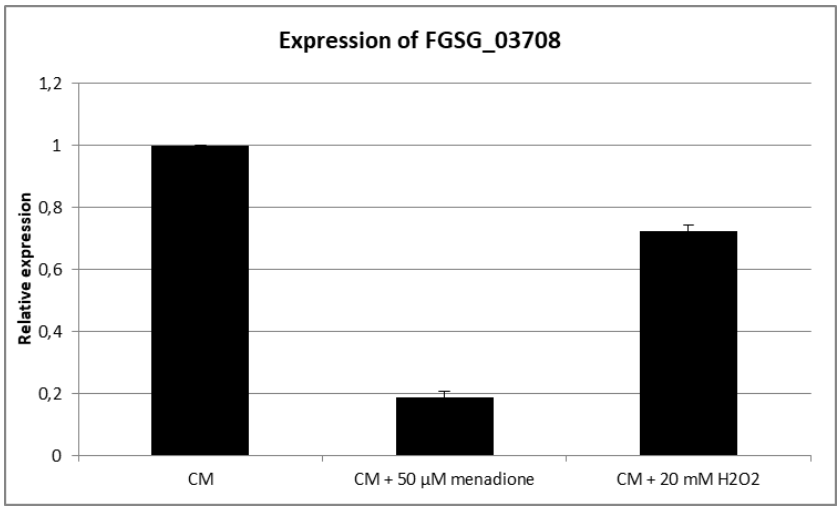

Figure 20: Quantitative real-time PCR of FGSG_03708. Relative expression of FGSG_03708 in WT cells was assessed during growth on CM-agar without stress-inducing agent (left bar), with 50 µM menadione (central bar), and with 20 mM H_2O_2 (right bar). Relative expression on normal CM-agar is set to 1. Relative to this value the expression level of FGSG_03708 is at 0.186 on 50 µM menadione and at 0.725 on 20 mM H_2O_2. Error bars indicate the standard deviation (n = 3).

ROS-accumulation of peroxidase deletion mutants was tested by staining 3 days old mycelia on CM agar with 0.2% NBT. After an incubation of 40 min, the rim of the Δ*FGSG_03708*, ΔΔ*FGSG_02341;03708*, and ΔΔΔ*FGSG_02341;03708;03436* colonies showed a halo of dark blue colouration that was broader and more intense than in the WT colony (Figure 21) suggesting higher ROS-accumulation in hyphal tips. Colouration of the other peroxidase deletion mutants (Δ*FGSG_04434*, Δ*FGSG_16013*) was WT-like.

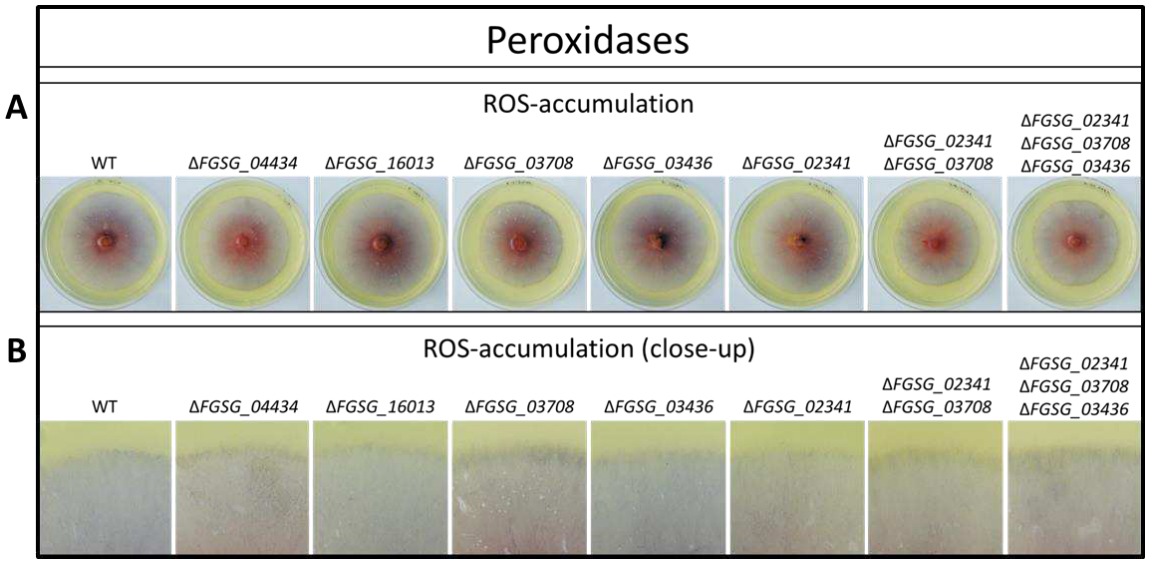

Figure 21: ROS-accumulation of peroxidase deletion mutants. Strains were cultivated on CM-agar for 3 days before flooding of the plate with 0.2% NBT. Upon reaction with superoxide NBT forms a blue precipitate. The intensity of blue colouration serves as an indicator for ROS-accumulation. **A:** Whole plate view. **B:** Detailed view of the colony rim. WT mycelium shows a narrow halo of dark blue colouring in hyphal tips. In mutants lacking the chloroperoxidase FGSG_03708 (Δ*FGSG_03708*, ΔΔ*FGSG_02341;03708*, ΔΔΔ*FGSG_02341;03708;03436*) the halo is broader and more intense suggesting stronger ROS-accumulation. n = 4

Pathogenicity of peroxidase deletion mutants was assessed on wheat heads. At 21 dpi, all spikelets of wheat heads inoculated with WT and peroxidase deletion mutant conidiospores showed premature bleaching, demonstrating that all mutants were able to fully infect wheat heads at 21 dpi (Figure 22).

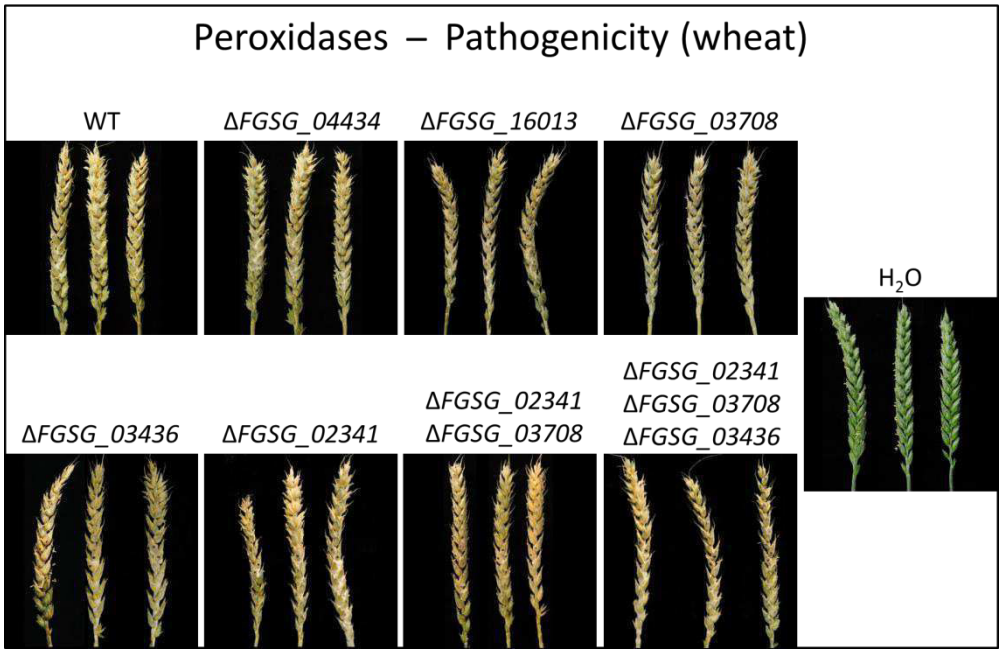

Figure 22: Pathogenicity of peroxidase deletion mutants on wheat heads. 200 conidiospores of the tested strains were inoculated in 2 wheat spikelets in the centre of wheat heads in early anthesis. After an incubation period of 21 days in controlled conditions, the disease pattern was assessed. The pictures show infected wheat heads at 21 dpi. Yellow spikelets indicate premature bleaching, a typical sign for infected plant tissue. Non-infected plant tissue is green, as shown in the water control (H_2O). All mutants and the WT were able to fully infect wheat heads. n = 5

In addition to virulence on wheat heads, the chloroperoxidase triple deletion mutant ΔΔΔ*FGSG_02341;03708;03436* was tested for virulence on maize cobs by inoculating the silk channels of maize cobs with conidiospores. The experiment showed that the triple deletion mutant, like the WT, is able to fully infect maize cobs within 5 weeks after infection (Figure 23).

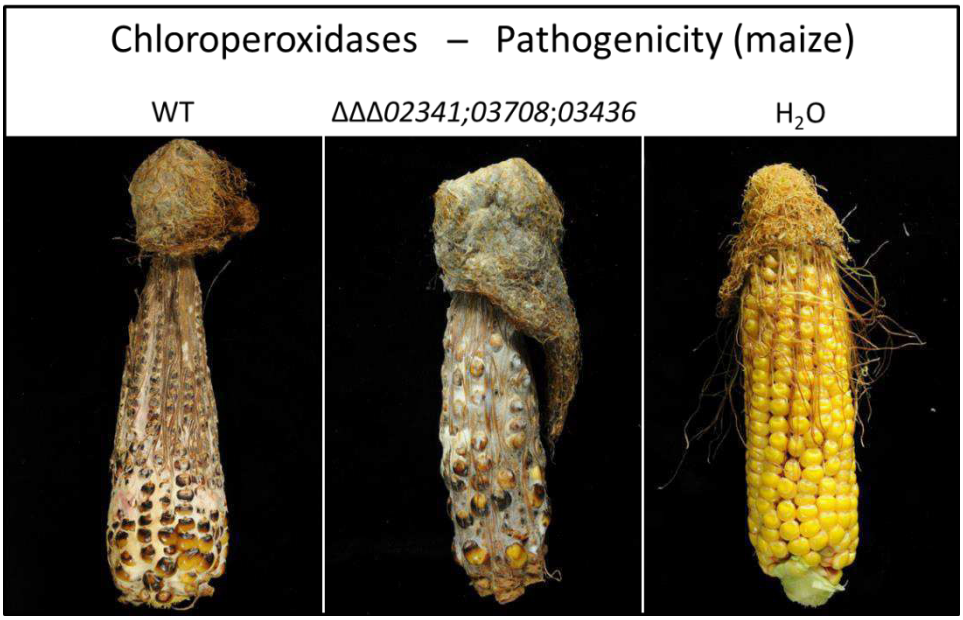

Figure 23: Pathogenicity of the chloroperoxidase triple deletion mutant ΔΔΔ*FGSG_02341;03708;03436* on maize cobs. 2×10^5 conidiospores of tested strains were injected in the silk channel of maize cobs and incubated for 5 weeks. The left picture shows a cob infected by the WT, the middle picture shows a cob infected by ΔΔΔ*FGSG_02341;03708;03436*, the right one shows the water control. Black coloured kernels and white mycelia visible on the cob surface indicate infected tissue. Both the WT and ΔΔΔ*FGSG_02341;03708;03436* are able to infect maize cobs after 5 weeks. n = 18

Fertility of peroxidase deletion mutants was tested by inoculating detached wheat nodes with conidiospores of the respective strains. Interestingly, the double and triple chloroperoxidase deletion mutants showed increased perithecia production compared to the WT (Figure 24). All chloroperoxidase single deletions were WT-like in this regard which indicates a cumulative effect. Deletion of the ascorbate/cytochrome c peroxidase FGSG_04434 also led to increased perithecia production (Figure 24). The perithecia assays were subject to strong variations in all mutants regarding the amount of produced perithecia which resulted in high standard deviations. The lignin-peroxidase deletion mutant Δ*FGSG_16013* was WT-like in all experiments.

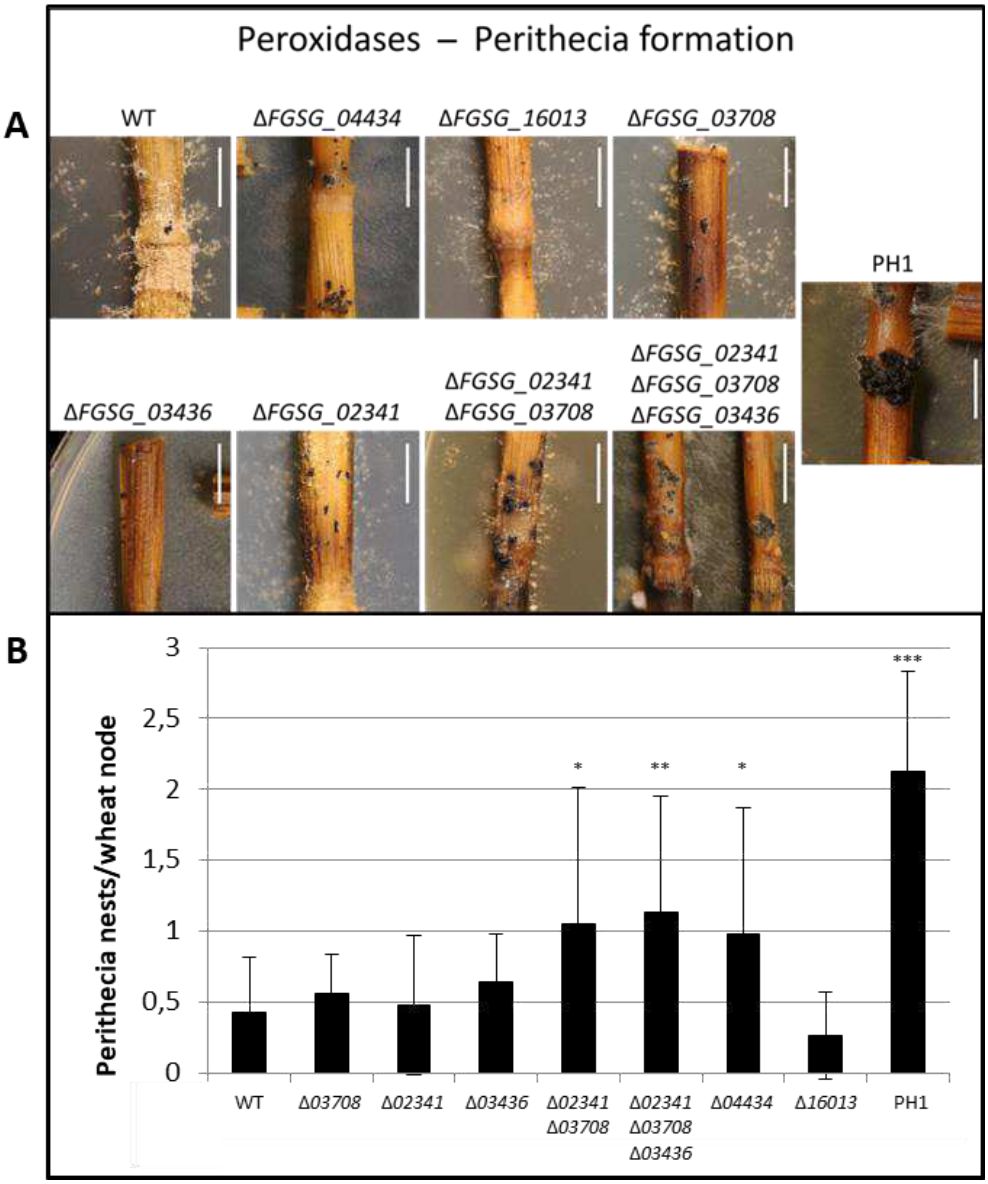

Figure 24: Fertility of peroxidase deletion mutants. Detached wheat nodes from straw were inoculated with 1000 conidiospores of tested strains and incubated for 2 months with artificial night-daylight-cycle to induce perithecia formation. **A:** Close-up photographs of grown perithecia to demonstrate fertility. Perithecia are visible a little black dots on the wheat nodes. All peroxidase deletion mutants were able to produce perithecia. Scale bars = 5 mm. **B:** Statistical evaluation of perithecia assays. Wheat nodes were subdivided in three sections (left edge, centre, right edge). If any amount of perithecia was present on one section this was counted as 1 perithecia nest. The sum of perithecia nests was divided by the number of assessed wheat node sections constituting the perithecia nests/wheat node ratio. Deviations from the WT were tested for significance using a two-tailed homoscedastic t-test (1 asterisk: significant, $p < 0.05$; 2 asterisks: very significant $p < 0.005$; 3 asterisks: highly significant, $p < 0.0005$). While the chloroperoxidase single deletion mutants Δ*FGSG_03708*, Δ*FGSG_02341*, and Δ*FGSG_03436* showed WT-like perithecia production, the double deletion mutant ΔΔ*FGSG_02341;03708* and triple deletion mutant ΔΔΔ*FGSG_02341;03708;03436* showed a significantly and very significantly increased perithecia production, respectively. The WT showed a perithecia nests/wheat node ratio of 0.43, ΔΔ*FGSG_02341;03708* a ratio of 1.05, and ΔΔΔ*FGSG_02341;03708;03436* a ratio of 1.13. Also, the deletion of ascorbate/cytochrome c peroxidase FGSG_04434 led to significantly increased perithecia production with a ratio of 0.98. Deletion of lignin peroxidase FGSG_16013 did not lead to significant changes in perithecia production. Error bars indicate the standard deviation (n = 54).

3.1.3.3 Characterisation of oxidases

2 secreted oxidases (FGSG_11399, FGSG_09093) were deleted in this study. Growth rate of the deletion mutants on CM-agar with and without oxidative stress inducing agents was identical to the WT (Figure 25).

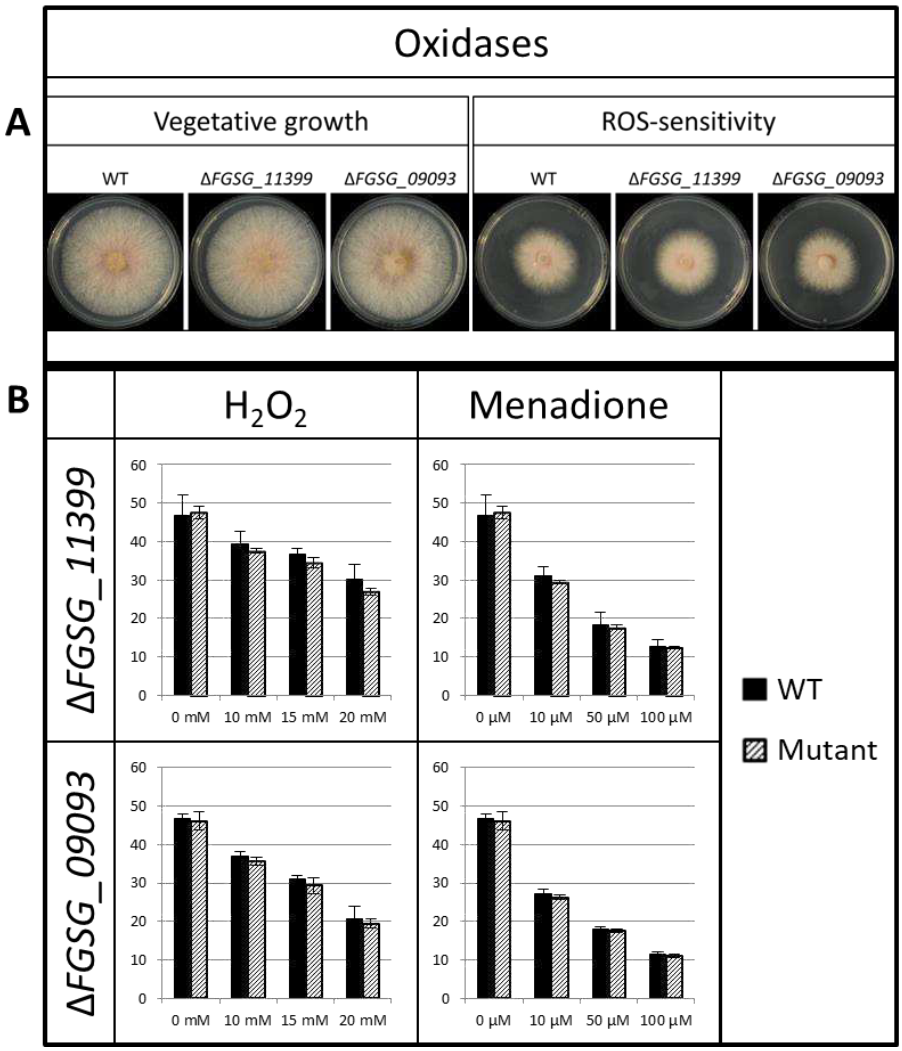

Figure 25: Vegetative growth of oxidase deletion mutants with and without oxidative stress. Strains were cultivated on CM-agar without additives and CM-agar containing H_2O_2 (10 mM, 15 mM, 20 mM) or menadione (10 µM, 50 µM, 100 µM) for three days before the colony area was measured. **A:** Exemplary photographs showing colony morphology on CM-agar (vegetative growth) and on CM-agar containing 50 µM menadione (ROS-sensitivity). Colony morphology of oxidase deletion mutants did not differ from the WT. **B:** Colony area of both mutants compared to the WT represented as a bar diagram. Each mutant is presented individually because growth rate of WT (black bars) and mutants (striated bars) differed between individual experiments. Y-axis represents the colony area, X-axis the applied concentrations of H_2O_2 and menadione. Deviations from the WT were tested for significance using a two-tailed homoscedastic t-test (significant: $p < 10^{-3}$). None of the mutations led to significant colony area deviations on any of the applied additive concentrations. Error bars indicate the standard deviation (n = 6).

ROS-accumulation of oxidase deletion mutants was tested by staining 3 days old mycelia on CM agar with 0.2% NBT. After an incubation of 40 min the colouration of both mutants was WT-like (Figure 26).

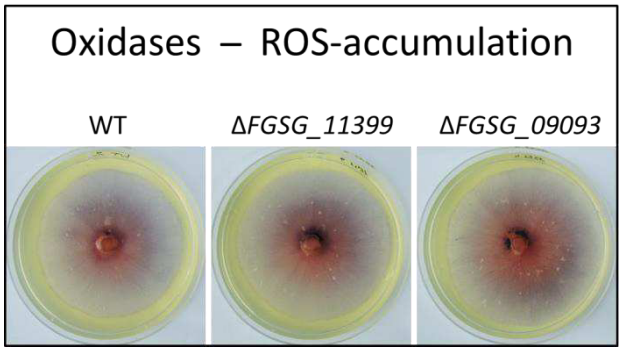

Figure 26: ROS-accumulation of oxidase deletion mutants. Strains were cultivated on CM-agar for 3 days before flooding the plates with 0.2% NBT. Upon reaction with superoxide NBT forms a blue precipitate. The intensity of blue colouration serves as an indicator for ROS-accumulation. The mutants show no deviation from the WT phenotype. n = 4

Pathogenicity of oxidase deletion mutants was assessed on wheat heads. At 21 dpi, all spikelets of wheat heads inoculated with WT and oxidase deletion mutant conidiospores showed premature bleaching, demonstrating that both mutants were able to fully infect wheat heads at 21 dpi (Figure 27).

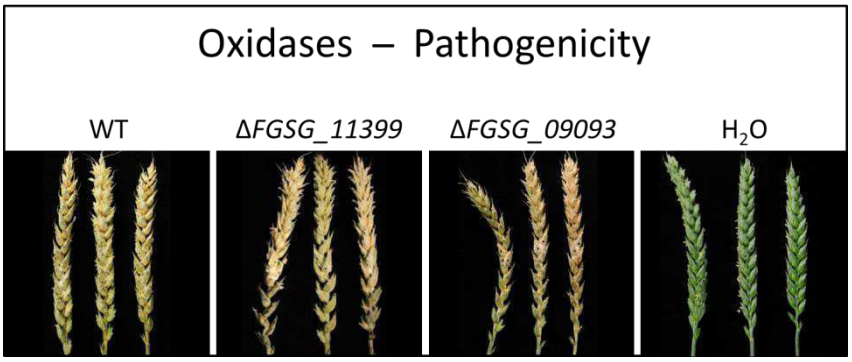

Figure 27: Pathogenicity of oxidase deletion mutants on wheat heads. 200 conidiospores of the tested strains were inoculated in 2 wheat spikelets in the centre of wheat heads in early anthesis. After an incubation period of 21 days in controlled conditions, the disease pattern was assessed. The pictures show infected wheat heads at 21 dpi. Yellow spikelets indicate premature bleaching, a typical sign for infected plant tissue. Non-infected plant tissue is green, as shown in the water control (H_2O). Both mutants and the WT were able to fully infect wheat heads. n = 5

Fertility of oxidase deletion mutants was tested by inoculating detached wheat nodes with conidiospores of the respective strains. The amount of produced perithecia on detached wheat nodes did not differ significantly from the WT (Figure 28).

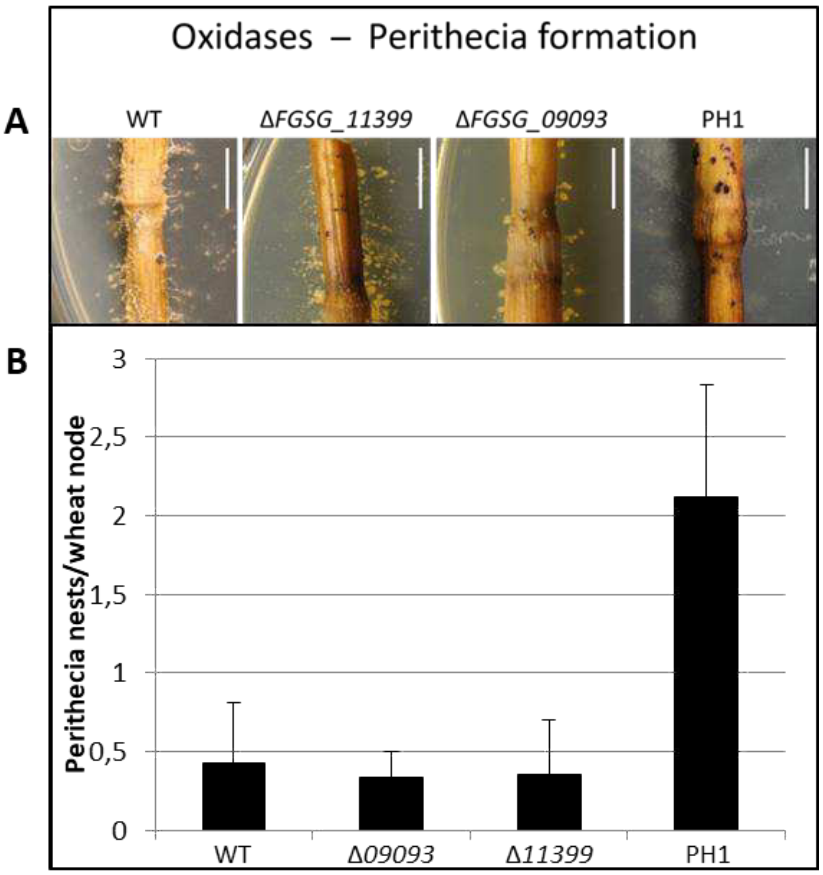

Figure 28: Fertility of oxidase deletion mutants. Detached wheat nodes from straw were inoculated with 1000 conidiospores of tested strains and incubated for 2 months with artificial night-daylight-cycle to induce perithecia formation. **A:** Close-up photographs of grown perithecia to demonstrate fertility. Perithecia are visible a little black dots on the wheat nodes. Both oxidase deletion mutants were able to produce perithecia. Scale bars = 5 mm. **B:** Statistical evaluation of perithecia assays. Wheat nodes were subdivided in three sections (left edge, centre, right edge). If any amount of perithecia was present on one section this was counted as 1 perithecia nest. The sum of perithecia nests was divided by the number of assessed wheat node sections constituting the perithecia nests/wheat node ratio. Deviations from the WT were tested for significance using a two-tailed homoscedastic t-test (significant: $p < 0.05$). Neither mutant showed a statistically significant deviation from the WT ratio. Error bars indicate the standard deviation (n = 21).

3.1.3.4 Characterisation of metallothioneins

F. graminearum expresses three metallothioneins, FGSG_17054, FGSG_12456, and FGSG_16151. A deletion mutant of the metallothionein FGSG_17054 (Δ*FGSG_17054.1*) showed strongly increased production of perithecia (Figure 29). On average, the ratio of perithecia clusters per wheat node was five times higher than in the WT and even higher than in the hyperfertile WT strain PH1 (Figure 30). Single deletion mutants of FGSG_12456 and FGSG_16151 did not change the amount of produced perithecia.

Simultaneous deletion of FGSG_12456 and FGSG_16151 in Δ*FGSG_17054.1* (ΔΔ*FGSG_17054.1;12456*, ΔΔΔ*FGSG_17054.1;12456;16151*) showed the same phenotype as Δ*FGSG_17054.1*. The hyperfertility of Δ*FGSG_17054.1*, however, was not reproducible upon repetition of the gene deletion. Both repetitions of the FGSG_17054 deletion (*ΔFGSG_17054.2* and Δ*FGSG_17054.3*) showed WT 8/1-like perithecia formation.

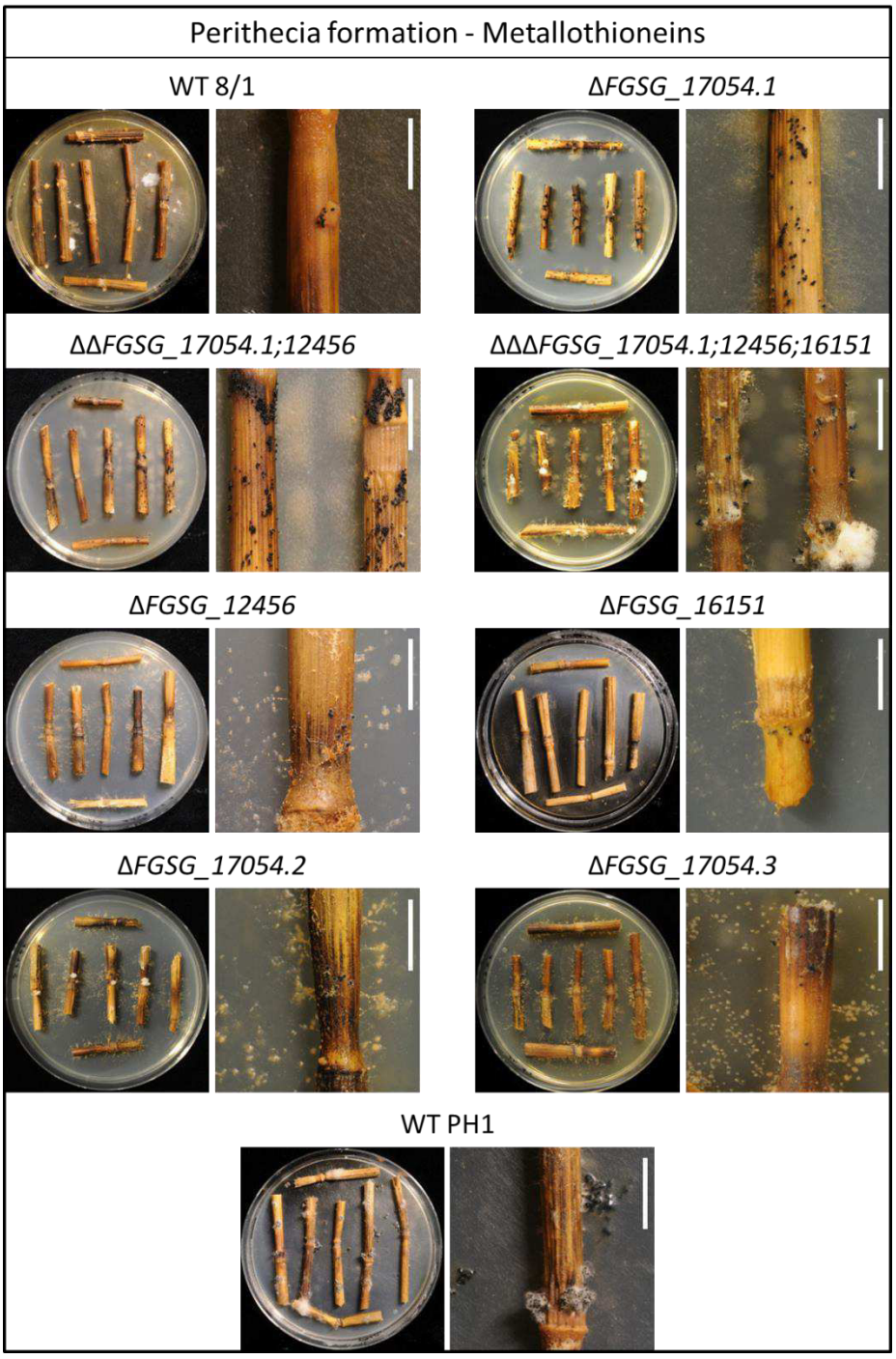

Figure 29: Fertility of metallothionein deletion mutants - photographs. Detached wheat nodes from straw were inoculated with 1000 conidiospores of tested strains and incubated for 2 months with artificial night-daylight-cycle to induce perithecia formation. Perithecia are visible as little black dots on the wheat nodes. All metallothionein deletion mutants were able to produce perithecia. For each mutant an overview (left) and a close-up (right) picture is shown. While the WT 8/1 mostly produced only sporadic and small nests of perithecia, FGSG_17054 deletion mutant Δ*17054.1* produced large amounts of perithecia on all wheat

nodes on the plate, similar to WT PH1. Repetitions of the FGSG_17054 deletion (Δ*17054.2* und Δ*17054.3*) did not show this increase in fertility. Deletions of FGSG_12465 and FGSG_16151 did not alter perithecia production and have no further influence on the phenotype during simultaneous deletion in the Δ*17054.1* background. Scale bars = 5 mm.

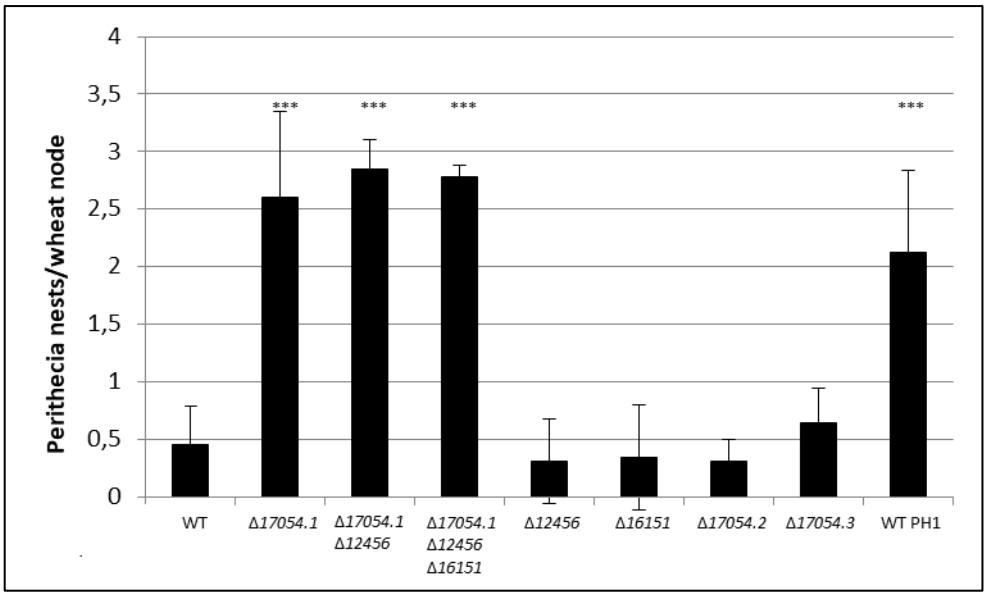

Figure 30: Fertility of metallothionein deletion mutants – statistical analysis. The bar diagram presents the statistical evaluation of the perithecia assays. Wheat nodes were subdivided in three sections (left edge, centre, right edge). If any amount of perithecia was present on one section this was counted as 1 perithecia nest. The sum of perithecia nests was divided by the number of assessed wheat node sections constituting the perithecia nests/wheat node ratio. Deviations from the WT 8/1 were tested for significance using a two-tailed homoscedastic t-test (1 asterisk: significant, $p < 0.05$; 2 asterisks: very significant, $p < 0.005$; 3 asterisks: highly significant, $p < 0.0005$). The first FGSG_17054 deletion mutant Δ*17054.1* and the simultaneous deletion mutants established in this background showed at least a 5-fold increase of the perithecia cluster/wheat node ratio compared to the WT 8/1. These changes were highly significant ($p < 0.0005$). The WT 8/1 showed a perithecia nests/wheat node ratio of 0.43, Δ*FGSG_17054.1* a ratio of 2.60, ΔΔ*FGSG_17054.1;12456* a ratio of 2.84, and ΔΔΔ*FGSG_17054.1;12456;16151* a ratio of 2.79. Deletion of the metallothioneins FGSG_12456 and FGSG_16151 caused no deviations from the WT 8/1 phenotype. Also, repetitions of the FGSG_17054 deletion (Δ*17054.2* and Δ*17054.3*) showed WT 8/1-like perithecia cluster/wheat node ratio. The hyperfertile WT PH1 strain was used as a positive control. Error bars indicate the standard deviation (n = 14).

Since Δ*FGSG_17054.1,* Δ*FGSG_17054.2* and Δ*FGSG_17054.3* showed contradictory results in the fertility assays, the mutants were screened for genetical differences. Southern-blotting of Δ*FGSG_17054.1* revealed a second integration of the deletion construct into the genome (Figure 31) which is not present in the repetitions (Δ*FGSG_17054.2* and Δ*FGSG_17054.3*). Considering the non-reproducibility of the fertility phenotype it is safe to assume that the increase in sexual activity in Δ*FGSG_17054.1* is caused by the second integration of the deletion construct and not by the deletion of FGSG_17054.

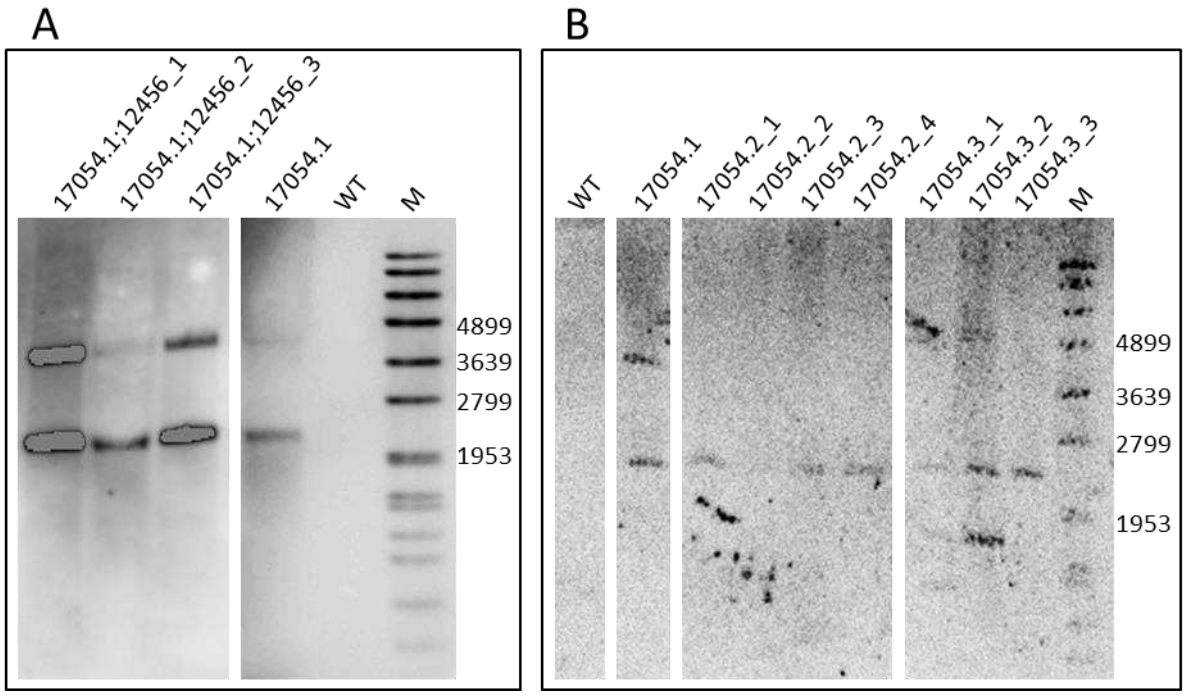

Figure 31: Southern blots of metallothionein FGSG_17054 deletion mutants. DNA was digested with *Hin*dIII, a digoxigenin labelled HYG cassette was used as a probe. The labelled fragment has a length of 2255 bp. **A:** Southern blot of the WT, the single deletion mutant of the first transformation 17054.1, and three mutants with a simultaneous deletion of metallothionein FGSG_12456 in the Δ*17054.1*-background. No band is visible in the WT column which was to be expected as no HYG cassette is present in the WT. The other columns show two bands. The lower band lies between the marker bands at 1953 bp and 2799 bp and presumably represents the expected fragment (2255 bp). The upper band lies between the marker bands at 3639 bp and 4899 bp. This band is not expected and shows that the deletion construct was integrated in an additional and unknown genetic locus. **B:** Southern blot of the WT, the single deletion mutant of the first transformation Δ*17054.1*, the mutants of the second independent deletion of FGSG_17054 (Δ*17054.2_1-4*), and the mutants of the third independent deletion of FGSG_17054 (Δ*17054.3_1-3*). As presented in A, Δ*17054.1* shows a second band between the marker bands at 3639 bp and 4899 bp. The mutants Δ*17054.2_1-4* and Δ*17054.3_1-3* show only the expected band between the marker bands at 1953 bp and 2799 bp. This shows that no second integration of the deletion construct took place in these mutants.

Vegetative growth of metallothionein mutants was assessed by incubating the tested strains on CM agar for 3 days. The deletion mutants showed the same colony diameter as the WT (Figure 32). When growing on CM-agar containing H_2O_2 (10 mM, 15 mM, and 20 mM) or menadione (10 µM, 50 µM, and 100 µM) for 3 days, no significant differences to WT colony area were observed (Figure 32). Since Δ*FGSG_17054.1,* Δ*FGSG_17054.2* and Δ*FGSG_17054.3* showed the same behaviour in all of the following assays they are depicted as Δ*FGSG_17054*.

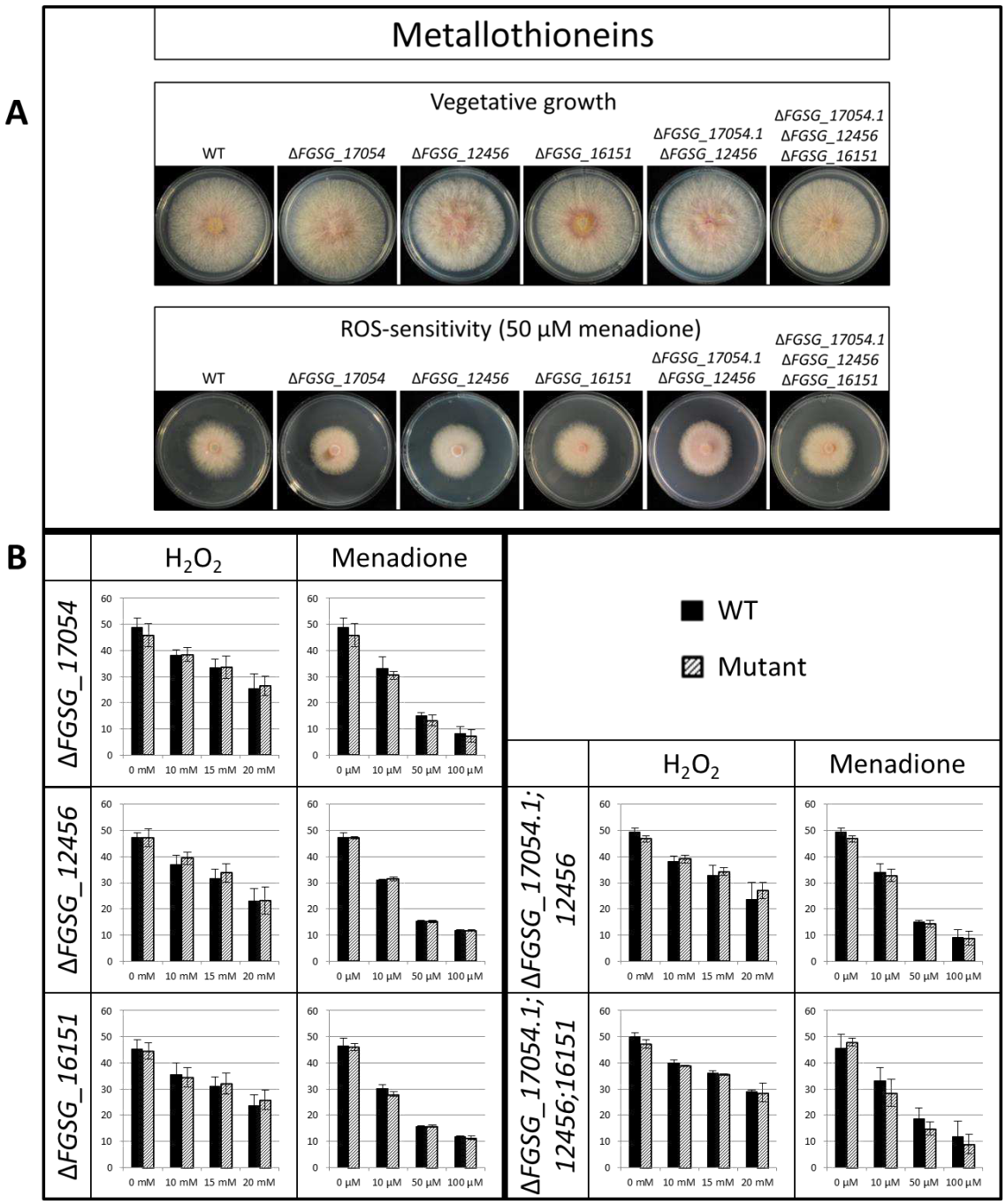

Figure 32: Vegetative growth of metallothionein deletion mutants with and without oxidative stress. Strains were cultivated on CM-agar without additives and CM-agar containing H_2O_2 (10 mM, 15 mM, 20 mM) or menadione (10 µM, 50 µM, 100 µM) for three days before the colony area was measured. **A:** Exemplary photographs showing colony morphology on CM-agar (vegetative growth) and on CM-agar containing 50 µM menadione (ROS-sensitivity). Colony morphology of metallothionein deletion mutants did not differ from the WT. **B:** Colony area of all mutants compared to the WT represented as a bar diagram. Each mutant is presented individually because the growth rate of WT (black bars) and mutants (striated bars) differed between individual experiments. Y-axis represents the colony area, X-axis the applied concentrations of H_2O_2 and menadione. Deviations from the WT were tested for significance using a two-tailed homoscedastic t-test (significant: $p < 0.05$). None of the mutations led to significant colony area deviations on any of the applied additive concentrations. Error bars indicate the standard deviation (n = 6).

ROS-accumulation of metallothionein deletion mutants was tested by staining 3 days old mycelia on CM agar with 0.2% NBT. After an incubation of 40 min the colouration of all mutants was WT-like (Figure 33).

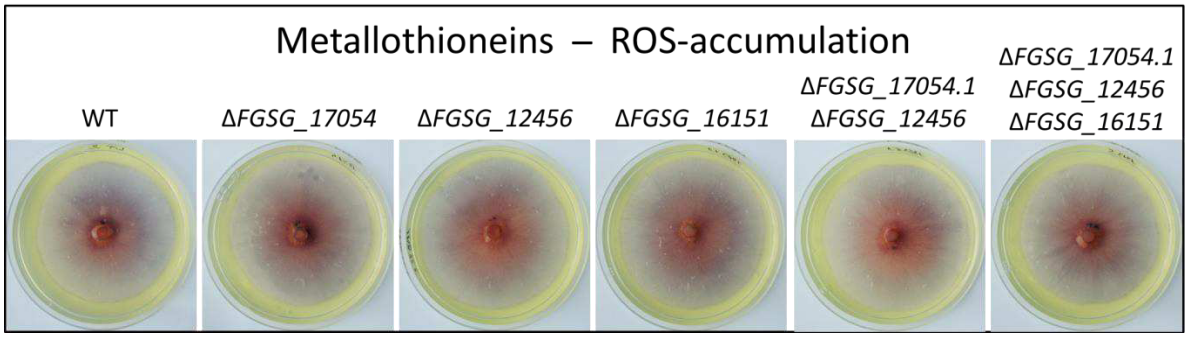

Figure 33: ROS-accumulation of metallothionein deletion mutants. Strains were cultivated on CM-agar for 3 days before flooding the plates with 0.2% NBT. Upon reaction with superoxide NBT forms a blue precipitate. The intensity of blue colouration serves as an indicator for ROS-accumulation. None of the mutants show a deviation from the WT phenotype. n = 2

Pathogenicity of metallothionein deletion mutants was assessed on wheat heads. At 21 dpi, all spikelets of wheat heads inoculated with WT and metallothionein deletion mutant conidiospores showed premature bleaching, demonstrating that all mutants were able to fully infect wheat heads at 21 dpi (Figure 34).

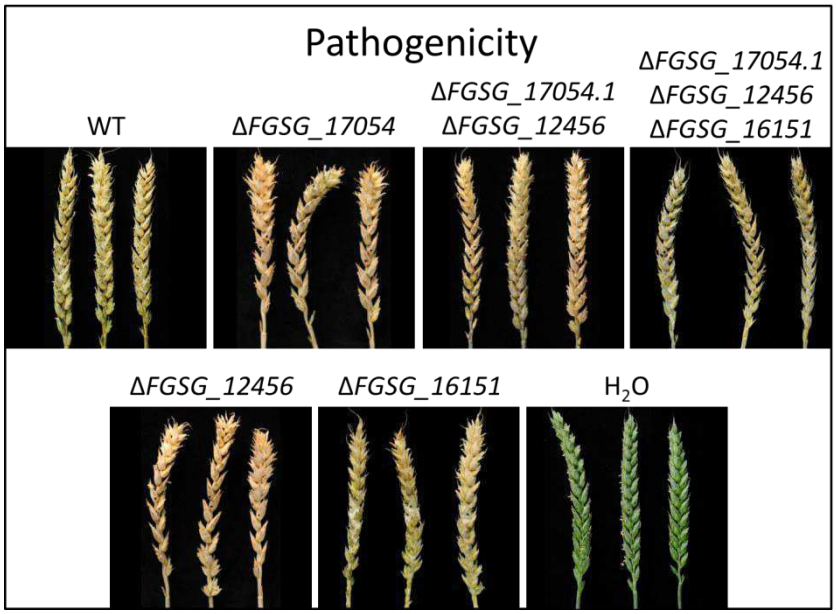

Figure 34: Pathogenicity of metallothionein deletion mutants on wheat heads. 200 conidiospores of the tested strains were inoculated in 2 wheat spikelets in the centre of wheat heads in early anthesis. After an incubation period of 21 days in controlled conditions, the disease pattern was assessed. The pictures show infected wheat heads at 21 dpi. Yellow spikelets indicate premature bleaching, a typical sign for infected plant tissue. Non-infected plant tissue is green, as shown in the water control (H_2O). All mutants were able to fully infect wheat heads. n = 10

In addition to virulence on wheat heads, the metallothionein triple deletion mutant (ΔΔΔ*FGSG_17054.1;12456;16151*) was tested for virulence on maize cobs by inoculating the silk channels of maize cobs with conidiospores. The experiment showed that the triple deletion mutant, like the WT, is able to fully infect maize cobs within 5 weeks after infection (Figure 35).

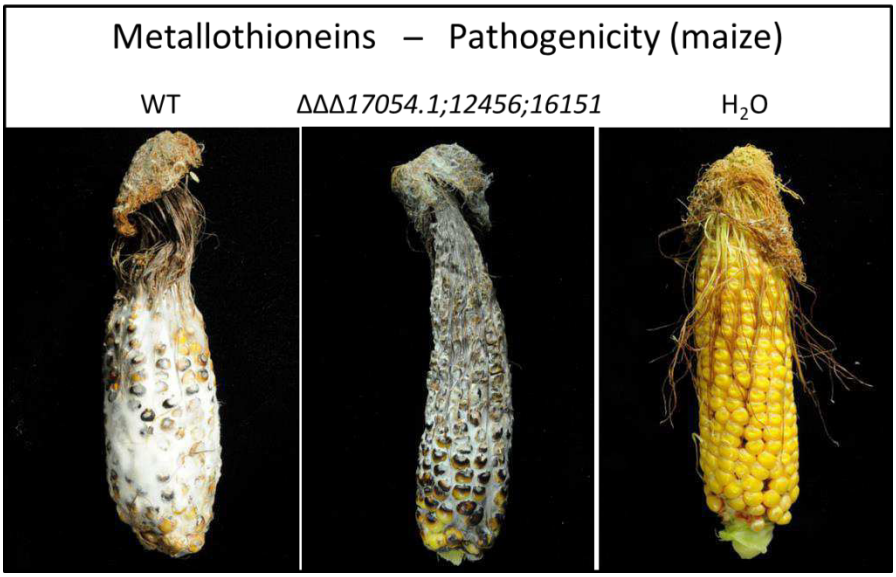

Figure 35: Pathogenicity of the metallothionein triple deletion mutant ΔΔΔ*FGSG_17054.1;12456;16151* on maize cobs. 2×10^5 conidiospores of tested strains were injected in the silk channel of maize cobs and incubated for 5 weeks. The left picture shows a cob infected by WT, the middle picture shows a cob infected by ΔΔΔ*FGSG_17054.1;12456;16151*, the right one shows the water control. Black coloured kernels and white mycelia visible on the cob surface indicate infected tissue. Both WT and ΔΔΔ*FGSG_17054.1;12456;16151* are able to infect maize cobs after 5 weeks. n = 15

Apart from ROS-detoxification, metallothioneins are mainly used as heavy metal ion chelators. To assess the role of *F. graminearum* metallothioneins in detoxification of heavy metal ions, metallothionein deletion mutants (Δ*FGSG_17054.1, ΔFGSG_17054.3*, ΔΔ*FGSG_17054.1;12456,* ΔΔΔ*FGSG_17054.1;12456;16151*) were grown on CM agar containing $CdCl_2$ (50 µM, 100 µM, 200 µM), $ZnCl_2$ (0.1 mM, 0.5 mM), or $CuCl_2$ (0.1 mM, 0.5 mM, 1.0 mM). After three days the colony area was measured. The metallothionein KOs showed a slightly lower colony area in the presence of cadmium. No phenotype was observed in the presence of zinc. In the presence of 0.5 mM copper the triple KO mutant showed a lower colony area compared to the other strains (Figure 36) which was not statistically significant. Together, application of heavy metal ion stress led to only minor changes in colony area of the mutants. Metallothioneins, therefore, do not play a major role in metal detoxification in *F. graminearum*.

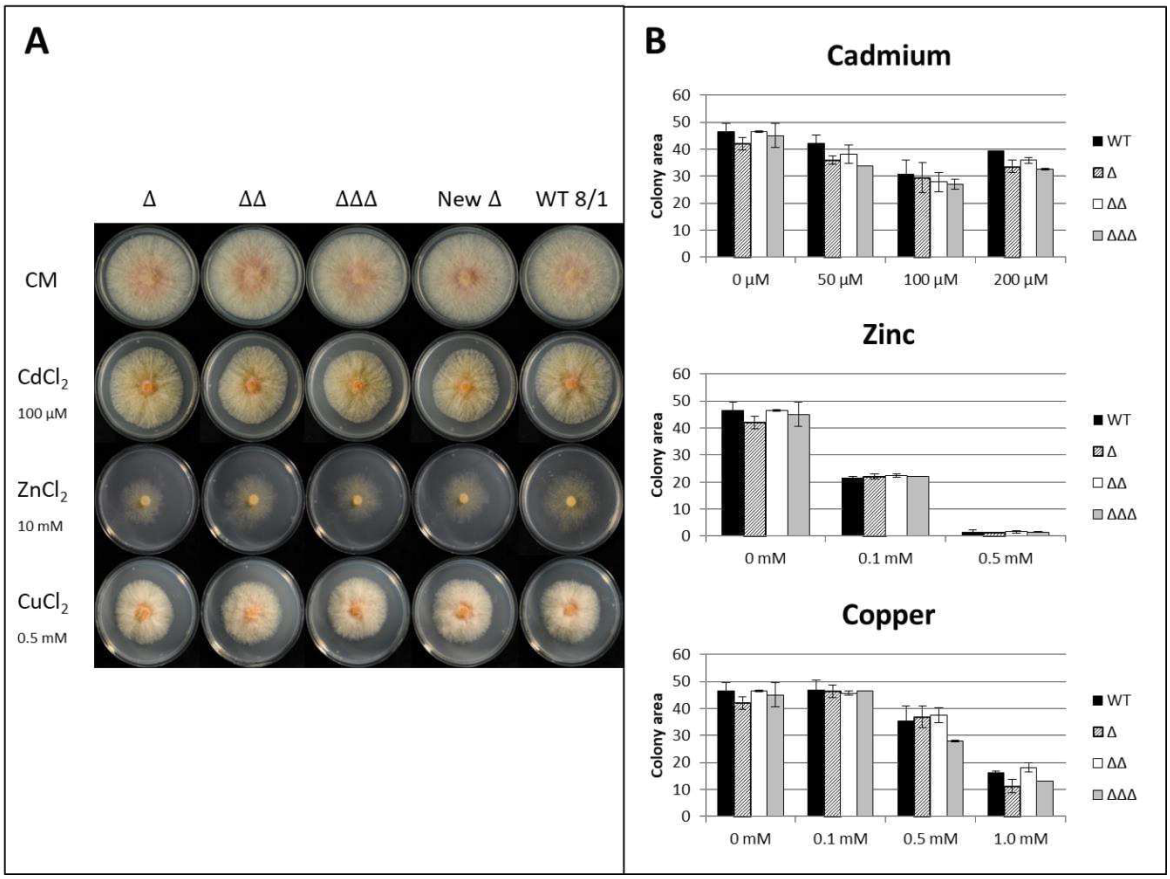

Figure 36: Growth assay to assess the resistance of metallothionein deletion mutants towards Cd^{2+}, Zn^{2+}, and Cu^{2+}. The metallothionein FGSG_17054 single deletion mutants Δ*FGSG_17054.1* (Δ) and Δ*FGSG_17054.3* (New Δ), the double deletion mutant ΔΔ*FGSG_17054.1;12456* (ΔΔ), and the triple deletion mutant ΔΔΔ*FGSG_17054.1;12456;16151* (ΔΔΔ) were cultivated on CM-agar containing harmful concentrations of the heavy metal ions Cd^{2+} (50 µM, 100 µM, 200 µM), Zn^{2+} (0.1 mM, 0.5 mM), and Cu^{2+} (0.1 mM, 0.5 mM, 1.0 mM) dispensed as $CdCl_2$, $ZnCl_2$, and $CuCl_2$. **A:** Exemplary photographs showing the growth habit of the tested strains on CM agar containing 100 µM $CdCl_2$, 10 mM $ZnCl_2$, and 0.5 mM $CuCl_2$, respectively. Even the triple deletion mutant shows no major growth reductions in presence of any of the applied heavy metals. In presence of cadmium the deletion mutants show slightly reduced growth. **B:** Bar diagram representing the growth assay results. Deviations from the WT were tested for significance using a two-tailed homoscedastic t-test (significant: $p < 10^{-3}$). Growing on CM agar without additives mutants showed WT-like colony area. Metallothionein deletion mutants showed slight growth retardation in the presence of cadmium, albeit not significantly. All strains displayed concentration dependent decrease of colony area at $CdCl_2$ concentrations of 50 µM and 100 µM. At 200 µM $CdCl_2$ the growth retardation is less severe compared to 100 µM. At $ZnCl_2$ concentrations 0.1 mM and 0.5 mM colonies of metallothionein deletion mutants showed the same area as WT colonies. At 0.1 mM $CuCl_2$ all strains showed the same colony area as on CM without additives. At 0.5 mM $CuCl_2$ the metallothionein triple deletion mutant (ΔΔΔ) showed slightly reduced colony area compared to the other strains. This reduction, however, is not statistically significant. At 1.0 mM $CuCl_2$ the single (Δ) and the triple deletion mutant (ΔΔΔ) showed slightly reduced colony area compared to the other strains. Error bars indicate the standard deviation (n = 2).

To investigate whether instead metal deprivation leads to a non-WT phenotype the metallothionein triple deletion mutant was cultivated on deprivation medium (DM, contains no metal ion trace elements) containing the metal chelator bathocuproinedisulfonic acid (BCS). After a growth period of three days no deviation from the WT phenotype was observed (Figure 37). Hence, *F. graminearum* metallothioneins FGSG_17045, FGSG_12456, and FGSG_16151 are dispensable during metal stress and metal deprivation in this fungus.

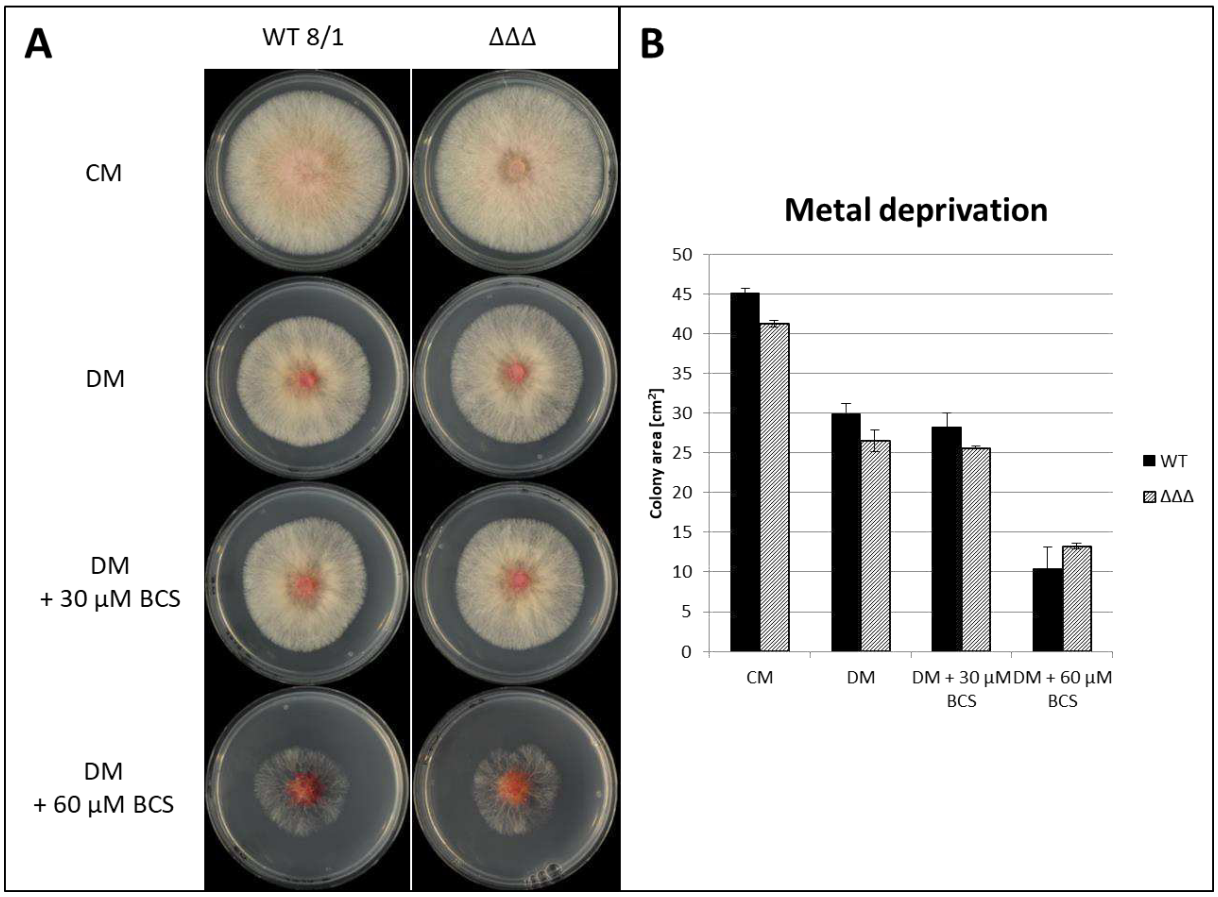

Figure 37: Growth assay to assess the resistance of the metallothionein triple deletion mutant (ΔΔΔ) towards deprivation of metal ions caused by the metal chelator bathocuproinedisulfonic acid (BCS). A: Photographs showing the vegetative growth of the tested strains on CM agar and deprivation medium (DM) agar with increasing concentrations of BCS (30 µM, 60 µM). **B:** Growth assay result presented as a bar diagram. Deviations from the WT were tested for significance using a two-tailed homoscedastic t-test (significant: $p < 10^{-3}$). The metallothionein triple deletion mutant displayed no significant deviations from the WT phenotype. Error bars indicate the standard deviation (n = 3).

3.1.3.5 Characterisation of Cupredoxins

Of three secreted plant induced cupredoxins (FGSG_06023, FGSG_09742, FGSG_07829) single and simultaneous deletions of FGSG_06023 and FGSG_09742 were established in *F. graminearum*. Vegetative growth was assessed by incubating the tested strains on CM agar for 3 days. The deletion mutants showed the same colony diameter as the WT (Figure 38). When growing on CM-agar containing H_2O_2 (10 mM, 15 mM, and 20 mM) or menadione (10 µM, 50 µM, and 100 µM) for 3 days, no significant differences to WT colony area were observed (Figure 38).

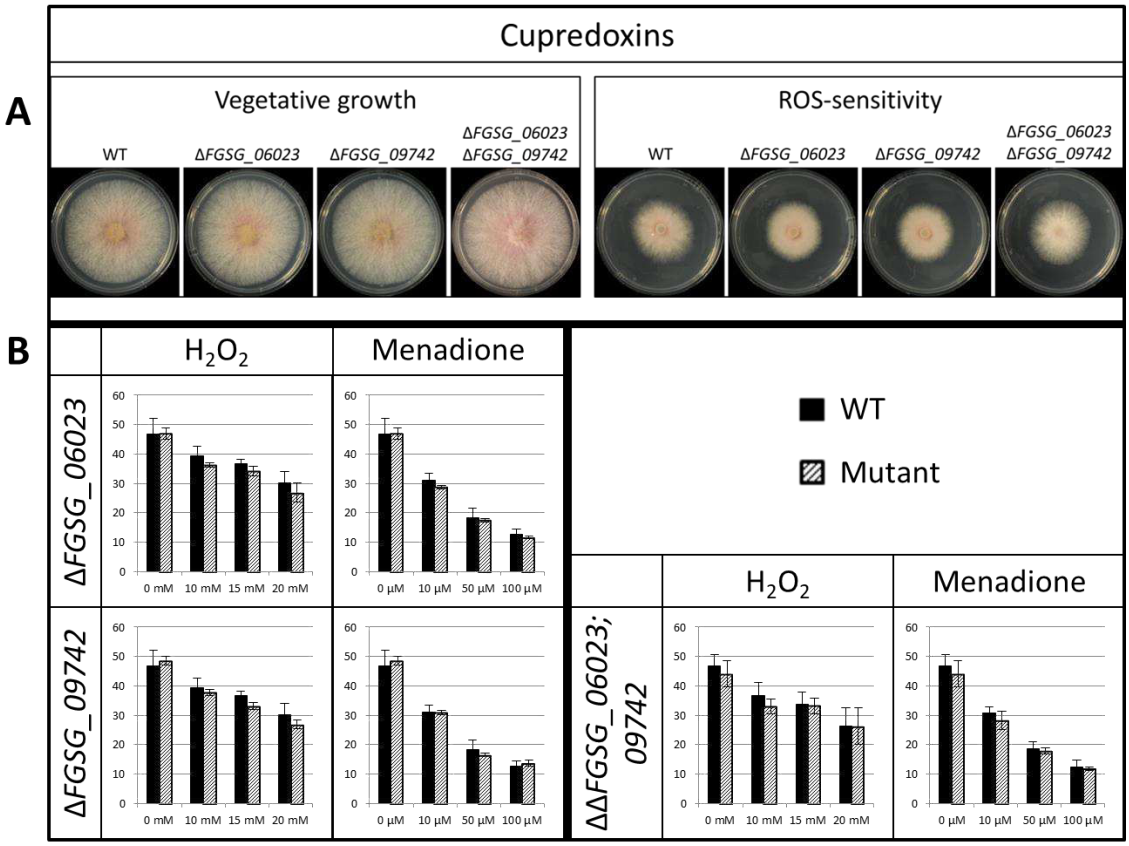

Figure 38: Vegetative growth of cupredoxin deletion mutants with and without oxidative stress. Strains were cultivated on CM-agar without additives and CM-agar containing H_2O_2 (10 mM, 15 mM, 20 mM) or menadione (10 µM, 50 µM, 100 µM) for three days before the colony area was measured. **A:** Exemplary photographs showing colony morphology on CM-agar (vegetative growth) and on CM-agar containing 50 µM menadione (ROS-sensitivity). Colony morphology of cupredoxin deletion mutants did not differ from the WT. **B:** Colony area of all mutants compared to the WT represented as a bar diagram. Each mutant is presented individually because the growth rates of WT (black bars) and mutants (striated bars) differed between individual experiments. Y-axis represents the colony area, X-axis the applied concentrations of H_2O_2 and menadione. Deviations from the WT were tested for significance using a two-tailed homoscedastic t-test (significant: $p < 10^{-3}$). None of the mutations led to significant colony area deviations on any of the applied additive concentrations. Error bars indicate the standard deviation (n = 12).

ROS-accumulation of cupredoxin deletion mutants was tested by staining 3 days old mycelia on CM agar with 0.2% NBT. After an incubation of 40 min the colouration of all mutants was WT-like (Figure 39).

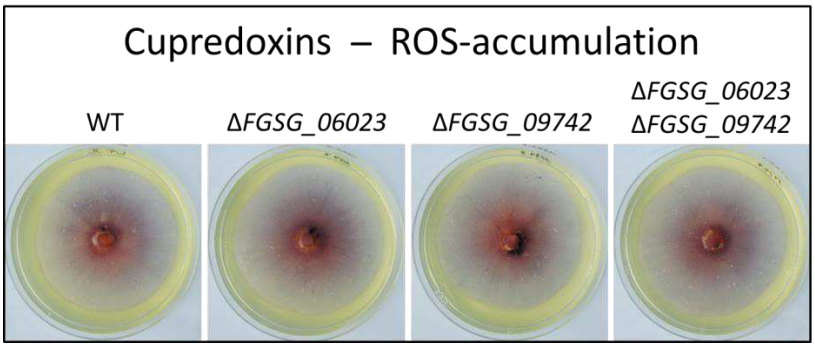

Figure 39: ROS-accumulation of cupredoxin deletion mutants. Strains were cultivated on CM-agar for 3 days before flooding the plates with 0.2% NBT. Upon reaction with superoxide NBT forms a blue precipitate. The intensity of blue colouration serves as an indicator for ROS-accumulation. None of the mutants show a deviation from the WT phenotype. n = 4

Pathogenicity of cupredoxin deletion mutants was assessed on wheat heads. At 21 dpi, all spikelets of wheat heads inoculated with WT and cupredoxin deletion mutant conidiospores showed premature bleaching, demonstrating that all mutants were able to fully infect wheat heads at 21 dpi (Figure 40).

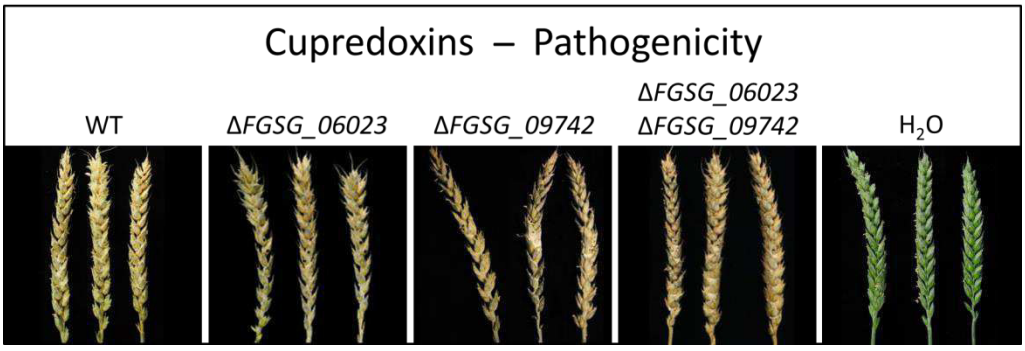

Figure 40: Pathogenicity of cupredoxin deletion mutants on wheat heads. 200 conidiospores of the tested strains were inoculated in 2 wheat spikelets in the centre of wheat heads in early anthesis. After an incubation period of 21 days in controlled conditions, the disease pattern was assessed. The pictures show infected wheat heads at 21 dpi. Yellow spikelets indicate premature bleaching, a typical sign for infected plant tissue. Non-infected plant tissue is green, as shown in the water control (H_2O). All mutants were able to fully infect wheat heads. n = 9

Fertility of cupredoxin deletion mutants was tested by inoculating detached wheat nodes with conidiospores of the respective strains. The amount of produced perithecia on detached wheat nodes did not differ significantly from the WT (Figure 41).

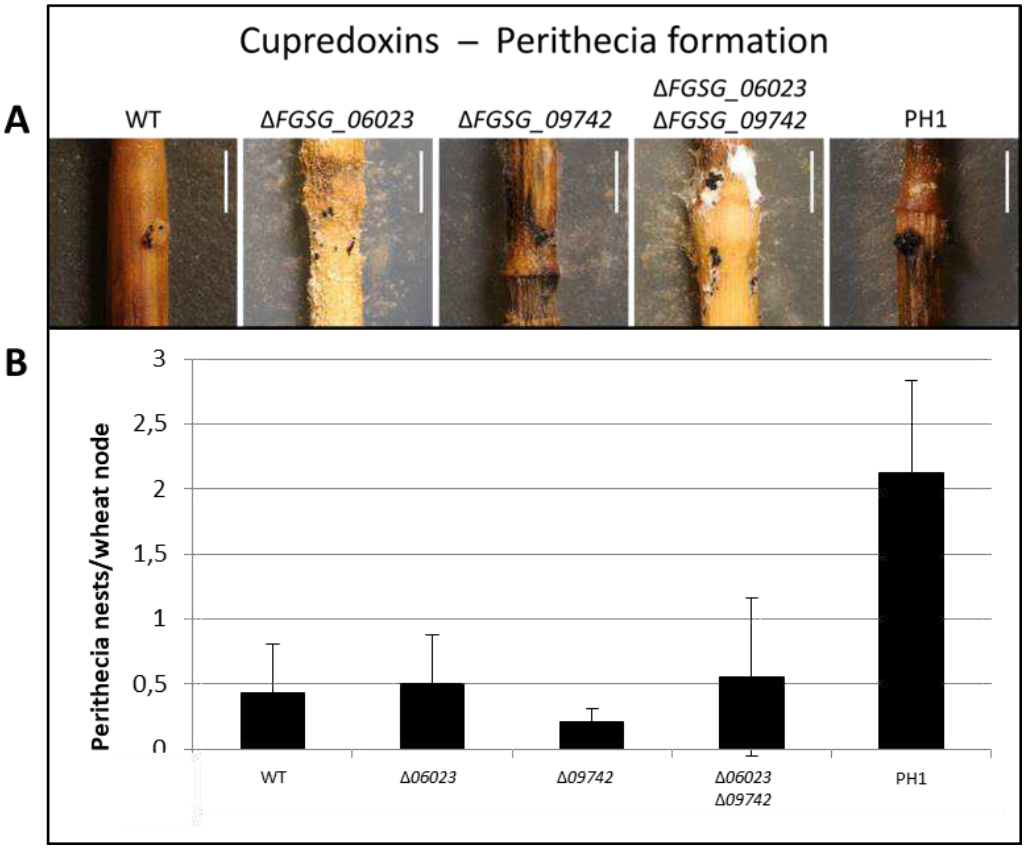

Figure 41: Fertility of cupredoxin deletion mutants. Detached wheat nodes from straw were inoculated with 1000 conidiospores of tested strains and incubated for 2 months with artificial night-daylight-cycle to induce perithecia formation. **A:** Close-up photographs of grown perithecia to demonstrate fertility. Perithecia are visible a little black dots on the wheat nodes. All cupredoxin deletion mutants were able to produce perithecia. Scale bars = 5 mm. **B:** Statistical evaluation of perithecia assays. Wheat nodes were subdivided in three sections (left edge, centre, right edge). If any amount of perithecia was present on one section this was counted as 1 perithecia nest. The sum of perithecia nests was divided by the number of assessed wheat node sections constituting the perithecia nests/wheat node ratio. Deviations from the WT were tested for significance using a two-tailed homoscedastic t-test (significant: $p < 0.05$). None of the mutants showed a statistically significant deviation from the WT ratio. Error bars indicate the standard deviation (n = 14).

3.1.3.6 Characterisation of other enzymes

4 enzymes were deleted that do not belong to the aforementioned enzyme groups. Those are the secreted cellobiose dehydrogenase FGSG_02917, the secreted reductase FGSG_09124, the secreted superoxide dismutase (SOD) FGSG_00576, and the nicotinamide nucleotide transhydrogenase (NNT) FGSG_09006. Vegetative growth of these genes' deletion mutants was assessed by incubating the tested strains on CM agar for 3 days. The deletion mutants showed the same colony diameter as the WT (Figure 42).

When growing on CM-agar containing H_2O_2 (10 mM, 15 mM, and 20 mM) or menadione (10 µM, 50 µM, and 100 µM) for 3 days no significant differences to WT colony area were observed (Figure 42).

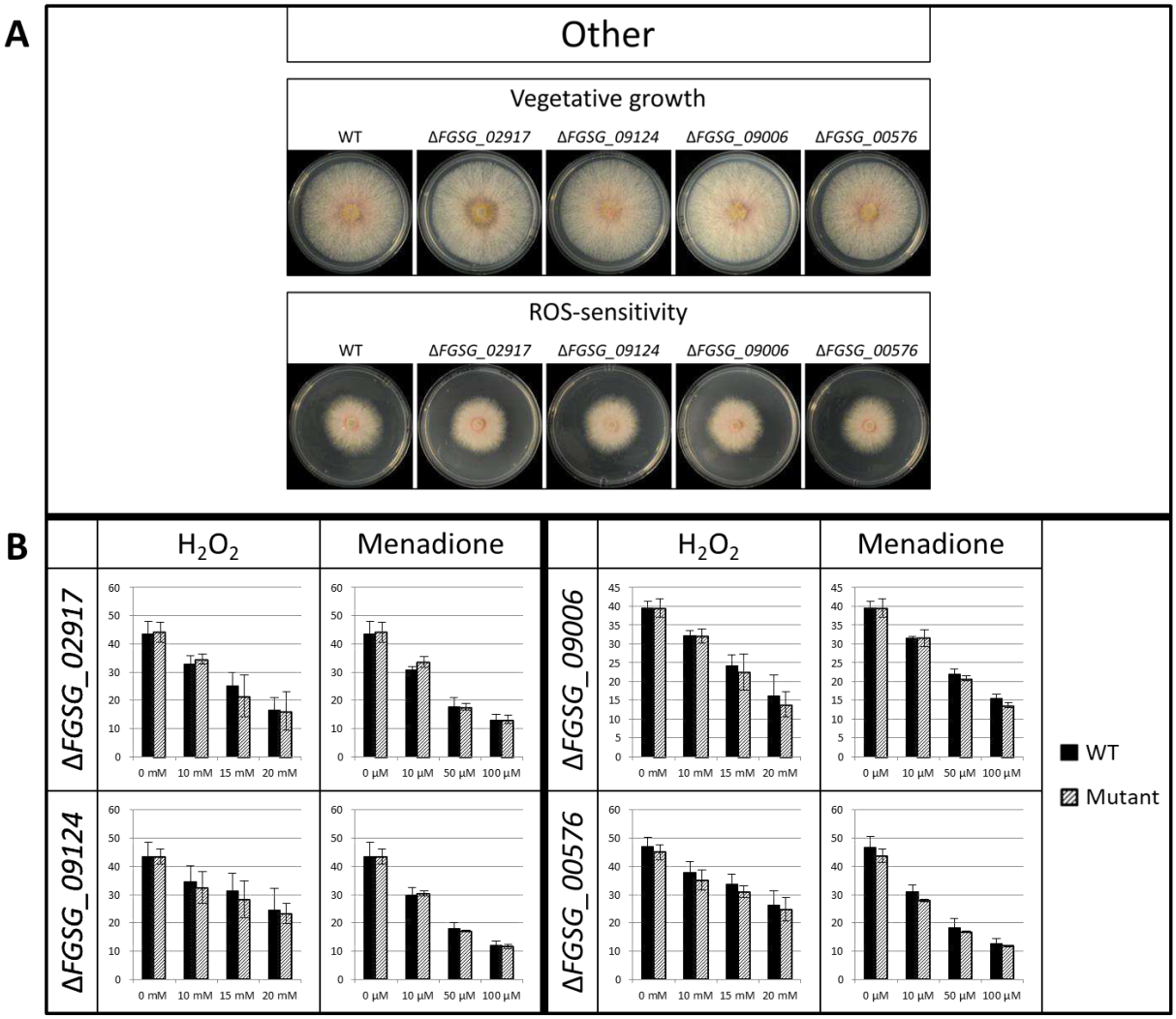

Figure 42: Vegetative growth of single deletion mutants of cellobiose dehydrogenase FGSG_02917, reductase FGSG_09124, NNT FGSG_09006, and SOD FGSG_00576 with and without oxidative stress. Strains were cultivated on CM-agar without additives and CM-agar containing H_2O_2 (10 mM, 15 mM, 20 mM) or menadione (10 µM, 50 µM, 100 µM) for three days before the colony area was measured. **A:** Exemplary photographs showing colony morphology on CM-agar (vegetative growth) and on CM-agar containing 50 µM menadione (ROS-sensitivity). Colony morphology of the deletion mutants did not differ from the WT. **B:** Colony area of all mutants compared to the WT represented as a bar diagram. Each mutant is presented individually because the growth rates of WT (black bars) and mutants (striated bars) differed between individual experiments. Y-axis represents the colony area, X-axis the applied concentrations of H_2O_2 and menadione. Deviations from the WT were tested for significance using a two-tailed homoscedastic t-test (significant: $p < 10^{-3}$). None of the mutations led to significant colony area deviations on any of the applied additive concentrations. Error bars indicate the standard deviation (n = 3).

ROS-accumulation of the non-grouped deletion mutants was tested by staining 3 days old mycelia on CM agar with 0.2% NBT. After an incubation of 40 min the colouration of all mutants was WT-like (Figure 43).

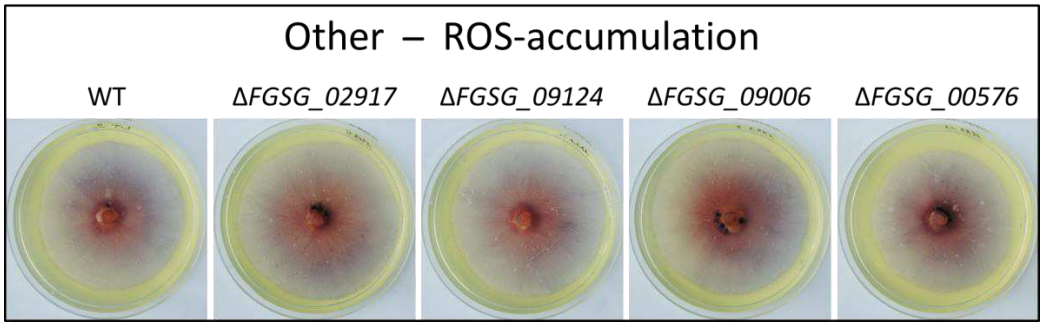

Figure 43: ROS-accumulation of single deletion mutants of cellobiose dehydrogenase FGSG_02917, reductase FGSG_09124, NNT FGSG_09006, and SOD FGSG_00576. Strains were cultivated on CM-agar for 3 days before flooding the plates with 0.2% NBT. Upon reaction with superoxide NBT forms a blue precipitate. The intensity of blue colouration serves as an indicator for ROS-accumulation. None of the mutants show a deviation from the WT phenotype. n = 2

Pathogenicity of the non-grouped deletion mutants was assessed on wheat heads. At 21 dpi, all spikelets of wheat heads inoculated with WT and deletion mutant conidiospores showed premature bleaching, demonstrating that all mutants were able to fully infect wheat heads at 21 dpi (Figure 44).

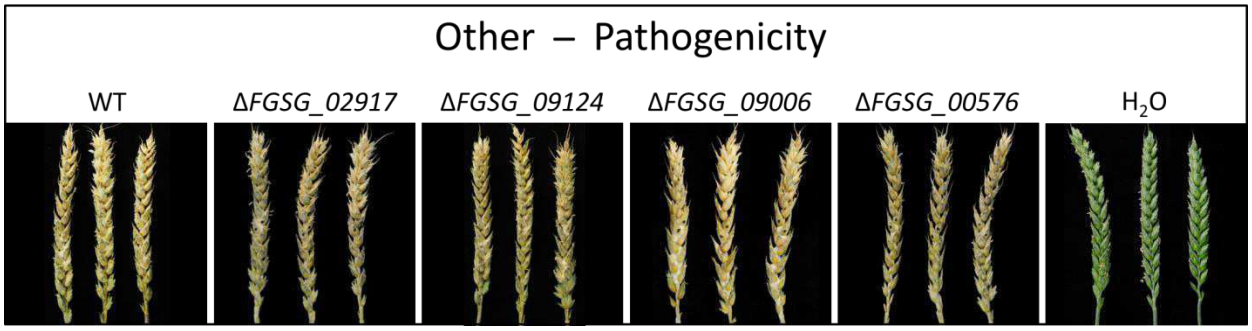

Figure 44: Pathogenicity of single deletion mutants of cellobiose dehydrogenase FGSG_02917, reductase FGSG_09124, NNT FGSG_09006, and SOD FGSG_00576. 200 conidiospores of the tested strains were inoculated in 2 wheat spikelets in the centre of wheat heads in early anthesis. After an incubation period of 21 days in controlled conditions, the disease pattern was assessed. The pictures show infected wheat heads at 21 dpi. Yellow spikelets indicate premature bleaching, a typical sign for infected plant tissue. Non-infected plant tissue is green, as shown in the water control (H_2O). All mutants were able to fully infect wheat heads. n = 5

Fertility of non-grouped deletion mutants was tested by inoculating detached wheat nodes with conidiospores of the respective strains. The amount of produced perithecia on detached wheat nodes did not differ significantly from the WT (Figure 45).

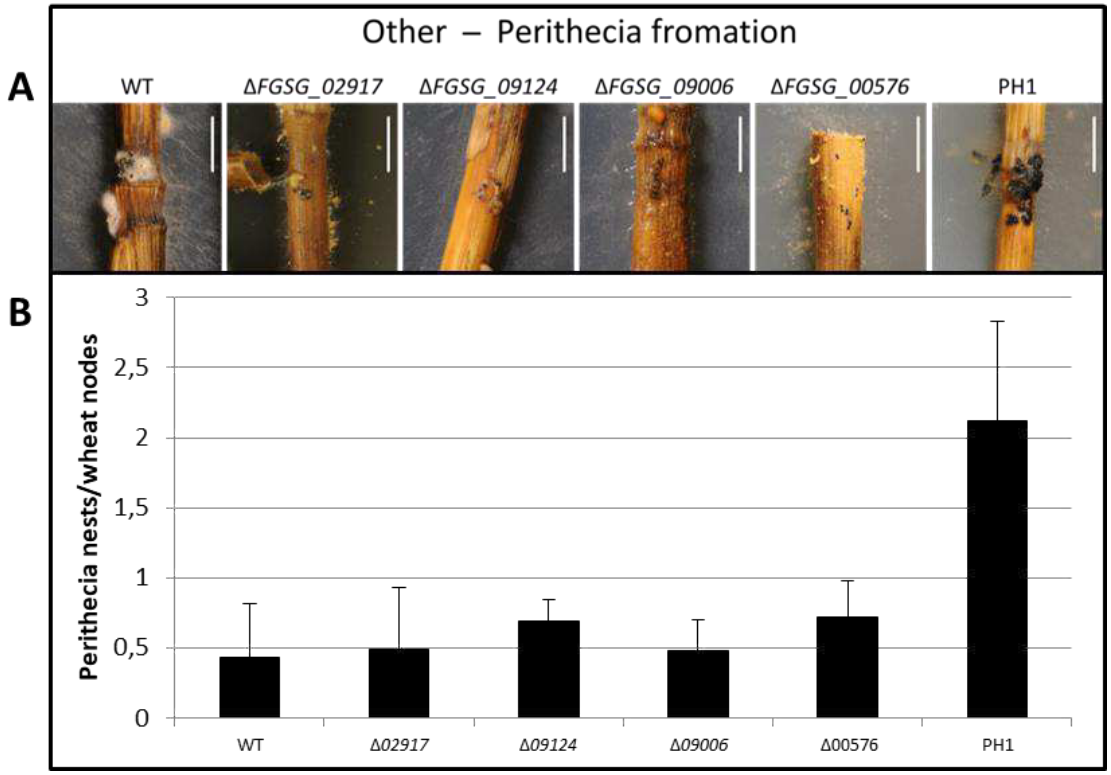

Figure 45: Fertility of single deletion mutants of cellobiose dehydrogenase FGSG_02917, reductase FGSG_09124, NNT FGSG_09006, and SOD FGSG_00576. Detached wheat nodes from straw were inoculated with 1000 conidiospores of tested strains and incubated for 2 months with artificial night-daylight-cycle to induce perithecia formation. **A:** Close-up photographs of grown perithecia to demonstrate fertility. Perithecia are visible a little black dots on the wheat nodes. All deletion mutants were able to produce perithecia. Scale bars = 5 mm. **B:** Statistical evaluation of perithecia assays. Wheat nodes were subdivided in three sections (left edge, centre, right edge). If any amount of perithecia was present on one section this was counted as 1 perithecia nest. The sum of perithecia nests was divided by the number of assessed wheat node sections constituting the perithecia nests/wheat node ratio. Deviations from the WT were tested for significance using a two-tailed homoscedastic t-test (significant: $p < 0.05$). None of the mutants showed a statistically significant deviation from the WT ratio. Error bars indicate the standard deviation (n = 21).

In summary, of 25 ROS-related enzymes characterised in this study only peroxidases revealed involvement in the life cycle of *F. graminearum*. Secreted chloroperoxidase FGSG_03708 has been shown to be needed in vegetative growth. During oxidative stress FGSG_03708 is downregulated. It is not involved in ROS-resistance but seems to be somehow involved in ROS-metabolism as shown by an NBT-stain that revealed increased superoxide levels in hyphal tips. Secreted chloroperoxidases FGSG_03708, FGSG_02341, and FGSG_03436 might be cumulatively involved in sexual reproduction. While chloroperoxidase single deletions have no effect on perithecia formation, the double and triple deletion mutants (ΔΔ*FGSG_02341;03708* and ΔΔΔ*FGSG_02341;03708;03436*) show

an increased perithecia nest/wheat node ratio. Also, the secreted ascorbate/cytochrome c peroxidase FGSG_04434 is connected to sexual reproduction. Upon deletion of FGSG_04434 the perithecia nest/wheat node ratio is increased. No other ROS-related enzymes characterised in this study could be shown to have an effect on vegetative growth, ROS-resistance, ROS-accumulation, or sexual reproduction. None of the characterised enzymes is involved in pathogenicity.

3.2 The modified H_2O_2 sensor GPI-HyPer is a new tool for subcellular H_2O_2 monitoring

3.2.1 Attachment of a GPI-anchor to HyPer

In previous work the H_2O_2 reporter system HyPer was established in *F. graminearum* (Mentges & Bormann, 2015). HyPer is an artificial sensor protein generated by fusion of circularly permutated yellow fluorescent protein (cpYFP) and the regulatory domain of the bacterial H_2O_2 sensor OxyR (Belousov et al., 2006). It has two excitation peaks (420 nm and 500 nm) that exhibit reciprocal behaviour when reacting to H_2O_2: the 420 nm peak decreases and the 500 nm peak increases upon contact with H_2O_2. This allows ratiometric measurement of H_2O_2. By expression of HyPer in cells, assessment of the intracellular H_2O_2-level is possible. The mutant used by Mentges and Bormann (2015) expressed HyPer in the cytosol (cytHyPer). In this study HyPer was genetically modified with the aim to grapple the protein to the cell surface in order to analyse HyPer oxidation at the area of contact between pathogen and host. For this purpose the N-terminal and C-terminal signal peptides of a putatively GPI-anchored protein (FGSG_00576, superoxide dismutase) were added to the HyPer ORF integrated in the overexpression vector pII99. The online N-terminal signal peptide prediction tool SignalP (http://www.cbs.dtu.dk/services/SignalP/) predicts a potential signal peptide cleavage site between positions 20 and 21 in the amino acid chain of FGSG_00576. The online GPI-modification site prediction tool fungal big-Pi (http://mendel.imp.univie.ac.at/gpi/fungi/gpi_fungi.html) predicts a potential modification site at position 242 (Figure 46).

FGSG_00576:

MRAQALAAVL LSACAGQAIA EDAPRVNDNP PGVGFKATLP KESFFKDAAI DGNVKGYIHA QATDSGQGVK
FIVKFSNLPK EGGPFTYHIH VDPVPDNGNC TATLAHLDPF ARGEDPPCDA EKPESCQVGD NSGKHGKITS
DPFETEYIDY YASTKEGIGA FFGNRSFVLH YANKTRITCA NFVSQIKPPA TNESYSAPGY LPTPTETVTL
TPTPSSKVPA STATSGVTSA PTSTATDVVG P**NAGSSMAVP VNLVLAGVFA LAFAL**

Figure 46: Amino acid chain of the superoxide dismutase FGSG_00576. FGSG_00576 served as a template for the N- and C-terminal signal peptides for GPI-HyPer. The sequence was analysed with the online tools SignalP and Fungal big-Pi which predicted the N-terminal signal peptide (position 1-21, orange letters) and the C-terminal signal peptide (position 242-265, red letters), respectively. Underlined letters illustrate predicted cleavage sites.

The respective nucleotide sequences for the N-terminal (MRAQALAAVLLSACAGQAIAE, N --> C) and C-terminal signal peptide (NAGSSMAVPVNLVLAGVFALAFAL, N --> C) were cloned together with the HyPer-2 ORF (without the initial start codon) in the overexpression vector pII99. The HyPer-2 ORF and the C-terminal signal peptide were separated by a spacer (GAGAGA) which was inserted during the same process. As promoter, 844 bp upstream of the non-annotated gene FGSG_04399 - which has been identified as one of the strongest constitutively expressed genes in the *F. graminearum* genome - were chosen and cloned upstream of the N-terminal signal peptide. Nucleotide sequences of all fragments cloned into vector pII99 are presented in Supplementary table 2. Figure 47 shows an overview for the GPI-HyPer expression vector.

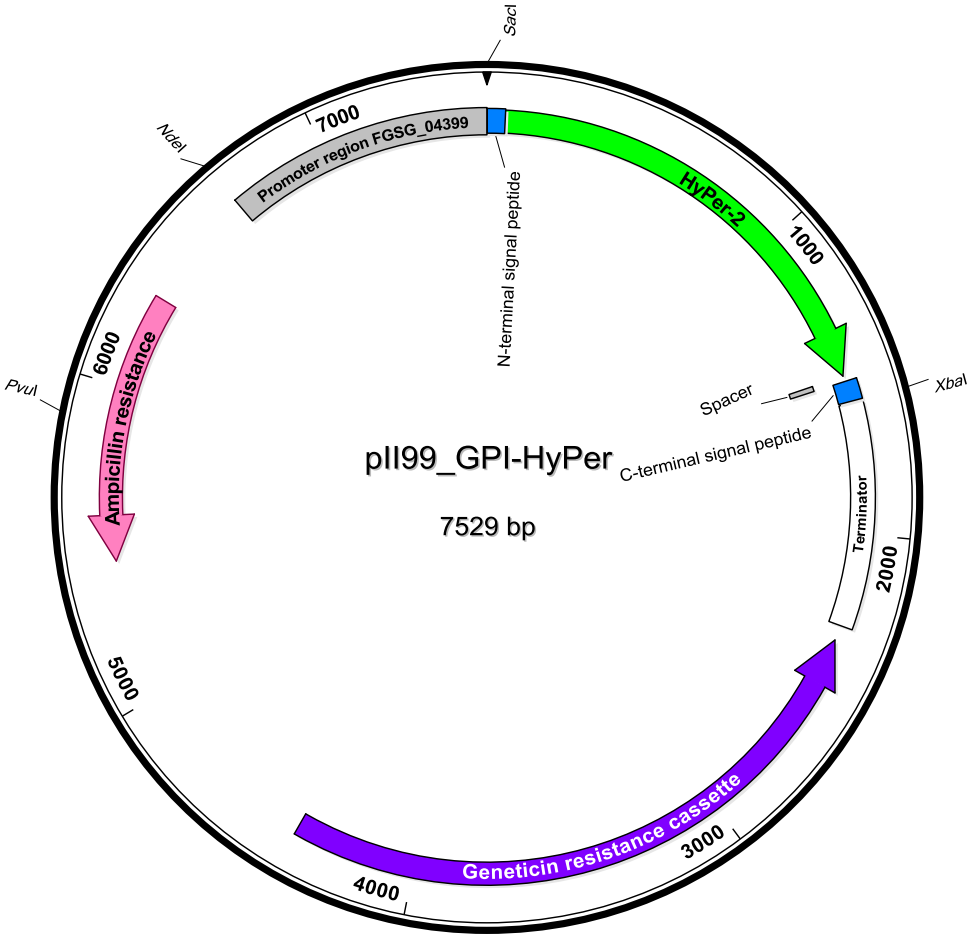

Figure 47: Vector map of the GPI-HyPer overexpression vector pII99_GPI-HyPer. Promoter region, signal peptides, HyPer ORF, and spacer were cloned into the overexpression vector pII99. The HyPer-ORF (green) is flanked by the N-terminal signal peptide upstream and the spacer and C-terminal signal peptide downstream (blue). As promoter 844 bp upstream of the gene FGSG_04399 were chosen (grey). Ampicillin (pink) and geneticin (purple) resistance cassettes were used as selection markers for *E. coli* and *F. graminearum* transformation, respectively. *Sac*I and *Xba*I represent the resitriction sites where HyPer and the signal peptides were cloned in pII99. *Nde*I and *Sac*I represent the restriction sites where the promotor region of FGSG_04399 was cloned in pII99. After successful cloning, the vector was linearised with *Nde*I and transformed into *F. graminearum* 8/1.

To verify that the HyPer-ORF does not interrupt or alter the sequences of the signal peptides, another *in silico* analysis of the transgenic GPI-HyPer amino acid sequence was performed. SignalP and Fungal big-Pi both predicted the same modification sites for the transgenic GPI-HyPer ORF as for FGSG_00576 (Figure 48).

GPI-HyPer:

MRAQALAAVL LSACAGQAIA EMASQQGETM SGPLHIGLIP TVGPYLLPHI IPMLHQTFPK LEMYLHEAQT
HQLLAQLDSG KLDCVILALV KESEAFIEVP LFDEPMLLAI YEDHPWANRE CVPMADLAGE KLLMLEDGHC
LRDQAMSAGY NSDNVYIMAD KQKNGIKANF KIRHNVEDGS VQLADHYQQN TPIGDGPVLL PDNHYLSFQS
VLSKDPNEKR DHMVLLEFVT AAGITLGMDE LYNVDGGSGG TGSKGEELFT GVVPILVELD GDVNGHKFSV
SGEGEGDATY GKLTLKLICT TGKLPVPWPT LVTTLGYGLK CFARYPDHMK QHDFFKSAMP EGYVQERTIF
FKDDGNYKTR AEVKFEGDTL VNRIELKGIG FKEDGNILGH KLEYNGTGFC FEAGADEDTH FRATSLETLR
NMVAVGSGIT LLPALAVPPE RKRDGVVYLP CIKPEPRRTI GLVYRPGSPL RSRYEQLAEA IRARMDGHFD
KVLKQAVGAG AGANAGSSMA VPVNLVLAGV FALAFAL

Figure 48: Amino acid chain of GPI-HyPer. After addition of the N-terminal and C-terminal signal peptides of FGSG_00576 to the HyPer ORF, the sequence was analysed with the online tools SignalP and Fungal big-Pi which predicted the same N-terminal signal peptide (position 1-21, orange letters) and C-terminal signal peptide (position 242-265, red letters) as for FGSG_00576. Underlined letters illustrate the cleavage sites. The spacer is highlighted in grey.

3.2.2 GPI-HyPer is attached to ER and mitochondria but not endocytotic membranes

The vector pII99_GPI-HyPer was linearised and transformed in *F. graminearum* protoplasts. Transformants were checked for and selected by strength of the YFP-signal using fluorescence microscopy. No apparent YFP signal at the cell surface was shown by mutants with GPI-HyPer expression. However, GPI-HyPer could be detected in subcellular structures. Circular and elongated structures were visible upon excitation of YFP. Experiments with ER-Tracker™ Blue-White DPX, MitoTracker™ Red FM, and FM™ 4-64 (Thermo Scientific) were conducted to identify these structures. As indicated in Figure 49, circular and elongated structures tagged with GPI-HyPer match the ER-Tracker™ signal. Co-expression of the histone-tag H1mCherry shows that the circular structures surround the nucleus. These finding strongly indicate that GPI-HyPer is attached to the ER.

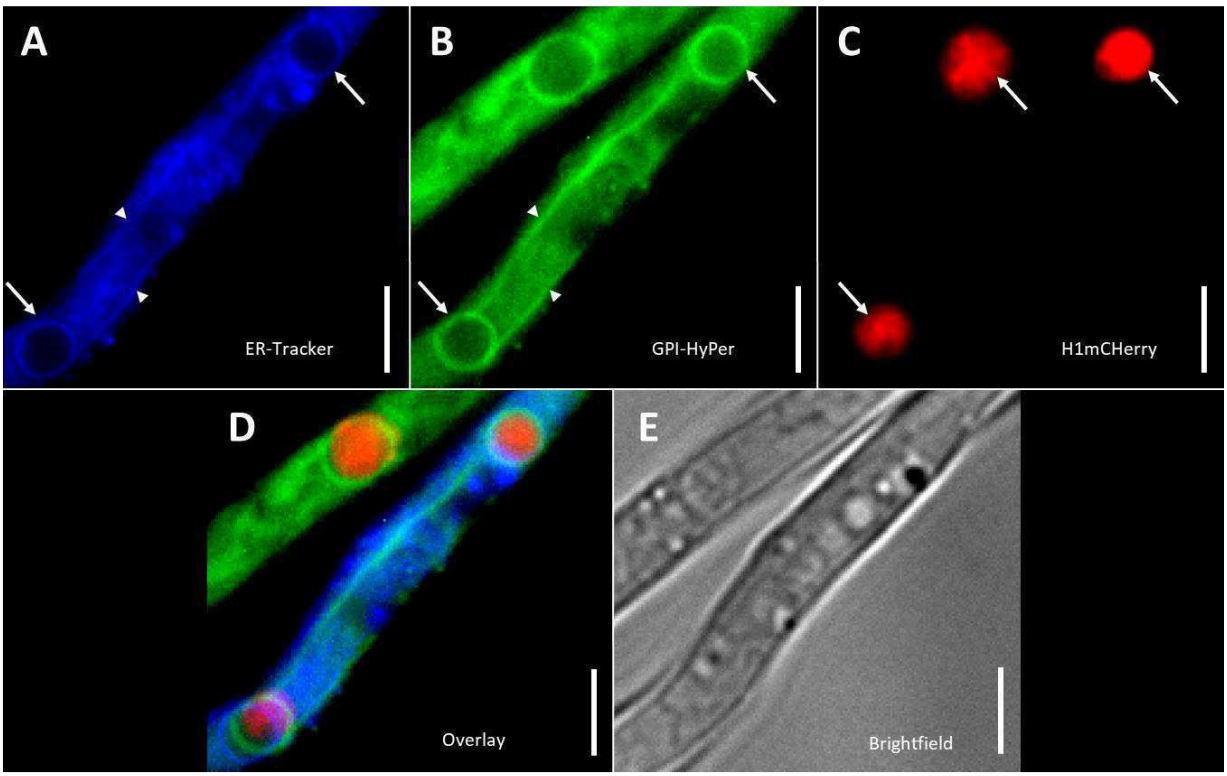

Figure 49: Fluorescence microscopy captures of vegetative hyphae expressing GPI-HyPer and H1mCherry stained with ER-Tracker™ Blue-White DPX. **A:** ER-Tracker™ Blue-White DPX signal. Of the 2 parallel hyphae visible in these photographs only the lower one was effectively stained with ER-Tracker. Circular (white arrows) and elongated structures (white arrowhead) are silhouetted against unspecifically stained background. **B:** GPI-HyPer signal. Circular (white arrows) and elongated structures (white arrowhead) are silhouetted against a background with less fluorescence intensity. **C:** mCherry tagged to histone 1 colouring parts of the nuclei. Nuclei are visible as round red structures (white arrows) **D:** Merge. GPI-HyPer-tagged circular structures (green) surround the nuclei stained with H1mCherry (red). GPI-HyPer-tagged circular and elongated structures match with the ER-Tracker signal indicating that GPI-HyPer is attached to the ER. The displacement of the ER-Tracker and the GPI-HyPer signal of the circular ER at the bottom of the picture can be explained with the motility of the organelle. The structure showed lateral movement between capturing of the ER-Tracker and the GPI-HyPer picture. **E:** brightfield capture. Scale bars = 1 µm.

To some extend the GPI-HyPer signal also colocalises with mitochondria (Figure 50). Figure 50 shows matching of different elongated structures with MitoTracker™. The circular putatively ER-bound GPI-HyPer-signals do not match with MitoTracker™ indicating that GPI-HyPer is attached to multiple membrane types.

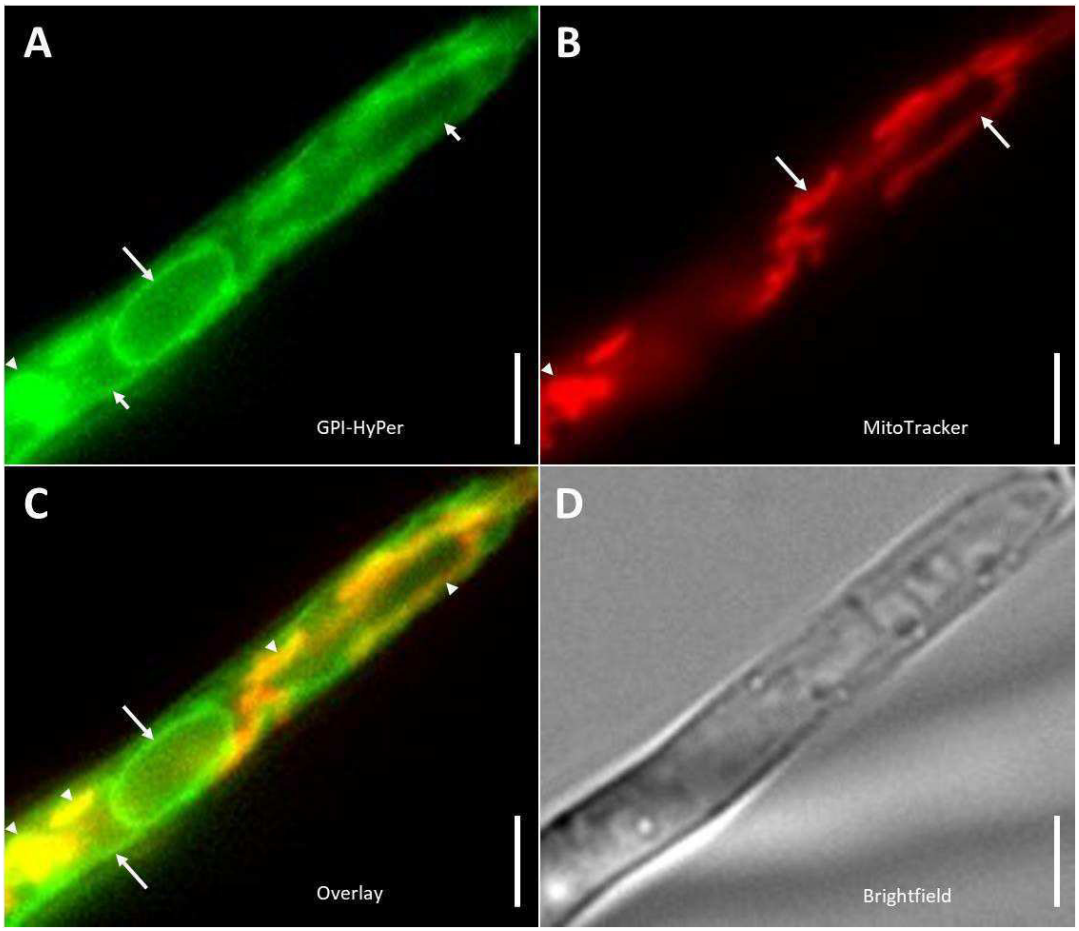

Figure 50: Fluorescence microscopy captures of vegetative hyphae expressing GPI-HyPer stained with MitoTracker™ Red FM. A: GPI-HyPer signal. Circular (long white arrow), elongated (short white arrows), and aggregated (white arrowhead) structures are visible. **B:** MitoTracker™ Red FM signal. Elongated (white arrows) and aggregated structures (white arrowhead) are stained. **C:** Merge. Some of the GPI-HyPer structures match with the MitoTracker signal (white arrowheads) indicating that GPI-HyPer is attached to the mitochondria. Circular and some elongated structures (white arrows) do not match the MitoTracker signal. **D:** Brightfield capture. Scale bars = 1 µm.

A fluorescence intensity plot profile (Figure 51) was established with the image processing program ImageJ to verify this optical analysis. The plot showed multiple intensity peaks at identical position on the plot profile line for GPI-HyPer and MitoTracker. Notably, high peaks of GPI-HyPer could be shown that were not exhibited by the MitoTracker profile. This confirmed the hypothesis that GPI-HyPer is attached to multiple subcellular structures.

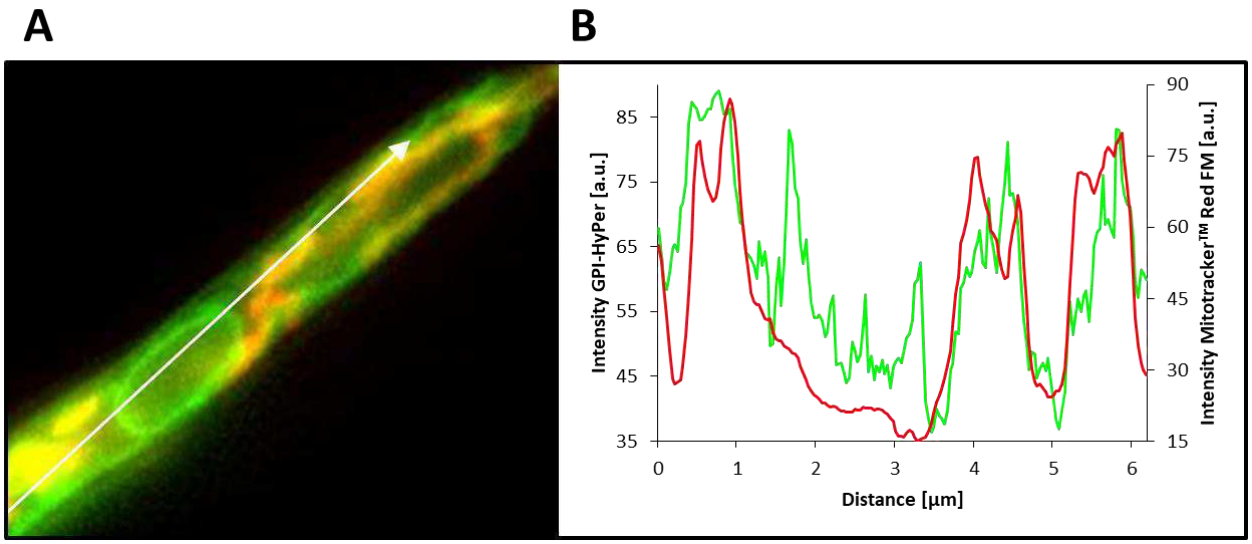

Figure 51: Fluorescence intensity plot profile projection of GPI-HyPer and MitoTracker™ Red FM composite picture. A: Composite picture of a vegetative *F. graminearum* hypha expressing GPI-HyPer stained with MitoTracker Red FM. The white arrow represents the approximately 6.0 µm long line of interest from which the values for the plot profile were taken. **B:** Plot profile of GPI-HyPer and MitoTracker fluorescence intensity. The MitoTracker profile (red line) exhibits three zones of high intensity separated by long minimum between 1.5 and 3.5 µm and one at 5 µm. These three high intensity zones are shared by the GPI-HyPer profile. However, between 1.5 and 3.5 µm the GPI-HyPer profile exhibits two main signal peaks which represent the intersections of the plot line with the perinuclear ER and are not shown by the MitoTracker profile. This demonstrates the partial colocalisation of GPI-HyPer and MitoTracker.

To gain a better understanding of the subcellular structures bound by GPI-HyPer, cells expressing GPI-HyPer were stained with FM4-64, a colouring agent that binds the plasma membrane before getting ingested by endocytosis. After an incubation time of 1 h, the agent was ingested staining endocytotic membranes. Fluorescence microscopy suggested that GPI-HyPer and FM4-64 were attached to exclusive structures and did not colocalise (Figure 52).

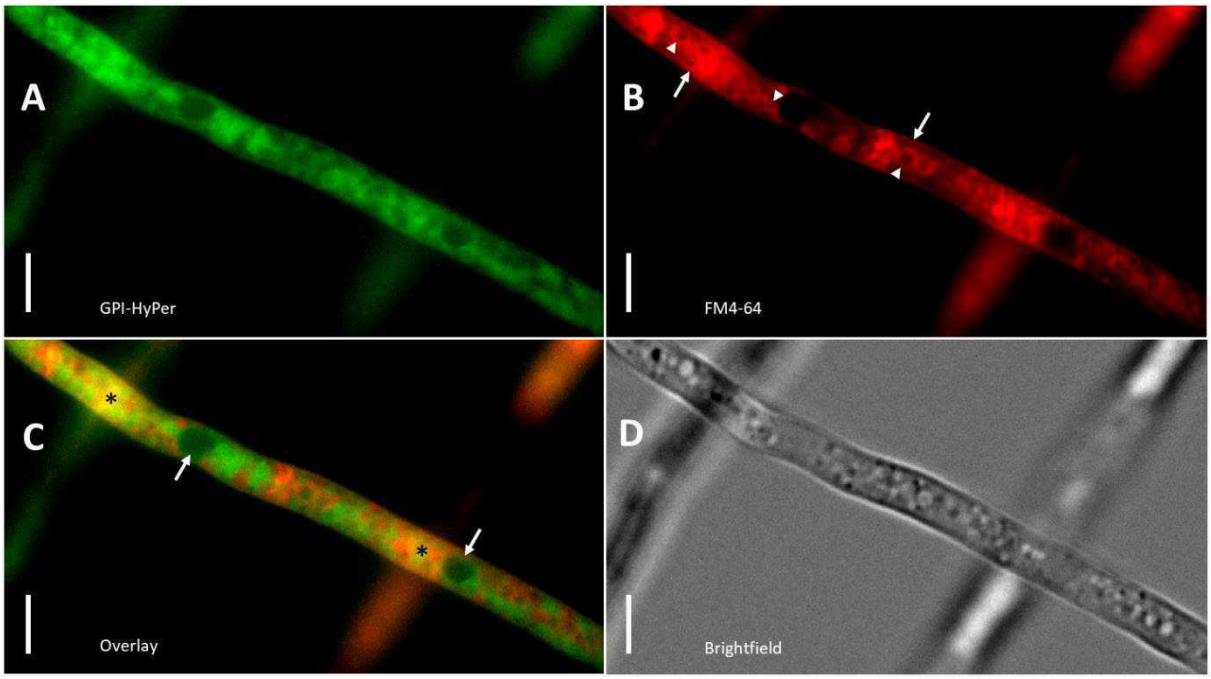

Figure 52: Fluorescence microscopy captures of a vegetative hypha expressing GPI-HyPer stained with FM™ 4-64. A: GPI-HyPer signal. **B:** FM™ 4-64 signal. The plasma membrane (white arrows) and multiple intracellular circular structures (white arrowheads), likely vacuoles and endocytotic vesicles, are visible. **C:** Merge. There is no overlap of GPI-HyPer signals and FM™ 4-64 signals. Areas occupied by the circular GPI-HyPer structures (white arrows) are devoid of any FM™ 4-64 signal. This indicates that GPI-HyPer is attached to no endocytotic structures. Yellow sections (black asterisks) are caused by overlap with the signal of the 2 hyphae in the background. **D:** Brightfield capture. Scale bars = 1 µm.

Again, a fluorescence intensity plot profile (Figure 53) was established to verify this optical analysis. The plot showed reciprocal behaviour of the GPI-HyPer and MitoTracker plot profiles. The peaks of the profiles did not overlap and were mostly faced by a minimum of the respective other profile. This confirmed the hypothesis that GPI-HyPer and FM4-64 did not colocalise suggesting that GPI-HyPer is not attached to endocytotic membranes.

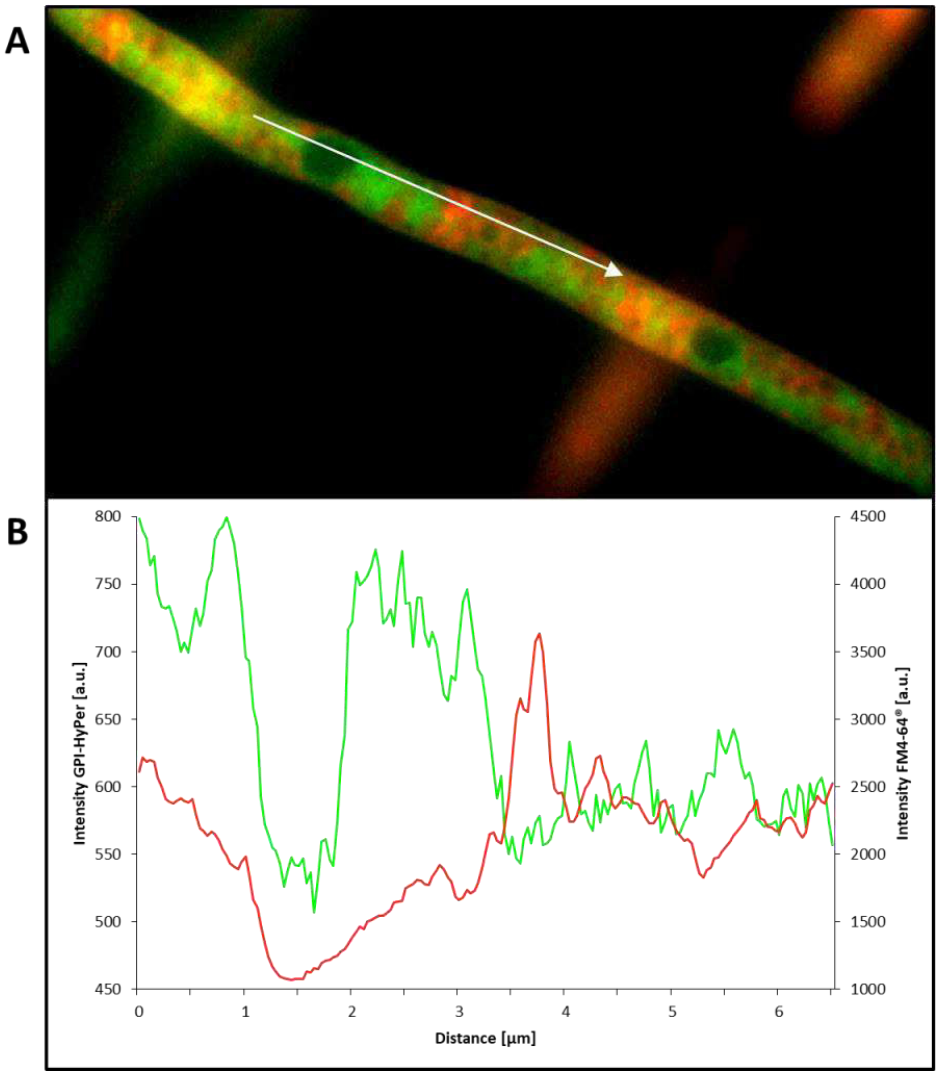

Figure 53: Fluorescence intensity plot profile projection of GPI-HyPer and FM4-64® composite picture. A: Composite picture of a vegetative *F. graminearum* hypha expressing GPI-HyPer stained with FM4-64. The white arrow represents the approximately 6.5 µm long line of interest from which the values for the plot profile were taken. **B:** Plot profile of GPI-HyPer and FM4-64 fluorescence intensity. The two profiles exhibit a reciprocal behaviour towards each other. When one plot shows an intensity peak the other mostly shows a minimum. The GPI-HyPer plot shows two high intensity peaks separated by a ca. 1 µm broad minimum within the first 3 µm of the plot. The FM4-64 plot starts with a decline until reaching the same minimum and increases afterwards. While the GPI-HyPer intensity declines after 3 µm reaching a minimum at 3.5 µm the FM4-64 plot increases until reaching a peak after 4.8 µm. Within the next 3 µm the GPI-HyPer profile and the FM4-64 profile show alternating peaks and minima underlining that the GPI-HyPer and FM4-64 signals do not colocalise.

Together, the results suggest that GPI-HyPer binds the ER and mitochondria but not endocytotic membranes. The asserted subcellular localisation of GPI-HyPer allows for new areas of application for the HyPer probe since ROS play a fundamental role in the function of ER and mitochondria. GPI-HyPer could therefore be used to monitor ROS fluctuations specifically in these organelles during live-cell imaging.

3.2.3 ER-stress leads to no deviation of the H_2O_2-level

Disrupting the correct interplay between the ER and the Golgi apparatus can lead to an accumulation of immature proteins inside the ER which is accompanied by an increase of the ER's ROS level (Santos et al., 2009). This reaction is called unfolded protein response (UPR) and is inducible by chemicals such as brefeldin A which interrupts the formation of ER vesicles and triggers the collapse of the Golgi apparatus leading to a reflux of proteins into the ER (Ripley et al., 1993), or tunicamycin which inhibits correct protein folding in the ER causing accumulation of misfolded proteins. Given that GPI-HyPer is a H_2O_2 probe located at the ER it posed a promising tool to visualise these cellular adaptations. To test whether ER-stress is detectable with GPI-HyPer, cells of the GPI-HyPer and cytHyPer mutant strains were cultivated in a 96-well plate and challenged with brefeldin A and tunicamycin diluted in DMSO. The fluorescence intensity ratio (F485/F380) of the two absorption maxima was measured for over 12 h using a microtiter plate reader. The WT, expressing no HyPer, shows a F485/F380 ratio of 2 which presumably derives from a natural fluorescence of the fungal cells (autofluorescence) which is independent of fluorescence proteins. The WT ratio only very slightly increased in all samples, suggesting that treatment with brefeldin A or tunicamycin has no major influence on the HyPer-independent autofluorescence of the cells. The cytHyPer and GPI-HyPer mutants show a decrease of the ratio from the start in all samples. The cytHyPer ratio is constantly decreasing until the end of the measurement. The GPI-HyPer ratio decreases until reaching a minimal value which is followed by a very slight increase for the rest of the measurement. The cells stressed with the brefeldin A or tunicamycin showed the same ratio progression as the negative controls (cells supplemented only with the solvent without tunicamycin or brefeldin A) (Figure 54) which shows that the observed decrease of the cytHyPer and GPI-HyPer ratios was not caused by the ER-stress inducing agents. It is likely that the gradual decrease of the cytHyPer and GPI-HyPer ratios is caused by bleaching of the sample due to constant excitation of HyPer by the plate reader. The experiments were also performed adding Triton X-100 (0.2%) and Tween 20 (0.02%) to the solvent to increase fungal cell permeability for tunicamycin and brefeldin A. The results, however, were the same. Together, the results suggest that neither cytHyPer nor GPI-HyPer react towards ER-stress.

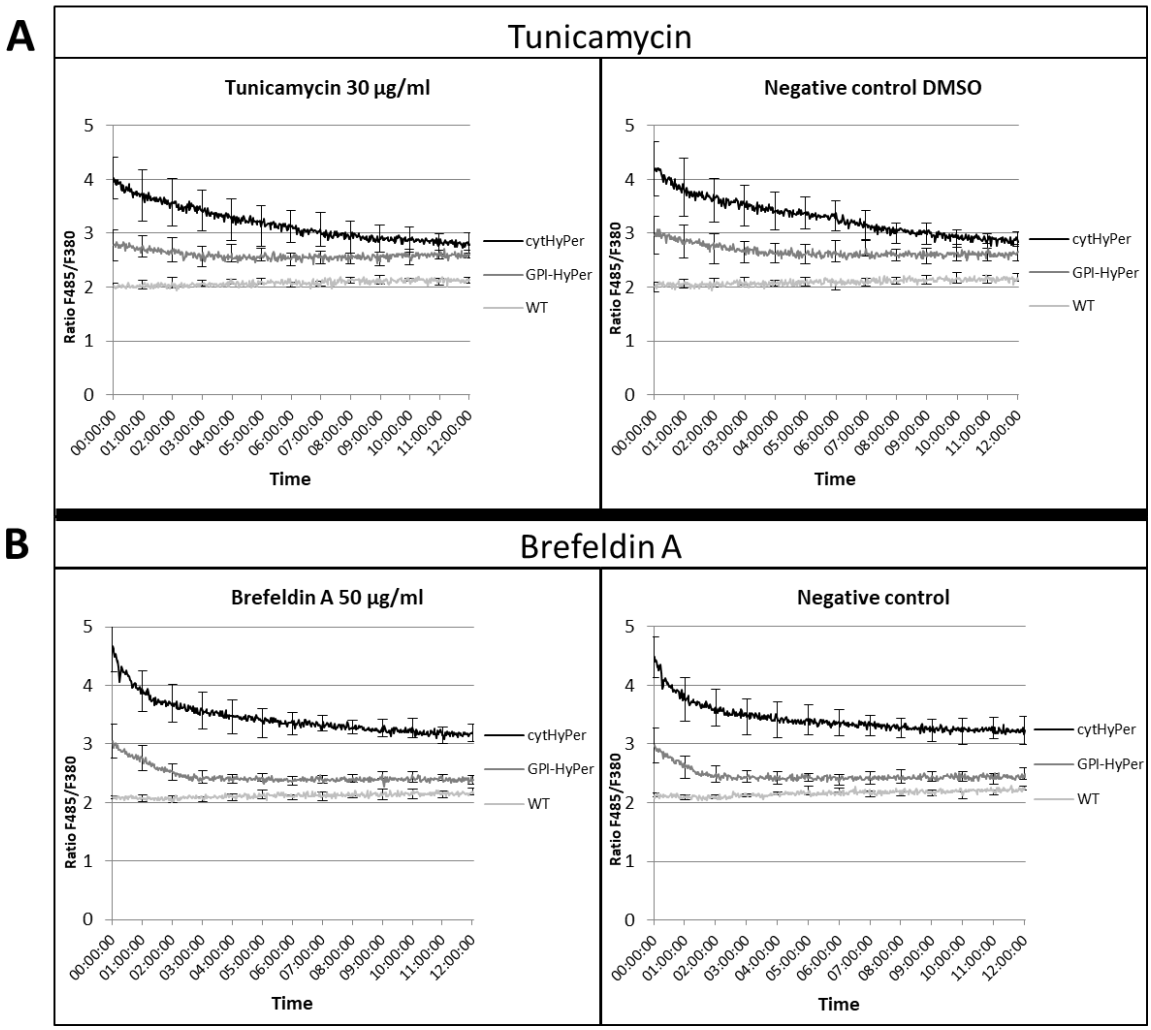

Figure 54: cytHyPer and GPI-HyPer ratio (F485/F380) progression upon ER-stress induction. cytHyPer and GPI-HyPer expressing strains were cultivated on minimal medium agar in a 96-well microtiter plate for 3 days. Immediately before starting the fluorescence measurement in a microtiter plate reader, 30 µg/ml tunicamycin or 50 µg/ml brefeldin A diluted in DMSO were added to each well. For negative controls, only the solvent without tunicamycin or brefeldin A was added. Fluorescence was measured continuously for 12 h. **A:** Ratio progression upon tunicamycin supplementation. The cytHyPer (black line) ratio starts at an initial value of 4.0. The ratio decreases consistently until reaching a value of 2.9 at the end of the measurement. The initial GPI-HyPer ratio (dark grey line) is 2.6. The ratio decreases until reaching a minimum of 2.37 after 6 h. Afterwards the ratio slightly increases until reaching a value of 2.5 at the end of the measurement. The ratio of the WT (light grey) starts at a value of 1.9 and increases continuously slightly until reaching a value of 2.15 at the end of the measurement. The ratio progressions in the negative controls are almost identical with the tunicamycin experiment ratio progressions. **B:** Ratio progression upon brefeldin A supplementation. The cytHyPer (black line) ratio starts at an initial value of 4.7. The ratio decreases consistently until reaching a value of 3.1 at the end of the measurement. The initial GPI-HyPer ratio (dark grey line) is 3.0. The ratio decreases until reaching a minimum of 2.4 after 3 h. Afterwards the ratio stays constant until end of the measurement. The ratio of the WT (light grey) starts at a value of 2.1 and increases continuously slightly until reaching a value of 2.2 at the end of the measurement. The ratio progressions in the negative controls are nearly identical with the brefeldin A experiment ratio progressions. The indistinguishable curve progressions of the ratio after ER-stress induction and of the negative control indicate that neither cytHyPer nor GPI-HyPer show a reaction to tunicamycin and brefeldin A.

3.2.4 GPI-HyPer still shows ratiometric reaction to H_2O_2

The absence of a GPI-HyPer ratio change upon ER-stress raised the question of whether the modifications that were performed on the HyPer sequence had abolished the ability for H_2O_2-dependent ratiometric behaviour. To rule out this possibility, experiments specifically assessing the ratiometric behaviour of GPI-HyPer towards oxidation by H_2O_2 and reduction by dithiothreitol (DTT) were conducted. As previously reported (Mentges & Bormann, 2015), the fluorescence intensity of the cells expressing GPI-HyPer increases after supplementation with H_2O_2 and decreases again after supplementation with DTT. To test if the attachment of the signal peptides impedes HyPer's ratiometric reaction towards H_2O_2, GPI-HyPer expressing cells of *F. graminearum* were cultivated in 96-well plates containing minimal medium agar. A microtiter plate reader equipped with multiple injectors successively measured fluorescence at 485 nm and 380 nm for 105 min with intermittent injections of H_2O_2 and DTT (Figure 55). The experiment showed that GPI-HyPer reacts to these agents in a similar way as was shown for HyPer. Shortly after injection of 20 mM H_2O_2, the ratio increases until reaching a peak value which is constant until injection of 50 mM DTT. After DTT injection the ratio decreases until the end of the measurement. The WT also showed a very slight ratio increase after H_2O_2 injection and decrease after DTT injection, suggesting that oxidation and reduction have a minor influence on the autofluorescence of *F. graminearum* cells as well. This result demonstrates that the modifications necessary to generate GPI-HyPer did not impede its H_2O_2-sensitivity and its typical reactions towards oxidation and reduction.

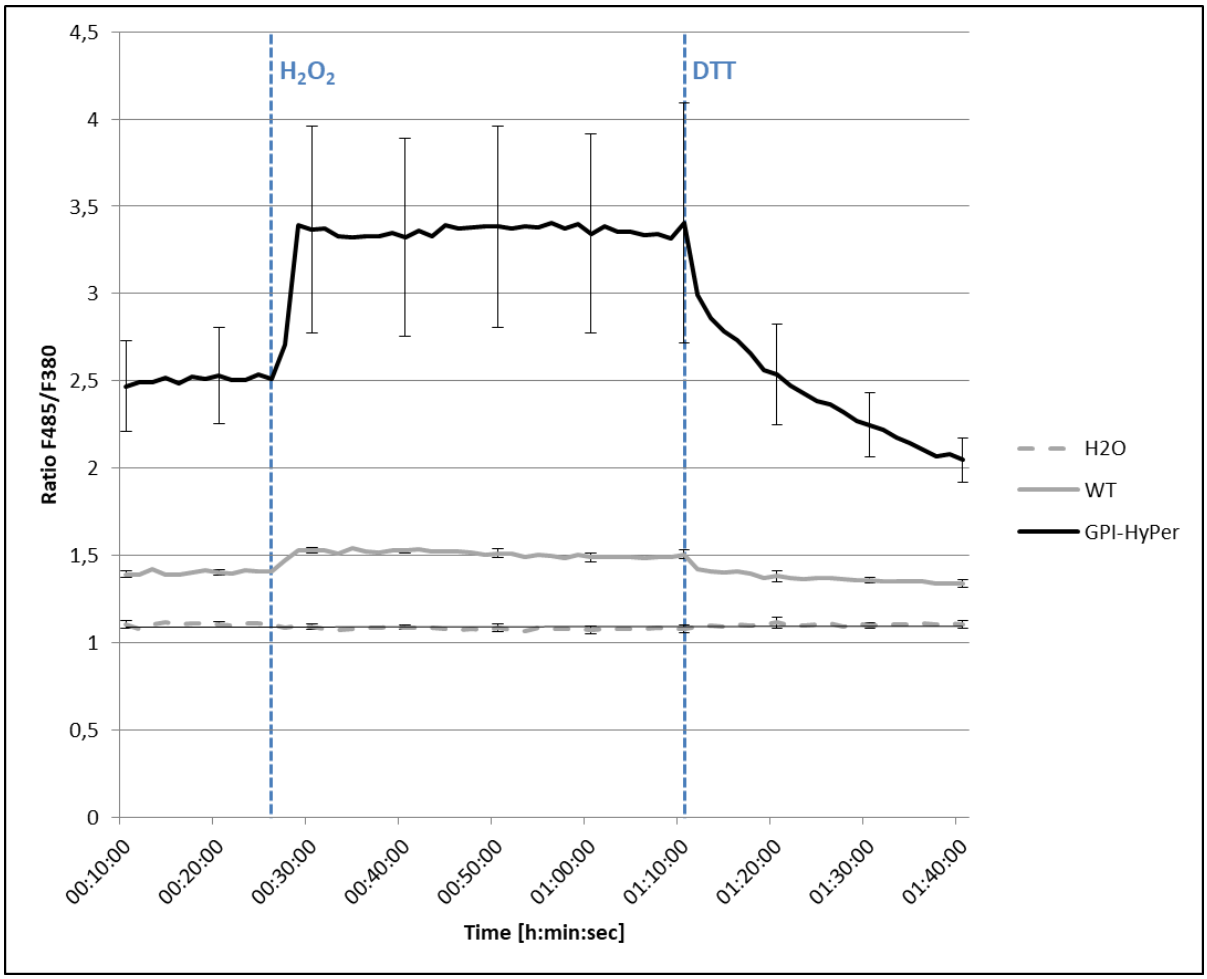

Figure 55: Oxidation and reduction reaction of GPI-HyPer. The figure shows the F485/F380 ratio measured with a microtiter plate reader over time. The vertical dashed lines indicate the time points of H_2O_2- and DTT-injection, respectively. After injection of 20 mM H_2O_2 the F485/F380 ratio in the GPI-HyPer mutant (black line) increases from 2.5 to 3.4 within 3 minutes. This value stays constant until addition of 50 mM DTT which is followed by a sudden decrease of the ratio. The decrease gradually slows down until the end of the measurement where the ratio reaches a value of 2.1. The WT (grey line) which does not express HyPer also shows a ratiometric reaction towards H_2O_2. Its base line ratio of 1.4 increases to 1.5 within 3 minutes. This value stays constant until addition of DTT which is followed by an immediate decrease of the ratio back to a value of 1.4. The ratio further decreases slightly until reaching a value of 1.35 at the end of the measurement. The water control (grey dashed line) shows no reaction to either substance. Error bars indicate the standard deviation. For the purpose of a better overview only every seventh standard deviation is shown.

A promising potential field of application for GPI-HyPer would be live-cell fluorescence microscopy allowing real-time visualisation of subcellular ROS-fluctuations. To determine GPI-HyPer's potential in this regard, an experimental setup based on the work of Michael Mentges (Master thesis) was established to enable the supplementation of GPI-HyPer expressing cells with H_2O_2 during confocal laser scanning microscopy (CSLM). GPI-HyPer mutant strains were cultivated on objective slides carrying minimal medium agar fixed in a Gene Frame®. Through an opening in the Gene Frame® and with the help of a syringe connected to a syringe pump, 20 mM H_2O_2 was applied on the mycelia. At the same time the hyphae were observed by CLSM with alternating excitation with 405 nm and 488 nm

(Figure 56). Within a period of 1 min to up to 20 min after H_2O_2 application, a specific, transient increase of the ratio between emission at 488 nm and 405 nm (ratio F488/F405) excitation wavelengths could be observed. Figure 56 presents a 30 min observation of an exemplary hypha exhibiting this behaviour. In this example, the reaction occurred approximately 11 min after starting the pump. The fluorescence intensity at 405 nm (left column) very slightly decreases until about 2 min after the reaction initiated before increasing again until the end of the measurement. The fluorescence intensity at 485 nm (middle column) increases until reaching a maximum after about 2 min, followed by a continuous decrease of fluorescence intensity until the end of the measurement. The ratio F488/F405 accordingly increases until 2 min after the start of the reaction before decreasing until the end of the measurement. The experiment revealed that the site of the ratio increase shown in Figure 55 corresponds to the observed subcellular localisation of GPI-HyPer shown in Figures 49-53. Also, the ratio increase of GPI-HyPer is not equal and not simultaneous throughout the cell but is first visible at the putative perinuclear ER followed by elongated structures. Throughout the measurement, the perinuclear ER shows the highest ratio in the hypha. This time dependent ratio increase of different subcellular structures suggests an irregular deposition and/or activity of GPI-HyPer in the subcellular structures it is attached to.

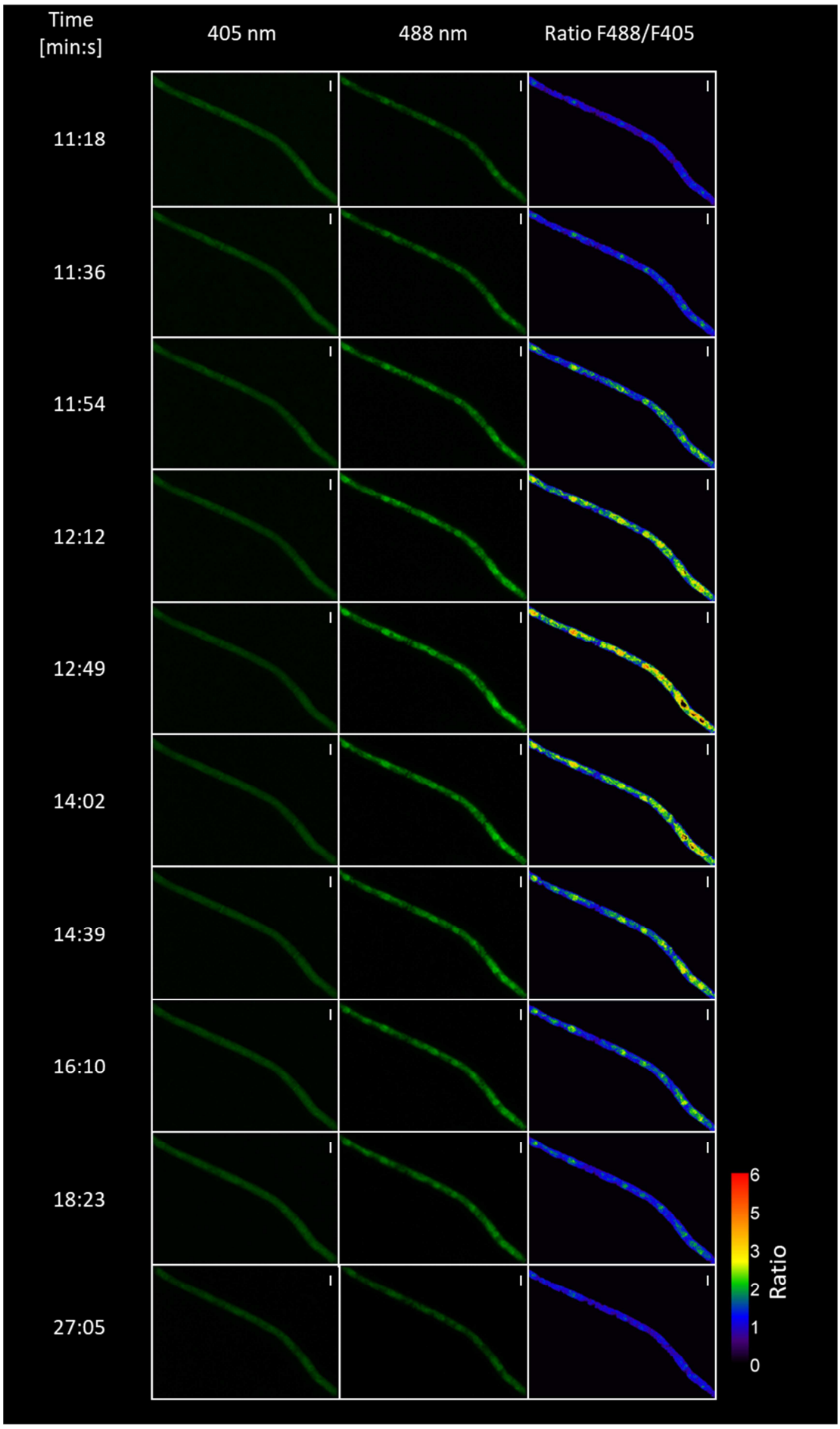
Time [min:s]
405 nm
488 nm
Ratio F488/F405
11:18
11:36
11:54
12:12
12:49
14:02
14:39
16:10
18:23
27:05
6
5
3
2
1
0
Ratio

Figure 56: Live-cell imaging of the GPI-HyPer reaction towards extracellular H_2O_2. GPI-HyPer expressing strains were cultivated on minimal medium agar carrying microscope slides. During live-cell imaging with confocal laser scanning microscopy the hyphae were supplemented with 20 mM H_2O_2. Throughout the experiment, fluorescence pictures were captured continuously. The figure shows the fluorescence intensity progression. Pictures were taken every 18 seconds during simultaneous excitation with wavelengths of 405 nm (left column) and 488 nm (middle column). Fluorescence intensity at 405 nm starts decreasing slightly at 11:18 min reaching a minimum at 12:49 min. Intensity increases afterwards again until the end of the measurement. Fluorescence intensity at 488 nm starts increasing at 11:18 min reaching a maximum at 12:49 min. Intensity decreases afterwards again until the end of the measurement. The right column shows the F488/F405 intensity ratio. The ratio starts increasing at 11:18 min until reaching a maximum at 12:49 min. The ratio decreases afterwards again until the end of the measurement. Values are indicated in the colour bar. The ratio increase is visible first at circular structures which were identified as perinuclear ER. At 11:36 min only these structures show increased ratio. At 11:54 min elongated structures show increased ratio as well. At 12:49 min, the moment of maximal GPI-HyPer oxidation in this experiment, putative perinuclear ER shows the highest ratio in the tested hypha. Scale bars = 1 µm.

The CLSM pictures where analysed *in silico* to gain comparable data of the observed GPI-HyPer reaction. A region of interest (ROI) was determined around the area with the strongest ratio increase (Figure 57). Measurement of the ROI's pixel intensity using the ratio plus function of the image processing program ImageJ revealed a ratio increase from 1.4 to 3.8 upon H_2O_2 exposure. The ratio increase is rapid and short. The maximum value of 3.8 is reached after 2 min immediately followed by a rapid decrease which slows down gradually before accelerating again after about 24 min. The initial ratio value is reached about 12 min after the maximum peak. At the end of the measurement, the ratio has reached a lower value than at the start of the experiment. An exact time difference between contact to H_2O_2 and rise of the ratio as in Figure 55 cannot be presented here because the time difference between starting of the pump and the reaction by GPI-HyPer varies from sample to sample and depends on the individual diffusion time of the H_2O_2 to the observed hyphae. Given the immediate reaction of GPI-HyPer after injection of H_2O_2 presented in Figure 55, it is to be expected that H_2O_2 contact and ratio increase are simultaneous.

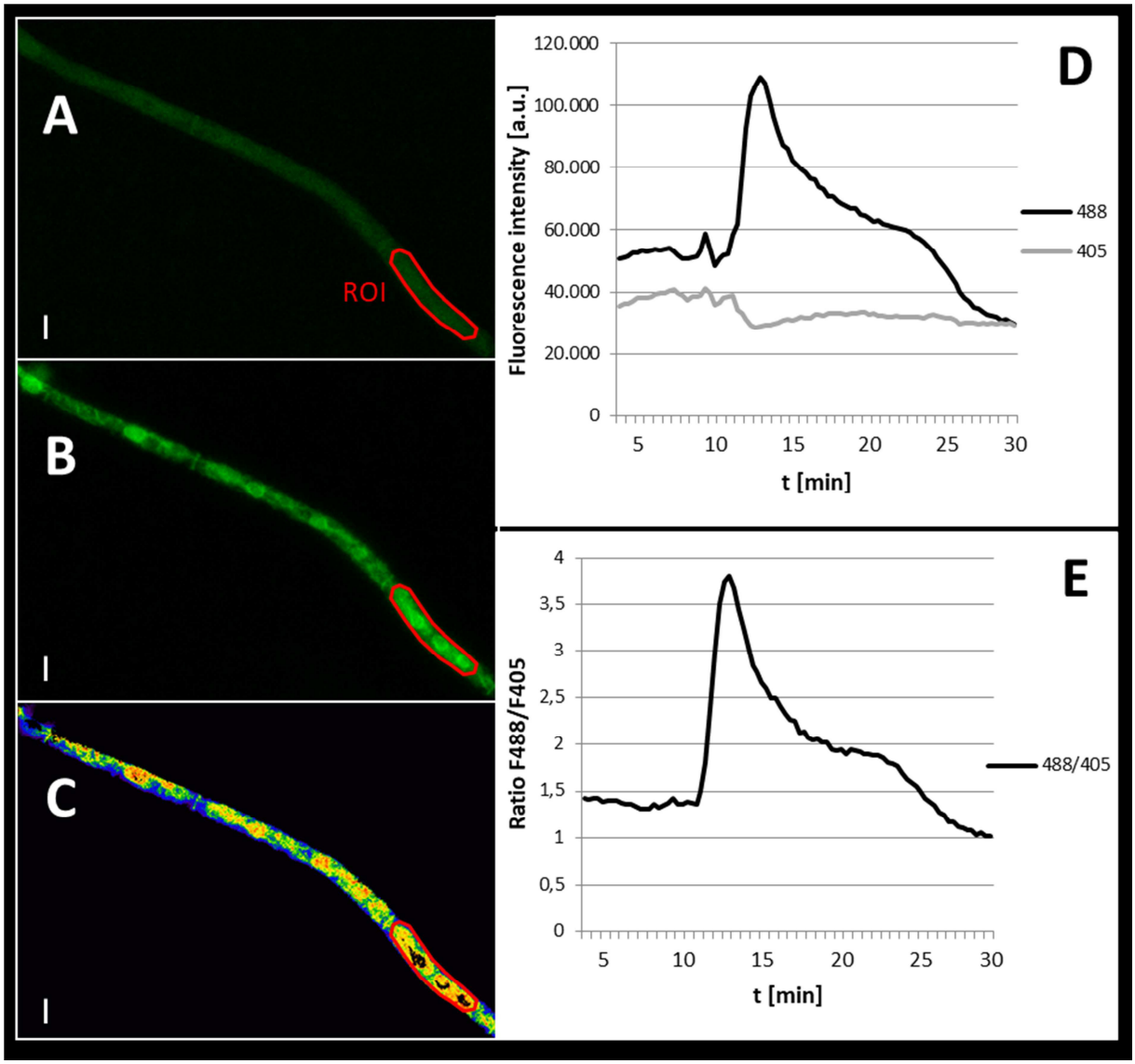

Figure 57: Region of interest evaluation during GPI-HyPer oxidation. Fluorescence pictures were captured every 18 seconds during excitation with wavelengths of 405 nm and 488 nm. A region of interest (ROI, red circle) was determined in which fluorescence intensities were calculated. **A:** Excitation with 405 nm. **B:** Excitation with 488 nm. **C:** F485/F405 ratio. **D:** Fluorescence intensity progression at 488 nm (black line) and 405 nm (grey line) excitation wavelength within the ROI until the end of the measurement. The small peak at the 9 minute mark before the putatively H_2O_2-triggered 485 nm intensity increase is due to focus adjustment. After 11 minutes the 488 nm fluorescence intensity increases from 50,000 to 110,000 a.u. within 2 minutes. Afterwards the fluorescence intensity decreases again. The decrease gradually slows down until the 24 minute mark before it accelerates again dropping to 29,000 a.u. at the end of the measurement. The 405 nm fluorescence intensity decreases after 11 minutes from 40,000 to 28,000 a.u. within 2 minutes. Afterwards the fluorescence intensity increases until reaching 33,000 a.u. at the 20 minute mark before very slightly decreasing again until the end of the measurement. **E:** F488/F405 intensity ratio progression within the ROI. After 11 minutes the ratio increases from 1.3 to 3.8 within 2 minutes before decreasing again. The decrease gradually slows down until the 24 minute mark before it accelerates again dropping to a ratio of 1.0. Scale bars = 1 µm.

3.2.5 Deletion of NoxR leads to increased ratio of cytHyPer but not of GPI-HyPer

With the functionality of GPI-HyPer verified its application in another ER-specific assay was attempted. One of the main sources of ROS in the cell is an enzyme complex termed nicotinamide adenine dinucleotide phosphate (NADPH)-oxidase (Nox). It has been suggested that members of the Nox family are located at the ER membrane (Marschall et al., 2016b). The catalytical subunits NoxA and NoxB are under control of the regulatory subunit NoxR (Sumimoto, 2008). In previous studies NoxR was deleted in a HyPer expressing *F. graminearum* mutant (Master thesis Michael Mentges, 2014). Microtiter plate reader measurements revealed a significantly increased ratio suggesting an increase in the cellular H_2O_2 level after NoxR deletion. The source of the H_2O_2, however, is unclear. With the ER-tagged GPI-HyPer a tool was at hand to gain further insights into this matter. If GPI-HyPer would show the same ratio increase in a NoxR-deletion mutant this would suggest that ER-resident Nox is involved in the observed raise of the H_2O_2 level in the HyPer mutant. For this purpose, deletion mutants of NoxR (Δ*NoxR*) were established in the cytHyPer and GPI-HyPer mutant background. Resulting mutants were termed cytHyPer_Δ*NoxR* and GPI-HyPer_Δ*NoxR* and screened for their 485/380 ratio using the same microtiter plate reader setup as in section 3.2.3. The cytHyPer_Δ*NoxR* mutants showed a significantly increased ratio compared to the cytHyPer mutant reproducing the results in Mentges' master thesis. Before addition of H_2O_2, the ratio of cytHyPer_Δ*NoxR* was increased suggesting a higher base oxidation level. After H_2O_2 injection, the ratio of cytHyPer_Δ*NoxR* stayed above the ratio of cytHyPer showing that supplementation with 20 mM H_2O_2 does not lead to maximal oxidation of HyPer. After reduction by DTT, the cytHyPer_Δ*NoxR* ratio gradually approaches the cytHyPer ratio until the end of the measurement. This indicates that the higher base oxidation of cytHyPer_Δ*NoxR* is reversible. In contrast to these results, the base oxidation level of the GPI-HyPer_Δ*NoxR* mutants was similar to that of the GPI-HyPer mutant (Figure 58). Injection of H_2O_2 and DTT led to an equal increase and decrease of the ratio in both strains. Together, these results suggest that the deletion of the Nox regulator leads to an elevated H_2O_2-level in the cytosol but not in the ER and demonstrate the benefit of the new subcellular H_2O_2 sensor GPI-HyPer.

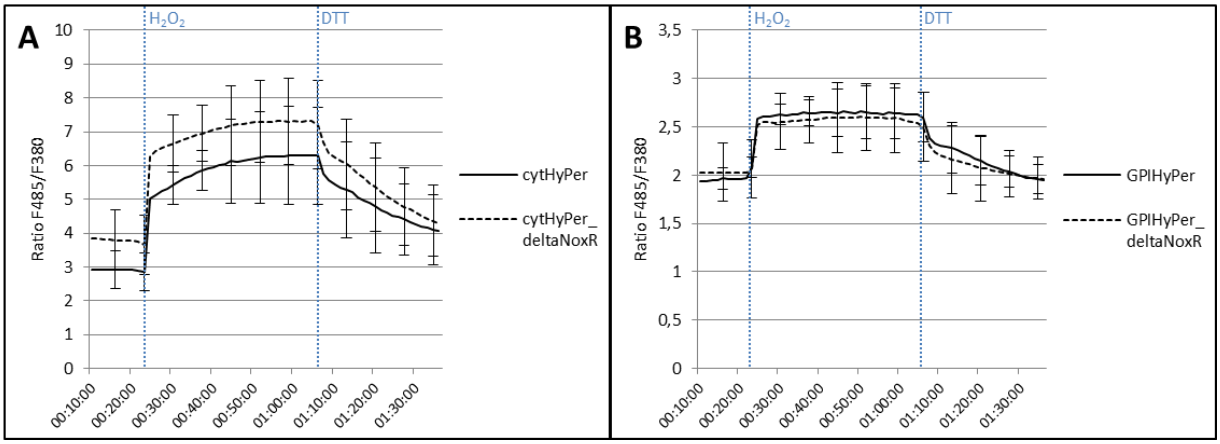

Figure 58: Comparison of cytHyPer ratio with GPI-HyPer ratio with and without deletion of NoxR. A: Progression of the ratio (F485/F380) of the cytHyPer mutant in WT background (solid line) and in *ΔNoxR*-background (dashed line). The vertical dotted lines indicate the time points of H_2O_2- and DTT-injection, respectively. cytHyPer_Δ*NoxR* shows a constantly increased oxidation level compared to cytHyPer. The average baseline ratios of cytHyPer and cytHyPer_Δ*NoxR* were 2.9 and 3.8, respectively. After addition of H_2O_2, the ratio of cytHyPer_Δ*NoxR* stays above the ratio of cytHyPer. The cytHyPer ratio initially reaches a value of 5.0 immediately after H_2O_2 substitution before gradually further increasing to a maximum of 6.3 at the moment of DTT substitution. The cytHyPer_Δ*NoxR* ratio initially reaches a value of 6.3 immediately after H_2O_2 substitution before gradually further increasing to a maximum of 7.3 at the moment of DTT substitution. After addition of DTT, the cytHyPer ratio drops to a value of 5.5 before gradually further decreasing until reaching a value of 4.0 at the end of the measurement. cytHyPer_Δ*NoxR* drops to a value of 6.3 before further decreasing and gradually approaching the cytHyPer ratio, reaching a value of 4.3 at the end of the measurement. GPI-HyPer_Δ*NoxR* shows the similar ratios as GPI-HyPer. GPI-HyPer and GPI-HyPer_Δ*NoxR* have an average initial value of 1.9 and 2.0, respectively. After H_2O_2 substitution the ratios increase to 2.6 and 2.55, respectively. These values stay constant until DTT substitution. After addition of DTT, the ratios drop to a value of 2.4 and 2.3, respectively, before gradually further decreasing to a value of 2.0 at the end of the measurement. Error bars indicate the standard deviation. For the purpose of a better overview only every fifth standard deviation is shown.

In summary, while GPI-HyPer failed to show a fluorescence signal at the surface of *F. graminearum* hyphae, making it unfit for measuring H_2O_2 at the area of contact between pathogen and host, it proved to be a valuable tool for monitoring intracellular H_2O_2 fluctuations. Organelle stains revealed that GPI-HyPer was attached to the ER and mitochondria. The combination of the HyPer ORF with the GPI-anchor did not abolish the sensor's function for ratiometric reaction to H_2O_2. Live-cell imaging during H_2O_2 supplementation using CLSM both confirmed the staining results and proved GPI-HyPer's functionality, revealing that the ER displayed the highest GPI-HyPer activity. Application of this novel H_2O_2 sensor in WT and Δ*NoxR* backgrounds suggested that a rise of intracellular ROS levels caused by a deletion of NoxR is not linked to an increasing H_2O_2 concentration in the ER. Instead, cytosolic H_2O_2 levels are significantly increased in Δ*NoxR* mutants. Application of GPI-HyPer in ER-stress experiments did not reveal any H_2O_2 based changes in the ER.

4. Discussion

It is evident that ROS are of major importance for virtually all aspects of cellular life (Mittler et al., 2011; Tudzynski et al., 2012; Foyer & Noctor, 2013; Vaahtera et al., 2014; Mittler, 2017). Of special interest for this thesis is the aspect of plant-pathogen interactions which are to a great extend governed by ROS: ROS are used as second messengers, control polarised hyphal growth and cellular differentiation and belong to the weaponry of both pathogen and host (Scott & Eaton, 2008; Heller & Tudzynski, 2011; Tudzynski et al., 2012), functions which are indispensable for fungal-plant interactions during infection. Previous studies showed that ROS are a key element for successful pathogenesis or symbiosis (Tiedemann, 1997; Toone & Jones, 1999; Schouten et al., 2002; Lyon et al., 2004; Nathues et al., 2004; Shetty et al., 2007; Molina & Kahmann, 2007; Walz et al., 2008; Abbà et al., 2009; Alkan et al., 2009; Williams et al., 2011; L'Haridon et al., 2011; Nguyen et al., 2012; Kiirika et al., 2012; Kobayashi et al., 2012; Bai et al., 2013; Kapoor & Singh, 2017). However, the nature of the fungus' response towards the ROS-mediated plant defence mechanism depends on the infection strategy of the pathogen. While biotrophic fungi inhibit or overcome the PTI, necrotrophic pathogens tend to use it to their advantage (Govrin & Levine, 2000). This fundamental difference might be deduced from the behaviour of hemibiotrophic fungi such as the plant pathogens *Septoria tritici*, *Verticillium dahliae*, or *Macrophomina phaseolina*. During the early, biotrophic, phase of infection no ROS accumulation was observed in these strains whereas high concentrations of ROS could be detected in the later, necrotrophic, phase of infection (Shetty et al., 2007; Chowdhury et al., 2017). Similar results for *F. graminearum* are presented by Zhang et al. (2012) who revealed a relatively higher expression of genes counteracting the plant-derived ROS-burst at early stages of infection followed by higher expression of genes contributing to ROS-production in later stages of infection. Regarding the infection strategy it needs to be noted here that the plant specific data presented by Zhang et al. (2012) was obtained from wheat coleoptiles which are not the typical site of infection of *F. graminearum*. It is still a matter of discussion how *F. graminearum* is to be integrated in the classification system of biotrophic, hemibiotrophic, and necrotrophic lifestyles. While Brown et al. (2010) discuss a unique lifestyle preceding the necrotrophic phase, Kazan et al. (2012) classify *F. graminearum* as a hemibiotrophic fungus. Boenisch & Schäfer (2011), however, observed necroses in the host tissue already during early infection phases on wheat florets, contradicting an early biotrophic phase. Further research is necessary to irrevocably define the lifestyle of *F. graminearum*.

Apart from virulence, ROS metabolism has been shown to control fungal growth and differentiation (Hansberg & Aguirre, 1990; Malagnac et al., 2004; Kayano et al., 2013). During differentiation events, local ROS levels increase and scavenging systems get upregulated. The aim of this work was to gain further insight into the highly complex world of ROS-related interactions between host and pathogen by monitoring ROS-

fluctuations relevant for infection and by characterising genes involved in the ROS-metabolism of *F. graminearum*. The main tool for the selection of target genes was an RNAseq-based transcriptomic analysis of *F. graminearum* growing *in planta* and *in vitro* performed by Mentges et al. (unpublished results). All genes chosen for deletion in this study shared one or multiple of the following parameters: involvement in ROS-metabolism, differential regulation *in planta*, low functional redundancy, secretion. 149 genes were identified that are linked to the metabolism of ROS and that were significantly induced in expression during palea colonisation. One fourth of those genes (34) are significantly up-regulated in IC compared to RH, whereas 10 genes are up-regulated in RH compared to IC.

Two genes, FGSG_17054 (FgMT1) and FGSG_12456 (FgMT2), that show characteristic features of metallothioneins, are among the highest plant-induced genes in the database and show no expression *in vitro* which made them promising targets for gene deletion. Metallothioneins are small (25-30 amino acids), cysteine-rich (25-30%) proteins that share a similar motif of seven cysteine residues constituting the proteins' metal binding capabilities. The *Neurospora crassa* metallothionein motif (X_2-[CXC]-X_5-[CXC]-X_3-[CXC]-X_2-C-X_3) (Lerch, 1980; Münger & Lerch, 1985) has been found in a variety of fungal metallothioneins and is also present in FGSG_17054 (MAGD-[CGC]-SGASS-[CNC]-GSS-[CSC]-SG-C-GK) and FGSG_12456 (MACDCGSS-[CNC]-GGASS-[CNC]-GES-[CTC]-KG-C-GK). Apart from FGSG_17054 and FGSG_12456 a third gene, FGSG_08172, was originally annotated as a metallothionein in the transcriptomic data this study is based on. FGSG_08172, however, is much longer (112 amino acids) and exhibits a lower cysteine proportion (14.3%) than typical fungal metallothioneins. Furthermore, while the amino acid sequence of FGSG_08172 exhibits 7 CXC patterns it does not contain the above mentioned characteristic metallothionein motif. Therefore, this thesis did not follow the annotation of FGSG_08172 being a metallothionein. Instead, a BLAST search of the metallothionein motif revealed a non-annotated hypothetical protein FGSG_16151 (former FGSG_04088) (MSG-[CGC]-ASSGS-[CGC]-GSS-[CTC]-AG-C-PCRNHAVSLLGR) that shares all other metallothionein characteristics such as low molecular weight and high cysteine content and was thusly considered a metallothionein. In contrast to FGSG_17054 and FGSG_12456, FGSG_16151 is not plant-induced and is expressed in axenic culture. Neither the single deletion nor the simultaneous deletion of all three metallothioneins led to changes in pathogenicity, oxidative stress tolerance, metal stress tolerance, metal starvation, vegetative growth, and sexual fruiting body formation. The single clone of the first Δ*FGSG_17054* protoplast transformation containing a successful deletion (Δ*FGSG_17054.1*) showed a phenotype which proved to be not reproducible. Δ*FGSG_17054.1* exhibited a strong increase and acceleration of perithecia formation. This phenotype is also prevalent in the and the simultaneous deletion mutant that were established in the Δ*FGSG_17054.1* background (ΔΔ*FGSG_17054.1;FGSG_12456* and ΔΔΔ*FGSG_17054.1;FGSG_12456;FGSG_16151*). Two additional protoplast transformations (Δ*FGSG_17054.2* and Δ*FGSG_17054.3*) did not show the increased

fruiting body formation. Indeed, southern blotting revealed a second integration of the deletion construct into the *F. graminearum* genome in Δ*FGSG_17054.1* which was not present in Δ*FGSG_17054.2* and Δ*FGSG_17054.3*. Therefore, it is safe to assume that the observed phenotype of Δ*FGSG_17054.1* and the simultaneous deletion mutants is caused by the second integration. Measures are taken to identify the location of this integration as it might reveal the gene responsible for the intriguing phenotype. *F. graminearum* WT strain 8/1 produces only small amounts of perithecia compared to the highly fertile *F. graminearum* WT strain PH1 (Trail & Common, 2000). During experiments with *F. graminearum* PH1 perithecia were visible as early as 10 dpi, whereas with *F. graminearum* 8/1 perithecia formation took 6-12 weeks. It is conceivable that the second integration in Δ*FGSG_17054.1* caused a genetic anomaly similar to the one being responsible for the hyperfertility of *F. graminearum* PH1.

Metallothioneins exhibit antioxidative properties that derive from either the sequestration of copper, which can potentially partake in the Fenton reaction generating hydroxyl radicals (Reddy et al., 2014), or by scavenging of ROS by free reduced cysteine moieties (Ruttkay-Nedecky et al., 2013) which otherwise constitute the binding positions for metals. Metals are an important factor in fungal virulence (Gerwien et al., 2017). While many metals are required as essential trace elements some also play an active role in weaponry of host and fungus during infection. They are either needed to be withdrawn from the aggressor by the host as it is the case with iron or zinc, or can be actively released in phagosomes as a defence reaction against a pathogen as with copper (White et al., 2009; Gerwien et al., 2017). Iron and zinc are vital cofactors that pathogen and host compete over. Copper is also used as a cofactor in cells but is highly toxic when accumulated. Metallothioneins take part in the metal metabolism of all eukaryotes and many prokaryotes (Coyle et al., 2002; Vasák, 2005) and therefore also in host-pathogen interactions, no matter if the host is plant or animal. Still, scientific literature covering functional characterisations of multicellular fungal metallothioneins in pathogenicity is scarce. The bacterial human pathogen *P. aeruginosa* expresses the metallothionein PmtA that is needed for oxidative stress resistance and production of a secondary metabolite which is vital for pathogenicity (Pietrosimone, 2014). In the opportunistic fungal human pathogen *Cryptococcus neoformans* Cu^{2+}-detoxifying metallothioneins are induced during infection as a reaction to the host's hyperaccumulation of copper. Deletion of metallothioneins significantly reduced virulence of the fungus (Ding et al., 2013). In *M. oryzae* the metallothionein MMT1 is a virulence factor (Tucker et al., 2004). Deletion of *mmt1* causes inability to penetrate the host cuticle which may be linked to the finding that MMT1 is located at the inner cell wall of the fungus. This would also imply that MMT1 is secreted, contrary to the metallothioneins in *F. graminearum*. Metal tolerance was not affected. In contrast to FGSG_17054 and FGSG_12456, MMT1 was highly expressed in *M. oryzae* at most stages of its life cycle (Tucker et al., 2004). The authors expect MMT1 to play a role in cell wall differentiation rather than a defensive agent against the plant's oxidative burst.

Considering the highly conserved metal binding capabilities of metallothioneins throughout all kingdoms and the low number of metallothionein genes in the *F. graminearum* genome, it is particularly surprising that even the simultaneous deletion of all three metallothioneins of *F. graminearum* had no significant impact on metal detoxification or during metal starvation (see Results, Figure 36 and Figure 37). Most fungal metallothioneins mainly sequester copper (Borrelly et al., 2002) and the vast majority of characterised fungal metallothioneins was shown to be upregulated under copper excess (Thorvaldsen et al., 1995; Riggle & Kumamoto, 2000; Ramesh et al., 2009; Ding et al., 2011; Reddy et al., 2014; Kalsotra et al., 2018). Zinc, cadmium, or silver are also frequently reported as inductors of metallothionein synthesis (Jacob et al., 2004; Reddy et al., 2014; Kalsotra et al., 2018). Generally, the metal specificity of metallothioneins differs interspecifically between copper, zinc, cadmium, silver, and mercury. *S. cerevisiae* modifies the copy number of its metallothionein gene CUP1 according to the ambient copper concentration. Together, it was reasonable to assume importance of *F. graminearum* metallothioneins at least during growth under high copper concentrations. If none of the predicted metallothioneins in *F. graminearum* are essential for metal detoxification the question arises which other strategies could be used by the fungus for this purpose. It is possible that FGSG_08172, which is annotated as a metallothionein but was not considered a metallothionein in this study, is of importance in this regard. Potentially, the thiol groups of the CXC patterns in its sequence could serve as binding residues for metal ions depending on its tertiary structure. Aside from generating a deletion mutant, the assessment of the FGSG_08172 transcript level during metal stress could offer valuable clues whether FGSG_08172 is involved in metal metabolism and could compensate for the loss of metallothioneins. Generally, yeasts and filamentous fungi are able to use a broad range of mechanisms to protect themselves against heavy metals such as chemical transformation, sequestration (by metallothioneins, calmodulin, polyphosphates, and polyamines), binding of metal ions to the cell wall (biosorption), compartmentalisation, immobilisation, and protection (Walker, 2004; Iskandar et al., 2011). It has been reported that metal tolerant species of filamentous fungi (e.g. species found in mining areas) possess cell walls with high heavy metal adsorption capacities and specific intracellular compartmentalisation (Blanquezet et al, 2004; Mohammadian et al., 2017) suggesting genetic adaption to extreme metal conditions. In yeast, the transporter CCC2 regulates transfer of copper into the Golgi apparatus, eventually resulting in its secretion (Walker, 2004). Five genes in *F. graminearum* are annotated as copper transporters. Assessing the regulation of metal ion transporters, particularly copper transporters, during metal stress in WT and metallothionein deletion backgrounds in *F. graminearum* could be worthwhile as these proteins might compensate for the lack of metal detoxification capabilities in the metallothionein deletion mutants.

While metallothioneins in *F. graminearum* are annotated as intracellular proteins, a fundamental part of this thesis revolved around secretion. Filamentous fungi are known

for being dependent on their exceptional ability to secrete large amounts of proteins, metabolites, and organic acids (Conesa et al., 2001; Peberdy et al., 2001). Owing to their degradive lifestyle they need to rely on an array of extracellular enzymes such as ligninases, cellulases, and pectinases (Kubicek et al., 2014; Lo Presti et al., 2015). The transcriptome of *F. graminearum* contains 1665 genes (12% of all predicted genes) predicted for secretion. 634 of these genes are plant-regulated with 328 being plant-induced while 306 are plant-repressed (Mentges et al., unpublished results). This suggests that indeed secreted genes in *F. graminearum* play an important role in infection.

Secretion of proteins is mainly mediated by the secretory pathway to which the endoplasmic reticulum (ER) constitutes the gateway. For the correct function of the ER the ROS-metabolism plays an important role (Krishnan & Askew, 2014). Furthermore, reduction of the secretory capacity has led to impaired pathogenicity in human- and plant-pathogenic fungi (Yi et al., 2009; Joubert et al., 2011; Cheon et al., 2011; Miyazaki et al., 2013; Krishnan & Askew, 2014), directly connecting ER-functionality and disease. In order to monitor H_2O_2-fluctuations in the ER the new modified H_2O_2-sensor generated in this study could prove useful. Originally, it was attempted to attach the ratiometric H_2O_2 sensor protein HyPer (Belousov et al., 2006) to the cell surface of *F. graminearum* in order to gain a new tool for visualizing ROS-based interactions in the immediate contact area between pathogen and host. For this purpose the N- and C-terminal signal peptides from the allegedly GPI-bound cell surface-attached superoxide dismutase (SOD) FGSG_00576 were cloned upstream and downstream of the HyPer ORF in the overexpression vector pII99. However, mutants expressing this modified HyPer (GPI-HyPer) showed no fluorescence on the cell surface. The exact reasons for this are unknown but it is likely that the extracellular milieu is unsuitable for HyPer, that the modified polypeptide is not folded correctly during secretion, or that the extracellular signal is too weak to be detected in the presence of unspecific background fluorescence. It has been shown previously that a putatively secreted SOD (FGSG_08721) (Paper et al., 2007; Brown et al., 2012; Lowe et al., 2015) was detected intracellularly after fusion with mRFP (Yao et al., 2016) suggesting that modifications of enzymes with fluorescence proteins may potentially influence their localisation. Interestingly, a strong signal of GPI-HyPer in intracellular organelle membranes could be detected. Labelling experiments with ER-Tracker™ Blue-White DPX, MitoTracker™ Red FM, and FM™ 4-64 revealed that GPI-HyPer mainly binds the ER, partially binds mitochondria, but never endocytotic vesicles (see Results, Figure 49-51). It is therefore also possible that these structures constitute the actual location of FGSG_00576, contrary to its annotation as cell surface attached. For a GPI-anchored protein, however, an intracellular localisation beyond structures involved in exo- or endocytosis (i.e. mitochondria) would be unusual. For GPI-HyPer the subcellular localisation opened up new possibilities in an unintended but nonetheless interesting application spectrum, namely the ROS-dynamics at the secretion-controlling ER and the mitochondria, two essential cellular ROS producers (Balaban et al., 2005; Santos et al., 2009). Life-cell-imaging via confocal laser scanning fluorescence microscopy as well as

analyses with a microplate reader proved that the ratiometric reaction towards H_2O_2 was functional in GPI-HyPer, although with a smaller ratio amplitude compared to cytosolic HyPer (cytHyPer), probably owing to its subcellular localisation (see Results, Figure 58).
The new GPI-HyPer probe was used to gain insight into ROS fluctuations during ER-stress. Interestingly, no deviation from the negative control was observed after challenging GPI-HyPer expressing cells with brefeldin A or tunicamycin, which lead to the ROS-inducing unfolded protein response (UPR). This suggests that ER-stress in *F. graminearum* does not lead to generation of H_2O_2. However, production of ROS is an integral part of the UPR (Santos et al., 2009; Laurindo et al., 2012; Zeeshan et al., 2016). In this regard, the question of which species of ROS is produced is important. The ER enzyme Ero1 is a vital player in ER functionality as it regenerates reduced protein disulfide isomerase (PDI), thereby enabling persistent protein folding. This mechanism generates H_2O_2 and is rising in activity during ER stress (Marciniak & Ron, 2006), a reaction that should be detectable with GPI-HyPer. In *Caenorhabditis elegans* Ero1 produces enough H_2O_2 to constitute a visible portion of tunicamycin-induced dichlorofluorescein (DCF) fluorescence (Harding et al., 2003). On the other hand, there is evidence that superoxide contributes to the ROS burst during the UPR as well. Santos et al. (2009) reported increased superoxide signals after tunicamycin-treatment of vascular smooth muscle cells. Although representing a precursor of H_2O_2 (being the substrate for SODs), superoxide itself does not cause changes in the HyPer ratio (Belousov et al., 2006). In addition to Ero1, mitochondria and Nox participate in UPR-associated ROS generation. In mammals, ER membrane-bound Nox4 is upregulated strongly during ER-stress and contributes greatly to UPR-associated ROS accumulation (Pedruzzi et al., 2004; Santos et al., 2009; Laurindo et al., 2014). There is contradictory evidence regarding the identification of the ROS produced by Nox4. While multiple studies describe Nox4 as a mainly H_2O_2 producing enzyme (Serrander et al., 2007; Dikalov et al., 2008; Helmcke et al., 2009; Takac et al., 2011; Nisimoto et al., 2014) there is literature suggesting that Nox4 produces superoxide as well (Serrander et al., 2007; Bedard & Krause, 2007; Kuroda et al., 2014). Since, in fungi, the Nox homologues NoxA and NoxB appear to be superoxide producers (Kim, 2014; Wang et al., 2014) and NoxC is predicted to be superoxide-producing (UniProt database), and given that the role of Nox4 is adopted in a similar fashion by a fungal homologue, the reported significance of Nox complexes for UPR-associated ROS-accumulation would imply a considerable superoxide production. Furthermore, it is speculated that superoxide generating cytochrome P450 isoenzymes (P450s) partake in the ROS burst during the UPR (Fleming et al., 2001; Santos et al., 2009). Depending on how ROS-production during the UPR is balanced in *F. graminearum* it could be possible that a major portion of the ROS-based response is conveyed through superoxide which would trigger no reaction of GPI-HyPer. The exact role of mitochondria in the UPR-related ROS burst is still subject of investigation. Mitochondria and ER communicate via different pathways comprising indirect mechanisms such as Ca^{2+}-mediated signalling but also immediate physical contact via mitochondria-associated membranes (MAMs) (Laurindo et al., 2012). It is still unclear whether ROS are directly transferred through the MAMs or not (van Vliet & Agostinis,

2017). If this is the case it would be debatable if the mitochondrial portion of UPR-associated ROS consists of hydrogen peroxide or superoxide or both. Given the existence of two SODs in the mitochondrial matrix and the mitochondrial intermembrane space it is likely that generated superoxide is quickly dismutated to H_2O_2. On the other hand, mitochondrial ROS generation is strongly increased during the UPR in mammalia (Margittai & Sitia, 2011; Zeeshan et al., 2016), possibly to an extend that exceeds the capacities of the mitochondrial SODs. Independent of a putative direct ROS transition: if indeed GPI-HyPer is located at mitochondria as well, a mitochondria-internal H_2O_2 accumulation should be detectable with GPI-HyPer. However, since mitochondria localisation of GPI-HyPer has been shown only partially, it is possible that a putative signal change is lost or that the H_2O_2-accumulation during the UPR in *F. graminearum* is simply too minor to be detected by GPI-HyPer. Additionally, GPI-HyPer might not be localised inside of mitochondria but attached to the outer mitochondrial membrane facing the cytosol. In that case no changes in the mitochondrial H_2O_2-level caused by SODs in the matrix or the intermembrane space would be detectable.

To verify the functionality of GPI-HyPer after observing no reactions upon ER-stress induction, the probe was tested directly for reactivity towards H_2O_2 and DTT. GPI-HyPer reacted to the chemicals with increasing and decreasing ratio at the ER, respectively. Marschall et al. (2016a) on the other hand observed only slight ratio changes of ER-targeted roGFP after application of 10 mM H_2O_2 compared to roGFP in the cytosol. They deduce from this that either the ER-glutathione pool differs from the cytosol in buffer capacity or that H_2O_2 is unable to cross the ER-membrane. In fact, even though H_2O_2 is an unpolar molecule that is widely believed to be able to diffuse through biological membranes (Chance et al., 1979), evidence has arisen that permeability of membranes to H_2O_2 is under cellular control and that membranes can pose an effective defence barrier against external H_2O_2 in *S. cerevisiae* (Branco et al., 2004; Miller et al., 2010). In this regard there is either a fundamental structural difference between the ER-membranes of *F. graminearum* and *B. cinerea* or the H_2O_2-permeability of the ER-membrane might be of lesser importance concerning this matter. Notably, the ER lumen is highly oxidised. A saturation of the local glutathione pool would prohibit further oxidation of roGFP by glutaredoxins even during further oxidation of the ER potentially explaining the minor rise in roGFP ratio in Marschall et al. (2016a). HyPer, reacting directly to H_2O_2, would not be restricted to the limitations of the glutathione redox system.

GPI-HyPer was also used to monitor intracellular ROS mediated by the enzyme class of NADPH-oxidases (Nox). Nox are unique in their sole function of ROS production and count as the most important enzymatic ROS generating system (Bedard & Krause, 2007). The finding by Marschall et al. (2016b) that NoxA in *B. cinerea* is presumably located at the ER membrane makes them a highly interesting target for analysis with GPI-HyPer. NoxA and NoxB in *F. graminearum* are under control of the regulator NoxR (Sumimoto, 2008). NoxR-deletions were conducted via transformation of cytoplasmic HyPer (cytHyPer) and GPI-HyPer expressing *F. graminearum* protoplasts. Interestingly, deletion of NoxR leads to a significantly elevated oxidation level of cytHyPer compared to cytHyPer in the WT

background. In contrast, GPI-HyPer shows no significant ratio change upon NoxR-deletion. These results suggest that disruption of Nox activity leads to H_2O_2-accumulation in the cytosol but not in the ER. This is counterintuitive with regard to previous findings that deletions of NoxA and NoxB in *F. graminearum* lead to decreased ROS formation (Wang et al., 2014). Nox deletions lead to reduced ROS levels in *Epichloë festucae* (Tanaka et al., 2008), in *M. oryzae* during appressoria formation (Egan et al., 2007), and in *A. nidulans* during sexual differentiation (Lara-Ortíz et al., 2003). On the other hand, contrary results were published for vegetative hyphae of *M. oryzae* where deletions of NoxA and NoxB cause higher hyphal ROS levels (Egan et al., 2007), for *A. nidulans* mycelia where disruption of NoxA leads to increased NBT staining (Semighini & Harris, 2008), for *P. anserina* where deletions of Nox1, Nox2, and NoxR lead to increased DAB and NBT staining (Brun et al., 2009), and for *B. cinerea* where deletions of NoxA, NoxB, and NoxR lead to no detectable decrease of the ROS level (Segmüller, 2008). Together these findings demonstrate the differences in the role of Nox in cellular ROS-metabolism between different species or cell types and underline that fungal Nox-deletion strains may accumulate high amounts of ROS as was suggested by the increased ratio in cytHyPer_Δ*NoxR*. With Nox-associated ROS production being challenged, the question concerning the source of these ROS arises. While mitochondria are the most plausible candidate producing predictably higher amounts of ROS than the Nox complex in many cell types (Balaban et al., 2005), ER-oxidoreductases which generate considerable amounts of oxidants in mammalian cells (Santos et al., 2009; Brown & Borutaite, 2012; Laurindo et al., 2012) and oxidoreductases that are involved in oxidative degradation of substrates, especially Nox-related ferric reductases (Brun et al., 2009; Grissa et al., 2010), represent additional possible ROS sources. Deregulation of these sources upon NoxR-deletion might account for the elevated HyPer ratio in the cytHyPer_Δ*noxR* mutants. Telling from the unchanged ratio of GPI-HyPer upon NoxR-deletion, the ROS generated by these sources are limited to the cytosol.

For both the ER-stress induction experiments and the NoxR-deletion experiments it is of great significance that other studies in mammals, plants, and fungi with ER-targeted HyPer or roGFP as ER redox sensors observed little to no response towards application of H_2O_2 (Meyer et al., 2007; Schwarzländer et al., 2008; Mehmeti et al., 2012; Marschall et al., 2016a). Concerning this matter, the fact that HyPer and roGFP oxidation is mediated via the formation of a disulfide bond in the regulatory domain OxyR (HyPer) and the β-barrel structure (roGFP) could generally be problematic for measuring ER-internal H_2O_2-concentrations. The extremely oxidising milieu, established by the PDI-mediated protein folding system, ought to be able to oxidize the redox sensors, and thereby raise their fluorescence ratio in an enzymatic and H_2O_2-independent fashion. Indeed, Mehmeti et al. (2012) present data suggesting this. The authors attempted to monitor the H_2O_2 generation during disulfide bond formation connected to protein folding in insulin-producing RINm5F cells using ER-targeted HyPer and detected strong ER oxidation. Since the ER-targeted expression of peroxiredoxin IV did not lower the ER-HyPer ratio the authors deduce that observed ratio changes of ER-HyPer derived from the formation of

an enzymatically mediated and H_2O_2-independent disulfide bond formation. They conclude that HyPer is not suitable for measuring ER-internal H_2O_2 concentrations.
Along this line, the exact location and orientation of GPI-HyPer is of utmost importance. While the location of GPI-HyPer at least regarding the ER is evident, it is unknown whether it is located in the ER lumen or in its membrane. If located in the membrane, an orientation to the ER lumen or the cytosol would make a strong difference concerning the interpretation of the data. The fact that GPI-HyPer is still oxidisable by H_2O_2 demonstrates that either the PDI-mediated enzymatic oxidation of HyPer as observed by Mehmeti et al. (2012) is not equally significant in *F. graminearum* and does not fully oxidise GPI-HyPer, or that GPI-HyPer is oriented to the cytosol resulting in GPI-HyPer's reactivity towards external H_2O_2 and DTT. This is supported by the missing ratio change during ER-stress. However, this would raise the question of why GPI-HyPer is unaffected by the deletion of NoxR, in the course of which cytHyPer shows a significant ratio increase. The signal peptides deriving from FGSG_00576 which were used to aim HyPer to the cell surface would furthermore imply that GPI-HyPer is in the secretory pathway, meaning inside the ER.
While the localisation of GPI-HyPer at the ER can be explained by the presence of signal peptides that direct it to the secretory pathway the reasons for the localisation at mitochondria are more difficult to deduce. The online tool TargetP 1.1 predicts the secretory pathway for the GPI-HyPer polypeptide but excludes mitochondrial targeting. Several causes of alternative peptide targeting are known: It is described that differential splicing or differential initiation of translation may lead to different N-terminal signal peptides (Ma & Taylor, 2008; reviewed in Danpure, 1995 and Small et al., 1998). For P450s and the amyloid precursor protein (APP) composite signal peptides containing patterns of both ER- and mitochondria-targeting signal peptides are described. These require activation through phosphorylation or proteolytic cleavage (reviewed in Anandatheerthavarada et al., 2003, Karniely & Pines, 2005, and Avadhani et al., 2011). Pfeiffer et al. (2013) suggest that certain structural features within a peptide's nascent chain can mediate targeting of secreted proteins to mitochondria. The protozoan parasite *Toxoplasma gondii* possesses a superoxide dismutase that is targeted to the mitochondria and the apicoplast, an Apicomplexa-specific chloroplast-like organelle, putatively due to inefficient binding of its nascent signal peptide to the signal recognition particle (Pino et al., 2007). Bodył and Mackiewicz (2007) describe a superoxide dismutase of the dinoflagellate *Lingulodinium polyedrum* that is located in three different compartments. The protein possesses a mitochondria/ER ambiguous signal peptide as well as two in-frame AUG start codons in its mRNA and a C-terminal signal peptide. The polypeptide can bind either the signal recognition particle (SRP) or the nascent polypeptide-associated complex (NAC). In the former case the polypeptide will be cotranslationally imported into the ER, in the latter case it will be post-translationally imported into mitochondria. When translation initiates at the second start codon the polypeptide is transported to peroxisomes due to its C-terminal signal peptide.

While several questions regarding the localisation of GPI-HyPer remain to be answered, GPI-HyPer still represents a valuable and functional ratiometric H_2O_2-sensor at the ER, an organelle that is specifically important for filamentous fungi which exhibit high secretion capacities. Among the core components of the ER responsible for key functions are cytochrome P450 monooxygenases (P450s). P450s are prevalent in all kingdoms and mainly located in the smooth ER membrane facing the cytosol (Monier et al., 1988; Black, 1992). In addition to their assumed role as superoxide producers during the UPR (Fleming et al., 2001; Santos et al., 2009) their ability to introduce reactive hydroxyl groups into organic molecules spawns a vast array of possible functions such as hydroxylation, dealkylation, epoxidation, deamination, desulfuration, dehalogenation, sulfoxidation, and N-oxide reduction (Sono et al., 1996; Mansuy, 1998). Hence the wide variety of metabolic processes they are involved in (Črešnar & Petrič, 2011; Shin et al., 2018). The number of P450 genes varies greatly between different species (Shin et al., 2018) with only three known P450s in *S. cerevisiae* (Shin et al., 2017) and 120 P450s in *F. graminearum* according to the transcriptomic data used in this study. Generally, plant pathogenic fungi tend to bear a comparatively large array of P450 enzymes (Črešnar & Petrič, 2011). As ROS production by ER-bound P450s contributes to the oxidizing conditions within the lumen which are necessary for proper folding of secreted proteins, the high number of P450s in filamentous fungi correlates with their extraordinary secretory capacities.

Concomitant with the importance of the secretome for filamentous fungi, secreted proteins found particular attention in this study. Among the 1665 *F. graminearum* genes predicted for secretion, 175 encode ROS-related enzymes which demonstrates that, along with effectors and plant cell wall degrading enzymes (CWDEs) (Kubicek et al. 2014, Mentges et al., unpublished data), ROS-related enzymes constitute an integral part of the fungus' secretome. 29 secreted ROS-related enzymes (SREs) are plant-induced and 16 are plant repressed. To this day only two secreted fungal virulence factors are known, namely the secreted lipase FGL1 (Voigt et al., 2005; Blümke et al., 2014) and the mycotoxin DON (Maier et al., 2006). However, given the relevance of a functioning secretory system (Krishnan & Askew, 2014) it is likely that these are not the only secreted virulence factors in *F. graminearum*. 24 SREs are upregulated in ICs, 7 of which are also upregulated compared to RH. Together, these findings suggest that ICs bear an arsenal of secreted enzymes which are of high relevance in the initial infection process and constitute the basis of the gene deletion experiments performed in this study. Via homologous recombination in *F. graminearum* protoplasts 26 single and 5 simultaneous deletions of ROS-related enzymes were conducted of which 16 single and 3 simultaneous deletions targeted SREs. Virulence, vegetative growth, resistance towards oxidative stress, ROS-accumulation, and sexual reproduction were assessed. Many P450 polypeptides contain a secretion signal which directs them to the secretory pathway; however, they are retained in the ER membrane. Therefore, they were not counted among the SREs despite carrying a signal peptide. With five deleted P450s (FGSG_03700, FGSG_07765, FGSG_03498, FGSG_01745, and FGSG_16458) they represent the largest group of genes characterised

in this study. FGSG_03498 is not plant-induced based on the threshold of a log_2-fold expression change of 2 compared to *in vitro* mycelia but upregulated after treatment with the fungicide tebuconazole according to Liu et al. (2009) posing a promising deletion target as a potential ROS-related stress-induced protein. The other four deleted genes belong to the group of 19 plant-induced P450s. FGSG_07765 is specifically upregulated in ICs compared to RH and *in vitro* mycelia, FGSG_16458 specifically upregulated in RH compared to ICs and *in vitro* mycelia. Notably, while the deletions in this study failed to generate any phenotype regarding virulence, vegetative growth, ROS-sensitivity, ROS-accumulation, and fertility, Shin et al (2017), who generated deletion mutants for all P450 genes in *F. graminearum*, observed decreased pathogenicity after deletion of FGSG_03700 and in 4 other P450 deletion mutants, despite using 5-fold higher conidia concentrations for virulence assays. With *F. graminearum* wildtype strain GZ-3639 and wheat cultivar Eunpamil the authors used a different fungus- and plant-background. Speculatively, susceptibility of the wheat cultivar or genetic background of the fungal wildtype strain differ from the strains used in this study, resulting in diverging phenotypes.

Once the plant's immune response in triggered, the fungus has to defend itself against toxic plant-produced xenobiotics. While P450s have often been associated with the degradation of xenobiotics (Werck-Reichhart & Feyereisen, 2000) and upregulation of P450s in presence of xenobiotics has been shown (Shin et al, 2017), only one P450 (FGSG_01972) led to increased xenobiotic sensitivity after deletion (Shin et al., 2017) suggesting strong functional redundancy. In addition to P450 monooxygenases, flavin-dependent monooxygenases are associated with xenobiotic detoxification. MAK1 of the filamentous fungus *Nectria haematococca* is one of the best known flavin monooxygenases in phytopathogenic fungi (Pigné et al., 2017) and has been shown to be involved in detoxification of antifungal xenobiotics (Covert et al., 1996). Similarly, *Alternaria brassicicola* induces expression of a flavin monooxygenase gene (*abmak1*) in response to the antifungal agent camalexin (Sellam et al., 2007), the major phytoalexin produced by *Arabidopsis thaliana* (Pigné et al., 2017). *F. graminearum* expresses 44 enzymes annotated as FAD-binding monooxygenases according to InterPro database and secretes 8 of which 2 are plant induced (FGSG_11215, FGSG_17478) thereby classifying as SREs. Both secreted plant-induced FAD-binding monooxygenases were deleted in this study but did not cause deviations from the wildtype phenotype regarding vegetative growth, virulence, ROS-sensitivity, ROS-accumulation, and sexual reproduction. Pigné et al. (2017) deleted the FAD-binding monooxygenase *abmak1* of *A. brassicicola* and observed decreased melanin production and aberrant cell wall structure but no effect on growth, conidiation, pathogenicity, cell wall stress, and H_2O_2-sensitivity, as well as resistance against plant defence metabolites (e.g. camalexin). The unaffected susceptibility to plant defence metabolites is counterintuitive regarding the above mentioned connections between flavin monooxygenases and camalexin. These findings show a comparable system in which the deletion of a flavin monooxygenase did not affect

pathogenicity or ROS-sensitivity. Also, the role of MAK1 and the camalexin-sensitive regulation of AbMak1 are suggestive enough to make the discovery of the function of FGSG_11215 and FGSG_17478 in antifungal xenobiotics degradation a promising future endeavour as these enzymes demonstrate an extracellular system contrary to the highly redundant intracellular P450s system. Respective experiments could improve the understanding of the role of flavin monooxygenases in *F. graminearum*. Supposed that FGSG_11215 and FGSG_17478 do play a role in xenobiotics detoxification, the presented data show suggest this function has no impact on the pathogenicity of the fungus. However, a simultaneous deletion of FGSG_11215 and FGSG_17478 with the six remaining secreted flavin-dependent monooxygenases would be necessary to be able to exclude functional substitution.

Along with P450s and flavin-dependent monooxygenases, tyrosinases constitute the third class of monooxygenases characterised in this study. *F. graminearum* expresses 15 tyrosinases of which 12 are secreted and 4 plant-induced. Fungal tyrosinases are generally associated with pigmentation, e.g. through the production of melanins (Sanchez-Ferrer et al., 1995; Halaouli et al., 2005). Melanins have been discovered as virulence factors in a broad range of plant pathogenic and human pathogenic fungi (Langfelder et al., 2003) such as *M. oryzae* (Chumley & Valent, 1990; Howard & Valent, 1996), *A. alternata* (Kawamura et al., 1999), *Bipolaris oryzae* (Moriwaki et al., 2004) *C. neoformans* (Kwon-Chung & Rhodes, 1986; Polacheck & Kwon-Chung, 1988), *A. fumigatus* (Jahn et al., 1997; Tsai et al., 1998; Langfelder et al., 1998), and *Wangiella* (*Exophiala*) *dermatitidis* (Dixon et al., 1987; Schnitzler et al., 1999; Feng et al., 2001). Also, they are involved in protection from environmental stress and plant enzymes, in conidial pigmentation, survival, sporulation, as well as ascospore protection (Cordero & Casadevall, 2017). 2 of 4 plant-induced secreted tyrosinases were deleted in this study, namely FGSG_01988 and FGSG_11528. Both deletions, however, led to no impairments in the tested functional categories. In *M. oryzea* the role of melanin in pathogenicity lies in the constitution of a semipermeable layer required to build mechanical pressure in appressoria (Howard & Valent, 1996). Since *F. graminearum* apparently does not rely on mechanical pressure for host penetration these findings do not apply in equal gravity to this fungus. Notably, whereas in basidiomycetes and mammals melanin is synthesised by tyrosinases (Sanchez-Ferrer et al., 1995; Feng et al., 2001), melanin of ascomycetes is claimed to usually be synthesised by polyketide synthases (PKS) (Bell & Wheeler, 1986; Feng et al., 2001). The black colour of *F. graminearum* perithecia for instance arises from the accumulation of melanin synthesised by the polyketide synthase PGL1 (Frandsen et al., 2016). Luo et al. (2017) on the other hand expect FGSG_01988 and FGSG_11528 to be involved in melanin synthesis. Also, in *N. crassa* tyrosinase has been long known to be responsible for melanin synthesis during perithecial development (Hirsch, 1954). Of the 15 annotated tyrosinases in the *F. graminearum* genome 12 carry a secretion signal. If involved in melanin synthesis, the secretion signals of FGSG_01988 and FGSG_11528 might hint at a role in melanisation of the cell wall where it is typically located in fungi

(Nosanchuk et al., 2015). In any case, the large number of other secreted tyrosinases demonstrates the high functional redundancy of this enzyme class. The single deletions performed in this study are likely to be made up for by alternative genes, maintaining the WT phenotype.

The next class of SREs under investigation were blue copper proteins or cupredoxins, small proteins with a single type-1 copper centre. Of 6 putative *F. graminearum* cupredoxins 4 are secreted of which 3 are plant-induced (FGSG_06023; FGSG_07829; FGSG_09742). All three genes also show a strongly reduced expression in ICs of the deletion mutant of the MAP kinase Gpmk1 (Δ*gpmk1*) (M. Mentges, University of Hamburg, pers. comm.). Δ*gpmk1* is avirulent due to malfunctional ICs that are unable to penetrate the plant surface. The downregulation of FGSG_06023, FGSG_07829, and FGSG_09742 compared to WT ICs suggested that these genes might be involved in the Δ*gpmk1* phenotype making them promising deletion targets. Genes FGSG_06023 and FGSG_09742 were deleted separately and simultaneously in this study but caused no effect on virulence, vegetative growth, resistance towards oxidative stress, ROS-accumulation, and sexual reproduction suggesting that these genes are not responsible for the Δ*gpmk1* phenotype. A protein BLAST and a query in the *F. graminearum* database from ZhaoGroup for Computational System Biology of Fudan University revealed that they are orthologues to SS1G_00809 and SS1G_07784 of *S. sclerotiorum* which are hypothesised to be laccases involved in melanin biosynthesis, sclerotia formation and pathogenicity of this fungus (Fan et al., 2016). Laccases are multicopper-oxidases which are common in fungi and have been associated with sporulation, melanin biosynthesis, lignin degradation, and virulence (Tsai et al., 1999; Leonowicz et al., 2001; Zhu et al., 2001; Zhu & Williamson, 2004). In *F. graminearum* the laccase FGSG_02338 is involved in aurofusarin synthesis. Notably, while laccases are defined to contain three cupredoxin-like domains (Enguita, 2011) SS1G_00809 and SS1G_07784 and their orthologues FGSG_06023 and FGSG_09742 contain only one cupredoxin-like domain according to an InterPro protein sequence analysis. This, together with the fact that these proteins are 299, 237, 295, and 214 amino acids long whereas laccases usually have an average length of around 600 amino acids, challenges the annotation of SS1G_00809 and SS1G_07784 as laccases.

Small, single copper centre-containing cupredoxins are shown to function as electron shuttles between proteins, e.g. between components of electron transport chains (de Rienzo et al., 2000). The upregulation of three secreted cupredoxins *in planta*, and in the case of FGSG_09742 specifically in ICs, suggests that *F. graminearum* increases its electron supply during infection. The electrons could be used as redox-mediators for extracellular oxidoreductases e.g. for lignin-degrading Fenton reactions: Chen & Pignatello (1997) showed in a cell-free system that quinones serving as electron shuttles can catalyse the reduction of Fe^{3+} to Fe^{2+} by facilitating electron transfer between phenolic HO· adducts and Fe^{3+}. The absence of phenotypes suggests that the fungus does

not rely on such catalysis or that the remaining cupredoxins or other electron shuttles compensate for the deletions.

In the following sections the results regarding peroxidase deletion mutants are discussed which constitute the only enzyme class that showed reproducible phenotypes upon deletion in this study. *F. graminearum* expresses five chloroperoxidases according to InterPro database of which two are not plant-induced and not secreted. The other three (FGSG_03708, FGSG_02341, FGSG_03436) are plant-induced and secreted and were therefore selected for gene deletion. The FGSG_03708 deletion mutant Δ*FGSG_03708* showed retarded vegetative growth under non-stress conditions which is restored after application of oxidative stress inducing agents, as well as slightly elevated ROS-levels in the hyphal tips in axenic culture (see Results, Figures 18-21). The pathogenicity of the mutant is WT-like. Quantitative real-time PCR analysis revealed that FGSG_03708-expression is repressed when the fungus is growing in presence of menadione or H_2O_2. This intriguing expression pattern of FGSG_03708 provides a plausible explanation as to why the deletion mutant is fully virulent on wheat. The observed downregulation of FGSG_03708 in the presence of ROS-stress suggests that the gene is dispensable or even harmful when facing external oxidative stress as for example encountered in the interaction with the plant host (Heller & Tudzynski, 2011; Segal & Wilson, 2018). Plants produce considerable amounts of ROS during defence reactions such as the oxidative burst. Consequently, deletion of FGSG_03708 does not affect plant-pathogen interaction. Along that line, this result also suggests that ROS-related defence reactions are initiated against the invading pathogen during systemic infections rather than during plant-surface colonisation by the fungus. An overexpression of FGSG_03708 might give clues regarding reasons for its downregulation. If an overexpression mutant would still be able to infect wheat, FGSG_03708 is likely to simply be dispensable during infection and gets downregulation to save resources. A virulence reduction of an overexpression mutant would instead suggest that the presence of FGSG_03708 is harmful during infection for the pathogen, for example due to FGSG_03708-mediated quenching of ROS that are needed for damaging the host. The vegetative growth retardation of Δ*FGSG_03708* was not observed by Lee et al. (2017) who deleted all putative peroxidases in *F. graminearum*. Lee et al. (2017) measured the radial growth of the mutants after five days. In this study the radial growth was measured after three days. Repeated growth assays reliably showed that after five days under the conditions described in the materials & methods section *F. graminearum* had completely overgrown a Ø 92 mm plate. The complete medium (CM) agar that was used in this study was similar to the complete medium used by Lee et al. (2017), albeit less rich.

Simultaneous deletion mutants of the three secreted plant-induced chloroperoxidases (ΔΔ*FGSG_02341;03708* and ΔΔΔ*FGSG_02341;03708;03436*) were established. ΔΔ*FGSG_02341;03708* and ΔΔΔ*FGSG_02341;03708;03436* showed the same growth and ROS-accumulation phenotypes described for Δ*FGSG_03708*. Virulence was still WT-like, on wheat as well as on maize. Interestingly, the simultaneous deletion mutants showed

increased production of perithecia compared to the WT which was not observable in the chloroperoxidase single deletion mutants. Another secreted peroxidase, FGSG_04434, also led to a higher perithecia nests/wheat node ratio after deletion contrary to the peroxidase characterisation study by Lee et al. (2017) who observed no such phenotype. FGSG_04434 is not plant regulated according to the transcriptomic data used in this study but Harris et al. (2016) show a downregulation of FGSG_04434 in wheat spikelets 4 days after infection and Zhang et al. (2012) found it significantly upregulated in wheat coleoptiles. Given the importance of ROS in cell differentiation a change in fertility through the disruption of the ROS equilibrium caused by peroxidase deletions would be comprehensible. Deletion of superoxide-producing Nox complex members impair sexual fruiting body formation in *P. anserina* (Malagnac et al., 2004), hyphal fusion in *E. festucae* (Kayano et al., 2013), and sclerotia formation in *S. sclerotiorum* and *B. cinerea* (Segmüller et al., 2008; Kim et al., 2011), meaning that the loss of a ROS-producer leads to attenuated sexual behaviour. That the loss of ROS-scavengers leads to accelerated sexual development would be the reverse conclusion of this and finds evidence in the peroxidase phenotypes presented in this study. Indeed, FGSG_04434 is a hybrid ascorbate/cytochrome c peroxidase according to the fungal peroxidase database fPoxDB (http://peroxidase.riceblast.snu.ac.kr). Cytochrome c peroxidases are known to play an important role in ROS-metabolism functioning both as an effective ROS scavenger and as a mitochondrial H_2O_2 sensing and signalling molecule in *S. cerevisiae* (Martins et al., 2013). Single deletion of FGSG_04434, however, did not influence the NBT-staining result. The involvement of the chloroperoxidase FGSG_03708 in ROS-detoxification was shown by the increased ROS-levels in hyphal tips in Δ*FGSG_03708*. In contrast to Δ*FGSG_04434*, however, Δ*FGSG_03708* alone had no influence on sexual reproduction. The observation that only simultaneous deletion of secreted chloroperoxidases affects perithecia formation suggests a cumulative effect of this enzyme class on fertility. Interestingly, Sikhakolli et al. (2012) describe that FGSG_04434 gets downregulated in the course of sexual development, indicating that its activity would be counterproductive in this process. On the basis of these data it is conceivable that *F. graminearum* actively raises the ROS-level in its vicinity to induce the sexual differentiation process. Since only a single Δ*FGSG_04434* clone was established, further independent deletion mutants are necessary to confirm the effect of ascorbate/cytochrome c peroxidase on fertility.

7 of the 16 SREs deleted in this study are putatively involved in plant cell wall degradation or exhibit features that suggest this function as is discussed below. The two plant-induced secreted chloroperoxidases FGSG_02341, FGSG_03436 as well as the secreted putative lignin-peroxidase FGSG_16013 belong to a group of 15 lignin metabolising enzymes annotated in the transcriptome used in this study of which 10 are secreted. 10 genes belong to the enzyme group of laccases, 4 to chloroperoxidases, and 1 gene is epoxide hydrolase-like. FGSG_16013 is the only annotated lignin-peroxidase in *F. graminearum*. Lignin has not been in the focus of *F. graminearum* research lately (its role in *F. graminearum* pathogenicity being termed unknown by Walter et al. (2009)) and

ascomycetes are usually not considered efficient lignin degraders (Xie et al., 2014). Still, lignin, constituting an important component of the plant cell wall of tissues relevant for *Fusarium* infection such as glumes, lemmas, paleas, and the rachis (Siranidou et al., 2002; Lahlali et al., 2016), has been shown to be involved in wheat resistance towards *Fusarium* Head Blight caused by *Fusarium culmorum* and *F. graminearum* (Ribichich et al., 2000; Kang & Buchenauer, 2000; Siranidou et al., 2002; Lahlali et al., 2016). FGSG_16013 shows unaltered expression in RH compared to *in vitro* mycelia but is repressed in ICs. This is consistent with data established by Harris et al. (2016) and visualised by Lee et al. (2017) who show a downregulation of FGSG_16013 in infected wheat spikelets at 4 dpi. Their data also show an upregulation at 1 dpi and, to a lesser extent, at 2 dpi. Considering the notion that ICs are harbouring an arsenal of plant cell wall degrading enzymes in order to penetrate the plant surface this is surprising. The transcriptomic data used in this study was established using cDNA isolated right after ICs had been formed (~5 dpi). While it is possible that FGSG_16013 is stable enough to be present and functional during the initial infection, an upregulation at 1 dpi before ICs are formed would suggest that FGSG_16013 does not belong to a putative arsenal of cell wall degrading enzymes of ICs. Its downregulation in ICs adds to this hypothesis. Since deletion of the only lignin-peroxidase did not alter the fungus' behaviour, its function might get compensated by similar enzymes. In this regard the seven secreted laccases of F. graminearum are potential candidates. Although typically being the main delignifiers only in basidiomycetes, laccases have been shown to be involved in wood degradation in ascomycetes as well (Xie et al., 2014). However, lignin, being an extremely complex and bulky polymer, needs a cocktail of different enzymes being active in the correct order to be efficiently degraded (Aro et al., 2005) which speaks against a simple substitution by a different enzyme class. The three chloroperoxidases with lignin as their annotated predicted substrate (FGSG_02341, FGSG_03436, FGSG_08911) could instead be able to take over the catalytic activity of FGSG_16013. The two secreted ones, FGSG_02341 and FGSG_03436, were deleted in this study. Since, contrary to FGSG_16013, FGSG_02341 and FGSG_03436 are plant-induced and specifically upregulated in ICs, they would be reasonable candidates for genes involved in plant cell wall degradation during early infection processes of *F. graminearum*. However, deletion of either candidate led to no phenotypical deviations concerning virulence, vegetative growth, resistance towards oxidative stress, ROS-accumulation, and sexual reproduction, suggesting that neither their role in ROS-metabolism nor their role in lignin degradation are important in these circumstances. The fact that also ΔΔΔ*FGSG_02341;03708;03436* was WT-like in this regard suggests that either delignification is a dispensable process during penetration of and dispersion inside the host, or that both IC-only expressed FGSG_02341 and FGSG_03436 are substituted for by genes with redundant function such as laccases or the secreted lignin-peroxidase FGSG_16013.

The degradation of lignin by fungi has been proven to be reliant on ROS. Extracellular fungal alcohol oxidases provide the H_2O_2 needed by lignin-peroxidases (Kersten & Kirk,

1987; Janse et al., 1998; Leuthner et al., 2005; Hernández-Ortega et al., 2012; Song et al., 2015). In *Fusarium* species a single glyoxal oxidase regulates virulence and mycotoxin production (Song et al., 2015) underlining the importance of this process. Extracellular alcohol oxidases, including carbohydrate oxidases, are all putatively involved in plant cell wall degradation as they produce H_2O_2 using aromatic compounds and sugars as substrate. While glyoxal oxidases have received much attention little research concerning the biological role has been conducted regarding galactose oxidases. Of 15 putative galactose oxidases in *F. graminearum* FGSG_09093 is the only plant-induced gene and is one of 7 secreted orthologues. The broad substrate specificity of this enzyme class (Knowles & Ito, 1993) making it adequate for hemicellulose degradation has raised the assumption that it is involved in plant cell wall degradation (Sierra-Campos & Pardo, 2009). This and its ROS-production capabilities adding to the fungus' lignin degradation capacities made FGSG_09093 a promising candidate as a virulence factor. However, its deletion has no influence on the assessed parameters suggesting a less pivotal role for the fungus as other alcohol oxidases or redundancy among the remaining galactose oxidases. Additionally, the secreted oxidase FGSG_11399 could be involved in providing ROS in this context. FGSG_11399 is highly upregulated specifically in ICs and has also previously been identified as an *in planta*-specific protein (Güldener et al., 2006; Lysøe et al., 2011; Boedi et al., 2016) but showed no phenotype upon deletion. A gene cluster analysis by Lee (2010) predicted FGSG_11399 to be part of a gene cluster of non-ribosomal peptide synthetase 14 (NPS14; FGSG_11395) which shows similarity to AM-toxin synthetase from *Alternaria mali* and to HC-toxin synthetase from *Beauveria bassiana*. In contrast to FGSG_11399 FGSG_11395 is not plant induced which suggests that FGSG_11399 serves a different purpose in early infection stages, e.g. as mentioned the production of ROS necessary for plant cell wall degradation.

Along with lignin, cellulose is one of the main components of plant cell walls. Therefore, degradation of cellulose is presumably of similar importance for successful penetration as delignification (Kubicek et al., 2014). The deletion of FGSG_02917, which encodes for a secreted cellobiose dehydrogenase, however, had no impact on virulence, vegetative growth, resistance towards oxidative stress, ROS-accumulation, and sexual reproduction. Cellobiose dehydrogenases participate in cellulose degradation and have been shown to degrade xylan and lignins as well (Henriksson et al., 1995; Cameron & Aust, 2001). Although not plant-induced according to the transcriptomic data used in this study, FGSG_02917 is attributed as upregulated in living wheat plants according to Boedi et al. (2016) who compared gene expression of *F graminearum* infecting living and dead wheat plants. Except FGSG_02917 there are four other secreted cellobiose-dehydrogenases, which are all highly plant-induced. Two of them (FGSG_03742, FGSG_04872) are specifically induced in ICs. Therefore, the probability of a compensation of FGSG_02917 function is in this case high. In *B. cinerea* a cellobiose dehydrogenase (BC1G_03188. 1/BofuT4_P082390.1) has been suggested as a potential potent ROS generator (Espino et al., 2010). In fact, a hypothesis regarding the function of cellobiose dehydrogenase

implies that the enzyme modifies its substrates through the production of hydroxyl radicals which are by-products of the reduction of iron (Fe^{3+} to Fe^{2+}) or copper (Cu^{2+} to Cu^{+}) during cellobiose oxidation. The reduced metal ions react with H_2O_2 in a Fenton-like reaction generating the highly aggressive hydroxyl radical (Kremer & Wood, 1992; Henriksson et al., 1995; Baldrian & Valášková, 2008). The ROS-production capabilities of FGSG_02917, however, are apparently not considerable enough to have an impact on the necrotrophic lifestyle or on the ROS-sensitivity of *F. graminearum* or get substituted for by a functionally redundant gene.

The first barrier that *F. graminearum* encounters upon colonisation of a host plant is the cuticle, a layer consisting of mainly of cutin, waxes, cellulose, and pectin. FGSG_09124 encodes a secreted reductase that is putatively related to the NADPH-dependent ß-ketoacyl reductase RhlG from the opportunistic human pathogenic bacterium *Pseudomonas aeruginosa* according to MIPS database. RhlG is involved in fatty acid synthesis, especially rhamnolipids which are secreted and constitute an important virulence factor of the bacterium (Campos-García et al., 1998; Miller et al., 2006). One other gene, FGSG_01857, in *F. graminearum* shares this characteristic but is neither secreted nor plant-induced. While RhlG has been associated with fatty acid synthesis the reversible nature of redox reactions would also allow FGSG_09124 to be involved in lipid degradation. In fact, a BLAST search revealed homology to genes from other ascomycetes such as *Coccoides immitis* and multiple *Aspergillus* species which are annotated as 3-hydroxyacyl-CoA dehydrogenase which takes part in beta oxidation of fatty acids. This function could be of value for the degradation of host tissue during infection. Previous studies showed that lipases can function as virulence factors in *F. graminearum* and *B. cinerea* (Comménil et al., 1998; Voigt et al., 2005). It is possible that these enzymes are involved in plant invasion through the degradation of lipid containing plant components such as the cuticle. While cutinases have been intensely studied as mediators of cuticle penetration (see below) little is known about the role of lipid degrading enzymes in this context. No experiments concerning lipid metabolism were conducted in this study. The wildtype-like behaviour of Δ*FGSG_09124* suggests that this enzyme's influence on extracellular synthesis of rhamnolipids or lipid degradation is negligible in regard to the tested conditions. The previous research on cutinases is controversial. While it was suggested that cutinases dissolve the plant cuticle enabling cell surface penetration (Woloshuk & Kolattukudy, 1986; Podila et al., 1988), single cutinases have not been identified as virulence factors (Stahl & Schäfer, 1992; Stahl et al., 1994; van Kan et al., 1997; Crowhurst et al., 1997; Reis et al., 2005) with the exception of Pbc1 from the brassica pathogen *Pyrenopeziza brassicae* (Li et al., 2003) which demonstrates the complexity of this system. The assumption of Voigt et al (2005) that, additionally to cutinases, secreted lipases are involved in the infection process includes the putative role of FGSG_09124 in lipid degradation. Conversely, this means that other lipases and/or cutinases would be able to compensate for the loss of FGSG_09124.

The discussed overlapping biochemical functions of CWDEs are plausible in regard to the high complexity and chemical stability of this barrier and the necessity of the pathogen to overcome it. However, the consequent notion that individual CWDEs would constitute virulence factors has yet to be demonstrated for most plant pathogens (Kubicek et al. 2014). Only few studies could show single CWDEs that were indispensable for pathogenicity and cover almost exclusively polygalacturanases with the exception of a xylanase in *B. cinerea* (Shieh et al., 1997; ten Have et al., 1998; Isshiki et al., 2001; Oeser et al., 2002; Brito et al., 2006; Douaiher et al., 2007; Fernández-Acero et al., 2010). In most cases plant-induced CWDEs do not seem to be involved in virulence (van Kan et al., 1997; Reis et al., 2005; Espino et al., 2005; Kubicek et al., 2014; Quarantin et al., 2016). Chloroperoxidases, lignin-peroxidases, and cellobiose-dehydrogenases have not been characterised in this context before. The results in this thesis are in line with the available literature which also attributes the resilience of the fungus in this regard to the strong functional redundancy of CWDEs. Concomitantly, this broad enzymatic arsenal leads to equally strong redundancy in ROS-metabolising functions due to the involved oxidoreductases as demonstrated by the low phenotype rate in this study.

In previous studies very insightful and generalizable results regarding the role of ROS in fungal infection have been gathered through broad scope disruptions of the ROS-metabolism e.g. via deletions of MAP-kinases or transcription factors (Nathues et al., 2004, 2007; Molina & Kahmann, 2007; Nguyen et al., 2012, 2013). Such a more general disruption was attempted in this study via the deletion of FGSG_09006 which encodes the single mitochondrial nicotinamide nucleotide transhydrogenase (NNT), an enzyme that couples the NADH and NADPH pools of mitochondria. Although highly favouring the production of NADPH under normal conditions, the reaction it catalyses ($NADH + NADP^+ \leftrightarrow NADPH + NAD^+$) is reversible, making it both a quencher and a potential producer of ROS. It could, therefore, play a major role in the redox balance of the mitochondria. In humans NNT-deficiency is a cause for familial glucocorticoid deficiency (Meimaridou et al., 2012). In PC12 cells silencing of the NNT leads to increased cellular H_2O_2 concentrations (Yin et al., 2012). NNT deletion mutants of *C. elegans* show a strongly reduced ROS resistance (Arkblad et al., 2005) underlining the importance of NNT in ROS-metabolism. While present in higher animals and most bacteria, little is known about the function of NNT in plants and fungi. *S. cerevisiae* and *Arabidopsis thaliana* do not contain a respective gene (Jackson et al., 1999; Arkblad et al., 2001) and the green alga *Acetabularia acetabulum* is the only plant known to express NNT (Arkblad et al., 2001; Rasmusson et al., 2008). Until now, fungal NNT has not been in the focus of scientific research. *F. graminearum* gene FGSG_09006 is annotated as related to mitochondrial NNT by MIPS database. A protein BLAST suggests NNT to be strongly conserved throughout bacteria, animals, and fungi. *F. graminearum* NNT amino acid sequence shows around 50 % similarity to NNT from animals, bacteria, and *A. acetabulum*. This is the first report on the functional characterisation of a putative NNT in a filamentous fungus. Δ*FGSG_09006* showed no deviations from the wildtype phenotype with respect to

vegetative growth, virulence, ROS-sensitivity, ROS-accumulation, and sexual reproduction. Considering the effect of NNT disruptions in animals, this is especially surprising in regard to ROS-sensitivity of *F. graminearum*. The data presented in this study suggest that NNT plays a less pivotal role in ROS-metabolism in *F. graminearum* compared to animals. FGSG_09006 is plant-repressed which might explain the ineffectiveness of the deletion regarding virulence. More clones of Δ*FGSG_09006* are needed to verify these results.

To achieve a more specific disruption of the ROS-metabolism, the sole secreted SOD FGSG_00576, which also served as a template for the GPI-HyPer signal peptides, was deleted. SODs constitute the first line of defence against superoxide making them key players within the ROS-detoxification cycle together with catalases. *F. graminearum* expresses 6 SODs of which 2 are plant-regulated with FGSG_08721 being induced and FGSG_00576 repressed *in planta*. Being the only SOD containing secretion and GPI-anchor signal peptides, FGSG_00576 posed a promising deletion target. However, virulence, vegetative growth, resistance towards oxidative stress, ROS-accumulation, and sexual reproduction were not affected in Δ*FGSG_00576*. This observation affirmed a publication by Rittenour and Harris (2013) regarding virulence and resistance towards menadione. Contrary to FGSG_00576, deletion of the cytosolic SOD FGSG_08721 in *F. graminearum* renders the fungus slightly reduced in vegetative growth and pathogenicity (Yao et al. 2016). Notably, while Yao et al. (2016) localised this SOD intracellularly, it was identified as non-classically secreted in a secretome prediction analysis by Brown et al. (2012), as well as by Lowe et al. (2015) and Paper et al. (2007). If indeed FGSG_08721 is secreted it is conceivable that FGSG_08721 and not FGSG_00576 is responsible for extracellular dismutation of superoxide in *F. graminearum* during infection.
Despite being highly conserved enzymes expressed exclusively for the detoxification of ROS in all aerobic organisms, and possessing a comparably low functional redundancy (see Results, Figure 11), disruption of SODs and catalases has led to varying results in previous studies. De Groot et al (2003) have identified three putative GPI-anchored SODs in *Candida albicans* and one in *Neurospora crassa*. In *Dictyostelium discoideum* the GPI-anchored superoxide dismutase *SodC* regulates the small GTPase Ras interfering with chemotaxis. The disuption of *SodC* leads to increased intracellular superoxide (Veeranki et al., 2008). The GPI-anchored superoxide dismutase *SOD5* of *Candida albicans* is involved in yeast to hyphal transition and response to osmotic or oxidative stresses. Its disruption leads to sensitivity to hydrogen peroxide when cells were grown in nutrient-limited conditions (Martchenko et al., 2004; Plaine et al., 2008). *C. purpurea* grows inside plant tissue without causing a change in ROS level (Scheffer & Tudzynski, 2006). Still, virulence was not significantly reduced after deletion of secreted ROS-detoxifying enzymes such as the single-secreted SOD and the major-secreted catalase (Garre et al., 1998; Moore et al., 2002). Disruption of all catalase activity via the deletion of the catalase regulator Cp*TF1*, however, leads to a reduction of virulence (Nathues et al., 2004). Deletion of the secreted SOD of *C. purpurea* did not affect resistance against superoxide stress induced by

paraquat (Moore et al., 2002). This experiment had been conducted in *N. crassa* as well (Chary et al., 1994) where the deletion of the intracellular Sod-1 did cause sensitivity to paraquat. *B. cinerea* experiences oxidative stress during infection. A secreted catalase is partly responsible for oxidative stress resistance in vitro. However, virulence on bean and tomato leaves is not affected by the deletion and neither does it change the amount of H_2O_2 that the fungus is exposed to during infection (Schouten et al., 2002). The deletion of a secreted SOD did lead to retarded lesion development (Rolke et al., 2004). Robbertse et al. (2003) revealed that none of the three monofunctional catalase genes of the maize pathogen *Cochliobolus heterostrophus* are essential for virulence. One secreted catalase is needed for H_2O_2 resistance *in vitro* but is dispensable for pathogenicity. In *S. sclerotiorum* it is vice versa. Deletion of the highly plant-induced catalase Scat1 leads to impaired pathogenicity and sensitivity to multiple stresses. H_2O_2-tolerence, on the other hand, was increased (Yarden et al., 2014). Deletion of a SOD leads to impaired pathogenicity, ROS-tolerance, hyphal growth and sclerotia development in this fungus (Veluchamy et al., 2012). Exemplary for the diverging functions of related enzymes in different organisms, the authors state here that a disrupted oxalate metabolism and not ROS-detoxification is the cause for the observed phenotypes in the SOD deletion mutant (Veluchamy et al. 2012). *F. graminearum* expresses 5 monofunctional catalases. While Nagygyörgy et al. (2014) assume a connection between peroxide sensitivity and catalase function in *F. graminearum*, Lee et al. (2014) showed that none of the monofunctional catalases lead to increased H_2O_2 sensitivity after deletion. Taken together, the literature demonstrates the variable and sometimes paradoxical nature of even those ROS-related enzymes whose only task is the maintenance of the ROS-metabolism (catalase and SOD). While the putative functions of most of the genes deleted in this study, with the exception of the SOD FGSG_00576 and the NNT FGSG_09006, do not in the first place aim at producing or detoxifying ROS, they all have in common that they trigger the activation of oxygen or using ROS as redox equivalents, thereby contributing at least passively to ROS-metabolism. Evidently, ROS-metabolism is a highly diverse and complex mechanism incorporating few essential and many redundant enzymes, which is substantiated by the minor role of ROS-related enzymes in virulence, growth, ROS-sensitivity, ROS-accumulation, and sexual reproduction suggested by the results presented in this study. It is reasonable to assume that *F. graminearum* in the course of evolution has evolved to possess a strong functional redundancy within the SREs to maintain a favourable ROS-balance during fungal-plant interaction. The outcome is a strongly secured system which is hardly to be perturbed by removing one of its members.

To achieve a perturbation of this system strong enough to cause a visible phenotypical effect, simultaneous deletions are indispensable. This study showed that simultaneous deletions of chloroperoxidases and metallothioneins had no effect on virulence indicating that a larger amount of functionally redundant enzymes would need to be deleted simultaneously. This is especially true for assessing the role of monooxygenases, oxidases, and dehydrogenases which constitute a large portion of the genome. However, with nourseothricin, hygromycin, and geneticin only 3 applicable selection markers are

available. Alternative recombination and genome editing systems such as Cre/*loxP* or CRISPR/Cas could be used to remove the resistance cassettes from the genome of deletion mutants and therefore allow serial deletions of ROS-related enzymes. Also, it is highlighted by the results of this study that the continuing identification of new potential virulence factors remains a highly necessary matter. At least 4432 of 13828 predicted genes (32%) of *F. graminearum* are still completely uncharacterised and have unknown function. This represents an enormous pool of potentially significant proteins with influence on the ROS-metabolism such as unknown epistatic factors with global regulatory function similar to FgAtf1and FgOS-2. Furthermore, the existence of unknown non-classically secreted enzymes, also among the identified enzymes in the proteome, is not to be disregarded. The prediction of non-classically secreted proteins is difficult as they do not carry an N-terminal signal peptide and need to be identified by their amino acid composition, secondary structure, and disordered regions (Orfanoudaki et al., 2017). With regard to the importance of functional redundancy of SREs indicated by this study it would be worthwhile to further improve the prediction accuracy of non-classically secreted enzymes in order to find new potential deletion targets.

5. Summary

F. graminearum is a necrotrophic filamentous ascomycete that is able to infect all major cereal crops causing plant diseases such as *Fusarium* Head Blight in wheat. The infection process is mediated mainly via differentiation of fungal cells into complex multicellular organs, so called infection cushions (ICs). In previous work an RNAseq-based transcriptomic and functional analysis indicated major transcriptional rearrangements between ICs and non-invasive cells. Data analysis revealed that expression of enzymes involved in the metabolism of reactive oxygen species (ROS) was elevated in ICs. ROS are integral components of every aerobic cell's metabolism and are formed as by-products of oxygen-based cellular reactions. While being harmful to the cell structure when accumulating, ROS are also necessary for cellular functions serving as an important second messenger mediating cellular differentiation. Particularly, they are essential elements in plant-pathogen interactions, such as fungal infection processes. Only few ROS-related enzymes involved in these interactions are known to this day, however. The aim of this study was to gain further insights into the role of ROS and specific ROS-related enzymes, particularly secreted ones, in different aspects of the fungal life-cycle. Via gene deletions 9 monooxygenases (4 of them secreted), 5 secreted peroxidases, 2 secreted oxidases, 1 secreted dehydrogenase, 1 secreted reductase, 2 secreted cupredoxins, 3 metallothioneins, 1 NAD(P) transhydrogenase (NNT), and 1 secreted superoxide dismutase (SOD) were disrupted. Mutants were tested for virulence, vegetative growth, ROS-sensitivity, ROS-accumulation, and fertility. It could be shown that secreted peroxidases are involved in vegetative growth, ROS-accumulation, and fertility. Other ROS-related enzymes deleted in this study caused no effect on the tested parameters. This low number of phenotypes indicates a high resilience of *F. graminearum* against disruptions of its ROS-metabolism. It seems that the ROS-equilibrium which the fungus seeks to maintain during infection is a highly secured system, fortified by a large array of enzymes with redundant function. Further experiments for gaining insights into *F. graminearum*-related ROS fluctuations were based on the genetically encoded ratiometric H_2O_2 probe HyPer which reacts towards H_2O_2 with an increase of the ratio of its two fluorescence peaks. HyPer had been expressed in the cytosol of *F. graminearum* previously (cytHyPer). In this study a GPI-anchor was attached to the probe. Organelle-specific staining revealed that this modified HyPer (GPI-HyPer) is attached to the endoplasmic reticulum (ER) and mitochondria. GPI-HyPer was used in ER-stress experiments. Substitution of GPI-HyPer expressing strains with brefeldin A and tunicamycin showed no reaction from GPI-HyPer suggesting that ER-stress in *F. graminearum* is not linked to a significant change of the ER's H_2O_2-level. Deletion of the NADP(H) oxidase regulator NoxR in cytHyPer and in GPI-HyPer expressing strains revealed a significant increase of the ratio of cytHyPer but not of GPI-HyPer. This showed, for the first time, that a NoxR deletion-mediated ROS-accumulation in *F. graminearum* is not caused by an increase of the ER's H_2O_2-level.

6. References

Online tools and databases:

ZhaoGroup for Computational System Biology of Fudan University, accessed 27.07.2018:

http://comp-sysbio.org/efg/

UniProt database:

Protein sequences and functional information, accessed 12.06.2018

https://www.uniprot.org/

SignalP:

N-terminal signal peptide prediction, accessed 28.04.2016

http://www.cbs.dtu.dk/services/SignalP/

big-PI Predictor:

C-terminal signal peptide prediction, accessed 28.04.2016

http://mendel.imp.ac.at/sat/gpi/gpi_server.html

Fungal big-PI Predictor:

C-terminal signal peptide prediction, accessed 28.04.2016

http://mendel.imp.univie.ac.at/gpi/fungi/gpi_fungi.html

Pedant database:

Genome sequences, accessed March 2015 – August 2018

http://pedant.helmholtz-muenchen.de

fPoxDB:

Fungal peroxidase database, accessed 07.07.2018

http://peroxidase.riceblast.snu.ac.kr

NEBioCalculator:

Calculating molar ratios for ligation, accessed 01.07.2018

http://nebiocalculator.neb.com/#!/ligation

Publications:

Abbà, S., Khouja, H.R., Martino, E., Archer, D.B., Perotto, S. (2009) SOD1-targeted gene disruption in the ericoid mycorrhizal fungus Oidiodendron maius reduces conidiation and the capacity for mycorrhization. Mol. Plant Microbe Interact. 22, 1412–1421.

Able, A.J. (2003) Role of reactive oxygen species in the response of barley to necrotrophic pathogens. Protoplasma 221:137–43

Abreu, I.A., Cabelli, D.E. (2010) Superoxide dismutases – a review of the metal-associated mechanistic variations. Proteins and Proteomics 1804(2):263-274

Aguirre, J., Ríos-Momberg, M., Hewitt, D., Hansberg, W. (2005) Reactive oxygen species and development in microbial eukaryotes. Trends Microbiol. 13:111–18

Alberts, B., Johnson, A., Lewis, J., Raff, M., Roberts, K., Walter, P. (2002) Molecular biology of the cell (4th ed.) New York: Garland Science

Alkan, N., Davydov, O., Sagi, M., Fluhr, R., Prusky, D. (2009) Ammonium secretion by *Colletotrichum coccodes* activates host NADPH oxidase activity enhancing host cell death and fungal virulence in tomato fruits. Mol. Plant-Microbe Interact. 22:1484–91

Anandatheerthavarada, H.K., Biswas, G., Robin, M.A., Avadhani, N.G. (2003) Mitochondrial targeting and a novel transmembrane arrest of Alzheimer's amyloid precursor protein impairs mitochondrial function in neuronal cells. J. Cell Biol. 161:41–54

Andersson, H., Kappeler, F., Hauri, H.-P. (1999) Protein Targeting to Endoplasmic Reticulum by Dilysine Signals Involves Direct Retention in Addition to Retrieval. J. Biol. Chem. 274:15080-15084

Arkblad, E. L., Betsholtz, C., Mandoli, D., Ryström, J. (2001) Characterization of a nicotinamide nucleotide transhydrogenase gene from the green alga *Acetabularia acetabulum* and comparison of its structure with those of the corresponding genes in mouse and *Caenorhabditis elegans*. Bioch. et Bioph. Acta. 1520(2):115-123

Arkblad, E. L., Tuck, S., Pestov, N. B., Dmitriev, R. I., Kostina, M. B., Stenvall, J., Tranberg, M., Rydström, J. (2005) A *Caenorhabditis elegans* mutant lacking functional nicotinamide nucleotide transhydrogenase displays increased sensitivity to oxidative stress. Free Radical Biol. and Med. 38(11):1518-1525

Aro, N., Pakula, T., Penttilä, M. (2005) Transcriptional regulation of plant cell wall degradation by filamentous fungi. FEMS Microbiol. Rev. 29(4):719-739

Arthur, J. C. (1891) Wheat scab. Indiana Agric. Exp. Stn. Bull. 36:129-138

Asai, S., Yoshioka, H. (2009) Nitric oxide as a partner of reactive oxygen species participates in disease resistance to necrotrophic pathogen *Botrytis cinerea* in *Nicotiana benthamiana*. Mol. Plant Microbe Interact. 22:619–629

Atanasoff, D. (1920) Fusarium-blight (scab) of wheat and other cereals. J. Agric. Res. 20:1-32

Auclair, C., Torres, M., Hakim, J. (1978) Superoxide anion involvement in NBT reduction catalyzed by NADPH-cytochrome P-450 reductase: a pitfall. FEBS Lett. 89(1):26-28

Avadhani, N.G., Sangar, M.C., Bansal, S., Bajpai, P. (2011) Bimodal targeting of cytochrome P450s to endoplasmic reticulum and mitochondria: the concept of chimeric signals. FEBS J. 278:4218–4229

Bai, T.-T., Xie, W.-B., Zhou, P.-P., Wu, Z.-L., Xiao, W.-C., Zhou, L., Sun, J., Ruan, X.-L., Li, H.-P. (2013) Transcriptome and expression profile analysis of highly resistant and susceptible banana roots challenged with *Fusarium oxysporum* f. sp. *cubense* tropical race 4. PLoS one 8:e73945.

Balaban, R.S., Nemoto, S., Finkel, T. (2005) Mitochondria, oxidants, and aging. Cell 120:483–495

Baldrian, P., Valášková, V. (2008) Degradation of cellulose by basidiomycetous fungi. FEMS Microbiol. Rev. 32:501-521

Bardwell, J. C. A. (2004) The dance of disulfide formation. Nat. Struc. & Mol. Biol. 11(7):582-583

Beck, E., Ludwig, G., Auerswald, E. A., Reiss, B., & Schaller, H. (1982) Nucleotide sequence and exact localization of the neomycin phosphotransferase gene from transposon Tn5. Gene 19(3):327-336.

Bedard, K., Krause, K.H. (2007) The NOX family of ROS-generating NADPH oxidases: physiology and pathophysiology. Physiol. Rev. 87:245–313.

Bell, A. A., Wheeler, M. H. (1986) Biosynthesis and functions of fungal melanins. Annu. Rev. Phytopath. 24:411-451

Belousov, V.V., Fradkov, A.F., Lukyanov, K.A., Staroverov, D.B., Shakhbazov, K.S., Terskikh, A.V., Lukyanov, S. (2006) Genetically encoded fluorescent indicator for intracellular hydrogen peroxide. Nat. Methods 3(4):281-6.

Bilan, D.S., Pase, L., Joosen, L., Gorokhovatsky, A.Y., Ermakova, Y.G., Gadella, T.W.J., Belousov, V.V. (2013) HyPer-3: A genetically encoded H2O2 probe with improved performance for ratiometric and fluorescence lifetime imaging. ACS Chem. Biol. 8(3):535-542

Black, S.D. (1992) Membrane topology of the mammalian P450 cytochromes. FASEB J. 6(2):680-685

Blanquezet, P., Casas, N., Font, X., Gabarrell, X., Sarra, M., Caminal, G., Vicent, T. (2004) Mechanism of textile metal dye biotransformation by Trametes versicolor. Water Res. 38:2166-2172

Blümke, A., Falter, C., Herrfurth, C., Sode, B., Bode, R., Schäfer, W., Feussner, I., Voigt, C. A. (2014) Secreted fungal effector lipase releases free fatty acids to inhibit innate immunity-related callose formation during wheat head infection. Plant Physiol. 165(1):346-358

Bodył, A., Mackiewicz, P. (2007) Analysis of the targeting sequences of an iron-containing superoxide dismutase (SOD) of the dinoflagellate *Lingulodinium polyedrum* suggests function in multiple cellular compartments. Arch. Microbiol. 187(4):281-296

Boedi, S., Berger, H., Sieber, C., Münsterkötter, M., Maloku, I., Warth, B., Sulyok, M., Lemmens, M., Schuhmacher, R., Güldener, U., Strauss, J. (2016) Comparison of *Fusarium graminearum* transcriptomes on living or dead wheat differentiates substrate-responsive and defense-responsive genes. Front. Microbiol. 7:1113

Boenisch, M.J., Schäfer, W. (2011) *Fusarium graminearum* forms mycotoxin producing infection structures on wheat. BMC Plant Biology 11:110

Borden, W.T., Hoffmann, R., Stuyver, T., Chen, B. (2017) Dioxygen: What Makes This Triplet Diradical Kinetically Persistent?. JACS. 139:9010–9018

Bormann, J., Boenisch, M.J., Brückner, E., Firat, D., Schäfer, W. (2014) The adenylyl cyclase plays a regulatory role in the morphogenetic switch from vegetative to pathogenic lifestyle of *Fusarium graminearum* on wheat. PLoS ONE 9(3):e91135

Borrelly, G.P.M., Harrison, M.D., Robinson, A.K., Cox, S.G., Robinson, N.J., Whitehall, S.K. (2002) Surplus zinc is handled by Zym1 metallothionein and Zhf endoplasmic reticulum transporter in *Schizosaccharomyces pombe*. J. Biol. Chem. 277:30394–400

Branco, M.R., Marinho, H.S., Cyrne, L., Antunes, F. (2004) Decrease of H_2O_2 plasma membrane permeability during adaptation to H_2O_2 in *Saccharomyces cerevisiae*. J. Biol. Chem. 279:6501-6506

Brandes, R.P., Janiszewski, M. (2005) Direct detection of reactive oxygen species ex vivo. Kidney Int. 67(5):1662-1664

Brito, N., Espino, J.J., Gonzalez, C. (2006) The endo-β-1,4-xylanase *xyn11A* is required for virulence in *Botrytis cinerea*. Mol. Plant-Microbe Interact. 19:25–32

Brown, N.A., Ruban, M., van de Meene, A.M.L., Hammond-Kosack, K.E. (2010) The infection biology of *Fusarium graminearum*: Defining the pathways of spikelet to spikelet colonisation in wheat ears. Fungal Biology 114:555-571

Brown, N. A., Antoniw, J., Hammond-Kosack, K. E. (2012) The predicted secretome of the plant pathogenic fungus *Fusarium graminearum*: a refined comparative analysis. PLoS ONE 7(4):e33731

Brown, G.C., Borutaite, V. (2012) There is no evidence that mitochondria are the main source of reactive oxygen species in mammalian cells. Mitochondrion 12(1):1-4

Brun, S., Malagnac, F., Bidard, F., Lalucque, H., Silar, P. (2009) Functions and regulation of the Nox family in the filamentous fungus Podospora anserina. A new role in cellulose degradation. Mol. Microbiol. 74(2):480-496

Cadet, J., Davies, K.J.A. (2017) Oxidative DNA Damage & Repair: An Introduction. Free Radical Biology and Medicine 107:2-12

Cameron, M.D., Aust, S.D. (2001) Cellobiose dehydrogenase – an extracellular fungal flavocytochrome. Enzyme and Microbial Technology 28:129-138

Campbell, N.A. (2000) Biologie. Heidelberg, Berlin, Oxford: Spektrum, Akad. Verl., 1997

Campos-García, J., Delia Caro, A., Nájera, R., Miller-Maier, R.M., Al-Tahhan, R.A., Soberón-Chávez, G. (1998) The *Pseudomonas aeruginosa rhlG* gene encodes an NADPH-dependent ß-ketoacyl reductase which is specifically involved in rhamnolipid synthesis. J. Bacteriol. 180(17):4442-4451

Cano-Domínguez, N., Alvarez-Delfín, K, Hansberg, W., Aguirre, J. (2008) NADPH oxidases NOX-1 and NOX-2 require the regulatory subunit NOR-1 to control cell differentiation and growth in *Neurospora crassa*. Eukaryot. Cell 7(8):1352-61

Carocho, M., Ferreira, I.C.F.R. (2013) A review on antioxidants, prooxidants and related controversy. Natural and synthatic compunds, screening and analysis methodologies and future perspectives. Food and Chemical Toxicology 51:15-25

Chance, B., Sies, H., Boveris, A. (1979) Hydroperoxide metabolism in mammalian organs. Physiological Reviews 59:527-605

Chary, P., Dillon, D., Schroeder, A.L. and Natvig, D.O. (1994) Superoxide dismutase (sod-1) null mutants of Neurospora crassa: oxidative stress sensitivity, spontaneous mutation rate and response to mutagens. Genetics 137:723–730

Chen, R., Pignatello, J.J. (1997) Role of Quinone Intermediates as Electron Shuttles in Fenton and Photoassisted Fenton Oxidations of Aromatic Compounds. Environ. Sci. Technol. 31(8):2399-2406

Chen, S.S., Li, Y.-H., Lin, M.-F. (2017) Chronic exposure to the *Fusarium* mycotoxin deoxynivalenol: Impact on performance, immune organ, and intestinal integrity of slow-growing chickens. Toxins (Basel) 9(10):334

Chen, T., Embree, H.D., Wu, L.-Q., Payne, G.F. (2002) In vitro protein-polysaccharide conjugation: tyrosinase-catalyzed conjugation of gelatin and chitosan. Biopolymers 64(6):292–302

Cheon, S.A., Jung, K.W., Chen, Y.L., Heitman, J., Bahn, Y.S., Kang, H.A. (2011) Unique evolution of the UPR pathway with a novel bZIP transcription factor, Hxl1, for controlling pathogenicity of *Cryptococcus neoformans*. PLoS Pathog. 7(8):e1002177

Chi, M.H., Park, S.Y., Kim, S., Lee, Y.H. (2009) A novel pathogenicity gene is required in the rice blast fungus to suppress the basal defenses of the host. PLoS Pathog. 5:e1000401

Chiu, W.K., Towheed, A., Palladino, M.J. (2014) Chapter Fourteen – Genetically Encoded Redox Sensors. Methods in Enzymology 542:263-287

Choi, M., Davidson, V.L. (2011) Cupredoxins – A study of how proteins may evolve to use metals for bioenergetic processes. Metallomics 3:140-151

Chowdhury, S., Basu, A., Kundu, S. (2017) Biotrophy-necrotrophy switch in pathogen evoke differential response in resistant and susceptible sesame involving multiple signaling pathways at different phases. Sci. Rep. 7(1):17251

Christianson, T.W., Sikorski, R.S., Dante, M., Shero, J.H., Hieter, P. (1992) Multifunctional yeast high-copy-number shuttle vectors. Gene 110(1):119-122

Chumley, F.G., Valent, B. (1990) Genetic analysis of melanin-deficient, non-pathogenic mutants of Magnaporthe grisea. Molecular Plant-Microbe Interactions 3(3):135-143.

Cochrane, R.V., Vederas, J.C. (2014) Highly selective but multifunctional oxygenases in secondary metabolism. Acc. Chem. Res. 47:3148-3161

Colot, H.V., Park, G., Turner, G.E., Ringelberg, C., Crew, C.M., Litvinkova, L., Weiss, R.L., Borkovich, K.A., Dunlap, J.C. (2006) A high-throughput gene knockout procedure for *Neurospora* reveals functions for multiple transcription factors. Proc. Natl. Acad. Sci. USA 103(27):10352-10357

Comménil, P., Belingheri, L., Dehorter, B. (1998) Antilipase antibodies prevent infection of tomato leaves by Botrytis cinerea. Physiol. Mol. Plant Pathol. 52:1-14

Conesa, A., Punt, P.J., van Luijk, N., van den Hondel, C.A.M.J.J. (2001) The secretion pathway in filamentous fungi: A biotechnological view. Fungal Genetics and Biology 33:155-171

Cooke, M.S., Evans, M.D., Dizdaroglu, M., Lunec, J. (2003) Oxidative DNA damage: mechanisms, mutation, and disease. FASEB J. 17(10):1195-1214

Cordero, R.J.B., Casadevall, A. (2017) Functions of fungal melanin beyond virulence. Fungal Biology Reviews 31:99-112

Covert, S.F., Enkerli, J., Miao, V.P., Van Etten, H.D. (1996) A gene for maackiain detoxification from a dispensable chromosome of *Nectria haematococca*. Mol. Gen. Genet. 251:397-406

Cowger, C., Weisz, R., Arellano, C., Murphy, P. (2016) Profitability of integrated management of *Fusarium* Head Blight in North Caroline winter wheat. Phytopathology 106(8):814-823

Coyle, P., Philcox, J.C., Carey, L.C., Rofe, A.M. (2002) Metallothionein: The multipurpose protein. Cell. Mol. Life Sci. 59:627-647.

Črešnar, B., Petrič, Š. (2011) Cytochrome P450 enzymes in the fungal kingdom. Bioch. et Bioph. Acta 1814:29-35

Crowhurst, R.N., Binnie, S.J., Bowen, J.K., Hawthorne, B.T., Plummer, K.M., Rees-George, J., Rikkerink, E.H.A., Templeton, M.D. (1997) Effect of disruption of a cutinase gene (*cut*A) on virulence and tissue specificity of *Fusarium solani* f. sp. *cucurbitae* race 2 toward *Cucurbita maxima* and *C. moschata*. Mol. Plant-Microbe Interact. 10(3):355-368

Danpure, C.J. (1995) How can the products of a single gene be localized to more than one intracellular compartment? Trends Cell Biol. 5:230–238

Debenham, M.J., Hao, Q., Hasnain, S.S., Dodd, F.E., Abraham, Z.H., Eady, R.R. (1996) Structure solution of azurin II from Alcaligenes xylosoxidans using the Laue method: Possibility of studying in situ redox changes using X-rays. Journal of Synchrotron Radiation 3:14-19

De Groot, P.W.J., Hellingwerf, K.J., Klis, F.M. (2003) Genome-wide identification of fungal GPI proteins. Yeast 20:781-796

De Rienzo, F., Gabdoulline, R. R., Menziani, M. C., Wade, R. C. (2000) Blue copper proteins: A comparative analysis of their molecular interaction properties. Protein Science 9:1439-1454

Dence, C.W. (1971) Halogenation and nitration. In: Sarkanen, K.V., Ludwig, C.H. (ed.), Lignins: occurrence, formation, structure and reactions. Wiley-Interscience, New York, N.Y. p. 373-432.

Desjardins, A.E., Proctor, R.H. (2001) Biochemistry and genetics of *Fusarium* toxins. In: Summerell, B.A., Leslie, J.F., Backhouse, D., Bryden, W.L., Burgess, L.W., editors. Fusarium. Paul E. Nelson Memorial Symposium. St Paul, MN: APS Press. p. 50-69

Dickson, J.G. (1929) Scab of wheat and barley and its control. USDA Farmers' Bull. No. 1599:1-17

Dickson, J. G. (1942) Scab of wheat and barley and its control. USDA Farmers' Bull. No. 1599 (revised):1-22

Diebold, B.A., Bokoch, G.M. (2001) Molecular basis for Rac2 regulation of phagocyte NADPH oxidase. Nat Immunol 2:211-5.

Dikalov, S.I., Dikalova, A.E., Bikineyeva, A.T., Schmidt, H.H., Harrison, D.G., Griendling, K.K. (2008) Distinct roles of Nox1 and Nox4 in basal and angiotensin II-stimulated superoxide and hydrogen peroxide production. Free Radic. Biol. Med. 45:1340-1351

Ding, C., Yin, J., Tovar, E.M., Fitzpatrick, D.A., Higgins, D.G., Thiele, D.J. (2011) The copper regulon of the human fungal pathogen *Cryptococcus neoformans* H99. Mol. Microbiol 81:1560-76.

Ding, C., Festa, R.A., Chen, Y.-L., Espart, A., Palacios, O., Espín, J., Capdevila, M., Atrian, S., Heitman, J., Thiele, D.J. (2013) Cryptococcus neoformans copper detoxification machinery is critical for fungal virulence. Cell Host Microbe. 13:265-276

Dixon, D.M., Polak, A., Szaniszlo P.J. (1987) Pathogenicity and virulence of wild-type and melanin-deficient Wangiella dermatitidis. J. Med. Vet. Mycol. 25(2):97-106

Dizdaroglu, M. (1992) Oxidative damage to DNA in mammalian chromatin. Mutat. Res. 275:331-42

Dooley, C.T., Dore, T.M., Hanson, G.T., Jackson, W.C., Remington, S.J., Tsien, R.Y. (2004) Imaging dynamic redox changes in mammalian cells with green fluorescent protein indicators. J. Biol. Chem. 279(21):22284-22293

Douaiher, M.-N., Nowak, E., Durand, R., Halama, P., Reignault, P. (2007) Correlative analysis of Mycosphaerella graminicola pathogenicity and cell wall-degrading enzymes produced in vitro: The importance of xylanase and polygalacturonase. Plant Pathol. 56:79-86

Egan, M.J., Wang, Z.Y., Jones, M.A., Smirnoff, N., Talbot, N.J. (2007) Generation of reactive oxygen species by fungal NADPH oxidases is required for rice blast disease. Proc. Natl. Acad. Sci. USA. 104:11772-11777.

Eisenhaber, B., Schneider, G., Wildpaner, M., Eisenhaber, F. (2004) A sensitive predictor for potential GPI lipid modification sites in fungal protein sequences and its application to genome-wide studies for *Aspergillus nidulans*, *Candida albicans*, *Neurospora crassa*, *Saccharomyces cerevisiae*, and *Schizosaccharomyces pombe*. J. Mol. Biol. 337:243-253

Enguita, F. J. (2011) Structural Biology of Fungal Multicopper Oxidases. Mycofactories 16:57-72

Espino, J.J., Brito, N., Noda, J., Gonzalez, C. (2005) *Botrytis cinerea* endo-β-1,4-glucanase Cel5A is expressed during infection but is not required for pathogenesis. Physiol. Mol. Plant Pathol. 66:213-21

Espino, J. J., Gutiérrez-Sánchez, G., Brito, N., Shah, P., Orlando, R., González, C. (2010) The *Botrytis cinerea* early secretome. Proteomics 10(19):3020-3034

Evans, M. L., Hollaway, G. J., Dennis, J. I., Correll, R., Wallwork, H. (2010) Crop sequence as a tool for managing populations of *Fusarium pseudograminearum* and *F. culmorum* in south-eastern Australia. Australasian Plant Pathology. 39(4):376-382

Fan, H., Yu, G., Liu, Y., Zhang, X., Liu, J., Zhang, Y., Rollins, J. A., Sun, F., Pan, H. (2016) An atypical forkhead-containing transcription factor SsFKH1 is involved in sclerotial formation and is essential for pathogenicity in *Sclerotinia sclerotiorum*. Molecular Plant Pathology 18(7):963-975

Fenaille, F., Guy, P.A., Tabet, J.C. (2003) Study of protein modification by 4-hydroxy-2-nonenal and other short chain aldehydes analyzed by electrospray ionization tandem mass spectrometry. Journal of the American Society for Mass Spectrometry 14(3):215-226

Feng, B., Wang, X., Hauser, M., Kaufmann, S., Jentsch, S., Haase, G., Becker, J.M., Szaniszlo, P.J. (2001) Molecular Cloning and Characterization of WdPKS1, a Gene Involved in Dihydroxynaphthalene Melanin Biosynthesis and Virulence in Wangiella (Exophiala) dermatitidis. Infection and Immunity 69(3):1781-1794

Ferguson, M.A.J., Williams, A.F.A. (1988) Cell-surface anchoring of proteins via glycosyl-phosphatidylinositol structures. Annu. Rev. Biochem. 57:285-320

Fernández-Acero, F.J., Colby, T., Harzen, A., Carbu, M., Wieneke, U., et al. (2010) 2-DE proteomic approach to the *Botrytis cinerea* secretome induced with different carbon sources and plant-based elicitors. Proteomics 10:2270-80

Feyereisen, R. (2012) Insect CYP genes and P450 enzymes. Insect Molecular Biology and Biochemistry 236-316

Fisher, M.C., Henk, D.A., Briggs, C.J., Brownstein, J.S., Madoff, L.C., McCraw, S.L., Gurr, S.J., (2012) Emerging fungal threats to animal, plant and ecosystem health. Nature 484:1-18.

Fleming, I., Michaelis, U.R., Bredenkötter, D., Fisslthaler, B., Dehghani, F., Brandes, R.P., Busse, R. (2001) Endothelium derived hyperpolarizing factor synthase (cytochrome P450 2C9) is a functionally significant source of reactive oxygen species in coronary arteries. Circ. Res. 88:44-51

Flodin, C., Johansson, E., Boren, H., Grimvall, H., Dahlman, O., Morck, R. (1997) Chlorinated structures in high molecular weight organic matter isolated from fresh and decaying plant material and soil. Environ. Sci. Technol. 31**:**2464-2468

Flohé, L., Ursini, F. (2008) Peroxidase: A term of many meanings. Antioxidants Redox Signaling 10(9):1485-1490

Foyer, C.H., Noctor, G. (2013) Redox signaling in plants. Antioxid. Redox Signal. 18:2087-2090

Frandsen, R.J.N., Rasmussen, S.A., Knudsen, P.B., Uhlig, S., Petersen, D., Lysøe, E., Gotfredsen, C.H., Giese, H., Larsen, T.O. (2016) Black perithecial pigmentation in *Fusarium* species is due to the accumulation of 5-deoxybostrycoidin-based melanin. Scientific Reports 6:26206.

Fridovich, I. (1983) Superoxide radical: An endogenous toxicant. Annu. Rev. Biochem. 23:239-257

Garre, V., Muller, U., Tudzynski, P. (1998) Cloning, characterization, and targeted disruption of *cpcat1*, coding for an in planta secreted catalase of *Claviceps purpurea*. Mol. Plant-Microbe Interact. 11:772-83

Gehrmann, W., Elsner, M. (2011) A specific fluorescence probe for hydrogen peroxide detection in peroxisomes. Free Radic. Res. 45:501-506

George, H.L., Hirschi, K.D., VanEtten, H.D. (1998) Biochemical properties of the products of cytochrome P450 genes (PDA) encoding pisatin demethylase activity in Nectria haematococca. Arch. Microbiol. 170:147-154

Gerwien, F., Skrahina, V., Kasper, L., Hube, B., Brunke, S. (2017) Metals in fungal virulence. FEMS Microb. Rev. doi: 10.1093/femsre/fux050

Giesbert, S., Schurg, T., Scheele, S., Tudzynski, P. (2008) The NADPH oxidase Cpnox1 is required for full pathogenicity of the ergot fungus *Claviceps purpurea*. Mol. Plant Pathol. 9:317–27

Gilbert, J., Haber, S. (2013) Overview of some recent research developments in *Fusarium* Head Blight of wheat. Canadian J. Plant Path. 35(2):149-174

Govrin, E.M., Levine, A. (2000) The hypersensitive response facilitates plant infection by the necrotrophic pathogen *Botrytis cinerea*. Curr. Biol. 10:751-57

Grant, J.J., Loake, G.J. (2000) Role of reactive oxygen intermediates and cognate redox signaling in disease resistance. Plant Physiol. 124:21-29

Greving, M.P., Patti, G.J., Siuzdak, G. (2011) Nanostructure-initiator mass spectrometry metabolite analysis and imaging. Analytical Chemistry 83(1):2-7

Grieve, A.G., Rabouille, C. (2011) Golgi bypass: skirting around the heart of classical secretion. Cold Spring Harb Perspect Biol. 3(4) a005298

Grissa, I., Bidard, F., Grognet, P., Grossetete, S., Silar, P. (2010) The Nox/Ferric reductase/Ferric reductase-like families of Eumycetes. Fungal Biol. 114:766-777

Güldener, U., Seong, K.Y., Boddu, J., Cho, S., Trail, F., Xu, J.R., Adam, G., Mewes, H.W., Muehlbauer, G.J., and Kistler, H.C. (2006) Development of a Fusarium graminearum Affymetrix GeneChip for profiling fungal gene expression in vitro and in planta. Fungal Genet. Biol. 43: 316-325

Halaouli, S., Asther, M., Sigoillot, J.-C., Hamdi, M., Lomascolo, A. (2005) Fungal tyrosinases: new prospects in molecular characteristics, bioengineering and biotechnological applications. J. Appl. Microbiol. 100:219-232

Hammel, K.E., Cullen, D. (2008) Role of fungal peroxidases in biological ligninolysis. Curr. Opin. Plant Biol. 11:349-355

Hansberg, W., Aguirre, J. (1990) Hyperoxidant states cause microbial cell differentiation by cell isolation from dioxygen. J. Theoret. Biol. 142:201-221

Hanson, G.T., Aggeler, R., Oglesbee, D., Cannon, M., Capaldi, R.A., Tsien, R.Y., Remington, S.J. (2004) Investigating mitochondrial redox potential with redox-sensitive green fluorescent protein indicators. The Journal of Biological Chemistry 279:13044-13053

Harding, H.P., Zhang, Y., Zeng, H., Novoa, I., Lu, P.D., Calfon, M., Sadri, N., Yun, C., Popko, B., Paules, R., Stojdl, D.F., Bell, J.C., Hettmann, T., Leiden, J.M., Ron, D. (2003) An integrated stress response regulates amino acid metabolism and resistance to oxidative stress. Mol. Cell 11:619-633

Hare, J.M., Beigi, F., Tziomalos, K. (2008) Chapter Twenty-One - Nitric Oxide and Cardiobiology-Methods for Intact Hearts and Isolated Myocytes Methods in Enzymology Volume 441:369-392

Harris, L.J., Balcerzak, M., Johnston, A., Schneiderman, D., Ouellet, T. (2016) Host-preferential *Fusarium graminearum* gene expression during infection of wheat, barley, and maize. Fungal Biology 120(1):111-123

Harrison, N., Cavinder, B., Townsend, J.P., Trail, F. (2013) Optimized primers and other critical conditions for efficient fusion PCR to generate knockout vectors in filamentous fungi. Fungal Genetics Reports

Haschek, W.M., Voss, K.A. (2013) Haschek and Rousseaux's handbook of toxicologic pathology (third edition). Volume II. Academic Press 1187-1258

Heck, D.E., Shakarjian, M., Kim, H.D., Laskin, J.D., Vetrano, A.M. (2010) Mechanisms of oxidant generation by catalase. Ann. N.Y. Acad. Sci. 1203:120-125

Heller, J., Tudzynski, P. (2011) Reactive oxygen species in phytopathogenic fungi: signaling, development, and disease. Annu. Rev. Phytopathol. 49:369-390.

Helmcke, I., Heumüller, S., Tikkanen, R., Schröder, K., Brandes, R.P. (2009) Identification of structural elements in Nox1 and Nox4 controlling localization and activity. Antioxid Redox Signal. 11(6):1279-1287

Henkel, G., Krebs, B. (2004) Metallothioneins: Zinc, cadmium, mercury, and copper thiolates and selenolates mimicking protein active site features—Structural aspects and biological implications. Chem. Rev. 104:801-824.

Henriksson, G., Ander, P., Pettersson, B., Pettersson, G. (1995) Cellobiose dehydrogenase (cellobiose oxidase) from Phanerochaete chrysosporium as a wood degrading enzyme – studies on cellulose, xylan and synthetic lignin. Appl. Microbiol. Biotechnol. 42:790-796.

Hernández-Ortega, A., Ferreira, P., Martínez, A.T. (2012) Fungal aryl-alcohol oxidase: a peroxide-producing flavoenzyme involved in lignin degradation. Appl. Microbiol. Biotechnol. 93(4):1395-1410

Hinkle, P.C., Butow, R.A., Racker, E., Chance, B. (1967) Partial Resolution of the Enzymes Catalyzing Oxidative Phosphorylation. Xv Reverse Electron Transfer in the Flavin-cytochrome beta region of the respiratory chain of beef heart. J. Biol. Chem. 242:5169-5173.

Hirsch, M.M. (1954) Environmental factors influencing the differentiation of protoperithecia and their relation to tyrosinase and melanin formation in *Neurospora crassa*. Physiologia Plantarum 7(1):72-97

Howard, R.J., Valent, B. (1996) BREAKING AND ENTERING: Host Penetration by the Fungal Rice Blast Pathogen Magnaporthe grisea. Annu. Rev. Microbiol. 50:491-512

Hrycay, E.G., Bandiera, S.M. (2012) The monooxygenase, peroxidase, and peroxygenase properties of cytochrome P450. Arch. Biochem. Biophys. 522(2):71-89

Hrycay, E.G., Bandiera, S.M. (2015) Monooxygenase, peroxidase and peroxygenase properties and reaction mechanisms of cytochrome P450 enzymes. Adv. Exp. Med. Biol. 851:1-61

Huijbers, M.M., Montersino, S., Westphal, A.H., Tischler, D., van Berkel, W.J. (2014) Flavin dependent monooxygenases. Arch. Biochem. Biophys. 544:2-17

Ikawa, M., Okazawa, H., Arakawa, K., Kudo, T., Kimura, H., Fujibayashi, Y., Kuriyama, M., Yoneda, M. (2009) PET imaging of redox and energy states in stroke-like episodes of MELAS. Mitochondrion 9(2):144-148

Ikner, A., Shiozaki, K. (2005) Yeast signaling pathways in the oxidative stress response. Mutat Res 569:13-27.

Iskandar, N.L., Zainudin, N.A., Tan, S.G. (2011) Tolerance and biosorption of copper (Cu) and lead (Pb) by filamentous fungi isolated from a freshwater ecosystem. Journal of Environmental Sciences 23(5):824-830

Isshiki, A., Akimitsu, K., Yamamoto, M., Yamamoto, H. (2001) Endopolygalacturonase is essential for citrus black rot caused by *Alternaria citri* but not brown spot caused by *Alternaria alternata*. Mol. Plant-Microbe Interact. 14:749-57

Jackson, J.B., Peake, S.J., White, S.A. (1999) Structure and mechanism of proton-translocating transhydrogenase. FEBS Letters 464(1-2):1-8

Jacob, C., Courbot, M., Martin, F., Brun, A., Chalot, M. (2004) Transcriptomic response to cadmium in the ectomycorrhizal fungus Paxillus involutus. FEBS Lett. 576:423-427.

Jahn, B., Koch, A., Schmidt, A., Wanner, G., Gehringer, H., Bhakdi, S., Brakhage, A.A. (1997) Isolation and Characterization of a Pigmentless-Conidium Mutant of Aspergillus fumigatus with Altered Conidial Surface and Reduced Virulence. Infection and Immunity 65(12):5110-5117

Jamieson, D.J. (1998) Oxidative stress responses of the yeast *Saccharomyces cerevisiae*. Yeast 14(16):1511-1527

Janiszewski, M., Souza, H.P., Liu, X., Pedro, M.A., Zweier, J.L., Laurindo, F.R. (2002) Overestimation of NADH-driven vascular oxidase activity due to lucigenin artifacts. Free Radic. Biol. Med. 32(5):446-453

Janse, B.J.H., Gaskell, J., Akhtar, M., Cullen, D. (1998) Expression of Phanerochaete chrysosporium genes encoding lignin peroxidases, manganese peroxidases, and glyoxal oxidase in wood. Appl. Environ. Microbiol. 64:3536-3538

Jastroch, M., Divakaruni, A.S., Mookerjee, S., Treberg, J.R., Brand, M.D. (2010) Mitochondrial proton and electron leaks. Essays in Biochemistry. 47:53-67. doi:10.1042/bse0470053.

Joubert, A., Simoneau, P., Campion, C., Bataille-Simoneau, N., Iacomi-Vasilescu, B., Poupard, P., Francois, J.M., Georgeault, S., Sellier, E., Guillemette, T. (2011) Impact of the unfolded protein response on the pathogenicity of the necrotrophic fungus *Alternaria brassicicola*. Molecular Microbiology 79:1305-1324

Kalsotra, T., Khullar, S., Agnihotri, R., Reddy, M. S. (2018) Metal induction of two metallothionein genes in the ectomycorrhizal fungus *Suillus himalayensis* and their role in metal tolerance. Microbiology 164:868-876

Kang, Z., Buchenauer, H. (2000) Ultrastructural and immunocytchemical investigation of pathogen development and host responses in resistant and susceptible wheat spikes infected by *Fusarium culmorum*. Physiological and Molecular Plant Pathology 57:255-268.

Kapoor, R., Singh, N. (2017) In: Wu, Q.-S. (Ed.), Arbuscular Mycorrhiza and Reactive Oxygen Species BT - Arbuscular Mycorrhizas and Stress Tolerance of Plants. Springer Singapore, pp. 225-243

Kapteyn, J.C., Montijn, R.C., Vink, E., de la Cruz, J., Llobell, A., Douwes, J.E., Shimoi, H., Lipke, P.N., Klis, F.M. (1996) Retention of Saccharomyces cerevisiae cell wall proteins through a phosphodiester-linked beta-1,3-/beta-1,6-glucan heteropolymer. Glycobiology 6:337-345

Karniely, S., Pines, O. (2005) Single translation–dual destination: mechanisms of dual protein targeting in eukaryotes. EMBO Rep 6:420-425

Kawamura, C., Tsujimoto, T., Tsuge, T. (1999) Targeted disruption of a melanin biosynthesis gene affects conidial development and UV tolerance in the Japanese pear pathotype of *Alternaria alternata*. Mol. Plant Microbe Inter. 12:59-63

Kayano, Y., Tanaka, A., Akano, F., Scott, B., Takemoto, D. (2013) Differential roles of NADPH oxidases and associated regulators in polarized growth, conidiation and hyphal fusion in the symbiotic fungus *Epichloë festucae*. Fungal Genet. Biol. 56:87-97.

Kazan, K., Gardiner, D.M., Manners, J.M. (2012) On the trail of a cereal killer: recent advances in *Fusarium graminearum* pathogenomics and host resistance. Mol. Plant Pathol. 13(4):399-413

Keller, T., Damude, H.G., Werner, D., Doerner, P., Dixon, R.A., Lamb, C. (1998) A plant homolog of the neutro-phil NADPH oxidase gp91phox subunit gene encodes aplasma membrane protein with Ca^{2+} binding motifs. PlantCell 10:255–266.

Kersten, P.J., Kirk, T.K. (1987) Involvement of a new enzyme, glyoxal oxidase, in extacellular hydrogen peroxide production by Phanerochaete chrysosporium. J. Bacteriol. 169:2195-2201

Kiirika, L.M., Bergmann, H.F., Schikowsky, C., Wimmer, D., Korte, J., Schmitz, U. (2012) Silencing of the Rac1GTPase MtROP9 in *M*. *truncatula* stimulates early mycorrhizial and oomycete root colonizations but negatively affects rhizobial infection. Plant Physiol. 159:501-516

Kim, J.K. (2014) Exploitation of reactive oxygen species by fungi: Roles in host-fungus interaction and fungal development. J. Microbiol. Biotechnol. 24(11):1455-1463

Kim, H., Chen, C., Kabbage, M., Dickman, M.B. (2011) Identification and characterization of Sclerotinia sclerotiorum NADPH oxidases. Appl. Environ. Microbiol 77(21):7721-7729

Kim, K.H., Willger, S.D., Park, S.W., Puttikamonkul, S., Grahl, N., Cho, Y., Mukhopadhyay, B., Cramer, R.A. Jr, Lawrence, C.B. (2009) TmpL, a transmembrane protein required for intracellular redox homeostasis and virulence in a plant and an animal fungal pathogen. PLoS Pathog. 5:e1000653

Kimura, Y., Asada, Y., Kuwahara, M. (1990) Screening of basidiomycetes for lignin peroxidase genes using a DNA probe. Appl Microbiol Biotechnol 32:436-442

Knowles, P.F., Ito, N. (1993) Galactose Oxidase. In Perspectives on Bioinorganic Chemistry; R. W. Hay, J. R. Dilworth, Eds.; JAI Press: London, Vol. 2, pp 208-243.

Kobayashi, M., Yoshioka, M., Asai, S., Nomura, H., Kuchimura, K., Mori, H., et al. (2012) StCDPK5 confers resistance to late blight pathogen but increases susceptibility to early blight pathogen in potato via reactive oxygen species burst. New Phytol. 196:223-237

Kosiak, B., Skjerve, E., Thrane, U., Torp, M. (2003) The prevalence and distribution of Fusarium species in Norwegian cereals: a survey. Acta Agric. Scand. 53:168-176

Kremer, S.M., Wood, P.M. (1992) Production of fenton reagent by cellobiose oxidase from cellulolytic cultures of Phanerochaete chrysosporium. Eur. J. Biochem. 208:807-814

Krishnan, K., Askew, D. S. (2014) Endoplasmic reticulum stress and fungal pathogenesis. Fungal Bio. Rev. 28(2-3):29-35

Kubicek, C.P., Starr, T.L., Glass, N.L. (2014) Plant cell wall-degrading enzymes and their secretion in plant-pathogenic fungi. Annual Review of Phytopathology 52:427-451

Kuroda, J., Ago, T., Nishimura, A., Nakamura, K., Matsuo, R., Wakisaka, Y., Kamouchi, M., Kitazono, T. (2014) Nox4 is a mojor source of superoxide production in human brain pericytes. J. Vasc. Res. 51(6):429-438

Kussmaul, L., Hirst, J. (2006) The mechanism of superoxide production by NADH:ubiquinone oxidoreductase (complex I) from bovine heart mitochondria. Proc. Natl. Acad. Sci. USA 103:7607-7612

Kwon-Chung, K.J., Rhodes, J.C. (1986) Encapsulation and melanin in Cryptococcus neoformans. Infect. Immun. 51:218-223

Lah, L., Podobnik, B., Novak, M., Korošec, B., Berne, S., Vogelsang, M., Kraševec, N., Zupanec, N., Stojan, J., Bohlmann, J., Komel, R. (2011) The versatility of the fungal cytochrome P450 monooxygenase system is instrumental in xenobiotic detoxification. Molecular Microbiology 81(5):1374-1389

Lahlali, R., Kumar, S., Wang, L., Forseille, L., Sylvain, N., Korbas, M., Muir, D., Swerhone, G., Lawrence, J.R., Fobert, P.R., Peng, G., Karunakaran, C. (2016) Cell Wall Biomolecular Composition Plays a Potential Role in the Host Type II Resistance to Fusarium Head Blight in Wheat. Frontiers in Microbiology 7:910

Langfelder, K., Jahn, B., Gehringer, H., Schmidt, A., Wanner, G. & Brakhage, A.A. (1998) Identification of polyketide synthase gene (pksP) of Aspergillus fumigatus involved in conidial pigment biosynthesis and virulence. Med. Microbiol. Immunol. 187:79-89

Langfelder, K., Streibel, M., Jahn, B., Hasse, G., Brakhage, A.A. (2003) Biosynthesis of fungal melanins and their importance for human pathogenic fungi. Fungal Genet. Biol. 38:143-158.

Lara-Ortíz, T., Riveros-Rosas, H., Aguirre, J. (2003) Reactive oxygen species generated by microbial NADPH oxidase NaxA regulate sexual development in *Aspergillus nidulans*. Mol. Microbiol. 50(4):1241-1255

Laurindo, F.R.M., Pescatore, L.A., Fernandes Dde, C. (2012) Protein disulfide isomerase in redox cell signaling and homeostasis. Free Radic. Biol. Med. 52:1954–1969

Laurindo, F.R.M., Araujo, T.L.S., Abrahão T.B. (2014) Nox NADPH Oxidases and the Endoplasmic Reticulum. Antioxidants & Redox Signaling 20(17):2755-2775

Lee, W. (2010) Comprehensive DIscovery of Fungal Gene Clusters: Unexpected Co-work Reflected at the Genomic Level. Dissertation, TU München

Lee, Y., Min, K., Son, H., Park, A.R., Kim, J.-C., Choi, G.J., Lee, Y.-W. (2014) ELP3 is involved in sexual and asexual development, virulence, and the oxidative stress response in *F. graminearum*. MPMI 27(12):1344-1355

Lee, Y., Son, H., Shin, J.Y., Choi, G.J., Lee, Y.-W. (2017) Genome-wide functional characterization of putative peroxidases in the head blight fungus *Fusarium graminearum*. Mol. Plant Pathol. 19(3):715-730

Lehmann, S., Serrano, M., L'Haridon, F., Tjamos, S.E., Metraux, J.-P. (2014) Reactive oxygen species and plant resistance to fungal pathogens. Phytochemistry 112:54-62

Leonowicz, A., Cho, N. S., Luterek, J., Wilkolazka, A., Wojtas-Wasilewska, M., Matuszewska, A., Hofrichter, M., Wesenberg, D., Rogalski, J. (2001) Fungal laccase: Properties and activity on lignin. J. Basic Microbiol. 41:185-227.

Lerch, K. (1980) Copper metallothionein, a copper-binding protein from *Neurospora crassa*. Nature 284:368–370.

Leuthner, B., Aichinger, C., Oehmen, E., Koopmann, E., Müller, O., Müller, P., Kahmann, R., Bölker, M., Schreier, P. H. (2005) A H_2O_2-producing glyoxal oxidase is required for filamentous growth and pathogenicity in Ustilago maydis. Mol. Genet. Genomics 272(6):639-650

Lev, S., Hadar, R., Amedeo, P., Baker, S.E., Yoder, O.C., Horwitz, B.A. (2005) Activation of an AP1-like transcription factor of the maize pathogen *Cochliobolus heterostrophus* in response to oxidative stress and plant signals. Eukaryotic Cell. 4:443-54

L'Haridon, F., Besson-Bard, A., Binda, M., Serrano, M., Abou-Mansour, E., Balet, F., Schoonbeek, H.-J., Hess, S., Mir, R., Leon, J., Lamotte, O., Metraux (2011) A permeable cuticle is associated with the release of reactive oxygen species and induction of innate immunity. PLoS Pathogens e1002148.

Li, D., Ashby, A.M., Johnstone, K. (2003) Molecular evidence that the extracellular cutinase Pbc1 is required for pathogenicity of Pyrenopeziza brassicae on oilseed rape. Mol. Plant Microbe Interact. 16:545-552

Lin, C., Yang, S.L., Chung, K. (2009) The YAP1 homolog-mediated oxidative stress tolerance is crucial for pathogenicity of the necrotrophic fungus *Alternaria alternata* in citrus. Mol. Plant-Microbe Interact. 22:942–52

Liu, X., Jiang, J., Shao, J., Yin, Y., Ma, Z. (2009) Gene transcription profiling of Fusarium graminearum treated with an azole fungicide tebuconazole. Appl Microbiol Biotechnol 85(4):1105-1014

Liu, Y., Fiskum, G., Schubert, D. (2002) Generation of reactive oxygen species by the mitochondrial electron transport chain. J. Neurochem. 80:780-787

Lo Presti, L., Lanver, D., Schweizer, G., Tanaka, S., Liang, L., Tollot, M., Zuccaro, A., Reissmann, S., Kahmann, R. (2015) Fungal effectors and plant susceptibility. Annu. Rev. Plant Biol. 66:513-545

Lowe, R.G.T., McCorkelle, O., Bleackley, M., Collins, C., Faou, P., Mathivanan, S., Anderson, M. (2015) Extracellular peptidases of the cereal pathogen *Fusarium graminearum*. Front. Plant Sci. 6:962

Lukyanov, K.A., Belousov, V.V. (2014) Genetically encoded fluorescent redox sensors. Biochim. Biophys. Acta. 1840(2):745-56.

Luo, K., DesRoches, C. L., Johnston, A., Harris, L. J., Zhao, H. Y., Ouellet, T. (2017) Multiple metabolic pathways for metabolism of l-tryptophan in *Fusarium graminearum*. Can. J. Microbiol. 63(11):921-927

Lyon, G.D., Goodman, B.A., Williamson, B. (2004) *Botrytis cinerea* perturbs redox processes as an attack strategy in plants. In: Botrytis: Biology, Pathology and Control, pp. 119-142. Dordrecht: Springer

Lysøe, E., Seong, K.Y., Kistler, H.C. (2011) The transcriptome of *Fusarium graminearum* during the infection of wheat. Mol. Plant Microbe Interact. 24(9):995-1000

Ma, Y., Taylor, S.S. (2008) A molecular switch for targeting between endoplasmic reticulum (ER) and mitochondria: conversion of a mitochondria-targeting element into an ER-targeting signal in DAKAP1. J. Biol. Chem. 283(17):11743-11751

Maier, F.J., Malz, S., Lösch, A.P., Lacour, T., Schäfer, W. (2005) Development of a highly efficient gene targeting system for *Fusarium graminearum* using the disuption of a polyketide synthase gene as a visible marker. FEMS Yeast Research 5:653-662

Maier, F.J., Miedaner, T., Hadeler, B., Felk, A., Salomon, S., Lemmens, M., Kassner, H., Schäfer, W. (2006) Involvement of trichothecenes in fusarioses of wheat, barley and maize evaluated by gene disruption of the trichodiene synthase (Tri5) gene in three field isolates of different chemotype and virulence. Molecular Plant Pathology 7(6):449-461.

Malagnac, F., Lalucque, H., Lepère, G., Silar, P. (2004) Two NADPH oxidase isoforms are required for sexual reproduction and ascospore germination in the filamentous fungus Podospora anserina. Fungal Genet. Biol. 41:982-997.

Malinouski, M., Zhou, Y., Belousov, V.V., Hatfield, D.L., Gladyshev, V.N. (2011) Hydrogen peroxide probes directed to different cellular compartments. PLoS One 6(1): e14564

Malonek, S., Rojas, M.C., Hedden, P., Tudzynski, B. (2004) The NADPH-cytochrome P450 reductase gene from *Gibberella fujikuroi* is essential for gibberellin biosynthesis. J. Biol. Chem. 279(24):25075-25084

Mansuy, D. (1998) The great diversity of reactions catalyzed by cytochromes P450. Comp. Biochem. Physiol. C Pharmacol. Toxicol. Endocrinol. 121:5–14

Manzl, C., Enrich, J., Ebner, H., Dallinger, R., Krumschnabel, G. (2004) Copper-induced formation of reactive oxygen species causes cell death and disruption of calcium homeostasis in trout hepatocytes. Toxicology 196:57-64

Marciniak, S.J., Yun, C.Y. , Oyadomari, S., Novoa, I., Zhang, Y., Jungreis, R., Nagata, K., Harding, H.P., Ron, D. (2004) CHOP insuces death by promoting protein synthesis and oxidation in the stressed endoplasmic reticulum. Genes Dev. 18(24):3066-3077

Marciniac, S.J., Ron, D. (2006) Endoplasmic reticulum stress signaling in disease. Physiol. Rev. 86:1133-1149

Margittai, E., Sitia, R. (2011) Oxidative protein folding in the secretory pathway and redox signaling across compartments and cells. Traffic 12:1-8

Marino, D., Dunand, C., Puppo, A., Pauly, N. (2012) A burst of plant NADPH oxidases. Trends Plant Sci. 17:9-15

Markvicheva, K.N., Bilan, D.S., Mishina, N.M., Gorokhovatsky, A.Y., Vinokurov, L.M., Lukyanov, S., Belousov, V.V. (2011) A genetically encoded sensor for H2O2 with expanded dynamic range. Bioorg. Med. Chem. 19(3):1079-84.

Marschall, R., Schumacher, J., Siegmund, U., Tudzynski, P. (2016a) Chasing stress signals – Exposure to extracellular stimuli differentially affect the redox state of cell

compartments in the wild type and signaling mutants of *Botrytis cinerea*. Fungal Genetics and Biology 90:12-22

Marschall, R., Siegmund, U., Burbank, J., Tudzynski, P. (2016b) Update on Nox function, site of action and regulation in *Botrytis cinerea*. Fungal Biol. Biotechnol. 3:8

Martchenko, M., Alarco A., Harcus, D., Whiteway, M. (2004) Superoxide dismutases in Candida albicans: Transcriptional regulation and functional characterization of the hyphal-induced SOD5 gene. Molecular Biology of the Cell 15:456-467

Martins, D., Kathiresan, M., English, A.M. (2013) Cytochrome c peroxidase is a mitochondrial heme-based H_2O_2 sensor that modulates antioxidant defense. Free Radical Biology and Medicine 65:541-551

McMullen M., Bergstrom G., De Wolf E., Dill-Macky R., Hershman D., Shaner G., Van Sanford D. (2012) A unified effort to fight an enemy of wheat and barley: Fusarium head blight. Plant Disease 96(12):1712-1728

Mehmeti, I., Lortz, S., Lenzen, S. (2012) The H_2O_2-sensitive HyPer protein targeted to the endoplasmic reticulum as a mirror of the oxidizing thio-disulfide milieu. Free Radical Biology and Medicine 53(7):1451-1458

Meimaridou, E., Kowalczyk, J., Guasti, L. et al. (2012) Mutations in NNT encoding nicotinamide nucleotide transhydrogenase cause familial glucocorticoid deficiency. Nat. Genet. 44:740-742

Mentges, M. (2014) Ratiometrische Analyse zur Dynamik reaktiver Sauerstoffspezies in *Fusarium graminearum*. Masterarbeit, Universität Hamburg

Mentges, M., Bormann, J. (2015) Real-time imaging of hydrogen peroxide dynamics in vegetative and pathogenic hyphae of Fusarium graminearum. Sci. Rep. 5:14980

Meyer, A.J., Brach, T., Marty, L., Kreye, S., Rouhier, N., Jacquot, J.P., Hell, R. (2007) Redox-sensitive GFP in Arabidopsis thaliana is a quantitative biosensor for the redox potential of the cellular glutathione redox buffer. Plant J. 52:973-986

Miller, D. J., Zhang, Y-M., Rock, C. O., White, S. W. (2006) Structure of RhlG, an essential ß-ketoacyl reductase in the rhamnolipid biosynthesis pathway of *Pseudomonas aeruginosa*. J. Biol. Chem. 281:18025-18032

Miller, E.W., Dickinson, B. C., Chang, C. J. (2010) Aquaporin-3 mediates hydrogen peroxide uptake to regulate downstream intracellular signaling. Proc. Natl. Acad. Sci. U.S.A. 107:15681-15686

Mittler, R. (2017) ROS are good. Trends Plant Sci. 22(1):11-19

Mittler, R., Vanderauwera, S., Suzuki, N., Miller, G., Tognetti, V.B., Vandepoele, K., Gollery, M., Shulaev, V., van Breusegem, F. (2011) ROS signaling: the new wave? Trends Plant Sci. 16(6):300-309

Miyazaki, T., Nakayama, H., Nagayoshi, Y., Kakeya, H., Kohno, S. (2013) Dissection of Ire1 functions reveals stress response mechanisms uniquely evolved in *Candida glabrata*. PLoS Pathog. 9(1):e1003160

Mohammadian, E., Ahari, A. B., Arzanlou, M., Oustan, S., Khazaei, S. H. (2017) Tolerance to heavy metals in filamentous fungi isolated from contaminated mining soils in the Zanjan Province, Iran. Chemosphere 19555

Molina, L., Kahmann, R. (2007) An *Ustilago maydis* gene involved in H_2O_2 detoxification is required for virulence. Plant Cell 19:2293-309

Møller, I.M., Jensen, P.E., Hansson, A. (2007) Oxidative Modifications to Cellular Components in Plants. Annu. Rev. Plant Biol. 58:459-481

Monier, S., Van Luc, P., Kreibich, G., Sabatini, D. D., Adesnik, M. (1988) Signals for the Incorporation and Orientation of Cytochrome P450 in the Endoplasmic Reticulum Membrane. The Journal of Cell Biology 107:457-470

Moore, S., De Vries, O.M.H., Tudzynski, P. (2002) The major cu,zn SOD of the phytopathogen *Claviceps purpurea* is not essential for pathogenicity. Mol. Plant Pathol. 3:9-22

Moriwaki, A., Kihara, J., Kobayashi, T., Tokunaga, T., Arase, S., Honda, Y. (2004) Insertional mutagenesis and characterization of a polyketide synthase gene (PKS1) required for melanin biosynthesis in *Bipolaris oryzae*. FEMS Microbiol. Lett. 238:1-8.

Moschini, R. C., Fortugno, C. (1996) Predicting wheat head blight incidence using models based on meteorological factors in Pergamino, Argentina. Eur. J. Plant Pathol. 102:211-218

Müller-Esterl, W., Brandt, U., Anderka, O., Kerscher, S., Kieß, S., Ridinger, K. (2017) Biochemie: Eine Einführung für Mediziner und Naturwissenschaftler. 3. Auflage. Springer-Verlag

Münger, K., Lerch, K. (1985) Copper metallothionein from the fungus *Agaricus bisporus*: chemical and spectroscopic properties. Biochemistry 24:6751-6756

Myneni, S.C.B. (2002) Formation of stable chlorinated hydrocarbons in weathering plant material. Science 295:1039-1041

Nagygyörgy, E.D., Kocács, B., Leiter, E., Miskei, M., Pócsi, I., Hornok, L., Adám, A.L. (2014) Toxicity of abiotic stressors to *Fusarium* species: differences in hydrogen peroxide and fungicide tolerance. Acta Microbiol. Immunol. Hung. 61(2):189-208

Nathues, E., Joshi, S., Tenberge, K.B., Von Den Driesch, M., Oeser, B., Bäumer, N., Mihlan, M., Tudzynski, P. (2004) CPTF1, a CREB-like transcription factor, is involved in the oxidative stress response in the phytopathogen *Claviceps purpurea* and modulates ROS level in its host *Secale cereale*. Mol. Plant-Microbe Interact. 17:383-93

Nathues, E., Jorgens, C., Lorenz, N., Tudzynski, P. (2007) The histidine kinase CpHK2 has impact on spore germination, oxidative stress and fungicide resistance, and virulence of the ergot fungus *Claviceps purpurea*. Mol. Plant Pathol. 8:653-65

Nelson, D.R., Koymans, L., Kamataki, T., Stegeman, J.J., Feyereisen, R., Waxman, D.J., Waterman, M.R., Gotoh, O., Coon, M.J., Estabrook, R.W. (1996) P450 superfamily: Update on new sequences, gene mapping, accession numbers and nomenclature. Pharmacogenetics 6:1-42

Neve, E.P., Ingelman-Sundberg, M. (2010) Cytochrome P450 proteins: retention and distribution from the endoplasmic reticulum. Curr. Opin. Drug Discov. Devel. 13(1):78-85

Nganje, W.E., Kaitibie, S., Wilson, W.W., Leistritz, F.L., Bangsund, D.A. (2004) Economic impacts of Fusarium head blight in wheat and barley: 1993-2001. Agribusiness and Applied Economics Rep. No. 528.

Nguyen, T.V., Schäfer, W., Bormann, J. (2012) The stress-activated protein kinase FgOS-2 is a key regulato in the life cycle of the cereal pathogen *Fusarium graminearum*. MPMI 25(9):1142-1156

Nguyen, T.V., Kröger, C., Bönninghausen, J., Schäfer, W., Bormann, J. (2013) The ATF/CREB transcription factor Atf1 is essential for full virulence, deoxynivalenol production, and stress tolerance in the cereal pathogen *Fusarium graminearum*. MPMI 26(12):1378-1394

Nickel, A.G., von Hardenberg, A., Hohl, M., Löffler, J.R., Kohlhaas, M., Becker, J., Reil, J.-C., Kazakov, A., Bonnekoh, J., Stadelmaier, M., Puhl, S.-L., Wagner, M., Bogeski, I., Cortassa, S., Kappl, R., Pasieka, B., Lafontaine, M., Lancaster, C.R.D., Blacker, T.S., Hall, A.R., Duchen, M.R., Kästner, L., Lipp, P., Zeller, T., Müller, C., Knopp, A., Laufs, U., Böhm, M., Hoth, M., Maack, C. (2015) Reversal of mitochondrial transhydrogenase causes oxidative stress in heart failure. Cell Metabolism 22(3):472-484

Nickel, W. (2005) Unconventional secretory routes: Direct protein export acress the plasma membrane of mammalian cells. Traffic 6(8):607-614

Nisimoto, Y., Diebold, B.A., Cosentino-Gomes, D., Lambeth, J.D. (2014) Nox4: a hydrogen peroxide-generating oxygen sensor. Biochem. 53(31):5111-5120

Nosanchuk, J.D., Stark, R.E, Casadevall, A. (2015) Fungal melanin: what do we know about structure? Frontiers in Microbiology 6:1463

Oerke, E.C. (2006) Crop losses to pests. Journal of Agricultural Science 144:31-43.

Oeser, B., Heidrich, P.M., Muller, U., Tudzynski, P., Tenberge, K.B. (2002) Polygalacturonase is a pathogenicity factor in the *Claviceps purpurea*/rye interaction. Fungal Genet. Biol. 36:176-86

Orfanoudaki, G., Markaki, M., Chatzi, K., Tsamardinos, I., Economou, A. (2017) MatureO: prediction of secreted proteins with exclusive information from their mature regions. Scientific Reports 7:3264

Ortiz-Bermúdez, P., Srebotnik, E., Hammel, K.E. (2003) Chlorination and Cleavage of Lignin Structures by Fungal Chloroperoxidases. Appl. Environ. Microbiol. 69(8):5015-5018

Oteiza, P.I. (2012) Zinc and the modulation of redox homeostasis. Free Radic. Biol. Med. 53:1748-1759

Paper, J.M., Scott-Craig, J.S., Adhikari, N.D., Cuomo, C.A., Walton, J.D. (2007) Comparative proteomics of extracellular proteins *in vitro* and *in planta* from the pathogenic fungus *Fusarium graminearum*. Proteomics 7:3171-3183

Pedruzzi, E., Guichard, C., Ollivier, V., Driss, F., Fay, M., Prunet, C., Marie, J. C., Pouzet, C., Samadi, M., Elbim, C., O'Dowd, Y., Bens, M., Vandewalle, A., Gougerot-Pocidalo, M.A., Lizard, G., Ogier-Denis, E. (2004) NAD(P)H oxidase Nox-4 mediates 7-ketocholesterol-induced endoplasmic reticulum stress and apoptosis in human aortic smooth muscle cells. Mol. Cell. Biol. 24:10703-10717

Peberdy, J.F., Wallis, G.L.F., Archer, D.B. (2001) Protein secretion by fungi. Applied Mycology and Biotechnology 1:73-113

Pereyra, S., Lori, G.A. (2013) Crop residues and their management in the epidemiology of *Fusarium* head blight. In: *Fusarium* Head Blight in Latin America. Magliano, T.M.A. and Chulze, S.N. (eds.) Springer, Dordrecht, the Netherlands, pp. 143-156

Pestka, J.J. (2010) Toxicological mechanisms and potential health effects of deoxynivalenol and nivalenol. World Mycotoxin Journal 3:323-347

Pfaffl, M.W., Horgan, G.W., Dempfle, L. (2002) Relative expression software tool (REST) for group-wise comparison and statistical analysis of relative expression results in real-time PCR. Nucleic Acids Res. 30(9):e36

Pfeiffer, N. V., Dirndorfer, D., Lang, S., Resenberger, U. K., Restelli, L. M., Hemion, C., Miesbauer, M., Frank, S., Neutzner, A., Zimmermann, R., Winklhofer, K.F., Tatzelt, J. (2013) Structural features within the nascent chain regulate alternative targeting of secretory proteins to mitochondria. The EMBO Journal 32(7):1036-1051.

Pigné, S., Zykwinska, A., Janod, E., Cuenot, S., Kerkoud, M., Raulo, R., Batillé-Simoneau, N., Marchi, M., Kwasiborski, A., N'Guyen, G., Mabilleau, G., Simoneau, P., Guillemette, T. (2017) A flavoprotein supports cell wall properties in the necrotrophic fungus *Alternaria brassicicola*. Fungal Bio. Biotechnol. 4(1)

Piedras, P., Hammond-Kosack, K.E., Harrison, K., Jones, J.D.G. (1998) Rapid, cf-9 and Avr9-dependent production of active oxygen species in tobacco suspension cultures. Mol. Plant-Microbe Interact. 11:1155-1166

Pietrosimone, K.M. (2014) Characterization of the Bacterial Metallothionein, PmtA in the Human Pathogen *Pseudomonas aeruginosa*. Doctoral Dissertations 498

Pino, P., Foth, B.J., Kwok, L.Y., Sheiner, L., Schepers, R., Soldati, T., Soldati-Favre, D. (2007) Dual targeting of antioxidant and metabolic enzymes to the mitochondrion and the apicoplast of *Toxoplasma gondii*. PLoS Pathog. 3(8):e115

Plaine, A., Walker, L., Da Costa, G., Mora-Montes, H. M., McKinnon, A., Gow, N. A. R., Gaillardin, C., Munro, C. A., Richard, M. L. (2008) Functional analysis of Candida albicans GPI-anchored proteins. Roles in cell wall integrity and caspofungin sensitivity. Fungal Genetics and Biology 45:1404-1414

Podila, G.K., Dickman, M.B., Kolattukudy, P.E. (1988) Transcriptional activation of a cutinase gene in isolated fungal nuclei by plant cutin monomers. Science 242:922-925

Polacheck, I., Kwon-Chung, K.J. (1988) Melanogenesis in Cryptococcus neoformans. J. Gen. Microbiol. 134:1037-1041

Quarantin, A., Glasenapp, A., Schäfer, W., Favaron, F., Sella, L. (2016) Involvement of the *Fusarium graminearum* cerato-platanin proteins in fungal growth and plant infection. Plant Physiol. Biochem. 109:220-229

Rabouille, C. (2017) Pathways of unconventional protein secretion. Trends in Cell Biology 27(3):230-240

Ramesh, G., Podila, G.K., Gay, G., Marmeisse, R., Reddy, M.S. (2009) Copper and cadmium metallothioneins of the ectomycorrhizal fungus *Hebeloma cylindrosporum* have different patterns of regulation. Appl Environ Microbiol 75:2266-2274

Rasmusson, A.G., Geisler, D.A., Møller, I.M. (2008) The multiplicity of dehydrogenases in the electron transport chain of plant mitochondria. Mitochondrion 8:47-60

Reddy, M.S., Prasanna, L., Marmeisse, R., Fraissinet-Tachet, L. (2014) Differential expression of metallothioneins in response to heavy metals and their involvement in metal tolerance in the symbiotic basidiomycete *Laccaria bicolor*. Microbiology 160:2235-2242.

Reis, H., Pfiffi, S., Hahn, M. (2005) Molecular and functional characterization of a secreted lipase from Botrytis cinerea. Mol. Plant Pathol. 6:257-267

Reszka, K.J., Wagner, B.A., Burns, C.P., Britigan, B.E. (2005) Effects of peroxidase substrates on the Amplex red/ peroxidase assay: Antioxidant properties of anthracyclines. Anal. Biochem. 342:327-337.

Ribichich, K.F., Lopez, S.E., Vegetti, A.C. (2000) Histopathological spikelet changes produced by *Fusarium graminearum* in susceptible and resistant wheat cultivars. Plant Disease 84:794-802.

Riggle, P. J., Kumamoto, C. A. (2000) Role of a *Candida albicans* P1-type ATPase in resistance to copper and silver in ion toxicity. J. Bacteriol. 182:4899-4905

Ripley, R.C., Fant, J., Bienkowski, R.S. (1993) Brefeldin A inhibits degradation as well as production and secretion of collagen in human lung fibroblasts. J. Biol. Chem. 268(5):3677-3682

Rittenour, W.R., Harris, S.D. (2013) Glycosylphosphatidylinositol-anchored proteins in *Fusarium graminearum*. Inventory, variability, and virulence. PLoS One 8(11):e81603.

Robbertse, B., Yoder, O.C., Nguyen, A., Schoch, C.L., Turgeon, B.G. (2003) Deletion of all *Cochliobolus heterostrophus* monofunctional catalase-encoding genes reveals a role for one in sensitivity to oxidative stress but none with a role in virulence. Mol. Plant Microbe Interact. 16(11):1013-21

Rocha, O., Ansari, K., Doohan, F.M. (2005) Effect of trichothecene mycotoxins on eukaryotic cells: a review. Food addit. Contam. 22:369-378.

Rolke, Y., Liu, S., Quidde, T., Williamson, B., Schouten, A., et al. (2004) Functional analysis of H2O2-generating systems in *Botrytis cinerea*: the major cu-zn-superoxide dismutase (BCSOD1) contributes to virulence on french bean, whereas a glucose oxidase (BCGOD1) is dispensable. Mol. Plant Pathol. 5:17–27

Ron, D., Walter, P. (2007) Signal integration in the endoplasmic reticulum unfolded protein response. Nat. Rev. Mol. Cell Biol. 8(7):519-529

Ruch, W., Cooper, P.H., Baggiollini, M. (1983) Assay of H2O2 production by macrophages and neutrophils with Homovanillic acid and horseradish peroxidase. J. Immunol. Methods 63:347-357.

Ruttkay-Nedecky, B., Neijdl, L., Gumulec, J., Zitka, O., Masarik, M., Eckschlager, T., Stiborova, M., Adam, V., Kizek, R. (2013) The Role of Metallothionein in Oxidative Stress. In. J. Mol. Sci. 14(3):6044-6066

Ryder, L.S., Dagdas, Y.F., Mentlak, T.A., Kershaw, M.J., Thornton, C.R., Schuster, M., Chen, J., Wang, Z., Talbot, N.J. (2013) NADPH oxidases regulate septinmediated cytoskeletal remodeling during plant infection by the rice blast fungus. Proc. Natl. Acad. Sci. USA. 110:3179-3184

Rydström, J. (2006) Mitochondrial NADPH, transhydrogenase and disease. Biochimica et Biophysica Acta 1757(5-6):721-726

Sanchez-Ferrer, A., Rodriguez-Lopez, J.N., García-Cánovas, F., García-Carmona, F. (1995) Tyrosinase: a comprehensive review of its mechanism. Biochim. Biophys. Acta 1247:1-11.

Sano, R., Reed, J.C. (2013) ER stress-induced cell death mechanisms. Biochim. Biophys. Acta 1833:3460-3470

Santos, C.X.C., Tanaka, L.Y., Wosniak, J., Laurindo, F.R.M. (2009) Mechanisms and Implications of Reactive Oxygen Species Generation During the Unfolded Protein Response: Roles of Endoplasmic Reticulum Oxidoreductases, Mitochondrial Electron Transport, and NADPH Oxidase. Antioxidants & Redox Signaling 11(10):2409-2427

Sanz, V.C., Mena, M.L., González-Cortés, A., Yáñez-Sedeño, P., Pingarrón, J.A. (2005) Development of a tyrosinase biosensor based on gold nanoparticles-modified glassy carbon electrodes: application to the measurement of a bioelectrochemical polyphenols index in wines. Analytica Chimica Acta 528(1):1-8

Scala, V., Aureli, G., Cesarano, G., Incerti, G., Fanelli, C., Scala, F., Reverberi, M., Bonanomi, G. (2016) Climate, soil management, and cultivar affect *Fusarium* Head Blight incidence and deoxynivalenol accumulation in durum wheat of southern Italy. Front. Microbiol. 7:1014

Scheffer, J., Tudzynski, P. (2006) In vitro pathogenicity assay for the ergot fungus *Claviceps purpurea*. Mycol. Res. 110:465-70

Schnitzler, N., Peltroche-Llacsahuanga, H., Bestier, N., Zündorf, J., Lütticken, R., Haase, G. (1999) Effect of melanin and carotenoids of Exophiala (Wangiella) dermatitidis of phagocytosis, oxidative burst, and killing by human neutrophils. Infect. Immun. 67:94-101

Schouten, A., Tenberge, K.B., Vermeer, J., Stewart, J., Wagemakers, L., et al. (2002) Functional analysis of an extracellular catalase of *Botrytis cinerea*. Mol. Plant Pathol. 3:227

Schwarzländer, M., Fricker, M.D., Muller, C., Marty, L., Brach, T., Novak, J., Sweetlove, L.J., Hell, R., Meyer, A.J. (2008) Confocal imaging of glutathione redox potential in living plant cells. J. Microsc. 231:299-316

Scott, B., Eaton, C.J. (2008) Role of reactive oxygen species in fungal cellular differentiations. Curr. Opin. Microbiol. 11:488-493.

Segal, L.M., Wilson, R.A. (2018) Reactive oxygen species metabolism and plant-fungal interactions. Fungal Genet. Biol. 110:1-9

Segmüller, N., Ellendorf, U., Tudzynski, B., Tudzynski, P. (2007) BcSAK1, a stress-activated mitogen-activated protein kinase, is involved in vegetative differentiation and pathogenicity in *Botrytis cinerea*. Eukaryotic Cell. 6:211-21

Segmüller, N., Kokkelink, L., Giesbert, S., Odinius, D., van Kahn, J., Tudzynski, P. (2008) NADPH oxidases are involved in differentiation and pathogenicity in Botrytis cinerea. Mol Plant Microbe Interact. 21:808-1808.

Selinheimo, E., Autio, K., Kruus, K., Buchert, J. (2007a) Elucidating the mechanism of laccase and tyrosinase in wheat bread making. J. Agric. Food Chem. 55(15):6357-6365

Selinheimo, E., NiEidhin, D., Steffensen, C., Nielsen, J., Lomascolo, A., Halaouli, S., Record, E., O'Beirne, D., Buchert, J. & Kruus, K. (2007b) Comparison of the characteristics of fungal and plant tyrosinases. J. Biotechnol. 130(4):471-480.

Sellam, A., Dongo, A., Guillemette, T., Hudhomme, P., Simoneau, P. (2007) Transcriptional responses to exposure to the brassicaceous defence metabolites camalexin and allyl-isothiocyanate in the necrotrophic fungus *Alternaria brassicicola*. Mol. Plant Pathol. 8:195-208

Semighini, C.P., Harris, S.D. (2008) Regulation of apical dominance in *Aspergillus nidulans* hyphae by reactive oxygen species. Genetics 179(4):1919-1932

Serrander, L., Cartier, L., Bedard, K., Banfi, B., Lardy, B., Plastre, O., Sienkiewicz, A., Fórró, L., Schlegel, W., Krause, K.H. (2007) NOX4 activity is determined by mRNA levels and reveals a unique pattern of ROS generation. Biochem. J. 406:105-114

Shaw, C.F., Savas, M.M., Petering, D.H. (1991) Ligand substitution and sulfhydryl reactivity of metallothionein. Methods Enzymol. 205:401-414

Shaw, S.L., Long, S.R. (2003) Nod factor inhibition of reactive oxygen efflux in a host legume. Plant Physiol. 132:2196–204

Shetty, N.P., Mehrabi, R., Lutken, H., Haldrup, A., Kema, G.H.J., et al. (2007) Role of hydrogen peroxide during the interaction between the hemibiotrophic fungal pathogen *Septoria tritici* and wheat. New Phytol. 174:637-47

Shieh, M.T., Brown, R.L., Whitehead, M.P., Cary, J.W., Cotty, P.J., et al. (1997) Molecular genetic evidence for the involvement of a specific polygalacturonase, P2c, in the invasion and spread of *Aspergillus flavus* in cotton bolls. Appl. Environ. Microbiol. 63:3548-52

Shimomura, O., Johnson, F.H., Saiga, Y. (1962) Extraction, purification and properties of aequorin, a bioluminescent protein from the luminous hydromedusan, Aequorea. J. Cell. Comp. Physiol. 59:223-39

Shin, J.Y., Bui, D.-C., Lee, Y., Nam, H., Jung, S., Fang, M., Kim, J.-C., Lee, T., Kim, H., Choi, G.J., et al. (2017) Functional characterization of cytochrome P450 monooxygenases in the cereal head blight fungus *Fusarium graminearum*. Environ. Microbiol. 19:2053-2067

Shin, J.Y., Kin, J.-E., Lee, Y.-W., Son, H. (2018) Fungal cytochrome P450s and the P450 complement (CYPome) of *Fusarium graminearum*. Toxins 10(3):112

Siegmund, U., Heller, J., van Kan, J., Tudzynski, P. (2013) The NADPH oxidase complexes in Botrytis cinerea: evidence for a close association with the ER and the tetraspanin Pls1. PLoS One 8(6):e55879

Sierra-Campos, E., Pardo, J. P. (2009) The relationship between the antioxidant system and the virulence in *Ustilago maydis*, a fungal pathogen. Microbiología 51(1-2):7-17

Sikhakolli, U.R., Lopez-Gir aldez, F., Li, N., Common, R., Townsend, J.P., Trail, F. (2012) Transcriptome analyses during fruiting body formation in Fusarium graminearum and Fusarium verticillioides reflect species life history and ecology. Fungal Genet. Biol. 49:663-673

Siranidou, E., Kang, Z., Buchenauer, H. (2002) Studies on symptom development, phenolic compounds and morphological defence responses in wheat cultivars differing in resistance to *Fusarium* Head Blight. J. Phytopathology 150:200-208

Small, I., Wintz, H., Akashi, K., Mireau, H. (1998) Two birds with one stone: genes that encode products targeted to two or more compartments. Plant Mol. Biol. 38:265-277

Song, X.-S., Xing, S., Li, H.-P., Zhang, J.-B., Qu, B., Jiang, J.-H., Fan, C., Yang, P., Liu, J.-L., Hu, Z.-Q., Xue, S., Liao, Y.-C. (2015) An antibody that confers plant disease resistance targets a membrane-bound glyoxal oxidase in *Fusarium*. New Phytologist 210:997-1010

Sono, M., Roach, M.P., Coulter, E.D., Dawson, J.H. (1996) Heme-containing oxygenases. Chem. Rev. 96:2841-2888

Stahl, D.J., Schäfer, W. (1992) Cutinase is not required for fungal pathogenicity on pea. Plant Cell 4(6):621-629

Stahl, D.J., Theuerkauf, A., Heitefuss, R., Schäfer, W. (1994) Cutinase of *Nectria haematococca* (*Fusarium solani* f. sp. pisi) is not required for fungal virulence. Mol. Plant-Microbe Interact. 7(6):713-725

Sumimoto, H. (2008) Structure, regulation and evolution of Nox-family NADPH oxidases that produce reactive oxygen species. FEBS J. 275(13):3249-77

Sutherland, J.B. (1992) Detoxification of polycyclic aromatic hydrocarbons by fungi. J. Ind. Microbiol. 9:53-61

Szczesna-Skorupa, E., Kemper, B. (2000) Endoplasmic Reticulum Retention Determinants in the Transmembrane and Linker Domains of Cytochrome P450 2C1. J. Biol. Chem. 275(25):19409-19415

Tabas, I., Ron, D. (2011) Integrating the mechanisms of apoptosis induced by endoplasmic reticulum stress. Nat. Cell Biol. 13:184-190

Takac, I., Schröder, K., Zhang, L., Lardy, B., Anilkumar, N., Lambeth, J. D., Shah, A. M., Morel, F., Brandes, R. P. (2011) The E-loop is involved in hydrogen peroxide formation by the NADPH oxidase Nox4. J. Biol. Chem. 286(15):13304-13313

Takeda, J., Kinoshita, T. (1995) GPI-anchor biosynthesis. TIBS 20:367-371

Tanaka, A., Christensen, M.J., Takemoto, D., Park, P., Scott, B. (2006) Reactive oxygen species play a role in regulating a fungus-perennial ryegrass mutualistic interaction. Plant Cell. 18:1052-1066.

Tanaka, A., Takemoto, D., Hyon, G.S., Park, P., Scott, B. (2008) NoxA activation by the small GTPase RacA is required to maintain a mutualistic symbiotic association between *Epichloë festucae* and perrenial ryegrass. Mol. Microbiol. 68(5):1165-1178

Tarpey, M.M., Fridovich, I. (2001) Methods of detection of vascular reactive species: nitric oxide, superoxide, hydrogen peroxide, and peroxynitrite. Cric. Red. 89(3):224-236

Temme, N., Tudzynski, P. (2009) Does Botrytis cinerea ignore H2O2-induced oxidative stress during infection? Characterization of Botrytis Activator Protein 1. Mol. Plant Microbe Interact. 22:987-998

ten Have, A., Mulder, W., Visser, J., van Kan, J.A. (1998) The endopolygalacturonase gene *Bcpg1* is required for full virulence of *Botrytis cinerea*. Mol. Plant-Microbe Interact. 11:1009-1016

Thelwall, P.E., Yemin, A.Y., Gillian, T.L., Simpson, N.E., Kasibhatla, M.S., Rabbani, Z.N., MacDonald, J.M., Blackband, S.J., Gamcsik, M.P. (2005) Noninvasive *In vivo* Detection of Glutathione Metabolism in Tumors. Cancer Research 65(22):10149-10153

Thorvaldsen, J.L., Mehra, R.K., Yu, W., Sewell, A.K., Winge, D.R. (1995) Analysis of copper-induced metallothionein expression using autonomously replicating plasmids in *Candida glabrata*. Yeast 11(15):1501-1511

Tiedemann, A.V. (1997) Evidence for a primary role of active oxygen species in induction of host cell death during infection of bean leaves with *Botrytis cinerea*. Physiol. Mol. Plant Pathol. 50:151-166

Toone, W.M., Jones, N. (1999) AP-1 transcription factors in yeast. Curr. Opin. Genet. Dev. 9:55-61

Torres, M.A., Dangl, J.L., Jones, J.D. (2002) Arabidopsis gp91phox homologues AtrbohD and AtrbohF are required for accumulation of reactive oxygen intermediates in the plant defense response. Proc. Natl. Acad. Sci. USA 99(1):517-522

Torres, M.A., Onouchi, H., Hamada, S., Machida, C., Hammond-Kosack, K.E., Jones, J.D.G. (1998) Six *Arabidopsis thaliana* homologues of the human respiratory burst oxidase (gp91phox). Plant J. 14:365-70

Torres Pazmiño, D.E., Winkler, M., Glieder, A., Fraaije, M.W. (2010) Monooxygenases as biocatalysts: Classification, mechanistic aspects and biotechnological applications. J. Biotech. 146:9-24

Totah, R.A., Rettie, A.E. (2007) Principles of Drug Metabolism 3: Enzymes and Tissues. Comprehensive Medicinal Chemistry II 5:167-191

Trail, F., Common, R. (2000) Perithecial development by *Gibberella zeae*: a light microscopy study. Mycologia 92(1):130-138

Trail, F. (2009) For blighted waves of grain: *Fusarium graminearum* in the postgenomics era. Plant Physiol. 149(1):103-110

Tsai, H.F., Chang, Y.C., Washburn, R.G., Wheeler, M.H. & Kwon-Chung K.J. (1998) The Developmentally Regulated alb1 Gene of *Aspergillus fumigatus*: Its Role in Modulation of Conidial Morphology and Virulence. Journal of Bacteriology 180(12):3031-3038

Tsai, H.F., Wheeler, M.H., Chang, Y.C., Kwon-Chung, K.J. (1999) A developmentally regulated gene cluster involved in conidial pigment biosynthesis in *Aspergillus fumigatus*. J. Bacteriol. 181:6469-6477

Tucker, S.L., Thornton, C.R., Tasker, K., Jacob, C., Giles, G., Egan, M., Talbot, N.J. (2004) A fungal metallothionein is required for pathogenicity of *Magnaporthe grisea*. The Plant Cell 16:1575-1588

Tudzynski, P., Heller, J., Siegmund, U. (2012) Reactive oxygen species generation in fungal development and pathogenesis. Curr. Opin. Microbiol. 15:653-659

Vaahtera, L., Brosché, M., Wrzaczek, M., Kangasjärvi, J. (2014) Specificity in ROS signaling and transcript signatures. Antioxid. Redox Signal. 21:1422-1441

van Kan, J.A.L., van't Klooster, J.W., Wagemakers, C.A.M., Dees, D.C.T., Vlugt-Bergmans, V.D. (1997) Cutinase A of Botrytis cinerea is expressed, but not essential, during penetration of Gerbera and Tomato. Mol. Plant Microbe Interact. 10:30-38

van Vliet, A.R., Agostinis, P. (2017) Mitochondria-associated membranes and ER stress. Curr. Top. Microbiol. Immunol. 414:73-102

Vasák, M., Hasler, D.W. (2000) Metallothioneins: new functional and structural insights. Curr Opin Chem Biol. 4:177-183

Vasák, M. (2005) Advances in metallothionein structure and functions. J. Trace Elements Med Biol. 19:13-17.

Veeranki, S., Kim, B., Kim, L. (2008) The GPI-anchored superoxide dismutase SodC is essential for regulating basal Ras activity and for chemotaxis of Dictyostelium discoideum. Journal of Cell Science 121:3099-3108

Veluchamy, S., Williams, B., Kim, K., Dickman, M.B. (2012) The CuZn superoxide dismutase from Sclerotinia sclerotiorum is involved with oxidative stress tolerance, virulence, and oxalate production. Physiol. Mol. Plant Pathol. 78:14-23.

Vestal, E.F. (1964) Barley scab in South Korea in 1963 and 1964. Plant Dis. Rep. 48:754-755

Vilter, H. (1995) Vanadium-dependent peroxiodases. In: Vanadiumand Its Role in Life, edited by Sigel H and Sigel A. New York: M. Dekker, pp 365-362

Voigt, C.A., Schäfer, W., Salomon, S. (2005) A secreted lipase of *Fusarium graminearum* is a virulence factor required for infection of cereals. The Plant Journal 42:364-375

Wagacha, J.M., Muthomi, J.W. (2007) *Fusarium culmorum*: Infection process, mechanisms of mycotoxin production and their role in pathogenesis in wheat. Crop Protection 26:877-885

Walker, G.M. (2004) Metals in yeast fermentation processes. Advances in Appl. Microbiol. 54:197-229

Walter, S., Nicholson, P., Doohan, F.M. (2009) Action and reaction of host and pathogen during *Fusarium* head blight disease. New Phytologist 185(1):54-66

Walz, A., Zingen-Sell, I., Loeffler, M., Sauer, M., (2008) Expression of an oxalate oxidase gene in tomato and severity of disease caused by Botrytis cinerea and Sclerotinia sclerotiorum. Plant Pathol. 57:453-458.

Wang, L., Mogg, C., Walkowiak, S., et al. (2014) Characterization of NADPH oxidase genes NoxA and NoxB in Fusarium graminearum. Can. J. Plant Pathol. 36:12-21.

Weber, H., Engelmann, S., Hecker, M. (2004) Oxidative stress triggers thiol oxidation in the glyceraldehyde-3-phosphate dehydrogenase of Staphylococcus aureus. Molecular Microbiology 52(1):133-140

Wegulo, S.N. (2012) Factors influencing deoxynivalenol accumulation in small grain cereals. Toxins 4(11):1157-1180

Werck-Reichhart, D., Feyereisen, R. (2000) Cytochromes P450: a success story. Genome Biol. 1(6)

White, C., Lee, J., Kambe, T. et al. (2009) A role for the ATP7A copper transporting ATPase in macrophage bactericidal activity. J. Biol. Chem. 284:33949-56

Williams, B., Kabbage, M., Kim, H.J., Britt, R., Dickman, M.B. (2011) Tipping the balance: Sclerotinia sclerotiorum secreted oxalic acid suppresses host defenses by manipulating the host redox environment. PLoS Pathog. 7:e1002107

Windels, C.E. (2000) Economic and social impacts of Fusarium head blight: Changing farms and rural communities in the Northern Great Plains. Phytopathology 90:17-21

Winterbourn, C.C., Hampton, M.B. (2008) Thiol chemistry and specificity in redox signaling. Free Radic. Biol. Med. 45:549-561.

Woloshuk, C.P., Kolattukudy, P.E. (1986) Mechanism by which contact with plant cuticle triggers cutinase gene expression in the spores of *Fusarium solani* f. sp. pisi. Proc. Natl. Acaad. Sci. USA 83(6):1704-1708

Wu, F., Groopman, J.D., Pestka, J.J. (2014) Public health impacts of foodborne mycotoxins. Annu. Rev. Food Sci. Technol. 5:351-372

Wu, R.F., Ma, Z., Liu, Z., Terada, L.S. (2010) Nox4-derived H2O2 mediates endoplasmic reticulum signaling through local Ras activation. Mol. Cell. Biol. 30:3553–3568

Xie, N., Chapeland-Leclerc, F., Silar, P., Ruprich-Robert, G. (2014) Systematic gene deletions evideces that laccases are involved in several stages of wood degradation in the filamentous fungus *Podospora anserina*. Env. Microbiol. 16(1):141-161

Xu., F. (2005) Applications of oxidoreductases: Recent progress. Industrial Biotechnology 1(1):38-50

Yang, L., van der Lee, T., Yang, X., Yu, D., Waalwijk, C. (2008) Fusarium populations on Chinese barley show a dramatic gradient in mycotoxin profiles. Phytopathology 98, 719-727

Yang, S.L., Lin, C., Chung, K. (2009) Coordinate control of oxidative stress tolerance, vegetative growth, and fungal pathogenicity via the AP1 pathway in the rough lemon pathotype of *Alternaria alternata*. Physiol. Mol. Plant Pathol. 74:100-10

Yang, S.L., Chung, K.R. (2012) The NADPH oxidase-mediated production of hydrogen peroxide (H2O2) and resistance to oxidative stress in the necrotrophic pathogen Alternaria alternata of citrus. Mol. Plant Pathol. 13:900-914.

Yang, S.L., Chung, K.R. (2013) Similar and distinct roles of NADPH oxidase components in the tangerine pathotype of Alternaria alternata. Mol. Plant Pathol. 14:543-556.

Yao, S.-H., Guo, Y., Wang, Y.-Z., Zhang, D., Xu, L., Tang, W.-H. (2016) A cytoplasmic Cu-Zn superoxide dismutase SOD1 contributes to hyphal growth and virulence of *Fusarium graminearum*. Fungal Genetics and Biology 91:32-42

Yarden, O., Veluchamy, S., Dickman, M.B., Kabbage, M. (2014) Sclerotinia sclerotiorum catalase SCAT1 affects oxidative stress tolerance, regulates ergosterol levels and controls pathogenic development. Physiol. Mol. Plant Pathol. 85:34-41.

Yi, M., Chi, M.H., Khang, C.H., Park, S.Y., Kang, S., Valent, B., Lee, Y.H. (2009) The ER chaperone LHS1 is involved in asexual development and rice infection by the blast fungus *Magnaporthe oryzae*. The Plant Cell 21:681-695

Yin, F., Sancheti, H., Cadenas, E. (2012) Silencing of nicotinamide nucleotide transhydrogenase impairs cellular redox homeostasis and energy metabolism in PC12 cells. Bioch. et Bioph. Acta 1817(3):401-409

Zaidi, K.U., Ali, A.S., Ali, S.A., Naaz, I. (2014) Microbial tyrosinases: Promising enzymes for pharmaceutical, food bioprocessing, and environmental industry. Bioch. Res. Int. http://dx.doi.org/10.1155/2014/854687

Zeeshan, H.M.A., Lee, G.H., Kim, H.-R., Chae, H.-J. (2016) Endoplasmic Reticulum Stress and Associated ROS. In. J. Mol. Sci. 17(3):327

Zhang, D.X., Du, G.C., Chen, J. (2010) Fermentation production of microbial catalase and its application in textile industry. Chin. J. Biotech. 26:1473-1481

Zhang, X.-W., Jia, L.-J., Zhang, Y., Jiang, G., Li, X., Zhang, D., Tang, W.-H. (2012) In Planta Stage-Specific Fungal Gene Profiling Elucidates the Molecular Strategies of *Fusarium graminearum* Growing inside Wheat Coleoptiles. The Plant Cell 24(12):5159-5176

Zhao, H., Kalivendi, S., Zhang, H., Joseph, J., Nithipatikom, K., Vásquez-Vivar, J., Kalyanaraman, B. (2003) Superoxide reacts with hydroethidine but forms a fluorescent product that is distinctly different from ethidium: potential implications in intracellular fluorescence detection of superoxide. Free Radic. Biol. Med. 34(11):1359

Zhao, H., Joseph, J., Fales, H.M., Sokoloski, E.A., Levine, R.L., Vasquez-Vivar, J., Kalyanaraman, B. (2005) Detection and characterization of the product of hydroethidine and intracellular superoxide by HPLC and limitations of fluorescence. Proc. Natl. Acad. Sci. U.S.A. 102:5727-5732

Zhou, M., Diwu, Z., Panchuk-Voloshina, N., Haughland, R.P. (1997) A Stable nonfluorescent derivative of resorufin for the fluorometric determination of trace hydrogen peroxide: application in detecting the activity of phagocyte NADPH oxidase and other oxidases. Anal. Biochem 253:162-168.

Zhu, X., Gibbons, J., Garcia-Rivera, J., Casadevall, A., Williamson, P.R. (2001) Laccase of Cryptococcus neoformans is a cell wall-associated virulence factor. Infect. Immun. 69:5589-5596

Zhu, X., Williamson, P. R. (2004) Role of laccase in the biology and virulence of Cryptococcus neoformans. FEMS Yeast Res. 5:1-10.

7. Appendix

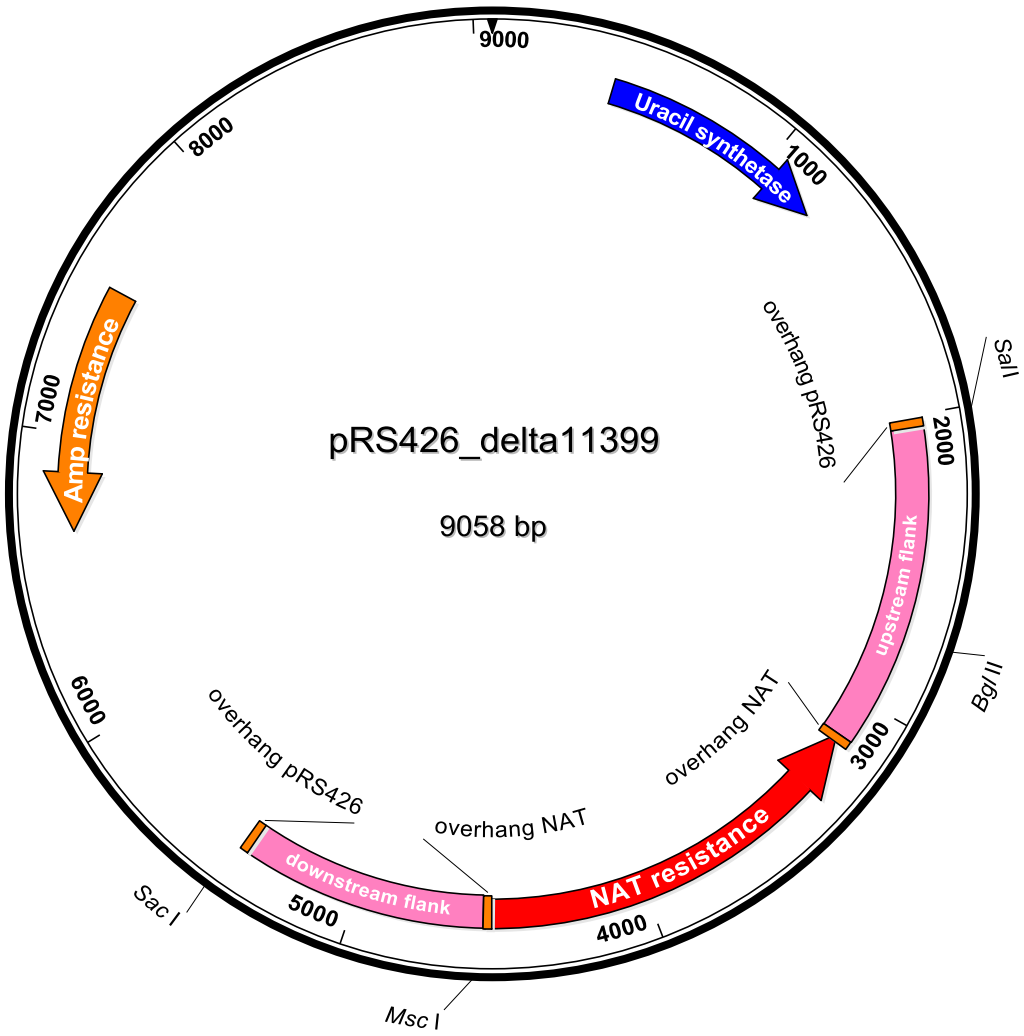

Supplementary figure 1: Map of deletion vector for oxidase gene FGSG_11399 pRS426_Δ11399. Uracil synthetase gene (dark blue), ampicillin resistance cassette (pink), and nourseothricin resistance cassette (red) were used as selection markers for *S. cerevisiae*, *E. coli* and *F. graminearum* cloning, respectively. Flanking regions (pink) of FGSG_11399 were cloned upstream and downstream of the resistance cassette in such a way that the resistance cassette would be integrated into the *F. graminearum* genome in antisense orientation of the target gene. Overhangs (orange) allowed correct assembly of the DNA fragments via yeast recombinational cloning. Restriction enzymes *Msc*I and *Bgl*II were used for verification of the correct assembly of the vector. Restriction enzymes *Sac*I and *Sal*I were used to cut the deletion construct (flanking region – resistance cassette – flanking region) out of the vector backbone for *F. graminearum* protoplast transformation.

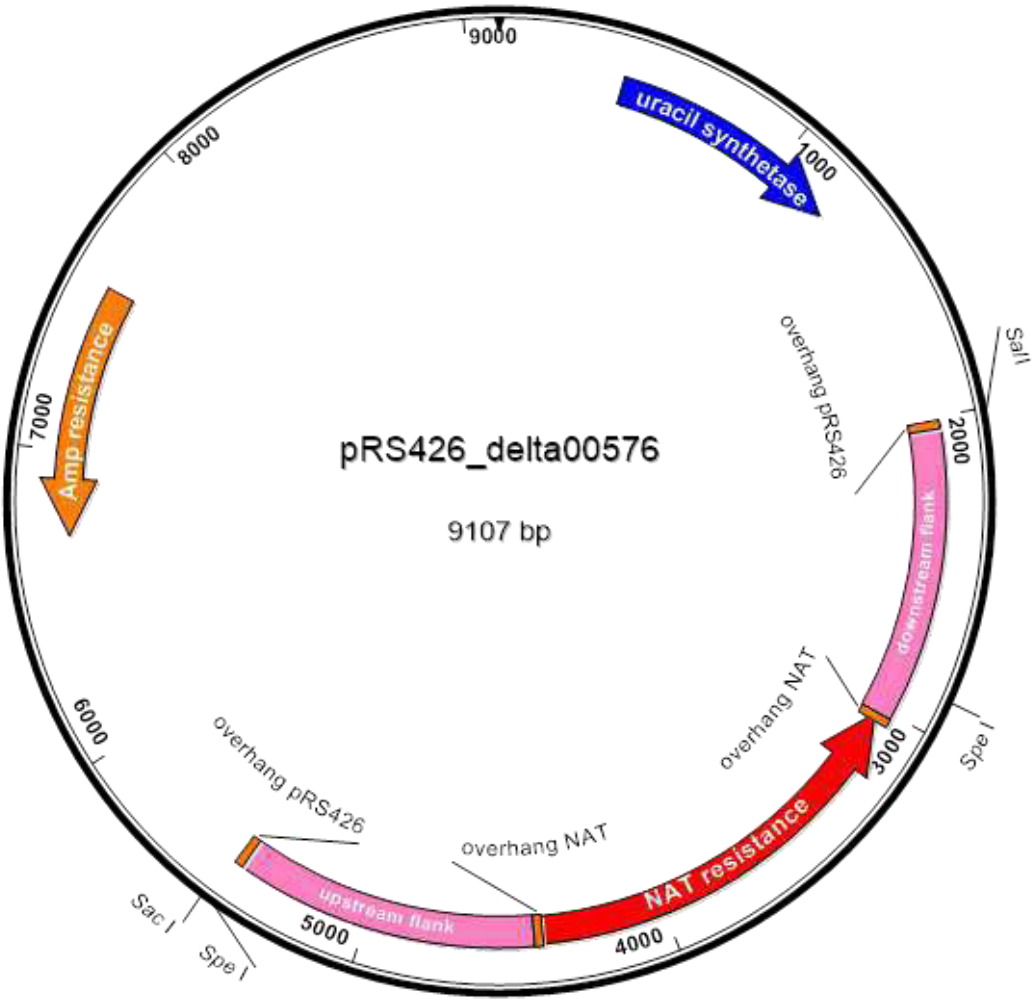

Supplementary figure 2: Map of deletion vector for superoxide dismutase gene FGSG_00576 pRS426_Δ00576. Uracil synthetase gene (dark blue), ampicillin resistance cassette (pink), and nourseothricin resistance cassette (red) were used as selection markers for *S. cerevisiae*, *E. coli* and *F. graminearum* cloning, respectively. Flanking regions (pink) of FGSG_00576 were cloned upstream and downstream of the resistance cassette in such a way that the resistance cassette would be integrated into the *F. graminearum* genome in antisense orientation of the target gene. Overhangs (orange) allowed correct assembly of the DNA fragments via yeast recombinational cloning. Restriction enzyme *Spe*I was used for verification of the correct assembly of the vector. Restriction enzymes *Sac*I and *Sal*I were used to cut the deletion construct (flanking region – resistance cassette – flanking region) out of the vector backbone for *F. graminearum* protoplast transformation.

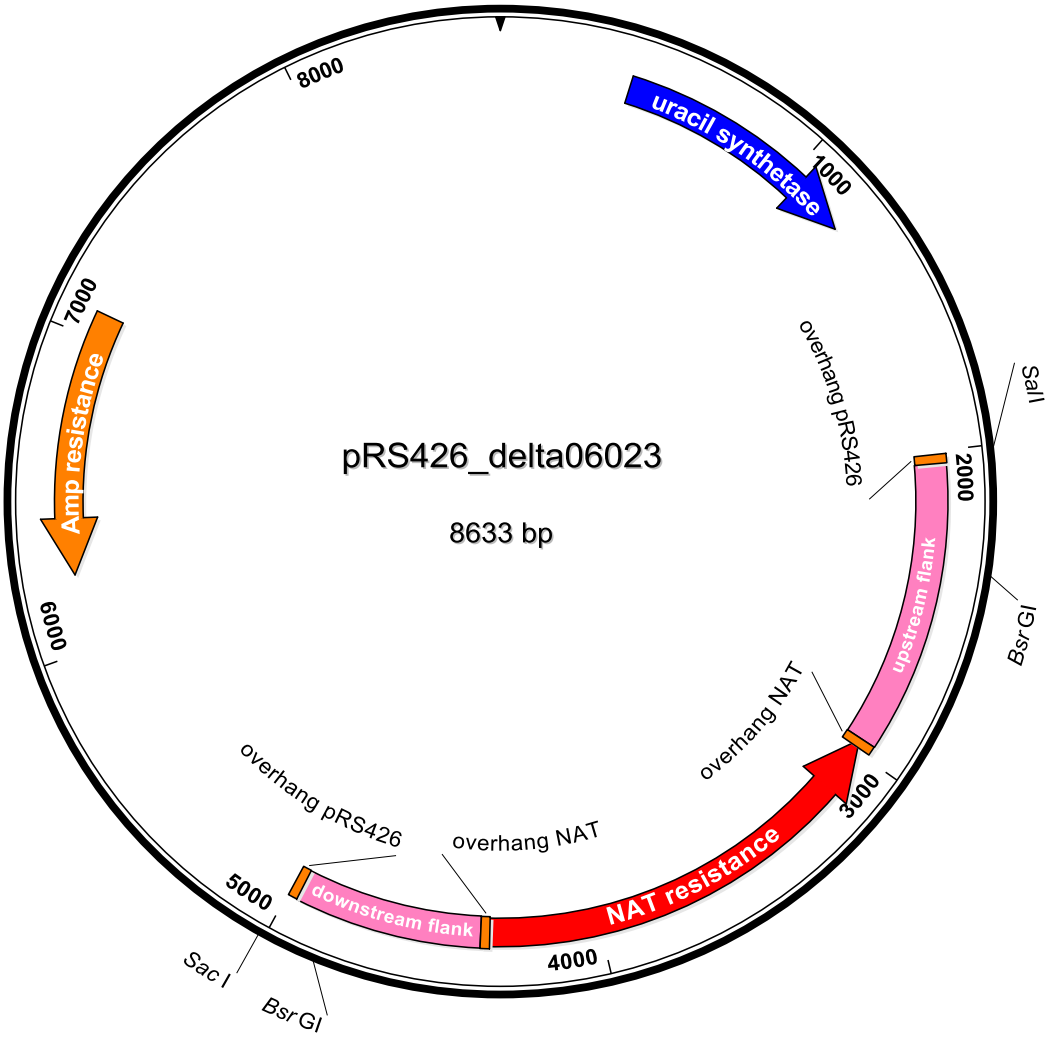

Supplementary figure 3: Map of deletion vector for cupredoxin gene FGSG_06023 pRS426_Δ06023. Uracil synthetase gene (dark blue), ampicillin resistance cassette (pink), and nourseothricin resistance cassette (red) were used as selection markers for *S. cerevisiae*, *E. coli* and *F. graminearum* cloning, respectively. Flanking regions (pink) of FGSG_06023 were cloned upstream and downstream of the resistance cassette in such a way that the resistance cassette would be integrated into the *F. graminearum* genome in antisense orientation of the target gene. Overhangs (orange) allowed correct assembly of the DNA fragments via yeast recombinational cloning. Restriction enzyme *Bsr*GI was used for verification of the correct assembly of the vector. Restriction enzymes *Sac*I and *Sal*I were used to cut the deletion construct (flanking region – resistance cassette – flanking region) out of the vector backbone for *F. graminearum* protoplast transformation.

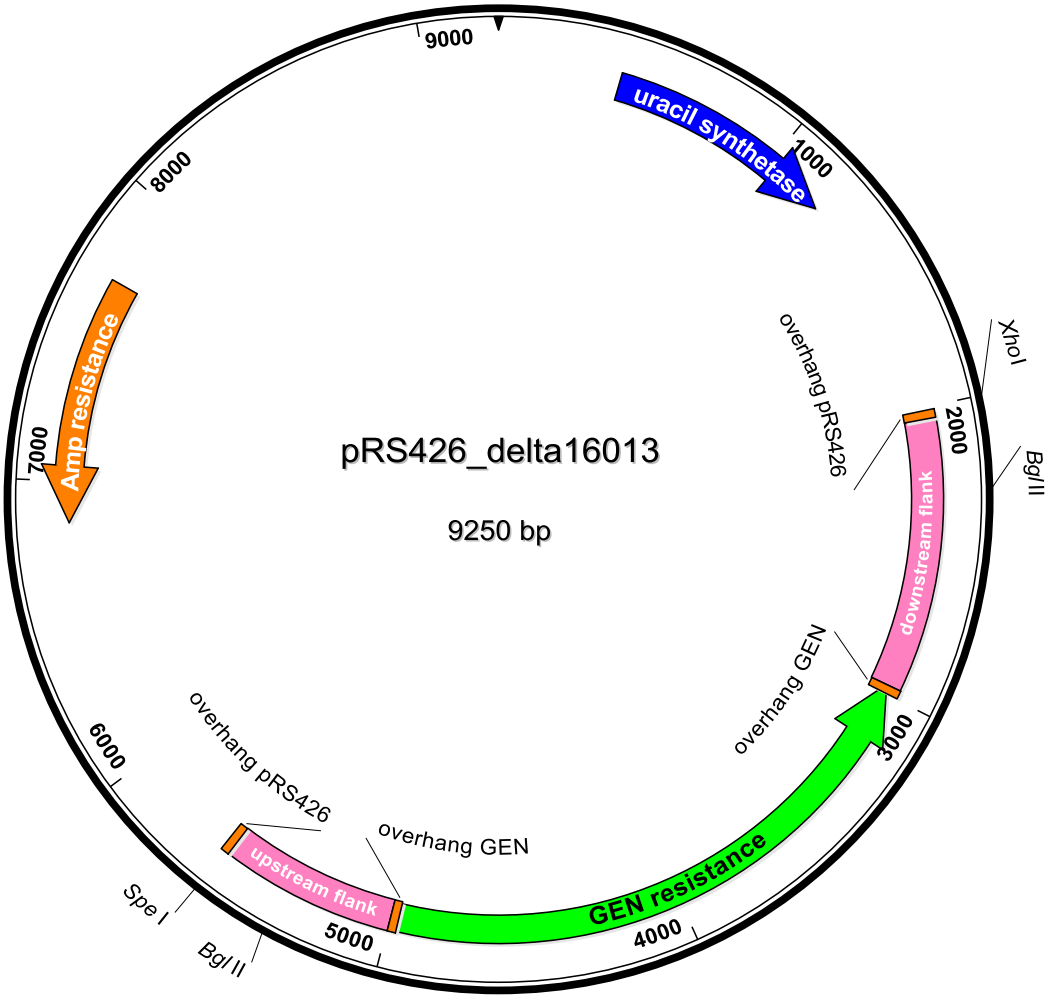

Supplementary figure 4: Map of deletion vector for lignin peroxidase gene FGSG_16013 pRS426_Δ16013. Uracil synthetase gene (dark blue), ampicillin resistance cassette (pink), and geneticin resistance cassette (green) were used as selection markers for *S. cerevisiae*, *E. coli* and *F. graminearum* cloning, respectively. Flanking regions (pink) of FGSG_16013 were cloned upstream and downstream of the resistance cassette in such a way that the resistance cassette would be integrated into the *F. graminearum* genome in antisense orientation of the target gene. Overhangs (orange) allowed correct assembly of the DNA fragments via yeast recombinational cloning. Restriction enzyme *Bgl*II was used for verification of the correct assembly of the vector. Restriction enzymes *Spe*I and *Xho*I were used to cut the deletion construct (flanking region – resistance cassette – flanking region) out of the vector backbone for *F. graminearum* protoplast transformation.

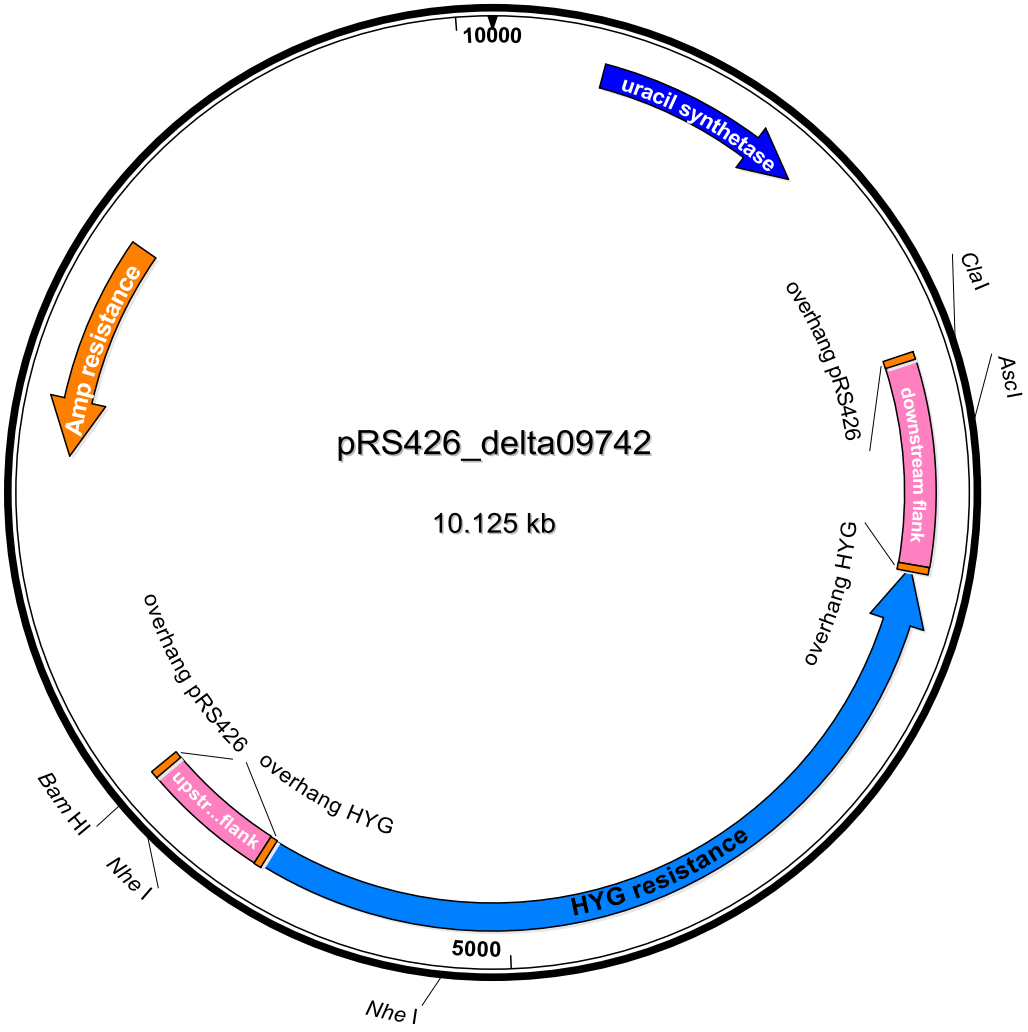

Supplementary figure 5: Map of deletion vector for cupredoxin gene FGSG_09742 pRS426_Δ09742. Uracil synthetase gene (dark blue), ampicillin resistance cassette (pink), and hygromycin resistance cassette (light blue) were used as selection markers for *S. cerevisiae*, *E. coli* and *F. graminearum* cloning, respectively. Flanking regions (pink) of FGSG_09742 were cloned upstream and downstream of the resistance cassette in such a way that the resistance cassette would be integrated into the *F. graminearum* genome in antisense orientation of the target gene. Overhangs (orange) allowed correct assembly of the DNA fragments via yeast recombinational cloning. Restriction enzymes *Nhe*I and *Asc*I were used for verification of the correct assembly of the vector. Restriction enzymes *Bam*HI and *Cla*I were used to cut the deletion construct (flanking region – resistance cassette – flanking region) out of the vector backbone for *F. graminearum* protoplast transformation.

Supplementary table 1: List of genes deleted in this study with corresponding FGSG_number, enzyme class, storage number, number of individual mutants with respective strain number, and selection markers. Genes are ordered by storage number of the respective deletion strain.

FGFG-number of deleted genes	Enzyme class	Storage number	Deletion strains	Selection marker
FGSG_11399	Oxidase	1641	.6, .9, .12	NAT
FGSG_06023	Cupredoxin	1667	.1, .4, .7, .8	NAT
FGSG_00576	SOD	1682	.3, .9, .11	NAT
FGSG_16013	Lignin peroxidase	1686	.4, .5, .7, .8	GEN
FGSG_09742	Cupredoxin	1687	.1, .6, .8, .15	HYG
FGSG_06023;09742	Cupredoxins	1729	.3, .7, .8	NAT/HYG
FGSG_03436	Chloroperoxidase	1762	.2	NAT
FGSG_03708	Chloroperoxidase	1791/1864	.1 / .1, .4, .5, .6, .8	HYG
FGSG_11528	Tyrosinase	1805	.7	NAT
FGSG_03700	P450 monooxygenase	1809	.1, .3, .13	NAT
FGSG_07765	P450 monooxygenase	1814	.20	NAT
FGSG_03498	P450 monooxygenase	1816	.3, .4, .6, .15	HYG
FGSG_01745	P450 monooxygenase	1819	.1, .19, .20	HYG
FGSG_09124	Reductase	1821	.4	HYG
FGSG_04434	Ascorbate/cytochrome c peroxidase	1822	.2	HYG
FGSG_17054	Metallothionein	1841/1931/1932	.2 / .1, .2, .4, .5, .6 / .1, .14, .22	HYG
FGSG_02341	Chloroperoxidase	1843	.5	GEN
FGSG_12456	Metallothionein	1848	.10, .22	NAT
FGSG_17054;12456	Metallothioneins	1863	.4, .5	HYG/NAT
FGSG_03708;02341	Chloroperoxidases	1865	.14	GEN/HYG
FGSG_03708;02341; 03436	Chloroperoxidases	1877	.3, .22	GEN/HYG/NAT
FGSG_16151	Metallothionein	1903	.1, .2, .8, .9	GEN
FGSG_17054;12456; 16151	Metallothioneins	1913	.5	HYG/NAT/GEN
FGSG_16458	P450 monooxygenase	1966	.1, .6, .13, .20	HYG
FGSG_09093	Galactose oxidase	1967	.2, .5, .8, .11	HYG
FGSG_02917	Cellobiose dehydrogenase	1968	.5, .9, .12, .23	GEN
FGSG_17478	FAD-dependent monooxygenase	1969	.1, .7, .15, .24	GEN
FGSG_01988	Tyrosinase	1970	.2, .13, .20, .37	NAT
FGSG_09006	NNT	1973	.2	NAT
FGSG_11215	FAD-dependent monooxygenase	1976	.9, .16, .23	HYG

Supplementary table 2: Nucleotide sequence of GPI-HyPer DNA fragments. Promotor, signal peptides, HyPer ORF, and spacer were cloned into vector pII99. Each row in the presented nucleotide sequences shows 50 bp.

Promotor region of FGSG_04399	TATGGCATTATAACATTACCTAACGAAGCATCAACACATAGACACTGGTT GAAAACAGAAGACATAAGTGGCGACGCAAAAGCACATGCTACTGCGAGGA AGACTTCCGCTTAAGAGGCGTACCGATCACATATAAAAGGCGGATGATGA TTTAGTTGAACATTTGAGTAAGACATGTCGAAGAAAACGCAGGTACTCGC ACTCATTTTGGATTTGTATGATTGGAGTTGTTGGCATGGCGTGATACAAA GGTGTCTGAATAATAGACAGTTTCGAAGTTTGTTAAACATAGCACAAGAA GCATGCACATGTTTGTATTCGATGTTGCTAGTGAGGTCAAGCTGTGATAT CACAAGAGACTATCTAAGCCTAGTCCCTCAGTGAGCAAAGAATATGACTT TGTTCAAGTTTACTATTCCTAACCAATATCTGACCCTCTATTCTCAAGTC TCCATTTGTTGCCAGCACAATGAGCTGTTTCTCACCCGACCAAGGCCTTC CATTCCCCACCTAGATCCCCATCTCACCAGGACCCAAGACCCTTCAAACT TCCTTTATCAAGATGGGGTGGGCTTGTGTATGCGTGTGTGTGTGTCACGG GCGAATCGCAAGAGGGGGTAAAACAAAGCAACAGCCCGCTATTTGCGCCA GGAAACCCCGCTTTGGGAAAGAGTCGACGTAAATCTCGTGTGAGGGAAGG ATGATTTGGTTTGGAGTTGATGGAGATACAGTAGTATATATAATTTAAAC CTTCCCTCCCCCTCTTTCTTCCCTTCCTCTCTTTTTCTACACAGCTTAAA CTTTGACACTTCTACACCTTGTACCACATACATCTCTCGAGCTC
N-terminal signal peptide	ATGCGCGCCCAGGCTCTTGCTGCTGTTCTTCTCTCTGCATGCGCTGGTCA AGCTATCGCT
HyPer-2 ORF (without initial start codon)	GAGATGGCAAGCCAGCAGGGCGAGACGATGTCCGGACCGCTGCACATTGG TTTGATTCCCACAGTTGGACCGTACCTGCTACCGCATATTATCCCTATGC TGCACCAGACCTTTCCAAAGCTGGAAATGTATCTGCATGAAGCACAGACC CACCAGTTACTGGCGCAACTGGACAGCGGCAAACTCGATTGCGTGATCCT CGCGCTGGTGAAAGAGAGCGAAGCATTCATTGAAGTGCCGTTGTTTGATG AGCCAATGTTGCTGGCTATCTATGAAGATCACCCGTGGGCGAACCGCGAA TGCGTACCGATGGCCGATCTGGCAGGGGAAAAACTGCTGATGCTGGAAGA TGGTCACTGTTTGCGCGATCAGGCAATGTCCGCCGGCTACAACAGCGACA ACGTCTATATCATGGCCGACAAGCAGAAGAACGGCATCAAGGCCAACTTC AAGATCCGCCACAACGTCGAGGACGGCAGCGTGCAGCTCGCCGACCACTA CCAGCAGAACACCCCCATCGGCGACGGCCCCGTGCTGCTGCCCGACAACC ACTACCTGAGCTTCCAGTCCGTCCTGAGCAAAGACCCCAACGAGAAGCGC GATCACATGGTCCTGCTGGAGTTCGTGACCGCCGCCGGGATCACTCTCGG CATGGACGAGCTGTACAACGTGGATGGCGGTAGCGGTGGCACCGGCAGCA AGGGCGAGGAGCTGTTCACCGGGGTGGTGCCCATCCTGGTCGAGCTGGAC GGCGACGTAAACGGCCACAAGTTCAGCGTGTCCGGCGAGGGCGAGGGCGA TGCCACCTACGGCAAGCTGACCCTGAAGCTGATCTGCACCACCGGCAAGC TGCCCGTGCCCTGGCCCACCCTCGTGACCACCCTCGGCTACGGCCTGAAG TGCTTCGCCCGCTACCCCGACCACATGAAGCAGCACGACTTCTTCAAGTC CGCCATGCCCGAAGGCTACGTCCAGGAGCGCACCATCTTCTTCAAGGACG ACGGCAACTACAAGACCCGCGCCGAGGTGAAGTTCGAGGGCGACACCCTG

	GTGAACCGCATCGAGCTGAAGGGCATCGGCTTCAAGGAGGACGGCAACAT CCTGGGGCACAAGCTGGAGTACAACGGCACCGGTTTCTGTTTTGAAGCCG GGGCGGATGAAGATACACACTTCCGCGCGACCAGCCTGGAAACTCTGCGC AACATGGTGGCGGTAGGTAGCGGGATCACTTTACTGCCAGCGCTGGCTGT GCCGCCGGAGCGCAAACGCGATGGGGTTGTTTATCTGCCGTGCATTAAGC CGGAACCACGCCGCACTATTGGCCTGGTTTATCGTCCTGGCTCACCGCTG CGCAGCCGCTATGAGCAGCTGGCAGAGGCCATCCGCGCAAGAATGGATGG CCATTTCGATAAAGTTTTAAAACAGGCGGTT
Spacer	GGAGCTGGAGCAGGTGCA
C-terminal signal peptide	AACGCTGGCTCTTCTATGGCTGTTCCGGTCAACCTGGTTCTTGCTGGTGT CTTTGCTCTCGCTTTCGCTCTG

Acknowledgments

An erster Stelle bedanke ich mich bei Herrn Prof. Wilhelm Schäfer für die Möglichkeit, in seiner Arbeitsgruppe promovieren zu können, und für die weitreichende wissenschaftliche Förderung und Betreuung. Danke auch für die zahlreichen Bundesligagespräche unter lauter Fußballverächtern.

Ein besonderer Dank geht an Herrn Prof. Jörg Bormann, der mein Forschungsprojekt ins Leben gerufen und den Großteil der Betreuung meiner wissenschaftlichen Arbeit übernommen hat. Selbst während seines Auslandsaufenthaltes war immer mindestens ein offenes Ohr für Fragen übrig.

Danke an Dr. Ana Lilia Martínez-Rocha für die vielen Tipps und Tricks und die ständige Aufmunterung. Vielen lieben Dank an das Herz der Arbeitsgruppe, Cathrin Kröger und Birgit Hadeler, für die ständige Unterstützung und die vielen Ratschläge und Erklärungen. Eure freundliche und fürsorgliche Art haben Vieles einfacher gemacht.

Ich danke den vielen Labor-Kollegen und -Freunden, die mit mir im gleichen Boot saßen und die immer aufmunternde Worte bei Frustration sowie guten Humor und Ablenkung parat hatten. Danke an Gunnar Baermann, Sophie Charlotte Brandt, Anika Glasenapp, Hoáng Xuan Chien, Tobias Hanack, Aimo Zurborg, Annemarie Glöckner, Christine Blum und Michael Mentges. Ihr habt mich oft genug daran erinnert, dass Misserfolge im Labor kein Weltuntergang sind.

Ich danke meinen Eltern, ohne deren Unterstützung mir dieser Schritt nicht möglich gewesen wäre.

Danke an Barbara Snow Titus für die Prüfung meiner Dissertation auf sprachliche Richtigkeit.

Außerdem möchte ich meiner Freundin Juliane danken. Ein Gedanke an dich hat immer wieder ausgereicht, um zu erkennen, dass es weit wichtigere Dinge im Leben gibt als beruflichen Erfolg. Es ist von unschätzbarem Wert, sich stets auf zu Hause freuen zu können. Du gibst mir Rat, Kraft und Mut und ich werde dir noch viele Jahre dafür danken.

Declaration of authorship

I hereby declare on oath that I have written the present dissertation by my own and have not used other than the acknowledged resources and aids. I further declare that I have not submitted this thesis at any other institution in order to obtain a degree.

Hamburg, 29.08.2018
(Place, Date)

(Signature)

Confirmation of Linguistic Correctness

I hereby declare that I have read the doctoral thesis "Investigation of the reactive oxygen species metabolism during the life cycle of *Fusarium graminearum*" by Karl Lewin Günther, and, as a native English speaker, confirm its linguistic correctness in English.

Albuquerque, August 26th 2018

Barbara Snow Titus